

UNIVERSIDADE DE LISBOA

FACULDADE DE CIÊNCIAS

DEPARTAMENTO DE FÍSICA



**SPECTROSCOPIC TECHNIQUES FOR CHARACTERIZING PORTUGUESE GLAZED  
CERAMICS: A CONTRIBUTION TO THE STUDY OF ANCIENT FAIENCES OF  
COIMBRA.**

Ana Cristina de Oliveira Guilherme Buzanich

DOUTORAMENTO EM FÍSICA

2013

UNIVERSIDADE DE LISBOA

FACULDADE DE CIÊNCIAS

DEPARTAMENTO DE FÍSICA



**SPECTROSCOPIC TECHNIQUES FOR CHARACTERIZING PORTUGUESE GLAZED  
CERAMICS: A CONTRIBUTION TO THE STUDY OF ANCIENT FAIENCES OF  
COIMBRA.**

Ana Cristina de Oliveira Guilherme Buzanich

Tese orientada por:

Prof. Doutora Maria Luisa de Carvalho Dias de Sousa Leonardo

Prof. Doutor João Paulo Pereira Freitas Coroado

DOUTORAMENTO EM FÍSICA

2013

To Günter  
and my dear parents.

"De tudo o que nós fazemos de sincero e bem intencionado alguma coisa fica."<sup>1</sup>

*Florbela Espanca, 1928*

---

<sup>1</sup> *"Something remains out of everything sincere and well intended you do."*



## ACKNOWLEDGMENTS

- First of all my deepest gratitude goes to my supervisor Professor Maria Luisa de Carvalho (*Centro de Física Atómica, Departamento de Física da Faculdade de Ciências da Universidade de Lisboa*). You made it possible for me to start a scientific career providing all kinds of resources and support. I recognize and deeply appreciate the effort you always put in finding means of supporting me financially, given the present difficult times. By granting me the possibility to participate in (national and international) projects related to X-ray Spectrometry applied to the Cultural Heritage, I have acquired experience and confidence to come forward. An important stage of my life was moving to Berlin and even though I never felt neglected. Thank you for your scientific guidance, advisory, comprehension, trust and above all friendship.

- My gratitude is also extended to my other supervisor Professor João Coroado (*Departamento de Arte e Conservação e Restauro do Instituto Politécnico de Tomar*), who I had the pleasure to meet during my masters studies. Your knowledge in glazed ceramics is outstanding and this was essential for me to get into this new field of investigation. Thanks for the long talks via Skype™ and for clarifying all my doubts. In your own words: “Talking about these subjects is like eating sweets.” In fact, your enthusiasm on this field kept me motivated to carry on and wanting to know more about it. Thank you for your suggestions, advises and knowledge transfer.

- To Professor Joaquim dos Santos (*GIAN – Grupo de Instrumentação Atómica e Nuclear, Departamento de Física da Faculdade de Ciências da Universidade de Coimbra*) I am deeply grateful. Thanks for having supported me financially. I will never forget your promptness in helping me to carry on my PhD. It would have been very hard otherwise.

- I would like to acknowledge Fundação para a Ciência e Tecnologia (FCT) for granting the bilateral collaboration between Portugal and Germany (FCT-DAAD: 2010/11) “Investigation on glazed Portuguese ceramics through spectroscopy techniques (EDXRF, 3D Micro-XRF, XRD and SEM-EDS)”. Thanks to this collaboration, I was able to develop important parts of my PhD.

- I want to express my sincere gratitude to Professor Birgit Kanngießner (*Institut für Optik und Atomare Physik, Technische Universität Berlin*), who was the responsible person from the

German side of this bilateral collaboration. Your immediate effort in receiving me and integrating me in your workgroup, as a guest scientist, was remarkable and very important to make me feel comfortable in a new country and working environment. Thank you for giving me space to perform my work. Also for granting me the opportunity to participate in all group activities: meetings, seminars and annual bike excursions. Above all, thank you for all your scientific and personal support as well as your friendship. I am glad that my first long experience abroad was in your workgroup.

- I thank the *Helmholtz Zentrum Berlin (HZB)* for the allocation of synchrotron radiation beamtime, three times (between 2010 and 2012), as well as financial support for travel expenses. I also thank Ivo Zizak for the technical support at the MySpot beamline.

- Special thanks go to the group responsible for the Synchrotron beam analysis from the Structure Analysis (division 1.3) from BAM (*Bundesanstalt für Materialforschung und -prüfung*) in Berlin. Namely, Heinrich Riesemeier, Uwe Reinholz, Martin Radtke and Günter Buzanich. Thank you for the opportunity to perform measurements at the BAMline, at BESSY-II, out of official allocated beamtime.

- Thank you to my dear friends and colleagues, from *Centro de Física Atómica da Universidade de Lisboa*, Marta Manso, Sofia Pessanha, Teresa Amorim, Diana Guimarães and Ana Cavaco. A special thank goes to Sofia, for having me accompanied with the *in situ* measurements at the *Museu Machado de Castro* in Coimbra. I was/am so lucky to have you as colleagues and friends. You provided me always an amazing working atmosphere both in personal and scientific ways. Thank you for keeping in touch though the long distance and for caring about me.

- To all members of the workgroup AG Kanngießler (*Institut für Optik und Atomare Physik, Technische Universität Berlin*), many thanks for having provided a warm working environment with very good moments. Among them, I will never forget the reaction that many of you had by eating snails, in Figueira da Foz. Thank you so much for the support you all gave me during the first two beamtime allocations. It was fantastic the effort from you all, working 24/7. Special thanks go to Lars Lühl, Timo Wollf, Christian Seim, Ioanna Mantouvalou, Wolfgang Malzer and Bernhard Hesse for the help with the data analysis and discussions. Maram Na'es, thank you for

reviewing my thesis and for the useful contributions to it. Above all thanks for the support by bearing my frustrations while writing – better times will come for sure. I appreciate your friendship and wish you all the best!

- Regarding SEM/EDX analyses, I want to acknowledge two institutions: *GeoBioTec at the University of Aveiro (Aveiro, Portugal)* and *BAM, Bundesanstalt für Materialforschung und -prüfung, Division 6.8: Surface Analysis and Interfacial Chemistry, Berlin, Germany*. Huge thanks to Mrs. Sigrid Benneman and Dr. Vasile-Dan Hodoroaba (BAM), for the support, promptness and knowledge transfer during my time there. Dan, thank you for the help with the SEM figures' layout – It was great what we were able to produce from these results.

- Thanks to Dr. Andreas C. Scheinost – *Rosendorf Beamline (BM20) at the European Synchrotron Radiation Facility (ESRF) in Grenoble, France* – for providing me with XAFS spectra of Sb-based reference compounds.

- I also want to thank Ricardo Pereira Triães (*Departamento de Arte e Conservação e Restauro do Instituto Politécnico de Tomar*) for his support in manufacturing replicas of glazed ceramics with me. Thank you for your time, patience and knowledge transfer.

- I want to thank Dr. Alexandre Pais (*Museu Nacional do Azulejo – MNAz – Lisboa*) for providing me with *Azulejos* samples and useful explanations about them, and to Mr. António Pacheco (*Museu Machado de Castro – MMC – Coimbra*) for allowing *in situ* measurements on whole original pieces.

- Thanks for the inspiring PhD thesis of Marta Manso, Diana Guimarães, Ioanna Mantouvalou, Lars Lühl, Günter Buzanich, Alexandre Pais and João Coroado.

- To my family, the most important people in my life. My husband, Günter, I want to thank for supporting and understanding me. Thanks for cherishing my good moments with me and keeping me optimistic in bad times. Your love kept me stronger when I most needed. “I’ve got a crush on you, sweetie pie...”. Thank you for the helpful comments while reviewing my thesis.

My dear parents, Maria Elina de Oliveira and Manuel Guilherme, I cannot thank you enough for the support you gave me throughout my whole life, at many levels. You are an inspiration to me. Thank you for always respecting my decisions and supporting them even if they were hard for you. That’s what family is all about. I love you!



## LIST OF PUBLICATIONS RESULTING FROM THIS WORK

- 1) A. Guilherme, V.-D. Hodoroaba, S. Benemann, J. Coroado, M. L. Carvalho. *Morphological and compositional features of blue and yellow pigments used in Portuguese glazed ceramics by SEM/EDX – unraveling manufacturing differences*. Submitted to *Microscopy and Microanalysis* (2013).
  
- 2) A. Guilherme, G. Buzanich, M. Radtke, U. Reinholz, J. Coroado, J. M. F. dos Santos and M. L. Carvalho. *Synchrotron Micro-XRF with Compound Refractive Lenses (CRLs) for tracing key elements on Portuguese glazed ceramics*. *Journal of Analytical Atomic Spectrometry* (2012), 27, 966-974.
  
- 3) A. Guilherme, J. Coroado, J.M.F. dos Santos, L. Lühl, T. Wolff, B. Kanngießler and M.L. Carvalho. *X-ray fluorescence (conventional and 3D) and scanning electron microscopy for the investigation of Portuguese polychrome glazed ceramics: Advances in the knowledge of the manufacturing techniques*. *Spectrochimica Acta part B – Atomic spectroscopy* (2011), 66 (5) 297-307.
  
- 4) A. Guilherme, M.L. Carvalho, S. Pessanha, J. M. F. dos Santos and J. Coroado. *Micro energy dispersive X-ray fluorescence analysis of polychrome lead-glazed Portuguese faiences*. *Spectrochimica Acta part B – Atomic spectroscopy* (2010), 65 (4), 328-333.
  
- 5) A. Guilherme, J. Coroado and M. L. Carvalho. *Chemical and mineralogical characterization on glazes of ceramics from Coimbra (Portugal) from XVI-XIX centuries*. *Analytical and Bioanalytical Chemistry* (2009), 395, 2051–2059.

# TABLE OF CONTENTS

<b>ACKNOWLEDGMENTS</b> .....	i
<b>LIST OF PUBLICATIONS RESULTING FROM THIS WORK</b> .....	iv
<b>TABLE OF CONTENTS</b> .....	v
<b>RESUMO</b> .....	1
<b>ABSTRACT</b> .....	6
<b>CHAPTER 1 – INTRODUCTION TO GLAZED CERAMICS</b> .....	7
1.1 Glazed ceramics in Portugal – historical context .....	9
1.2 Description of the analyzed samples – origin and features.....	13
1.2.1 Ceramic support / body .....	14
1.2.2 Glaze .....	16
1.2.3 Surface decoration .....	19
<b>CHAPTER 2 – OBJECTIVES OF THE WORK</b> .....	24
2.1 The necessity for investigation.....	24
2.2 Analytical requirements .....	25
<b>CHAPTER 3 – METHODS OF ANALYSIS</b> .....	29
3.1 X-ray Fluorescence Spectroscopy (XRF) .....	29
3.1.1 XRF principles.....	29
3.1.2 Conventional XRF.....	34
3.1.3 3D Micro-XRF .....	41
3.1.4 High-resolution Micro-XRF .....	45
3.2 X-ray Diffraction (XRD) .....	51
3.2.1 XRD principles.....	51
3.2.2 Experimental setup and methodology .....	54
3.3 Scanning Electron Microscopy / Energy Dispersive X-ray System (SEM/EDX).....	54
3.3.1 SEM/EDX principles .....	54
3.3.4 Experimental setup and methodology .....	61
3.4 X-ray Absorption Fine Structure (XAFS) .....	62

3.4.1 XAFS principles.....	62
3.4.2 Data handling.....	65
3.4.3 Experimental setup and methodology .....	66
3.5 Statistical data handling .....	68
<b>CHAPTER 4 – RESULTS .....</b>	<b>73</b>
4.1 – Suitability of XRF for glazed ceramics analyses.....	73
4.2 – Original samples: fragments.....	76
4.2.1 – Ceramic body .....	76
4.2.2 – Glaze .....	80
4.2.3 – Surface decoration.....	90
4.3 – Replicas.....	142
4.3.1 – Manufacturing processes .....	142
4.3.2 – Chemical and mineralogical characterization .....	146
4.4 – <i>In situ</i> analysis of whole Museum objects .....	151
4.4.1 – Blue pigment.....	152
4.4.2 – Yellow pigment .....	155
4.4.3 – Purple pigment .....	156
4.4.4 – Green pigment.....	157
<b>CHAPTER 5 – DISCUSSION, CONCLUSIONS and OUTLOOK .....</b>	<b>159</b>
5.1 Ceramic body.....	159
5.2 Glaze .....	160
5.3 Surface decoration .....	161
5.3.1 Blue.....	162
5.3.1 Yellow .....	163
<b>Outlook .....</b>	<b>165</b>
<b>BIBLIOGRAPHY.....</b>	<b>167</b>
<b>ANNEX.....</b>	<b>174</b>
Annex 1.1 – Chronological development of <i>Azulejos</i> (Wall-tiles) in Portugal. ....	174
Annex 1.2 – Chronological development of faiences from Coimbra. ....	176

Annex 1.3 – Description of the analyzed fragments. ....	178
Annex 1.4 – Description of the analyzed museum objects original from Coimbra. ....	186
Annex 1.5 – Papers published in peer reviewed international scientific journals in the framework of the present thesis. ....	197

## RESUMO

Este estudo tem como objectivo principal a análise e caracterização de cerâmicas vidradas (antigas) produzidas entre os séculos XVI e XVIII em Coimbra e Lisboa. Para tal recorreu-se a uma metodologia multianalítica de modo a fornecer informação científica a vários níveis para se obter parâmetros identificadores destas produções. Paralelamente, este estudo surge como uma oportunidade para o apuramento do conhecimento e da reconstituição da tecnologia e do sistema de produção usado em Coimbra, particularmente faianças.

De um modo geral, cerâmicas vidradas policromas são caracterizadas por três zonas: corpo cerâmico, vidrado e superfície decorativa. A escolha das matérias-primas bem como o processo de manufactura (aplicação do vidrado, temperatura de cozedura, entre outros) são factores que influenciam a peça final. O corpo cerâmico é composto maioritariamente por minerais argilosos, óxidos de silício (Si) e Alumínio (Al) e inclusões não plásticas (têmpera). Os minerais argilosos conferem plasticidade à pasta; sílica ( $\text{SiO}_2$ ) tem um papel estrutural e é refractário – ponto de fusão alto (1600 – 1725 °C); têmperas podem ser impurezas intrínsecas aos minerais argilosos ou adicionadas pelo oleiro para conferir as propriedades desejadas.

O vidrado é constituído por três (ou quatro) grupos de compostos: i) formadores de rede – maioritariamente sílica ( $\text{SiO}_2$ ); ii) modificadores de rede (ou fluxos) – maioritariamente óxidos de chumbo (ex.  $\text{PbO}$ ) e minerais argilosos (para baixar o ponto de fusão da estrutura silicatada); iii) intermediários - para repôr as propriedades perdidas pela introdução de fluxos; iv) agentes opacos – normalmente Cassiterite ( $\text{SnO}_2$ ).

Os escassos estudos cerâmicos já desenvolvidos privilegiam as manufacturas de Lisboa em detrimento das de Coimbra, encaradas como mais periféricas e de menor qualidade. No entanto, este preconceito exige uma reflexão mais profunda, pois aspectos considerados pouco cuidados (tipo de vidrados, tonalidades mais densas dos óxidos, maior porosidade das pastas) poderão dever-se a constrangimentos na aquisição de matérias-primas e consequente improvisação do que havia disponível. O facto é que qualquer peça da produção de Coimbra é avidamente coleccionada, mesmo fora das fronteiras nacionais. Através de uma caracterização visual, têm vindo a ser intuídos pelos ceramólogos alguns aspectos potencialmente marcadores

das cerâmicas de Coimbra, mas faltam critérios científicos que permitam confirmar estas hipóteses.

Os objectos de estudo pertencem a dois grupos de cerâmica vidrada: faianças utilitárias (originais de Coimbra) e azulejos (originais de Coimbra e Lisboa). Os fragmentos de faianças foram recolhidos do espólio existente no Mosteiro de Santa Clara-a-Velha (Coimbra) através do Museu Machado de Castro (MMC) em Coimbra e os fragmentos de azulejos – quer de Coimbra e de Lisboa – foram obtidos através do Museu Nacional do Azulejos (MNAz) em Lisboa. Tendo em conta o objectivo principal proposto, este estudo assenta em duas grandes vias de investigação: caracterização composicional de peças com origem conhecida (Coimbra e Lisboa) e preparação e caracterização de modelos laboratoriais. Os modelos criados em laboratório servirão para obter informação sobre a origem da matéria-prima utilizada, dos processos de fabrico, nomeadamente da temperatura de cozedura, processo de aplicação do vidrado e aplicação dos pigmentos. Pretende-se assim com este trabalho o desenvolvimento de um extenso programa analítico, que permitirá a caracterização elementar, composicional, mineralógica e morfológica ao nível do corpo cerâmico, vidrado e pigmentos. Além disto, as zona de interface (pigmento/vidrado e vidrado/corpo cerâmico) serão também analisadas, pois a interacção pigmento/vidrado e vidrado/corpo cerâmico depende das matérias primas utilizadas bem como da temperatura de cozedura.

Tendo em conta os objectivos propostos é necessário escolher técnicas espectroscópicas não destrutivas, isto é, que preservem a integridade física e química do objecto a analisar. As técnicas usadas neste trabalho são: espectroscopia por Fluorescência de Raios X (do inglês, XRF), Difracção de Raios X (do inglês, XRD), Microscopia por Varrimento Electrónico com sistema de espectroscopia por Fluorescência de Raios X acoplado (do inglês, SEM/EDX) e espectroscopia por Absorção de Raios X (do inglês, XAFS).

XRF permite a identificação simultânea bem como quantificação dos elementos presentes numa amostra, com número atómico superior a 9. O facto de esta técnica ser não destrutiva, faz dela um método de eleição para a análise de objects com valor histórico, artístico e arqueológico. Além do método convencional de XRF, foi também usada a vertente confocal (ou

3D) de XRF. Com esta vertente, consegue-se seleccionar volumes de amostra e efectuar varrimentos em profundidade, obtendo uma informação tri-dimensional elementar da amostra.

XRD fornece informação ao nível mineralógico que constitui as amostras. Acedendo a esta informação consegue-se assim aceder directamente às matérias-primas utilizada bem como a minerais que surgem como consequência das transformações térmicas que ocorrem durante o processo de cozedura.

SEM/EDX fornece informação ao nível morfológico, em que imagens dos cristais que pertencem à estrutura das matérias-primas são visualizados. Tendo esta informação disponível, conseguem-se estimar processos de cozedura utilizados, mais precisamente temperaturas utilizadas. O tamanho e a forma dos cristais é indício desta ultima propriedade.

Por fim, XAFS, vem complementar a informação que é “perdida” com XRD. A alta sensibilidade química para especiação de um único átomo, vem colmatar as dificuldades impostas pelos artefactos experimentais em XRD. Com XAFS, consegue-se averiguar o estado e oxidação de um dado átomo bem como a distância a que se encontram os átomos vizinhos mais próximos desse átomo. Assim sendo, informação acerca da geometria da molécula em que o que átomo se encontra bem como tipos de ligação entre este e os seus vizinhos, consegue ser obtida. Estas propriedades tornam a técnica de XAFS bastante apelativa para estudos em objects ligados ao património cultural. A única dificuldade é ter que recorrer a um sincrotrão para poder efectuar tais medições. O facto de ser uma técnica altamente sensível a nível atómico requer o uso de fontes de radiação X com determinadas propriedades que não se encontram em laboratório, tais como, coerência, alto brilho e muito baixa divergência.

Aplicando esta aproximação multianalítica aos objectos em estudo – e tendo em conta o objectivos propostos – foram obtidas diferenças entre as produções de Coimbra e Lisboa, destacando as faianças das demais. Resultados obtidos por XRF e XRD demonstram que o corpo cerâmico dos Azulejos é mais heretogéneo e mais poroso do que o das faianças. Mais ainda, foi obtido que os corpos cerâmicos de Azulejos terão sido submetidos a temperaturas de cozedura mais elevadas do que os de Faianças. Isto confirma-se pela presença de minerais metaestáveis que se formam a mais altas temperaturas, tais como a Cristobalite (um polimorfo da silica que se forma a alta temperatura). Foi também detectada a presença de chumbo (Pb)

(principalmente em Azulejos) na parte de trás do corpo cerâmico. Isto deve-se à elevada porosidade no corpo cerâmico de Azulejos que favorece a penetração de Pb pelos poros até ao fundo do corpo cerâmico. Este fenómeno está de acordo com o processo de manufactura das peças. Faianças são produzidas ao torno oleiro enquanto que os Azulejos são produzidos em placas, conferindo assim maior heterogeneidade.

Faianças têm um vidrado mais fino (espessura máx. 180  $\mu\text{m}$ ) do que os azulejos (espessura máx. 400  $\mu\text{m}$ ). Através de XRF foi possível identificar elementos-chave para vidrado e cores usadas para a camada decorativa: Cobalto (Co) para o azul, Antimónio (Sb) para o amarelo, Manganês (Mn) para o púrpura, Cobre (Cu) para o verde e Chumbo (Pb) para o vidrado.

Através de SEM/EDX foi possível observar que Estanho (Sn) foi adicionado intencionalmente pelo oleiro à mistura do pigmento azul. Isto deve-se ao facto de o azul de Co ser muito escuro (quase preto) e não é esse o tom de cor que se observa a olho nú. Sendo  $\text{SnO}_2$  um composto que confere uma cor esbranquiçada, confere-se a adição de este ao pigmento azul. Uma das grandes contribuições deste estudo foi verificar Co está associado a uma corrente de 5 elementos: Fe-Co-Ni-As-Bi. Apesar de Bi ter sido detectado por XRF, este não foi detectado com estando associado à fonte de Co. Mais ainda, em faianças de Coimbra, as estruturas de Co são ricas em Ferro (Fe) enquanto que em Azulejos estas são ricas em Níquel (Ni).

Outro resultado importante foi verificar diferenças na morfologia dos cristais que compõem o pigmento amarelo. Segundo fontes documentais, o pigmento amarelo mais usado e mais provável terá sido o Amarelo de Nápoles ( $\text{Pb}_2\text{Sb}_2\text{O}_7$ ). Através de SEM/EDX foi verificado que os cristais de amarelo de Nápoles em azulejos de Lisboa são hexagonos bem definidos – típico do pigmento em si e indicativo de uma temperatura de cozedura acima dos 1100 °C. Nas faianças de Coimbra estes cristais têm formas mais irregulares (triangulares) em vez de hexagonais. De acordo com a literatura esta forma de cristais indica temperaturas de cozedura inferiores a 1000 °C. Além do mais, através de XAFS obtiveram-se diferenças na própria estrutura cristalina do pigmento amarelo. Amostras de Coimbra (faianças e Azulejos) o composto na forma de  $\text{Pb}_2\text{Sb}_2\text{O}_7$  terá sido usado enquanto que nas amostras de Lisboa, uma mistura de compostos de Pb e Sb foi identificada.



Este trabalho é pioneiro no estudo científico de tão valioso espólio e com a informação obtida surgiram 4 publicações em revistas internacionais científicas com um factor de impacto significativo na área de espectroscopia. Foram fornecidas respostas acerca das matérias-primas e propriedades composicionais – ao nível mineralógico e morfológico. Assim sendo, o campo das artes em Portugal pode ser usado como base para desenvolver metodologias de conservação e restauro. Este trabalho proporcionou não só nova informação acerca das produções de Coimbra e Lisboa mas também a abertura de horizontes para dar continuidade a esta investigação. O universo de amostra aqui analisado se viu para extrair diferenças entre os centros de manufactura cerâmica mas há ficada implícita a necessidade de analisar cerâmicas de outros centros, como por exemplo Porto ou Alcobaça.

**Palavras-chave:** Faianças de Coimbra; Azulejos; Investigação multianalítica; Caracterização composicional; Diferenças entre técnicas de manufactura;

## ABSTRACT

Polychrome glazed ceramics (faïences and wall-tiles) originally produced in the two main manufacturing centers between the XVI and XVIII centuries, Coimbra and Lisbon (Portugal), were object of study. In order to overcome mislabeling of objects which are not properly identified – e.g. by potters marks – this investigation addresses to gain knowledge concerning manufacturing technological aspects by a multianalytical (non-destructive) approach. Since no scientific data was found regarding faïences produced in Coimbra, this serves as a contribution for the classification of “Faïence from Coimbra”.

The samples are characterized by ceramic support, a glaze and surface decoration. Depending on the raw materials as well as the manufacturing process involved – e.g. firing temperature – these three main regions will interact with each other differently. Therefore, information obtained at the interface-areas is important.

Considering the objectives of this work, the chosen analytical methods were: X-ray Fluorescence (XRF), X-ray diffraction (XRD), Scanning Electron Microscopy / Energy Dispersive X-ray System (SEM/EDX) and X-ray Absorption Fine Structure (XAFS). It was shown that faïences are a unique kind of glazed ceramics and differences between the productions from Coimbra and Lisbon arose. Faïences have thinner glazes (max. 180  $\mu\text{m}$ ) than wall-tiles (max. 400  $\mu\text{m}$ ). Key elements are: Co for blue, Mn for purple, Cu for green, Sb for yellow, Pb for glaze. Elemental and morphological features have shown that Sn is mixed in the blue to lighten the final hue and Co-structures are in a Fe-rich environment in faïences and in a Ni-rich environment in wall-tiles.

Regarding the yellows, the hexagonal shape found for wall-tiles from Lisbon indicates that a higher temperature was used ( $\geq 1100$  °C), in comparison to the samples from Coimbra (faïences and wall-tiles), which shape is irregular and triangular-like (from 950 °C). Furthermore, the compound used for yellow pigments is different between Coimbra and Lisbon.

**Keywords:** Coimbra faïences; Wall-tiles; Multianalytical investigation; Compositional characterization; Differences in manufacturing techniques.

## CHAPTER 1 – INTRODUCTION TO GLAZED CERAMICS

Pottery-wares are magnificent and complex objects carrying intrinsic historical, cultural and traditional values. Their high resistance to weathering mechanisms allows us to infer about past traditions through direct and indirect evidences on manufacturing techniques, raw materials and decoration employed, characteristic of a culture, region or country.

Features like the chemical composition (dependent on the raw materials and recipes used) and the firing stages applied, will dictate the type, or class of object. Nowadays there is huge variety of ceramics, including the traditional pottery for domestic use and decorative ware, porcelains, sanitary, bricks and tiles. Moreover, modern ceramic materials are used for example as thermal insulators, with high thermal and mechanical resistance, for medical proteases and even for computer memory devices.

Based on the properties of the processed products, traditional ceramics can be divided into two groups: porous (or permeable) and non-porous (or impermeable). The former are characterized by their ability of absorbing water and the latter by having practically no porosity, resulting in new crystalline phases during the firing process, at high temperature. Examples of porous bodies are faiences and refractory clays (with a melting point of  $> 1600$  °C) while non-porous bodies are typical in porcelain [1].

Ceramic objects can be classified according to body's porosity and firing range as resumed in Table 1.1 [2]. Based on this taxonomy all objects under consideration in this work are earthenware.

**Table 1.1** – General taxonomy of the ceramic bodies [2].

<b>Body</b>	<b>Porosity</b>	<b>Firing Range</b>
Terracotta	High: $\geq 10\%$	$< 1000$ °C
Earthenware	3% - 10%	900 – 1200 °C
Stoneware	0.5% - 3%	1200 – 1350 °C
Porcelain	0% - 1%	1300 – 1450 °C

Another feature that has been used to define the type of ceramic objects is surface treatment. Depending on it other object designations became known and accepted as definition for the pieces. Surface treatments have appeared to embellish the ceramic body and to reduce the permeability to fluids. They can cover the ceramic body partially or entirely, applied before or after firing [2]. The most common surface treatments are slips and glazes. Glazes are vitreous substances, having in its constitution a mixture of materials, which then are applied onto fired ceramic bodies (bisque) and submitted to a firing procedure, at high temperature. This was a great breakthrough in the history of ceramics manufacture, as it forms an impermeable, shiny, smooth layer, which is ideal for surface decoration application.

The origin of glazes production dates back to around 2000 B.C. in Mesopotamia. The development of glazes are interesting to observe and well documented by Gustav Weiss [3]. The glaze technology has evolved and improved. Until 550 A.D. glazes were of the alkali-lime-silica type, with similar composition to the contemporary glass, as the study on several glazed pottery from this period shows, reported by M. S. Tite [4]. Such studies have proven that there were no changes in the chemical composition of the glazes for a 2000-year period, and the glass and glaze content at this time was very similar, suggesting that glass ground to a powder (frit) and applied onto the bisque was used as glaze. The next important step on this path was the introduction of lead (Pb) into glazes' composition, with values between 45-60% (high-lead glazes), in the oxide form, during the I century B.C in Anatolia.

The introduction of Pb as one of the major components in the glaze has brought advantages like easier application due to its inherent insolubility, reduced possibility of cracking due to its low thermal expansion ( $0.106 \times 10^{-6}/^{\circ}\text{C}$ ) and it offers a higher optical brilliance.

A milestone in glaze's history was the introduction of tin (Sn) to their composition, around the IX century A.D. in Iraq, to imitate the white porcelain from China. Due to its high refractive index, small particle size and surface irregularity, tin oxide is an excellent opacifier. Later on, tin-opacified glazes started being produced in Egypt between the X – XI centuries A.D. At this time the glazes were lead-alkali type, with lead oxide concentrations ranging 25-30% and 5-10% alkali [4]. From this point on, this glaze technology spread through the Islamic world in North African and south European countries covering a big part of the Iberian Peninsula (Portugal and

Spain). To Italy it reached via the island Mallorca, and, therefore, the Italian named *Maiolica* (or *Majolica*) to the type of glazed ceramics based on the tin-opacifying technology. The spreading to other European countries such as France was from Faenza (in the north of Italy) and the French named this type of objects *Faïence*. In principle, both names are valid to classify them.

This is an important point to turn to the objects under investigation in this work – Portuguese glazed ceramics.

### **1.1 Glazed ceramics in Portugal – historical context**

From art historian point of view, the Islamic influence (661-750 A.D.) on Portuguese glazed ceramics is well noticed particularly in the recipes for ceramic production. *Azulejos* (wall tiles) and faïences are two examples with this technical influence.

From all the glazed ceramics in Portugal, the most famous ones are *Azulejos* (from Arabic: *al zulayj*, meaning “polished stone”). These *Azulejos*, Portuguese wall tiles, characterized by their square shape and elaborated decorative motifs are used in many (old) buildings in Portugal. The decorative motifs evolved between the Gothic and the Renaissance styles. Although these wall-tiles are also found in other countries like, Spain, Italy, Netherlands, Turkey, Morocco and Iran, they have assumed a special charisma in Portugal due to: i) their longevity in use (five centuries with no interruption); ii) its application mode, as element that supports the architecture, covering entire inner- and outer-walls; iii) the way it has been understood, not just as decorative art but also as support for taste renovation and as creativity proof [5]. A brief chronology of the development of *Azulejos* in Portugal is given in annex 1.1 [6].

In figure 1.1, a set of examples of the different uses for *Azulejos* in Portugal is shown.



**Figure 1.1** – Examples of the use of *Azulejos* in Portugal: a) “Armillary Sphere” motif at the *Carranca* courtyard in *Sintra* Palace [7]; b) pattern style at the main Church in *Argoncilhe (Aveiro)* [7]; c) Rococo style at the garden in *Queluz* palace [7]; d) Baroque style at the *Congregados* church in Porto (A. Guilherme, 2010); e) Publicity panel and street name in *Abrantes* [7]; f) Publicity panel in *Bom Jesus (Braga)* (A. Guilherme, 2010).

Given the development of *Azulejos* in Portugal, an important stage was in the mid XVI century, where a change of artistic taste in this matter was experienced. The embossed work in *Azulejos* became “old-fashioned” and a new wave of manufacturing appears. Pieces with flat, fine glazed surfaces (*faiences*) turned to be the “modern” style of glazed ceramics. This is the time where the first *Azulejos* with painted decoration (by Portuguese artists) appeared [6].

Other types of objects hereby investigated are utility *faiences* for domestic use, such as plates, vases, bowls, etc. Regarding *faiences*, Portugal has a big variety of factories (or potteries) and based on documental (non-scientific) proofs, the possibility that the different manufacturing centers adopted slightly different techniques has emerged [8]. One of the most

intriguing production centers is Coimbra. However, the lack of (scientific) data has raised mislabeling questions, which will be better explained in the next sections. Moreover, this investigation serves as a contribution to the missing scientific information. Just by 2007, a complete documental (and partially scientific) compilation about the Coimbra glazed ceramic production was published (in Portuguese) [9], but a good overview (in English) of the importance of faiences in Portugal is given in [10].

Still regarding the book of Pais et al. [9] one can find a detailed insight about the chronology related to faience production within Coimbra district. A whole list of potters and families protagonist of this type production is given, as well as stylist changes that have taken place between the XVI and XIX centuries. One of the most interesting facts is the lack of production indicatives before the ceramic factories appeared in this region. This is a strong hint that until that time, the ceramic objects were produced by craftsmen, mainly illiterate, who were not even aware of the craft and at that time the value of their productions was inexistent. Due to all of these difficulties, and as a first step for investigation, excavations at the places connected to “ancient” pottery workshops were executed, namely at the *Convento de Santa Clara-a-Velha* and at the *Museu Machado de Castro (MMC)*. The retrieved fragments there represent a concrete set of “ancient” samples. The term “ancient” is here connected to the fact that they are in the context of the earliest known Portuguese faience pieces (and therefore the oldest) produced in Portugal.

A brief chronology of art historical development regarding faiences from Coimbra is given in annex 1.2 [9]. From this description the main features characteristic of the faiences from Coimbra are: glazes more mate than the ones from Lisbon (for example); the use of earthy mate tones in which yellows tend to orange and blues tend to violet; the dark purple contours; embossed decorative motifs, which together with their lack of brightness suggest a third firing stage; and as a final remark the less use of oriental motifs, as it is known for the pieces from Lisbon [8, 9].

Another interesting fact is the strong influence of Spanish and Italian tin-glazes earthenwares in Portugal, especially from the quantity of faience produced in the XVII century. The most characteristic pieces from this period are decorated based on the exported Chinese

porcelain style. In fact, the Portuguese were the first Europeans to manufacture imitations of Chinese export porcelain in faience, preceding the Dutch with their 'Kraak' porcelain [10].

Citing the Portuguese ceramist, *Joaquim de Vasconcelos*, on faiences from Coimbra: "The only one in Portugal representing the oriental tradition and preserving characteristics from the Islamic style". The colored motifs (...) produce a unique effect at ones sight, gives to this ceramics an archaic aspect, which is impossible to confuse it with any other region" [9]. Figure 1.2 shows some examples of utility faience objects produced in Coimbra.



**Figure 1.2** – Examples of faiences from Coimbra: a) Tray from mid XVII century, 6 x Ø 27 cm (present location: *Museu Municipal de Viana do Castelo – MMVC* – in Viana do Castelo); b) Plate from late XVII century, 5.3 x Ø 33.6 cm (present location: *Museu Nacional de Arte Antiga – MNAA* – in Lisbon); c) Plate 1<sup>st</sup> half of XVIII century, 6.2 x Ø 39 cm (present location: *MMVC* – in Viana do Castelo); d) Plate from late XVIII century, 4.8 x Ø 27.4 cm (present location: *MMVC* – in Viana do Castelo); e) Bottle from late XVIII

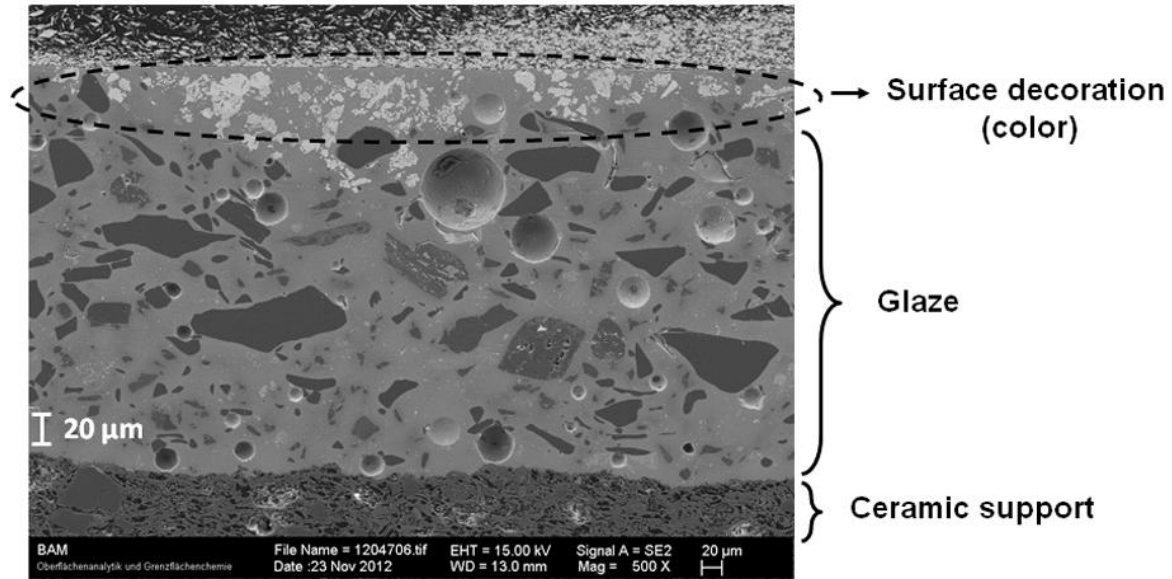


century, 25.2 x Ø 16 cm (present location: *Museu Nacional Machado de Castro – MNMC* – in Coimbra; f) Wall deposit from late XVIII century, 36.8 x 24 cm (present location: *MNAA* – in Lisbon) [9] (all photos by A. Guilherme, 2008).

## **1.2 Description of the analyzed samples – origin and features**

The sample set chosen for this investigation comprises two ceramic production centers: Coimbra and Lisbon. All samples belong to the class of Majolica (or faience) and two types are included: *Azulejos* (from Coimbra and Lisbon) and utility faiences (from Coimbra). All belong to the time period of XVI-XVIII centuries. The assignation to the manufacturing centre is based on the stylistic features that the pieces exhibit, according to documental proofs. Some of the pieces, at least the most erudite ones, have even potter trade-marks, which makes it easier to compare the artistic styles and assign the samples to Coimbra or to Lisbon.

The *Azulejo* samples (produced in Coimbra and Lisbon) were provided by the *Museu Nacional do Azulejo – MNAz* (Wall-tile National Museum in Lisbon), while the collection of utility faience samples (produced in Coimbra) were retrieved from the *Mosteiro de Santa Clara-a-Velha* (Santa Clara-a-Velha Monastery) in Coimbra. A list of the analyzed samples, describing their origin, estimated date of production and features observed by naked-eye, is presented in annex 1.3. In technical terms all of these pieces are characterized by three main parts: i) ceramic support (body); ii) glaze; iii) surface decoration, as indicated in figure 1.3. The micrograph of the cross-section was taken with a Scanning Electron Microscope (SEM) at the Federal Institute for Materials Research and Testing (BAM – *Bundesanstalt für Materialforschung und –prüfung*, Berlin, Germany – division 6.8: Surface Analysis and Interfacial Chemistry) (*cf.* chapter 3, section 3.3).



**Figure 1.3** – Scanning Electron Microscopy micrograph of a ceramic sample in cross-section taken at BAM (division 6.8 – Surface Analysis and Interfacial Chemistry). The three main parts characteristic of all samples are observable: surface decoration, glaze and ceramic support.

### 1.2.1 Ceramic support / body

The ceramic support is characterized mainly by clay minerals, Silicon (Si) and Aluminum (Al) oxides (with particle size  $\leq 2 \mu\text{m}$  in diameter) and non-plastic inclusions (temper). Clay minerals confer plasticity, which is necessary for molding the material [2]. These are basically alumina-silicate hydrated minerals ( $\text{Al}_2\text{O}_3 \cdot \text{SiO}_2 \cdot \text{H}_2\text{O}$ ) with lower quantities of other oxides, such as  $\text{TiO}_2$ ,  $\text{Fe}_2\text{O}_3$ ,  $\text{MgO}$ ,  $\text{CaO}$ ,  $\text{Na}_2\text{O}$  and  $\text{K}_2\text{O}$ . Silica ( $\text{SiO}_2$ ) has a structural role in the body and it is the refractory component, as it has a very high melting point (1600 – 1725 °C). The temper inclusions can be natural impurities within the clay minerals or added by the potter in order to change the properties of the ceramic material so that it could be easier to shape it and become more consistent [11].

The elements (or compounds) that hold a more informative character are the ones which are formed from igneous rocks and this is strongly dependent on the geology of the region [12]. Important minerals for the formation of igneous rocks are feldspars, quartz, olivines, pyroxenes, amphiboles and micas.

Feldspars are alumina-silicates ( $\text{SiO}_2$  and  $\text{Al}_2\text{O}_3$ ) and constitute 39% of the earth's crust. Potassium (K), sodium (Na) and calcium (Ca) are other elements which are present in feldspars as well. They are responsible for the division between potash or alkali feldspars (with K: orthoclase and microcline) and soda-lime feldspars (different relative quantities of Na and Ca: Albite, Oligoclase, Andesine, Labradorite, Bytownite and Anorthite) namely plagioclases. During the process of weathering, all the minerals in igneous rocks form clays, and different kinds of decomposition procedures form different clays [2]. There are still other elements (so-called "accessory" elements) that can either positively or negatively alter the properties of the paste, such as metallic sulphides, carbonates, sulphates, other salts and organic matter [13].

Apart from the chemical interactions within the water/clay system, physical and chemical characteristics are altered when the paste is submitted to a firing process. These alterations are function of three variables: firing cycle, temperature and atmosphere [2]. The atmosphere refers to the gases that are present while the paste is being heated and cooled down. If the whole process is taken place under a free air circulation and oxygen to bind with the elements, the atmosphere is said oxidizing; while if oxygen is lacking, the atmosphere is said reducing. This is important since the atmosphere during the firing affects the final product in terms of color, hardness, porosity and shrinkage [2, 13].

Regarding some of the most common components of the body, the first phenomenon under the first heat action (below  $300^\circ\text{C}$ ) is the loss of water which was not expelled during the drying process. The second important stage, between  $300 - 600^\circ\text{C}$ , is the dehidroxilation, which means that, at the end of this stage, the loss of plasticity is irreversible. Organic components start oxidizing at  $200 - 300^\circ\text{C}$ , which increases exponentially at temperatures around  $600 - 800^\circ\text{C}$  and together with the water elimination there is an increase in porosity that allows an intake of air into the piece. At  $573^\circ\text{C}$  there happens the so-called "quartz inversion". From  $800^\circ\text{C}$  the pores start closing and the material starts contracting. Between  $800 - 950^\circ\text{C}$  the decomposition of calcium and magnesium carbonates takes place and from  $900^\circ\text{C}$  vitrification phenomena starts occurring, which confers resistance to the material. So, in clayey materials the mechanical resistance is owed to the formation of glassy phases, mainly due to the fuser materials within the paste [1, 13-15].

All these transformations occur with the variation of temperature (or volume), which allows to infer about these phenomena, for example using X-ray Diffraction (XRD) (cf. chapter 3, section 3.2). In the case of faïences the firing temperature used for the ceramic body goes up to 950 – 1200 °C. The bisque (after firing) has a dim and opaque appearance, with low deformation, owed to the lower content in fuser elements. Faïence ceramic bodies have a higher mechanical resistance in comparison to the ball-clay ones. They have also an early vitrification phase, which makes it more difficult to have a good fit between body and glaze.

### 1.2.2 Glaze

Glazes are composed by three main categories of components: i) network formers, ii) network modifiers (fluxes) and iii) intermediates. Every one of these components is important for the properties of the final product.

The network formers, as the name itself suggests, create the structure and this is achieved by silica ( $\text{SiO}_2$ ). The network modifiers (fluxes) are oxides that are introduced in the tetrahedral structure of silica. These oxides have longer ionic radii than the ones of silica, which weakens the network connections, lowering the melting point of the system. The most common fluxes are  $\text{Na}_2\text{O}$ ,  $\text{K}_2\text{O}$ ,  $\text{PbO}$ ,  $\text{CaO}$  and  $\text{MgO}$ . The intermediates are oxides that substitute part of silica and have one or both of the functions:

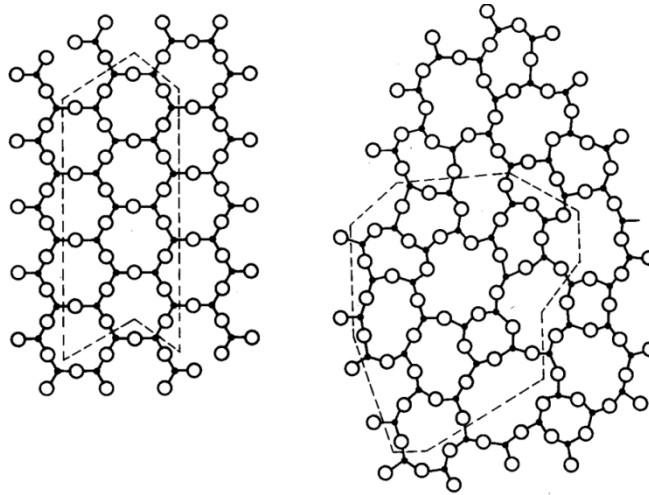
- Increase the glaze viscosity, which was lost by the introduction of fluxes;
- Strengthen the glaze during the firing process, avoiding fissures.

Common intermediates are  $\text{Al}_2\text{O}_3$ ,  $\text{PbO}$ ,  $\text{ZnO}$ ,  $\text{ZrO}_2$  and  $\text{CdO}$ . There is also a fourth category, the opacifiers, which make the glaze more opaque. As it was mentioned previously tin (Sn) is one of the best opacifiers and it is commonly found in the composition of *Maiolica* objects. The introduction of such components promotes the application of surface decoration onto the glazed pieces.

During the firing process these components react with each other and fuse to form the glaze layer. It can be fired simultaneously with the body (mono-firing) or fired after applied onto the bisque (bi-firing). In the case of the samples hereby studied, all glazes were applied onto the fired ceramic support and fired in an own stage. The surface decoration could have been

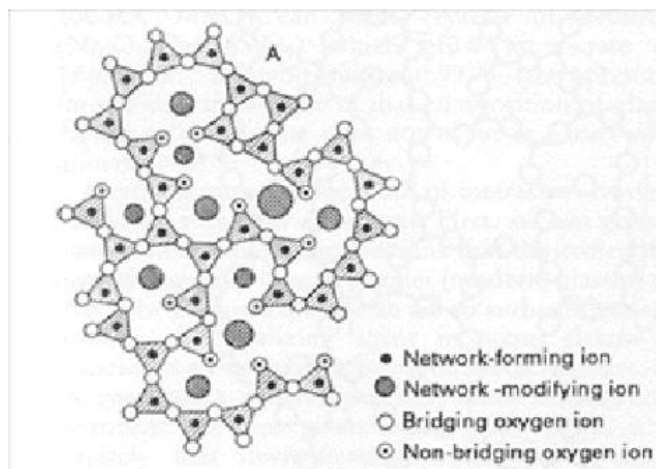
applied together with the base glaze onto the bisque or applied onto the glazed piece submitted to own firing stage, where the whole piece undergoes a third firing procedure. This is still an open question.

The glazes used for ceramics are a kind of glass, which is a non-crystalline substance cooled rapidly. Glazes are viscous coatings that are fused at high temperatures over a ceramic body and during the cooling process they solidify without the formation of a crystalline structure and retain some characteristics of a liquid. In fact glazes represent a mixture between amorphous and crystalline phases [2, 16] (figure 1.4).



**Figure 1.4** – Illustration of a crystalline material with theoretical composition of  $A_2O_3$  (left) and amorphous arrangement of  $A_2O_3$  (right) if the material is cooled down rapidly. The dashed lines surround 24 black dots and 36 open circles, representing the same chemical composition in both figures. The amorphous structure occupies a larger volume in comparison to the crystalline one [16].

Figure 1.5 shows what happens to a material with the insertion of network modifiers.



**Figure 1.5** – Insertion of network modifiers cations (larger grey filled circles) in the glass structure [17].

Glazes are normally applied in an aqueous suspension form either by submersion, or with a brush. After the water is absorbed through the pores of the body a sort of dusty layer remains on the surface [16, 17]. Once fired at sufficiently high temperature this layer forms an impermeable, more or less shiny glassy surface. During the firing process several phenomena occur, such as the decomposition of the raw materials (which were not fritted before) by the release of carbon dioxide ( $\text{CO}_2$ ) from the carbonates; dissolution of some compounds and separation of non-mixable phases. During the cooling process some substances crystallize and the glaze hardens.

The properties of glazes depend, of course, on the chemical composition. The higher the amount of silica the harder the glaze is but it needs a higher firing temperature. The oxides that act as fluxes have a stronger effect the shorter the cation is. Level of fusibility or fusing power varies using different alkaline oxides in the following order:



Yet, the presence of these oxides can be harmful since it diminishes the mechanical and chemical resistance of glazes and increase the thermal expansion coefficient<sup>2</sup>. Here the introduction of the so-called “network stabilizers” is necessary.

Taking all of these issues into account, glazes should have the following properties:

- Moderate viscosity, to avoid differences in thicknesses especially in irregular surfaces;
- The reaction between ceramic paste and glaze should be moderate in order to minimize the compounds exchange.
- The relationship between expansion coefficient and elasticity module (Young)<sup>3</sup> of the glaze should be towards a maximal resistance.
- It should be chemically stable, homogeneous, and abrasion resistant.

After applying the glaze either by submersion, or with a brush, onto the ceramic body, the piece is fired.

### **1.2.3 Surface decoration**

From all the analyzed samples, and from documental proofs [9], the base colors used for the surface decoration in Portuguese glazed ceramics are: blue, dark purple, yellow (and brown) and green – in rare cases. Different mixtures and concentrations (pigment to volume ratio) of the raw materials for the pigments result in different hues. For example different hues of blue and yellow were found among the sample set. Based on the colors used, the palette of inorganic pigments is broad as it is described in table 1.2.

---

<sup>2</sup> Thermal expansion coefficient: Thermal expansion is the tendency of matter to change in volume in response to a change in temperature. The degree of expansion divided by the change in temperature is called the material's coefficient of thermal expansion.

<sup>3</sup> Young's module: For the description of the elastic properties of objects, which are either stretched or compressed, a convenient parameter is the ratio of the stress to the strain, a parameter called the Young's modulus of the material.

**Table 1.2** – Inorganic pigments with their chemical formula as well as key-elements.

Color	Pigment name	Chemical formula	Key-element(s)
Blue	Azurite	$2\text{CuCO}_3 \cdot \text{Cu}(\text{OH})_2$	Cu
	Cerulean blue	$\text{CoO} \cdot \text{SnO}_2$	Co, Sn
	Cobalt blue	$\text{CoO} \cdot \text{Al}_2\text{O}_3$	Al, Co
	Cobalt violet	$\text{Co}_3(\text{PO}_4)_2$	Co
	Egyptian blue	$\text{CaO} \cdot \text{CuO} \cdot 4\text{SiO}_2$	Si, Ca, Cu
	Manganese blue	$\text{BaSO}_4 \cdot \text{Ba}_3(\text{MnO}_4)_2$	Mn, Ba
	Prussian blue	$\text{Fe}_4[\text{Fe}(\text{CN})_6]_3$	Fe
	<b>Smalt Co-glass</b>	<b><math>(\text{K}_2\text{O}, \text{SiO}_2, \text{CoO})</math></b>	<b>Si, K, Co</b>
	Ultramarine	$\text{Na}_{8-10}\text{Al}_6\text{Si}_6\text{O}_{24}\text{S}_{2-4}$	Na, Al, Si, S
Yellow	Auripigment	$\text{As}_2\text{S}_3$	As
	Cadmium yellow	$\text{CdS}$	Cd
	Chrome yellow	$2\text{PbSO}_4 \cdot \text{PbCrO}_4$	Cr
	Cobalt yellow	$\text{K}_3[\text{Co}(\text{NO}_2)_6] \cdot 1.5\text{H}_2\text{O}$	K, Co
	Lead-tin yellow	$\text{Pb}_2\text{SnO}_4 / \text{PbSn}_{12}\text{Si}_x\text{O}_7$	Sn
	Massicot	$\text{PbO}$	Pb
	<b>Naples yellow</b>	<b><math>\text{Pb}(\text{SbO}_3)_2 / \text{Pb}_3(\text{SbO}_4)_2</math></b>	<b>Sb, Pb</b>
	Strontium yellow	$\text{SrCrO}_4$	Cr, Sr
	Titanium yellow	$\text{NiO} \cdot \text{Sb}_2\text{O}_3 \cdot 20\text{TiO}_2$	Ti, Ni, Sb
Yellow ochre	$\text{Fe}_2\text{O}_3 \cdot n\text{H}_2\text{O}$ (20–70%)	Fe	
Zinc yellow	$\text{K}_2\text{O} \cdot 4\text{ZnO} \cdot 4\text{CrO}_3 \cdot 3\text{H}_2\text{O}$	Cr, Zn	
Green	Basic copper sulphate	$\text{Cu}_x(\text{SO}_4)_y(\text{OH})_z$	Cu
	Chromium oxide	$\text{Cr}_2\text{O}_3$	Cr
	Chrysocolla	$\text{CuSiO}_3 \cdot n\text{H}_2\text{O}$	Cu
	Cobalt green	$\text{CoO} \cdot 5\text{ZnO}$	Co, Zn
	Emerald green	$\text{Cu}(\text{CH}_3\text{COO})_2 \cdot 3\text{Cu}(\text{AsO}_2)_2$	Cu, As
	Guignet green	$\text{Cr}_2\text{O}_3 \cdot n\text{H}_2\text{O} + \text{H}_3\text{BO}_3$	Cr
	Malachite	$\text{CuCO}_3 \cdot \text{Cu}(\text{OH})_2$	Cu
	Verdigris	$\text{Cu}(\text{CH}_3\text{COO})_2 \cdot n\text{Cu}(\text{OH})_2$	Cu
Black; purple	Black iron oxide	$\text{FeO} \cdot \text{Fe}_2\text{O}_3$	Fe
	Cobalt black	$\text{CoO}$	Co
	Ivory black	$\text{C} + \text{Ca}_3(\text{PO}_4)_2$	P, Ca
	<b>Manganese oxide</b>	<b><math>\text{MnO} + \text{Mn}_2\text{O}_3</math></b>	<b>Mn</b>

During the XVIII century it was common that each workshop prepares its own colors and hues and kept it as a secret [9]. This is a challenge for such investigations, as there is a need for finding adequate strategies for reconstructing manufacturing procedures used.



From table 1.2 one can see that at a first approach, having elemental information only can be difficult in assigning the pigment that has been used. Nonetheless, given the time of manufacture and resources available, some hints can be given about the pigments used for surface decoration. For example, the source for the blue may have been Smalt, for the yellow the Naples Yellow and for the purple the Manganese oxide [9], as highlighted in table 1.2. However, the mixture of pigments to obtain the desired hues can be dependent on the production center and the special case of the Naples Yellow seems to require a deeper understanding on the type which was used [18, 19].

Naples yellow is a synthetically generated pigment produced by initial raw materials, which could have been sulphides, oxides or metals. Dik et al. [20] investigated whether the yellow pigment was produced from sulphides, oxides or metals. Three mixtures of Naples Yellow were calcinated<sup>4</sup> at 900 °C: (1) minium ( $Pb_3O_4$ ) + Stibnite ( $Sb_2S_3$ ); (2)  $Pb_3O_4 + Sb_2O_3$ ; and (3) Pb metallic + Sb metallic. The tests showed advantage of the oxides mixture (2) over the other two, as it produced almost pure lead antimonate yellow.

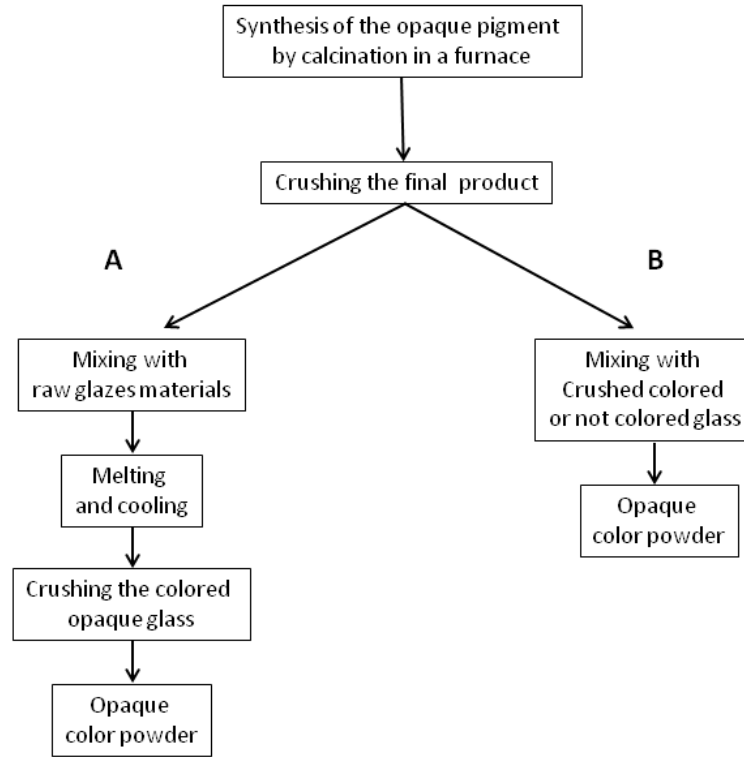
The work of Maggetti et al. [19] resumes the topology of four yellow mixtures used in glass manufacturers as well as in paintings, based on previous investigations on each one. These mixtures are: (1) cubic lead antimonate yellow (mineral: *bindheimite*),  $Pb_2Sb_2O_7$ ; (2) orthorhombic lead-tin yellow I,  $Pb_2SnO_4$ ; (3) cubic lead-tin yellow II,  $PbSn_{1-x}Si_xO_3$ ; and (4) cubic lead-tin antimonate yellow (a Pb-Sn-Sb solid solution),  $Pb_2Sb_{2-x}Sn_xO_{6.5}$ . In most ceramic glazes, lead antimonate is commonly found as coloring and opacifying agent [21, 22]. However, hints about the recipes used for this pigment production can be analytically identified by tracing the presence of other elements such as Al, Si, Fe or Zn. One way of predicting which of the four yellow mixtures was used is by the Sb/Pb weight ratio. If no other minor compounds are present in the yellow crystal structure, a stoichiometric composition of 58 wt% PbO and 42 wt%  $Sb_2O_5$  is expected, if  $Pb_2Sb_2O_7$  was used as yellow pigment. This corresponds to a PbO/ $Sb_2O_5$  ratio of 1.38 [19]. Further important informations are related to pigment thermal stability. Yellow mixtures (2) and (3) are thermally stable only up to 900 – 950 °C firing temperature

---

<sup>4</sup> Calcination: a thermal treatment process in which the compounds are heated below their fusing point, causing decomposition of carbonates, among others.

while mixtures (1) and (4) are thermally stable up to 1100 °C. The latter two would easily withstand temperatures of a second firing process (950 – 1050 °C) [19].

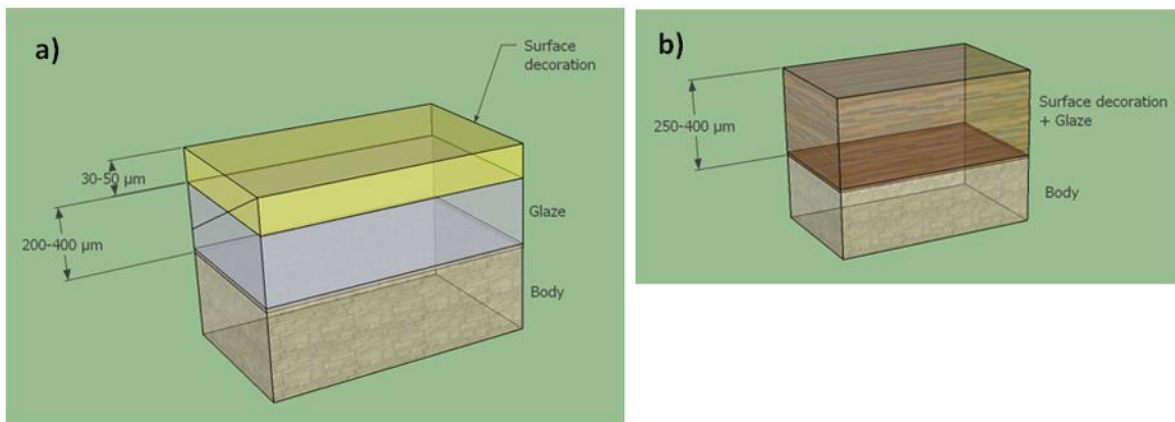
Another important factor that serves as a manufacturing production hint is the way the pigment was obtained. Such opaque glazed ceramic pigments could have been produced in two different ways according to Maggetti et al. [19], as shown in figure 1.6.



**Figure 1.6** – Production steps of opaque glazed ceramic colors [19]

Differences at the microscopic level are expected whether method A or B is chosen. In method A the pigments were subjected to high temperatures for an extended period and dissolution phenomena should have taken place; hence, more spherical or rounded-edge pigments grains are expected. In method B the pigments were fixed into the glassy matrix in the high temperature firing only – which implies that the pigment has less time left to react with glassy matrix; and the original pigment grain shape is preserved [19].

At this point one expects to have two main possible configurations regarding the base-glaze/color system. In figure 1.7 a schematic representation of both is shown.



**Figure 1.7** – Schematic representation of the two possible stratigraphic arrangements: a) three distinct layers (body, base glaze and color) or b) two layers (body and glaze+color).

For the particular case of opacified-colors, they were probably prepared as a frit (*cf.* figure 1.6) and therefore submitted to a third firing stage, which could lead to the situation in figure 1.7a. Conversely, pigment and base-glaze were submitted to the same firing stage (second), which would lead to the case in figure 1.7b.

## **CHAPTER 2 – OBJECTIVES OF THE WORK**

This work deals with polychrome glazed ceramics originally produced in the two main Portuguese manufacturing centers (Coimbra and Lisbon) between the XVI and XVIII centuries. With the premise of overcome mislabeling of objects that are not properly identified – either by potters marks or clear manufacturing tracers with unambiguous assignation – this investigation addresses to gain knowledge concerning manufacturing technological aspects by a multianalytical (non-destructive) approach. Literature survey shows a gap in scientific investigations concerning faiences produced in Coimbra, therefore a special output of this research work is to serve as a contribution – if not a basis – for the classification of “Faience from Coimbra”.

An important aspect is the choice of various analytical methods for the sought answers. For this purpose it is crucial to understand the advantages and limitations of each analytical method in order to extract results and conclusions as accurate as possible. This is briefed in the last section of this chapter.

### **2.1 The necessity for investigation**

According to the Portuguese history and traditions, glazed ceramics hold great artistic value based on the descriptions above and many more. This type of art has represented not only beauty to one’s eye but also a symbol of the influence from other nations as it has changed through times. Moreover, it has been a symbol of wealth for some and due to the importance in developing new manufacturing processes it has become a symbol of secrecy between different production centers. Taking this into account, information about the manufacturing processes is missing and from this point of view this investigation is important in order to fill the existing gaps.

Another issue is related to ceramic production in Coimbra, in particular. As it has been stated [9], there was always a difference between the two main ceramic production centers (Lisbon and Coimbra), at least in stylistic terms. In addition, Lisbon being the capital city, the monetary resources for such industry were larger and Coimbra has been known as a less wealthy

production center. Therefore, it has been thought that the expensive raw materials were spared as much as possible, which would imply a much broader range of materials in order to produce a single color or hue. One example is given by the blue pigments, in which the source of cobalt; smalt (a ground blue containing Cobalt), is the main and the most expensive mineral. In the samples from Coimbra, additional elements can be found, such as manganese (Mn) to spare the cobalt source.

An additional point is the fact that there are many pieces found with no labeling, which facilitates the erroneous assignation to a production center. Hence, the intrinsic value of a piece is put at stake, as based on historical and art historical facts “only” several opinions have been developed about e.g. the use of raw materials and manufacturing processes.

Regarding all the information above, it is of primary importance to have samples with unequivocal origin (pottery labels) to serve as a reference group for the whole investigation. This way one can validate a group and find similarities or dissimilarities between the samples from different production centers. This work is pioneer in terms of scientific criteria for such valuable pieces, improving the knowledge about Portuguese Cultural Heritage.

## **2.2 Analytical requirements**

The field of natural sciences applied to Cultural Heritage objects (also known as Archaeometry) has grown tremendously in the past decades, indicated by the big number of publications available. Concerning ceramic studies only, some examples can be found [21, 23-39].

The fact that most of the times the object cannot be taken away from its place (museum, building, etc.), triggered the fast development of portable equipment – as it is the case of X-ray Fluorescence (XRF) setups. In comparison to stationary equipment, portable XRF setups comprise low power X-ray tubes and X-ray detectors with a technology without external cooling (*cf.* chapter 3). Another issue is the growing demand for smaller spot sizes of analysis in order to resolve details in the sub-millimeter range. Hence, for example, the development of micro-focus X-ray tubes together with optical X-ray elements is evident, enabling beam focusing down

to the micrometer scale. Nowadays, several optical systems providing analysis at these ranges are found (*cf.* chapter 3).

Yet, the information obtained by the methods that allow portable setups is most of the times not enough for conclusive investigations. Information at other levels is also required and in that case only stationary systems are possible so far due to technical constraints. In this case a compromise has to be found and minimal sampling can be performed. Regarding this matter, X-ray Absorption (XAS) techniques became also very popular among Cultural Heritage (CH) objects [23]. This specific method is optimal for samples with high heterogeneity, as it provides high-sensitive chemical information (atom specific) irrespective of the complexity of the system. However, for this purpose the use of a high-brilliant X-ray source is required, such as in a synchrotron. The drawback of using synchrotron radiation is that one requires a beamtime application and, if accepted, the allowed beamtime is rather limited – most of the times not enough to have sufficient results. The tendency nowadays is to try to produce such high brilliant sources on a laboratory scale, allowing an “uncomplicated” use. This is, for example, one of the goals of BLiX – Berlin Laboratories for innovative X-ray technologies (at the Technical University of Berlin). It is still in a development process, but for example XAS measurements are already feasible for certain types of samples – mainly biological (<http://www.blix.tu-berlin.de/>).

The objects hereby investigated have great compositional variability, so there is a need for a multi-analytical approach. The analytical methods chosen have to be able to provide information about the chemical (or compositional) nature of the different parts of these artefacts, in order to identify raw materials. It is important here to remark that this approach is used for the objectives of this research work, and although it can be part of a scientific approach for provenance purposes but it should not be exclusively consider for this purpose. Even if the samples under investigation are fragments, these are artistic and historical objects playing a significant role in the context of Portuguese Cultural Heritage. Therefore the analytical requirements can be numbered in the following way:

- Non-destructive: in terms of keeping the physical integrity of glaze and surface decoration; the ceramic body (when exposed) is quite thick and if sampling is required for this part it would not represent a problem;

- Sensitive: in terms of the sought analytical answers; each method does not have to provide “all” the information required but it should be sensitive to the specific need.

- Versatile: in order to obtain information at different scales using the same technique, which in this case would be from millimeter (mm) down to micrometer ( $\mu\text{m}$ ) scale, and if possible, being able to analyze objects with different sizes, shapes and surface morphology.

All spectroscopic methods used for studying CH material based on X-ray, ultraviolet (UV), visible (VIS) and infrared (IR) radiation tend to be non-destructive. In many of CH objects a detailed surface decoration is visible, so one should aim for analytical systems that provide enough lateral resolution ( $< 1 \text{ mm}^2$ ) [40]. Furthermore, these objects have somewhat a layered system (or better explained, an interface system) and this is with most of the techniques a challenge for investigation. Therefore, depth resolved methods would provide useful information in this case and cancel out information overlap obtained in the conventional way.

Taking the above into account (and also based on the expected variability in these samples), within the group of non-destructive techniques, methods providing elemental, compositional, mineralogical and textural information are also needed.

As a good practice, one should start with the method that provides a fast and broad range of elemental information. An example that fulfills quite well these requirements is X-ray Fluorescence (XRF) spectrometry (*cf.* chapter 3, section 3.1). It is a well-established method for innumerable applications and, although there is a vast number of publications using this technique, a recent work by Tsuji et al. [41] gives an excellent overview about such applications.

As a complement, techniques that provide mineralogical and textural information are required. For this purpose, X-ray Diffraction (XRD) and Scanning Electron Microscopy with an attached Energy Dispersive X-ray System (SEM/EDX) are suitable (*cf.* chapter 3, section 3.2 and 3.3). The latter will be especially useful for cross-section analyses that comprise body/glaze/color in order to evaluate the interaction between these interfaces. This provides hints about the glazing process. At last, one must consider that changes in the chemical environment of some compounds may occur, which are indicative for differences in the manufacturing processes. Therefore X-ray Absorption Fine Structure (XAFS), a method sensitive

to the chemical environment of a certain atom, was also chosen for this investigation (*cf.* chapter 3, section 3.4)



## CHAPTER 3 – METHODS OF ANALYSIS

Considering the objectives of this work, the chosen analytical methods were: X-ray Fluorescence (XRF), X-ray diffraction (XRD), Scanning Electron Microscopy / Energy Dispersive X-ray System (SEM/EDX) and X-ray Absorption Fine Structure (XAFS). Therefore, this chapter is divided into four sections, each one dedicated to each of the mentioned techniques, pointing out the physical concepts and analytical features – enhancing advantages and limitations for the present investigation. Furthermore, a description of the experimental setup used is also provided in each section.

### 3.1 X-ray Fluorescence Spectroscopy (XRF)

As previously explained, XRF has innumerable advantages for the investigation of CH-related objects. XRF has undergone huge advances in the last decades improving both excitation and detection conditions, as well as the environment in which the whole analysis take place. One of the most significant upgrading resulted by the advent of X-ray optics devices, allowing XRF analysis at the micrometer scale. Concerning CH-related objects this was a great improvement, as it resolves tiny details both lateral and in depth. Several textbooks cover the fundamentals of this method – in its variants – in detail [42, 43].

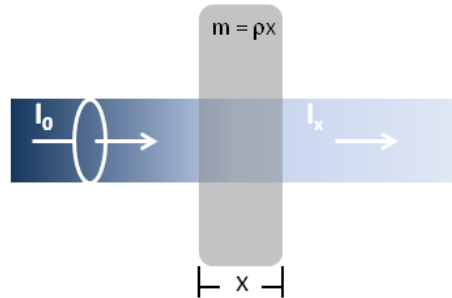
In the course of this work two variants of energy-dispersive XRF were used, conventional- and 3D Micro-XRF. Each of which will be covered in the second and third sub-sections, respectively.

#### 3.1.1 XRF principles

When interacting with matter and given their energy range ( $< 1$  MeV), X-rays undergo mainly absorption (photoelectric absorption) or scattering phenomena (Compton and Rayleigh), both of which will be described in the following sub-sections. Considering a parallel monochromatic X-ray beam of intensity  $I_0$  that impinges on a given homogeneous material (absorber), the transmitted beam – after passing through the absorber of thickness  $x$  – will have a reduced

intensity  $I_x$  due to absorption and scattering phenomena [44]. This attenuation process is described by the Lambert-Beer law according to:

$$I_x = I_0 \exp(-\mu_{lin}x) \quad (3.1)$$



**Figure 3.1** – Schematic representation of the attenuation of X-rays through a material (absorber).

where  $\mu_{lin}$  is the linear attenuation coefficient of the material for a specific wavelength. Knowing the density of the material,  $\rho$ , the mass of material in a unit section (white circle on figure 3.1) becomes  $m = \rho x$ . So, equation 3.2 can be re-written in the following way:

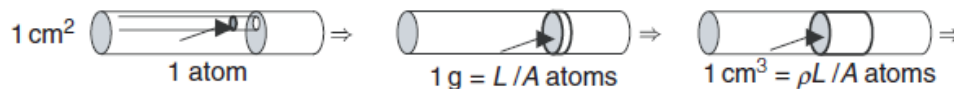
$$I_x = I_0 \exp \left[ -\left(\frac{\mu_{lin}}{\rho}\right)\rho x \right] \quad (3.2)$$

and for  $\mu = \mu_{lin}/\rho$ , equation 3.3 becomes:

$$I_x = I_0 \exp(-\mu m) \quad (3.3)$$

$\mu$  is the mass attenuation coefficient, as it refers to the mass of the material per unit section and it is expressed in  $\text{cm}^2 \cdot \text{g}^{-1}$  [44].

If one atom covers an area of  $\mu_{Atom}$  ( $\text{cm}^2$ ) within a beam of monochromatic photons with a cross-section of  $1 \text{ cm}^2$ , the practical unit is  $(10^{-24} \text{ cm}^2) = (\text{barns/atom})$  (figure 3.2).



**Figure 3.2** – Atomic cross-section, mass attenuation, linear attenuation [45].

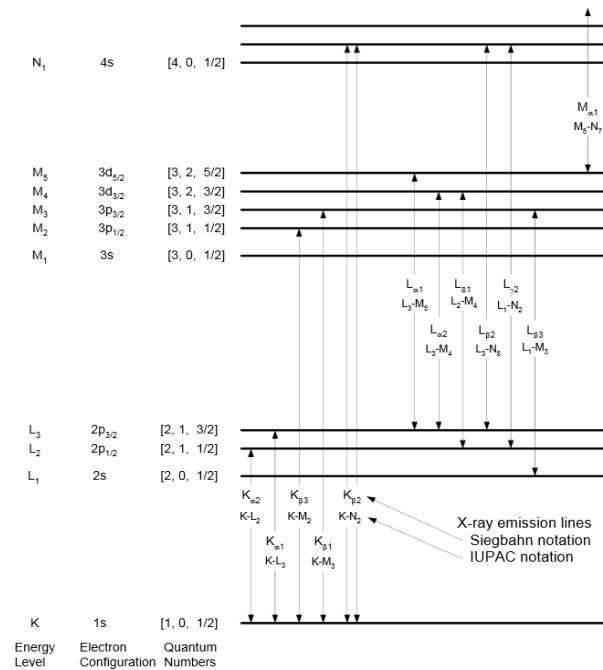
The total atomic cross-section comprises all three possible ways of interaction and is thereby an attenuation coefficient given by:

$$\mu_{Atom,total} = \tau_{Atom} + \sigma_{Atom,coh} + \sigma_{Atom,incoh} \quad (3.4)$$

Each of these terms will be described in the following sub-sections.

### 3.1.1.1 Photoelectric absorption

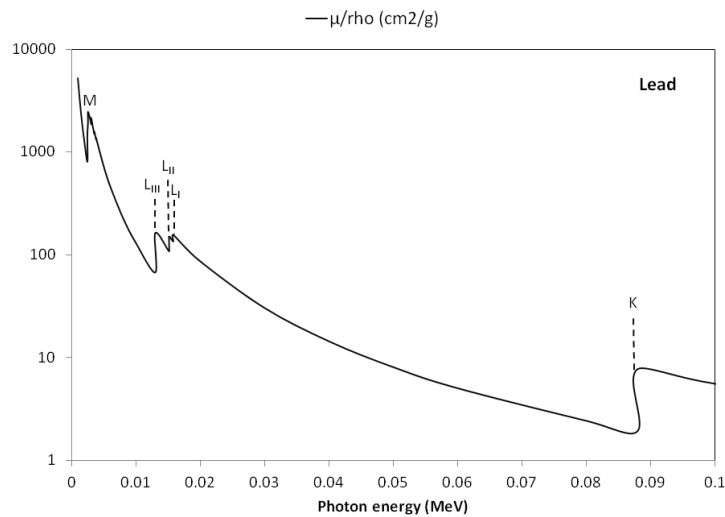
When X-rays of suitable energy impinge onto a sample, energy is transferred to core electrons and these can be ejected resulting in an excited atom with a vacancy in the inner orbital shell. The atom then reorganizes itself by successive vacancy-filling processes until it returns to its fundamental state. This means that a potential loss takes place and can be released by emission of fluorescent photons or by Auger transitions [42, 46]. The energy of each emitted photon equals the energy difference between the levels in which the transition has occurred. These fluorescent X-rays are characteristic for each transition in each atom (figure 3.3). The allowed transitions – according Hund’s rules – are organized in many tables according to their intensity. For example, the most intense characteristic line corresponds always to the transition between L3 – K (according the IUPAC notation), which is denoted as  $K\alpha_1$ , under the Siegbahn notation.



**Figure 3.3** – Schematics of the transitions between the atomic energy levels that give rise to the characteristic XRF lines. Both Siegbahn and IUPAC notations are displayed [47].

For the X-rays energy range considered (< 1 MeV), the photoelectric absorption coefficient accounts for at least 95% of the whole attenuation coefficient ( $\mu_{Atom, total}$ ) [44]. This means that

the experimental values of the attenuation coefficient reflect majorly the properties of the photoelectric coefficient. For a given element,  $\tau$  increases, i.e. the probability of a photon ejecting an electron from an atom increases with decreasing energy, within certain limits – which are characterized by sharp discontinuities that can be observed in any absorption curve [44]. An example is shown in figure 3.4 – photoelectric absorption coefficient of Pb.



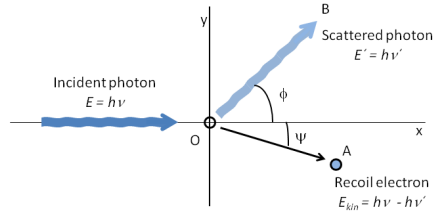
**Figure 3.4** – Photoelectric absorption coefficient of Pb as a function of photon energy [48].

### 3.1.1.2 Scattering

As previously mentioned, there are two types of scattering processes taking place in the photon-atom interaction: Compton (incoherent or inelastic) and Rayleigh (coherent or elastic) scattering. In the former energy and momentum are not conserved, which means that there is a change in energy and phase of the photon, while in the latter energy and momentum are conserved. The probability for Compton scattering increases for higher photon energies and lower atomic number ( $Z$ ) of the scattering atom, while the probability for Rayleigh scattering behaves exactly vice-versa.

#### Incoherent scattering

It results from the interaction between an incident photon ( $E = h\nu$ ) and a free electron – weakly bound to the atom (figure 3.5).



**Figure 3.5** – The Compton Effect.

An inelastic interaction takes place, which means that incident photon is deflected in the OB direction with lower energy ( $E'$ ) – at  $\phi < \pi$  - and the electron recoils in the OA direction – at  $\psi < \pi/2$ . This effect obeys to the laws of relativistic dynamics, so the principle of conservation of momentum implies that the wavelength change of the scattered photon is [44]:

$$\lambda' - \lambda = \frac{h}{m_0 c} (1 - \cos \phi) \quad (3.5)$$

with  $m_0$  being the mass of the electron at rest. Equation (3.5) is valid for all incident energies and any scattering atom. The pre-collision motion of the bound electron causes, due to the Doppler effect [49], a broadening of the Compton peak, compared with the fluorescence peaks, which can be and described by:

$$4\beta\lambda \sin\left(\frac{\theta}{2}\right) \quad (3.6)$$

with  $\beta = v/c$ .

### Coherent scattering

It is a process in which a photon interacts with a bound atomic electron without energy transfer. The scattered photon has the same energy as the incoming photon and only the direction is changed, leaving the atom neither ionized nor excited. The intensity of the radiation scattered by an atom is determined by summing the amplitudes of the radiation coherently scattered by each of the electrons bound in the atom. In Rayleigh scattering the coherence extends only over the Z electrons of individual atom and the interface is always constructive as long as the change over the diameter of the atom is less than one-half of a wavelength [42] :

$$\frac{4\pi}{\lambda} r_a \sin \frac{\theta}{2} < 1 \quad (3.7)$$

where  $r_a$  is the effective radius of the atom.

Rayleigh scattering is dominant at low energy incident photons and high-Z atoms.

### 3.1.2 Conventional XRF

In a simple form, in order to perform XRF analyses one needs an X-ray source and a suitable detector. Nowadays a big variety of XRF setups are found, according to the requirements for the investigations purposes. These setups can differ in the X-ray source, detector and some other devices used.

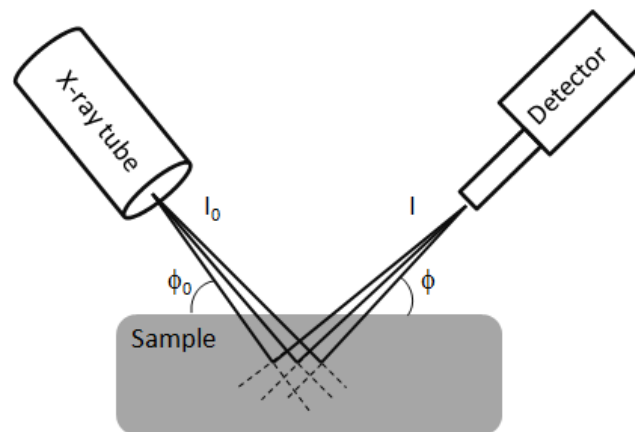
As previously explained, in addition to the emission of the characteristic radiation, several other X-ray interactions also occur. These interactions alter the overall appearance of the XRF spectrum, so it is vital to understand how these interactions occur when analyzing XRF spectra. Moreover, experimental artifacts mainly related to the detectors used for this purpose are visible in XRF spectra as well. Both qualitative and quantitative information can be withdrawn from performing XRF analysis. However, as no quantitative treatment was performed in this investigation by means of XRF, focus will be only given to the qualitative information.

XRF became possible due to the correlation between the energy of the fluorescence radiation  $E$  and the atomic number of the emitting element  $Z$ , proposed by Moseley, given as:

$$E = K (Z - \sigma)^2 \quad (3.8)$$

$Z$  and  $\sigma$  are constants related to the observed fluorescent line.

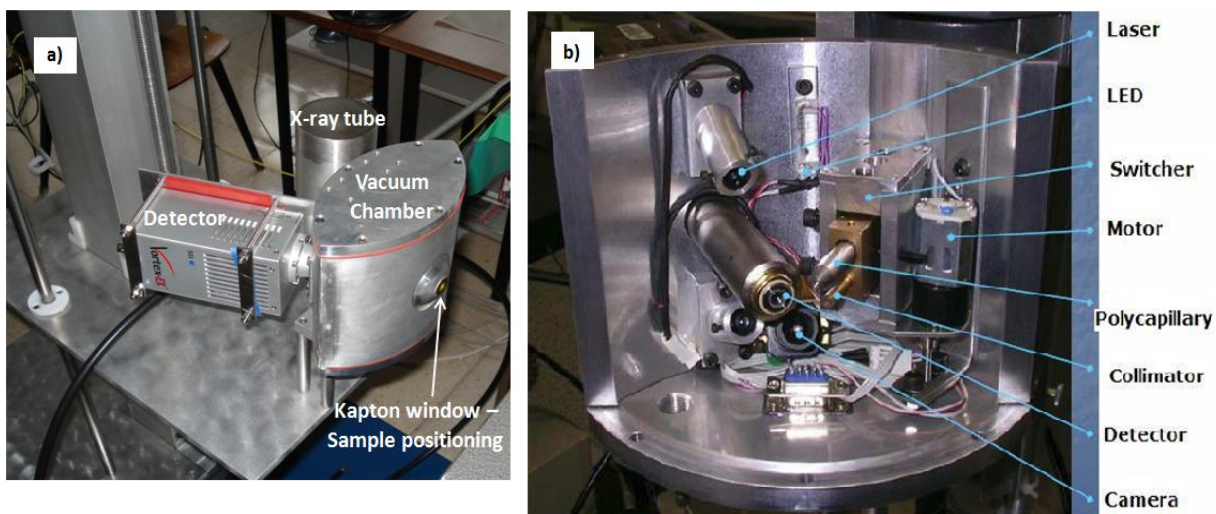
XRF measurements performed in the so-called “conventional” way are referred to bulk analysis, as it is shown in figure 3.6.



**Figure 3.6** – Sketch of a conventional XRF setup.

### 3.1.2.1 Experimental setup and methodology

The spectrometer used for conventional XRF measurements belongs to the *Atomic Physics Centre (Faculty of Sciences, University of Lisbon)*. Conventional XRF measurements were carried out in a 45° tube-detector geometry setup enclosed in a chamber submitted to a 10 mbar vacuum (figure 3.7a). The X-ray tube is a Be sided-window (125 µm thick) model with a Mo-anode and take-off angle of 20°, from Oxford Instruments (California, USA); the detector is a Vortex-60EX Silicon Drift Detector (SDD) with a 50mm<sup>2</sup> Si-area and 12.5 µm thick Be-window, from HITACHI USA Inc. (California, USA).



**Figure 3.7** – a) General view of the XRF experimental setup and b) the inside of the chamber [50] .

Inside the vacuum chamber (figure 3.7b) there is a motor stage which allows the incident radiation to be transmitted by means of a polycapillary full-lens from XOS (New York, USA) or a collimator made out of brass. The chamber is equipped with two laser pointers which overlap at the same position as the focus of the polycapillary and the detector axis. This allows positioning the sample at the proper distance of about 1.5 mm in front of the Kapton<sup>TM</sup> window. Due to this small distance the laser points as well as the spot of analysis can only be observed with the built-in camera.

The efficiency of an X-ray tube is very low (between 0.1 – 1%), due to the high thermal energy dissipation at the anode. The total irradiated X-ray power can be  $P[kW]$  can be estimated according to:

$$P[kW] = CZIU^2 \quad (3.9)$$

where  $[kV^{-1}] \approx 10^{-6}$ ,  $Z$  is related to the anode material,  $I[mA]$  is the anode current and  $U[kV]$  is the applied voltage. The maximum electric power of X-ray tubes can reach several kW for most operations and up to 100 kW in a pulsed mode – like for medical applications [43]. This implies that for many laboratory X-ray tubes a proper cooling system is crucial – in this case an air-cooling system was provided.

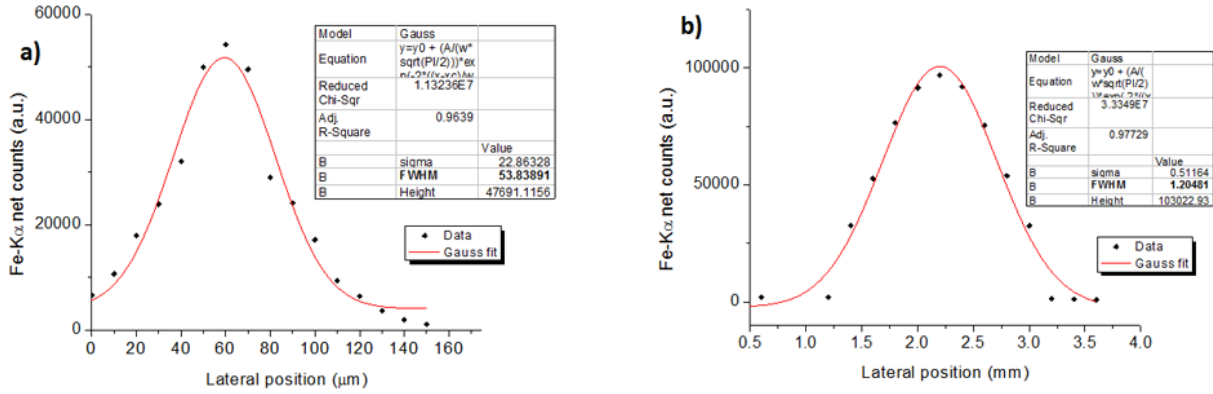
Silicon Drift Detectors (SDD) represent the latest technologic developments in collecting the charge (electron-hole pairs) created in the semiconductor material by the interaction of X-rays. The advantages of SDD compared to conventional energy dispersive detectors are lower electronic noise and capacitance, shorter shaping times, considerably higher pulse throughput and a pre-amplifying FET onto the detector chip. The energy-resolution is nowadays comparable to Si(Li) detectors and considerably high pulse throughput is achieved without detector cooling. The advantage of the Si(Li), nevertheless Si(Li) are still necessary because of their much higher detection efficiency – due to their thicker crystals – for high energy photons (up to 50 keV).

For the present investigation all measurements were performed with the collimator – in order to access larger areal information of at once – except when the decorative motifs were too close to each other and only by means of polycapillary they are laterally resolved [36-38]. As it was necessary to excite Sn- and Sb-K lines, the measuring conditions were always: 50 kV, 1 mA, 300 s and 10 mbar. Spectra were collected using a multichannel (4096 channels) and recorded in ASCII data mode in order to perform their evaluation using the PyMCA software code [51].

For beam-size measurements, a knife-edge scan with a snap-off blade was performed for the polycapillary, while an iron wire was used to perform the scans for the collimator. The step-size was 10  $\mu\text{m}$  for the polycapillary and 0.5 mm for the collimator. Figure 3.8 shows the scans performed for beam emitted with a) a polycapillary and b) a collimator. For the energy of Fe-K $\alpha$  (6.49 keV) the beam emitted with the polycapillary has a focal spot size of about 54  $\mu\text{m}$  and the collimator produces a beam of about 1.2 mm in diameter. One must keep in mind that the focal



spot of polycapillary lenses are energy dependent (explained further on) – assessed by the Full Width at Half Maximum (FWHM) of the profile obtained by such step-sized scans.



**Figure 3.8** – Scans performed for beam emitted with a) a polycapillary and b) a collimator. For the energy of Fe-K $\alpha$  (6.49 keV) the beam emitted with the polycapillary has a focal spot size of about 54  $\mu\text{m}$  and the collimator produces a beam of about 1.2 mm in diameter, both given by the Full Width at Half Maximum (FWHM) of the Gaussian fitted curves.

### X-ray polycapillary optics

The field of X-ray optics has grown tremendously in the past decades [52]. The necessity in analyzing samples with a high lateral or spatial resolution became evident to help understanding their properties or phenomena. This was the motivation for developing optical systems, which can focus or collimate an X-ray beam for the desired application. Nowadays we have at our disposal several optical systems, which provide different spot sizes for almost every requirement. Further information on the properties of the most common X-ray optics as well as their applications can be found in the review articles from Snigirev et al. [53], MacDonald [54] and Guilherme et al. [55]

Polycapillaries work under the principle of total reflection. It is meanwhile well-known that the interaction of X-rays with matter can be macroscopically described by an index of refraction. It can be derived from the interaction between a photon and a bound electron using the forced oscillator model, where an elastically bound electron is forced to oscillate in the electric field of the impinging photon. The whole derivation of the refraction index can be

found in James, 1962 [56]. An important result of this theory is that it leads to a complex index of refraction for X-rays, given by:

$$n = 1 - \frac{\lambda^2}{2\pi} r_0 \frac{\rho N_A}{A} f(\vec{k}) \quad (3.10)$$

with the wavelength of the photon  $\lambda$ , the scattering length  $r_0$ , the density of the matter  $\rho$ , the Avogadro constant  $N_A$ , the molar mass  $A$  and the atomic scattering factor:

$$f(\vec{k}) = f_0(\vec{k}) + f'_{(\lambda)} + if''_{(\lambda)} \quad (3.11)$$

where  $\vec{k}$  is the scattering vector between incident and scattered beam. Since only scattering in the forward direction is beneficial – while the rest accounts for attenuation – the atomic scattering factor (using the  $Z$  of the scattering element), can be re-written as:

$$f = Z + f'_{(\lambda)} + if''_{(\lambda)} \quad (3.12)$$

Hence, equation (3.10):

$$\text{With } \delta = \frac{\lambda^2}{2\pi} r_0 \frac{\rho N_A}{A} (Z + f'_{(\lambda)}) \quad \text{and} \quad \beta = \frac{\lambda^2}{2\pi} r_0 \frac{\rho N_A}{A} f''_{(\lambda)} \quad (3.13)$$

$$\text{can be rearranged in the following way: } n = 1 - \delta + i\beta \quad (3.14)$$

The value of the decrement  $\delta$  is in the order of  $10^{-5}$  to  $10^{-7}$  describes the refractive properties and depends on the energy of the X-rays ( $\lambda^2/2\pi$ ), the number of relevant electrons per atom ( $Z + f'_{(\lambda)}$ ) and the density of atoms  $\frac{\rho N_A}{A}$ . If  $N = \frac{Z N_A}{A} \rho$ , and  $\lambda$  is given in *Ångstrom*, an approximation can be found as:  $\delta = 2.72 \times 10^{-6} \frac{Z}{A} \rho \lambda^2 \approx 1.3 \times 10^{-6} \rho \lambda^2$  (3.15).

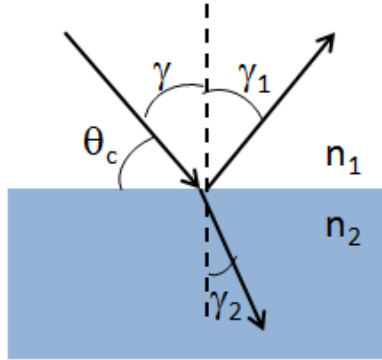
The imaginary part,  $\beta$ , describes the absorption of radiation in a medium and can be related to the linear attenuation coefficient  $\mu$  as:

$$\mu = \frac{4\pi\beta}{\lambda} \quad (3.16)$$

The small difference of the refraction index from the unit implies low reflection and refraction abilities of matter in the X-ray energy range. An important outcome from this derivation is that the real part of the refraction index is smaller than 1. This means that the optical density of any substance in the X-ray range is smaller than that of vacuum and the phenomenon of total external reflection can take place at grazing angles of incidence [43, 56].

Considering the scheme in figure 3.9 that represents the law of refraction formulated by Snell, it can be written as follows:

$$\frac{\sin(\gamma_2)}{\sin(\gamma)} = \frac{n_1}{n_2} \quad (3.17)$$



**Figure 3.9** – Representation of the law of refraction.

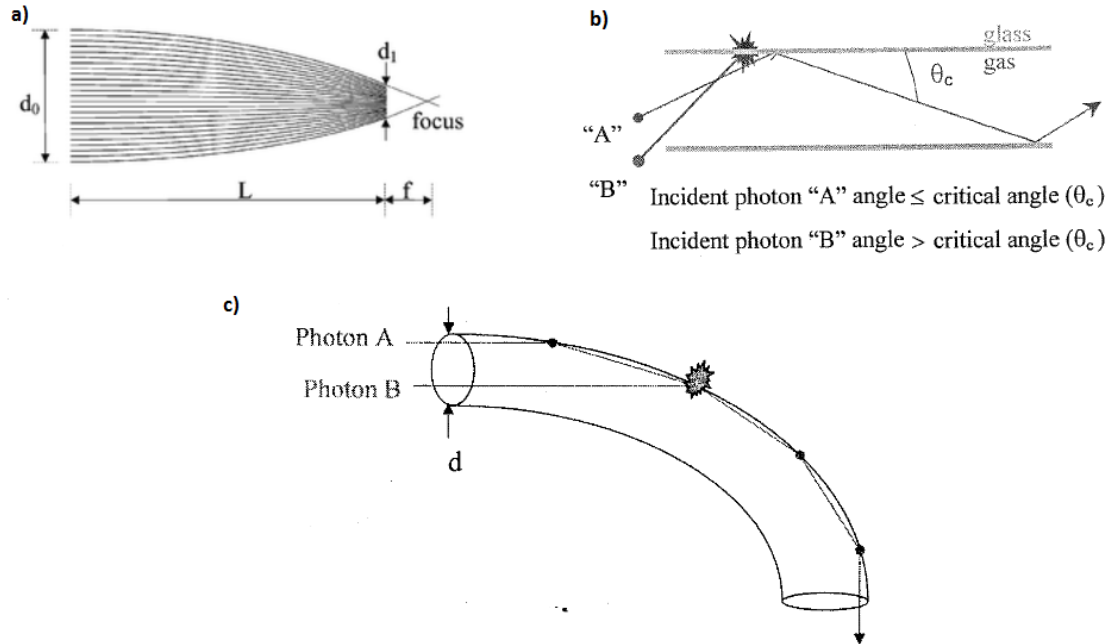
If  $\gamma_2 = 90^\circ$  and  $n_1 = 1$ , this leads to:  $\sin(\gamma) = \cos(\theta_c) = n_2 \approx 1 - \frac{\theta_c^2}{2}$  (3.18)

with  $\theta_c$  being the critical angle for total reflection. If one compares equation 3.17 with equation 3.14 – and having in mind  $E = h \cdot c / \lambda$  – one obtains:

$$\theta_c \approx (2\delta)^{1/2} \approx 1.6 \sqrt{\rho} \lambda \approx 20 \frac{\sqrt{\rho}}{E} \quad (3.19)$$

with E in keV,  $\rho$  in  $\text{g}/\text{cm}^3$  and  $\theta_c$  in mrad.

In the present case, focusing polycapillary half-lenses were used. They consist of thousands of bundles of hollow glass capillaries with different curvatures, as indicated in figure 3.10a.



**Figure 3.10** – a) Representation of focusing polycapillary half-lenses [57]; b) total reflection condition for X-ray photons [58] and c) Radiation capture for a bent capillary [58].

As the angle of the X-ray beam incident on the glass surface decreases from relatively high angles, the refracted beam in the glass will approach the critical angle ( $\theta_c$ ) and the increased probability of propagating along the channel by multiple reflections (figure 3.10b). Photons with  $\theta > \theta_c$  will not propagate and a shading effect happens (figure 3.10c). For a borosilicate glass, one has:

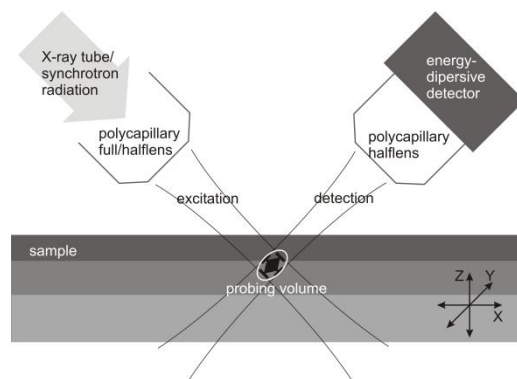
$$\theta_c [mrad] \cong \frac{30}{E [keV]} \quad (3.20)$$

Since the critical angle and the energy of the photon are inversely proportional, the transmission of a polycapillary has generally a maximum for medium-range energies and it decreases for both low-range and high-range energies. At higher energies, the angle of acceptance becomes smaller and the total reflection condition is not fulfilled anymore, while at lower energies, the reflectivity decreases.

### 3.1.3 3D Micro-XRF

A new mode of performing XRF analyses in depth was presented in 2003 by Kanngiesser et al. [59], where the first experimental applications were performed. The method consists in having two polycapillary lenses aligned in a confocal geometric arrangement, so 3D depth resolved analyses are feasible (figure 3.11). The model for this geometry was proposed by Malzer et al. [60] in 2005. Radiation from an X-ray source is focused by a polycapillary full or half-lens onto a sample. The resulting characteristic fluorescence radiation is transported with a second polycapillary half-lens to an energy-dispersive detector. The overlap of the foci of the two optics forms a probing volume from which information is derived. Due to the finite size of this probing volume information can be obtained three-dimensionally by moving the micro-volume through the sample. Absorption of exciting and fluorescence radiation limits the possible information depth and the extension of the probing volume affects the shape of the profiles [61].

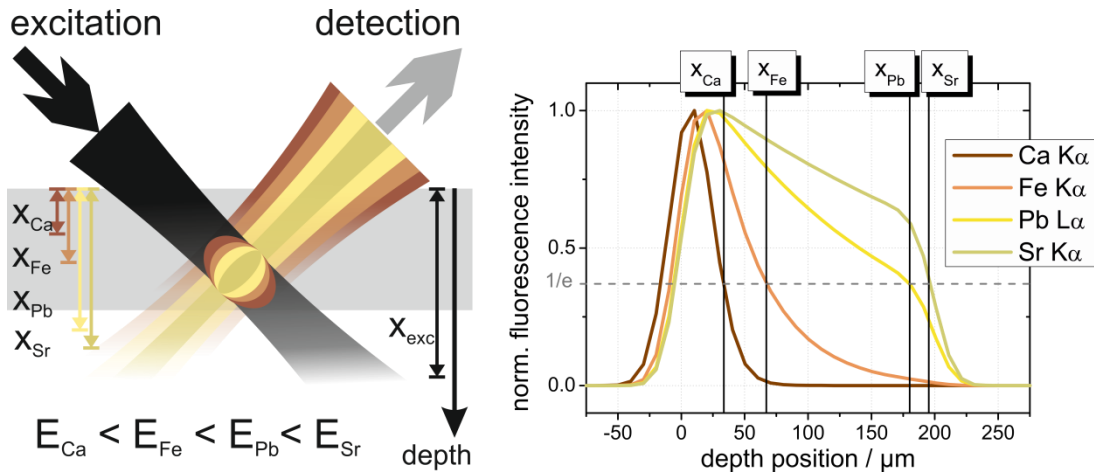
Both qualitative and quantitative analyses can be performed by means of 3D Micro-XRF. A review article published recently by Mantouvalou et al. [62] gives an overview of the work on 3D Micro-XRF.



**Figure 3.11** – 3D Micro-XRF sketch; the overlap of the foci from the two polycapillary half-lenses ensure three-dimensional resolution (sketch by I. Mantouvalou [61]).

When working with polycapillary X-ray optics some new features have to be taken into account. One of them is the energy-radiation dependence. The transmission and spot size of a polycapillary lens are functions of the radiation energy. The spot size decreases with increasing

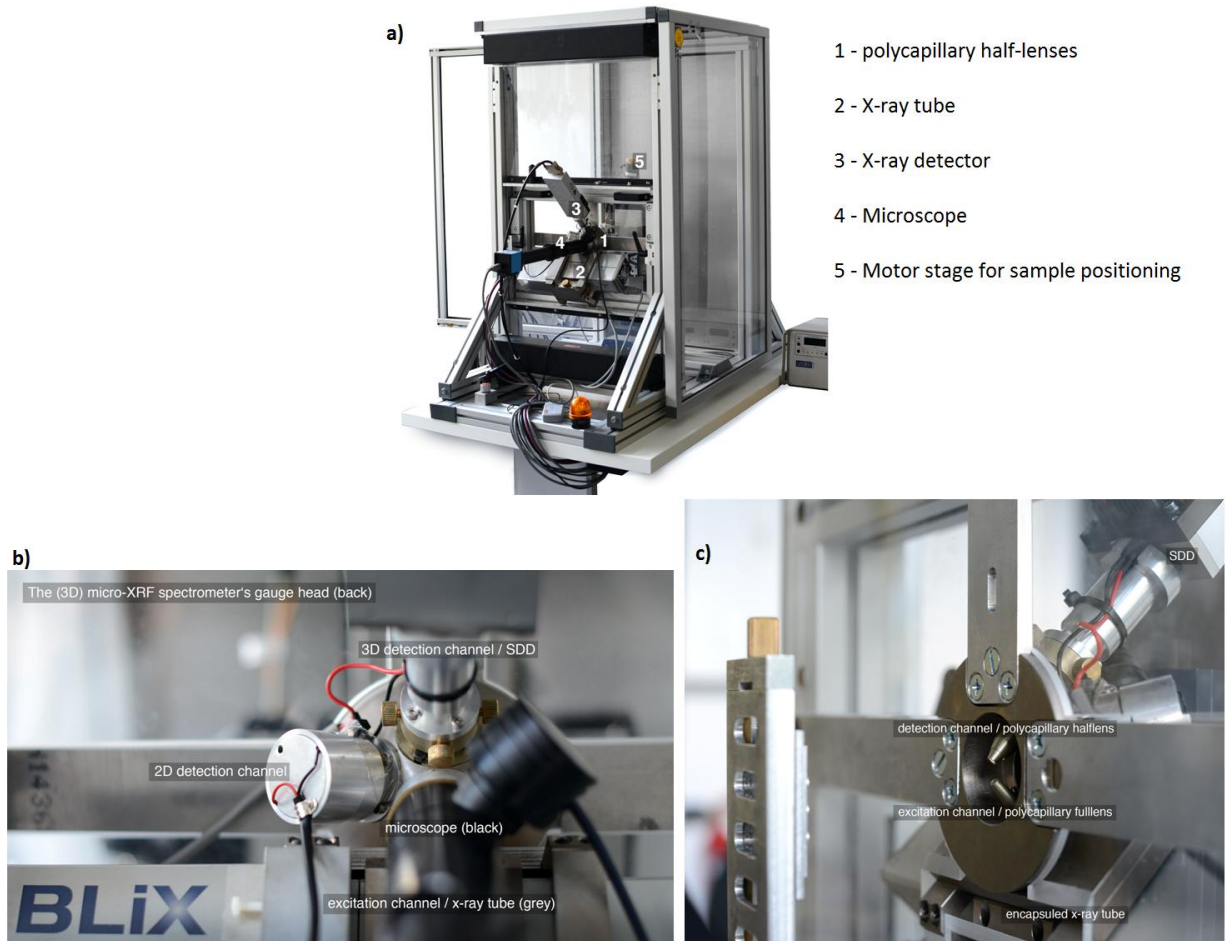
transported energy, which means that the size of the probing volume also decreases with increasing fluorescence energy (figure 3.12). The transmission of a polycapillary lens can be described by an asymmetric peak function, thus limiting the range of detectable elements through its decrease to higher and lower energies. Additionally, the absorption of radiation through matter is energy dependent and increases with decreasing energy.



**Figure 3.12** – Depth profile simulation on a 200  $\mu m$  thick glass samples with 50 ppm of CaO, Fe<sub>2</sub>O<sub>3</sub>, PbO and SrO homogeneously distributed in the sample matrix. Left: Sketch of the setup with respective attenuation depths  $x_i$ ; right: normalized depth profiles (sketch by I. Mantouvalou [62]).

### 3.1.3.1 Experimental setup and methodology

3D Micro-XRF measurements were carried out with a tabletop setup from *the Institute for Optics and Atomic Physics at the Technical University of Berlin*. This system is a commonly development with ifG (Institute for Scientific Instruments). The X-ray tube is from Rtw Röntgen-Technik (Neunhagen, Germany); the polycapillary optics are from IfG (Berlin, Germany); and the detector is from Bruker nano (Berlin, Germany).

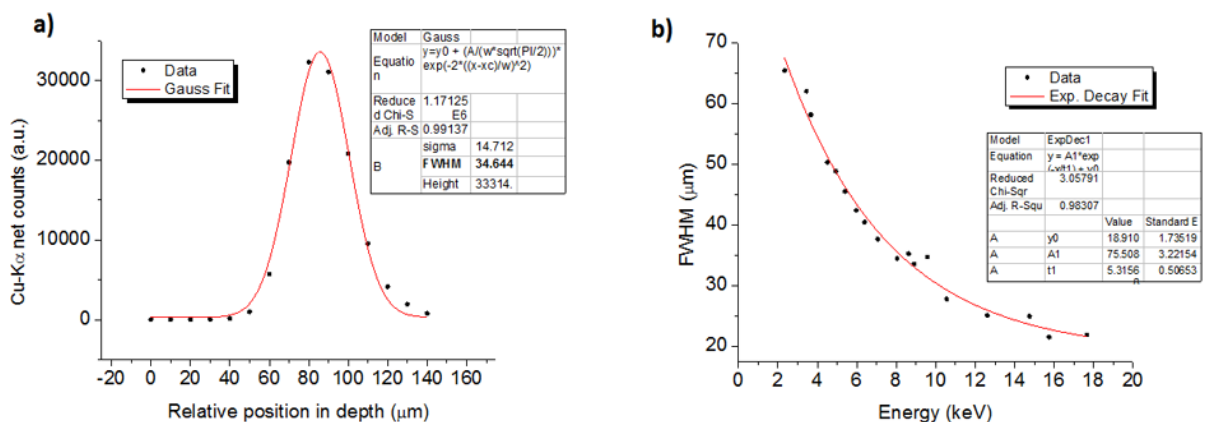


**Figure 3.13** – a) General view of the 3D Micro-XRF spectrometer; b) Spectrometer’s gauge head; c) view of the polycapillary half-lenses and sample holder (left-hand side) (pictures by C. Seim [63]).

With the aim of checking the stratigraphy of the samples in a non-destructive way, the choice of depth resolved XRF at the micrometer regime was justified. Therefore, a characterization of the spectrometer used was performed. Here the concept of probing volume plays a central role when using the confocal XRF – as explained above. Hence features such as beam resolution have to be known at front in order to properly evaluate information obtained from the scans performed on the samples.

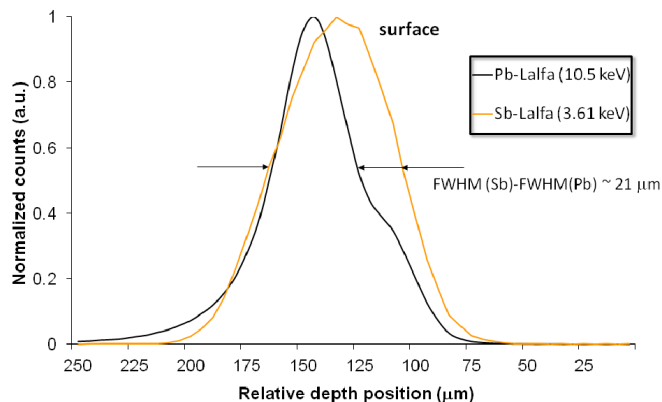
In order to evaluate the probing volume size, depth scans on thin single-element foils were carried out. As the thickness of each foil is 2  $\mu\text{m}$ , self absorption effects can be neglected since the probing volume will be larger than the foils thickness. Depth scans in steps of 5  $\mu\text{m}$  were performed and the sum of the most intense peak – characteristic of each foil – was collected

and plotted. The measuring time at each position was 10 s. In figure 3.14a the data collected from the depth scans performed with the Cu-foil are plotted. A Gaussian fit applied to the data spread showed a FWHM of  $\sim 34.6 \mu\text{m}$  for Cu-K $\alpha$  energy (8.05 keV). Figure 3.14b displays the FWHM for all analyzed elements (foils) with respect to the energy.



**Figure 3.14** – a) Determination of the FWHM for Cu-K $\alpha$  (8.05 keV):  $\sim 34.6 \mu\text{m}$ ; b) dependence of the FWHM as function of the energy. An exponential decrease of the FWHM is observed with increasing energy.

The leading feature of this system is the ability to perform depth-resolving analysis, as described above. However, due to the high amount of lead in the samples, strong absorption effects took place. In figure 3.15 an example of a depth scan performed perpendicular to the surface of a sample – with a stratigraphy (from top to bottom) of yellow-glaze-body – is shown.

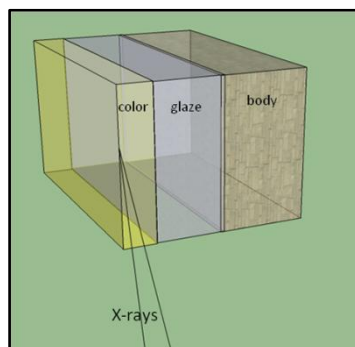


**Figure 3.15** – Depth profile from a faience sample from Coimbra. The Pb-L $\alpha$  and Sb-L $\alpha$  lines are characteristic from the glaze and yellow color, respectively.



From figure 3.15 one sees that the Full Width at Half Maximum (FWHM) for the Sb-L $\alpha$  line is larger than the one for the Pb-L $\alpha$ , which is due to the difference between probing volume sizes for different energies (*cf.* figure 3.14). At 10 keV, a probing volume size of ca. 27  $\mu\text{m}$  is expected, while at 3 keV a size of ca. 57  $\mu\text{m}$  is obtained, for the used lenses. This leads to a difference in about 30  $\mu\text{m}$ , which means that the existing 21  $\mu\text{m}$  difference between the Pb-L $\alpha$  and Sb-L $\alpha$  profiles gives no information about a possible layered system. This leads to an information depth of several tens of micrometers, only, which prevents further depth resolution.

Nevertheless, we took advantage of another feature of the confocal geometry, which is probing site selection – on the cross-section (figure 3.16). The probing volume created in the confocal geometry allows selective analysis in a certain volume in the micrometer regime, which reduces the amount of detected scattered radiation considerably. Therefore, scans just on the surface of the polished cross section of each sample were performed, in steps of 5  $\mu\text{m}$  (each during 60 s) through a length that varied according to the thickness of the relevant part of the sample [37]. The operating conditions were the maximum for this system: 50 kV and 600  $\mu\text{A}$ .



**Figure 3.16** – Schematic representation showing how the 3D Micro-XRF cross-section scans were performed.

### 3.1.4 High-resolution Micro-XRF

High-resolution Micro-XRF scans were performed at the synchrotron. More precisely, at the BAMline at BESSY-II (*Berliner Elektronen Speicherring für SYNchrotronstrahlung*) in Berlin,

Germany. The fact that a 1  $\mu\text{m}$  X-ray beam size is achieved was appealing for performing lateral cross-section scans to trace key-elements along the different “layers” of the samples.

Synchrotron radiation (SR) together with Compound Refractive Lenses (CRL) allowed having a 1  $\mu\text{m}$  beam, which provides information about the diffusion of the pigments throughout the glaze and the glaze throughout the ceramic support. The following sub-sections summarize the properties of SR and CRLs.

#### 3.1.4.1 Synchrotron Radiation

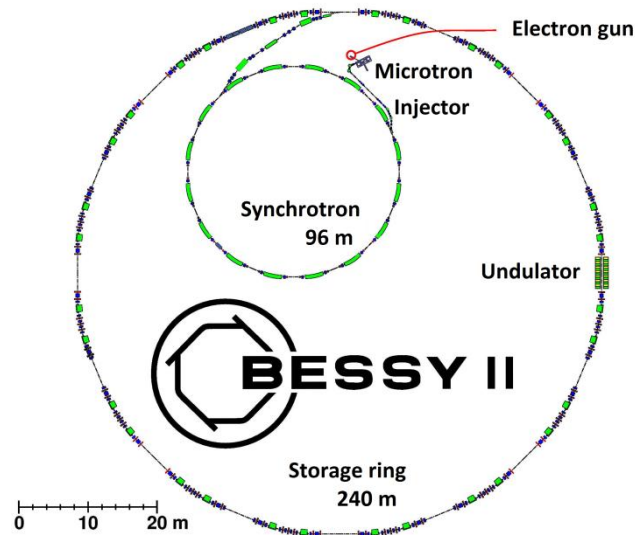
Synchrotron radiation (SR) is produced whenever electrons travelling at relativistic velocity ( $v \approx c$ ) are accelerated for example by forcing them to deviate from a straight line of motion. SR possesses unique features such as:

- High brilliance (photons/sec/mm<sup>2</sup>/mrad<sup>2</sup> in 0.1% bandwidth)
- Highly collimated (divergence in the mrad range)
- Polarization
- Time structure (pulse lengths down to 100 ps)
- Broad spectral range (IR to hard X-ray region)
- Small source size (size and divergence of the electron beam)

Due to the high energy  $E_{e^-}$  of the electrons, in the range of GeV, and the corresponding high velocity, close to  $c$ , the relativistic version of the total radiated power  $P$  of an accelerated electron (calculated by Larmor) has to be used to calculate the emitted radiation:

$$P \simeq \frac{2ec^2}{3R^2} \gamma^4 \propto E^2 B \quad (3.21)$$

with  $\gamma = E/m_e c^2$  and the orbit radius  $R \propto E/B$ . Further insight about SR properties can be found, for example, in Duke [64]. A 3<sup>rd</sup> generation synchrotron source consists basically of an electron gun, a microtron, the synchrotron and the storage ring (figure 3.17).



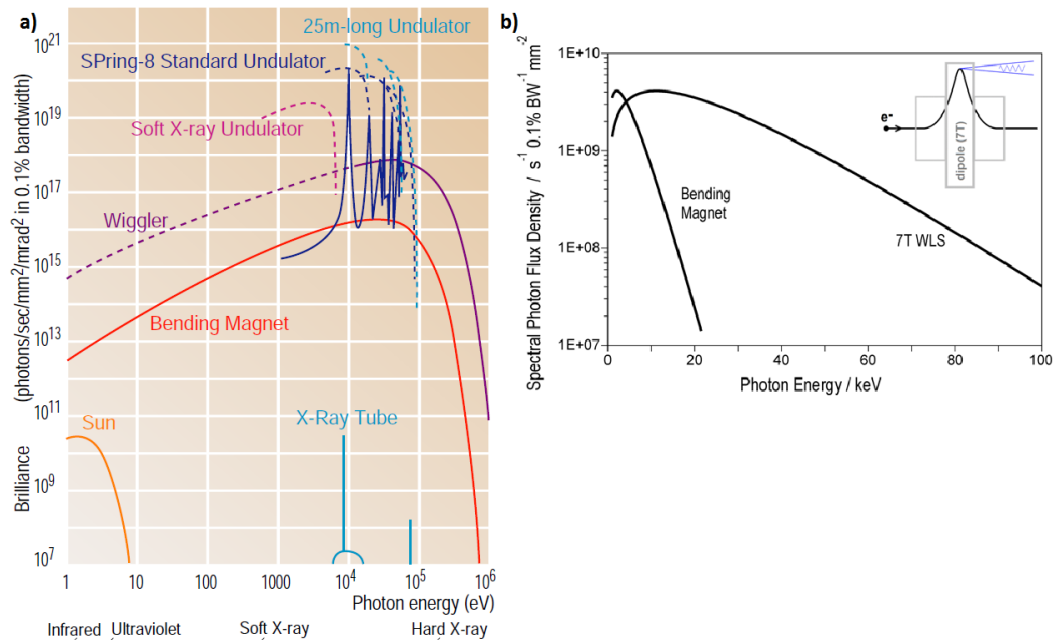
**Figure 3.17** – Main components and dimensions of the *Berliner Elektronen Speicherring für Synchronstrahlung* (BESSY-II) in Berlin, Germany [65].

Electrons emitted by an electron gun are first accelerated in a linear accelerator (Microtron) and then transmitted to a circular accelerator (booster synchrotron) where they are accelerated to reach an energy of 1.7 billion electron volts (1.7 GeV) – in the case of BESSY-II. These high-energy electrons are then injected into a large storage ring where they circulate in a vacuum environment, at a constant energy, for many hours. Each time these electrons pass through a magnetic device, they emit X-rays (SR), which are directed along beamlines.

SR radiation can be emitted either by a bending magnet (**BM**) – which makes the electron beam to undergo in circular trajectory – or by an insertion device, which comprise rows of magnets with alternating polarity, installed in straight sections of the electron path. Insertion devices are: wigglers (**W**), undulators (**U**) or wavelength shifters (**WLS**).

Each device provides different radiation features, being one of them related with the cone of divergence in which more or less brilliance is obtained (figure 3.18). Generally: **BM**: When stored electrons encounter a BM, they bent and emit SR in a continuous spectrum; **W**: the electron beam wiggles with a large deviation angle and, as a result, bright a spectral continuous light with short wavelengths is obtained; **U**: The electron beam wiggles with a small deviation angle and, as a result, highly bright and quasi-monochromatic light is obtained by the interference effect; **WLS**: The electron beam passes a three dipole magnet array with

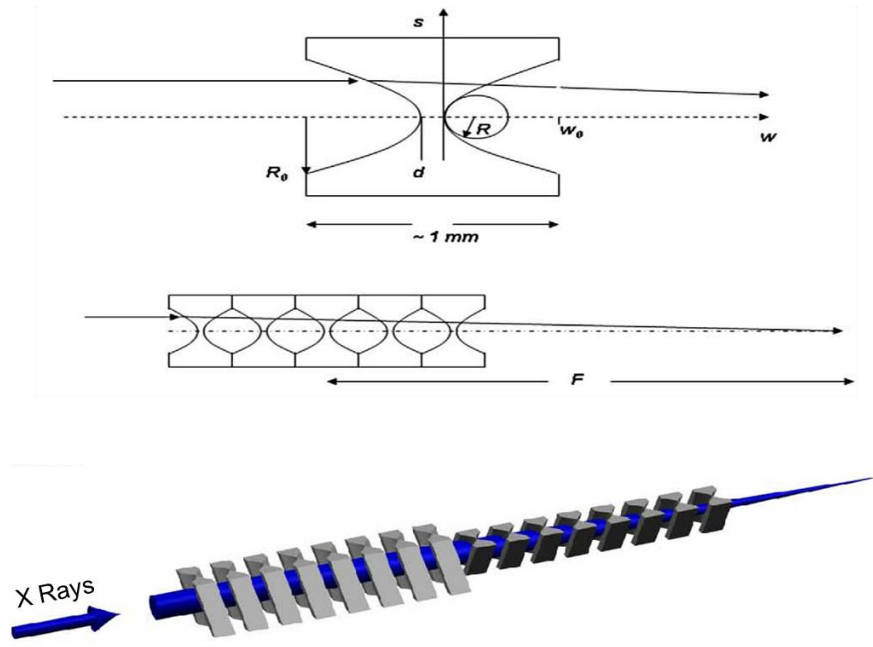
alternating magnetic field directions. The radiation is emitted at the central dipole of the wavelength shifter. The other two dipoles only compensate the deflection of the electron beam from its orbit, so that the electrons leave the device in the same direction as they entered.



**Figure 3.18** – a) comparison of brilliance vs photon energy obtained with different magnetic devices at the synchrotron and X-ray tubes (from Spring 8 [66]); b) Spectral Photon Flux of a 1.3T bending magnet and a 7T wavelength shifter. In the upper right corner, a schematic view of the electron trajectory in a WLS is shown (adapted by G. Buzanich [67]).

### 3.1.4.2 Compound Refractive Lenses (CRL)

CLRs belong to the group of refractive optics, in which the X-rays undergo refraction at the surfaces between different materials, as shown in figure 3.19. Since one lens only provokes a small change in the direction of the X-ray, an array of such lenses (therefore Compound Refractive Lenses) is necessary to obtain acceptable focal distances [68].



**Figure 3.19** – Example of a CRL and its working principle.

For thin lenses, the focal length  $f$  can be calculated as:

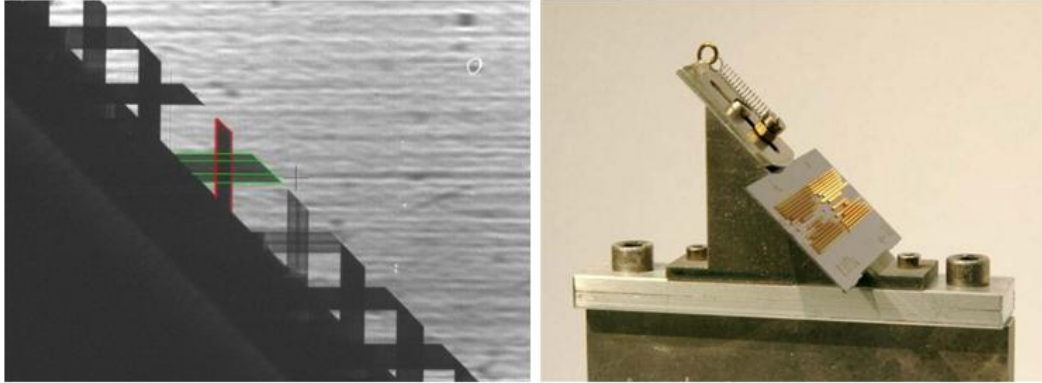
$$f = \frac{R}{2\delta N} \quad (3.22)$$

with the radius of curvature  $R$  and the number of lenses elements  $N$ . When the lens length  $L$  is in the range of the focal length, the formula for thick lenses can be applied [68]:

$$f = \frac{R}{2\delta N} + \frac{L}{6} \quad (3.23)$$

Due to their simple design and alignment, CRLs are one of the most popular X-ray focusing devices. The important features are: i) focusing in the region of 100 nm; and ii) focusing of X-rays with energies in the range from 5-200 keV is possible. The energy bandwidth of this kind of lenses (ca. 100 eV) is very small, meaning that for every energy an own lens has to be manufactured. The fact that the CRL's require a monochromatic and also parallel beam makes them suitable for synchrotron beamlines only.

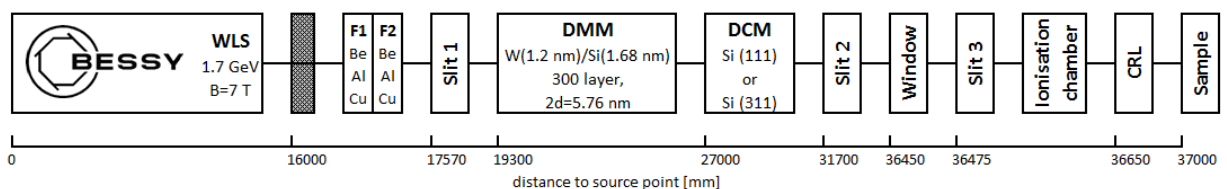
As an example, the CRL plate designed for the BAMline is shown in figure 3.20.



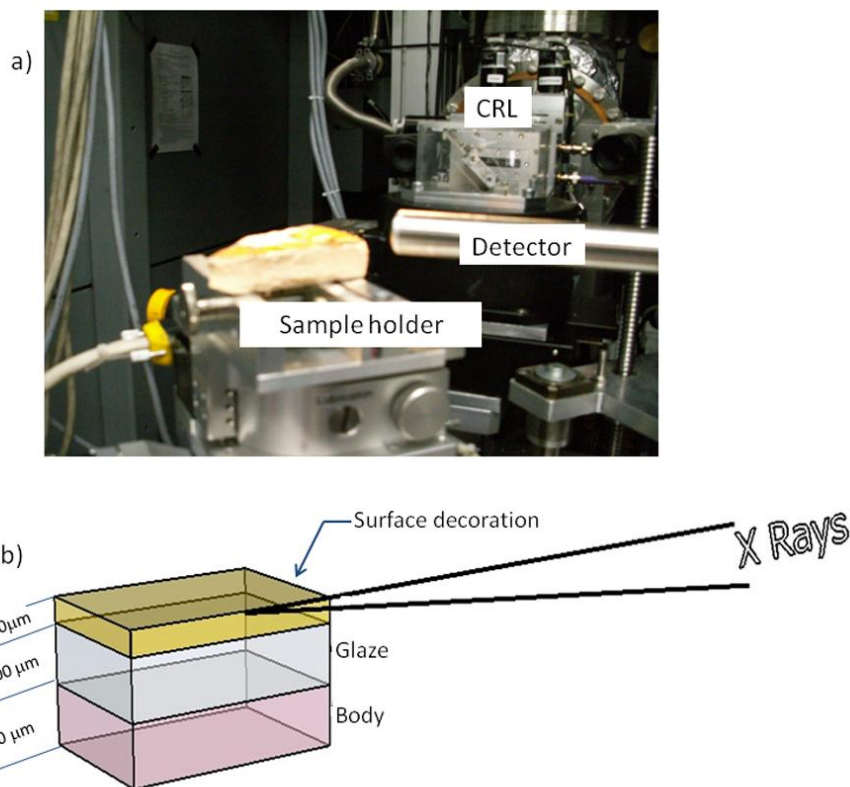
**Figure 3.20** – CRL @BAMline (from KIT: [www.x-ray-lenses.de](http://www.x-ray-lenses.de) pictures by G. Buzanich).

### 3.1.4.3 Experimental setup and methodology

The schematic of the BAMline @BESSY-II is shown in figure 3.21. In figure 3.22 the layout of the  $\mu$ -XRF experiment at the BAMline and a sketch of the sample composition (wall-tile) in terms of its layers is shown to illustrate how the scans were performed. For these measurements two lenses were used: one with a nominal energy of 33.2 keV and another with a nominal energy of 20.0 keV. This choice was taken due to the elemental variability present in the decorative motifs as well as in the glaze. For the pieces which have yellow (Sb:  $E_{C(K)} = 30.491$  keV) the 33.2 keV lens was ideal and for the pieces which have blue (Co:  $E_{C(K)} = 7.709$  keV), green (Cu:  $E_{C(K)} = 8.979$  keV) and purple (Mn:  $E_{C(K)} = 6.539$  keV; Fe:  $E_{C(K)} = 7.112$  keV) colors together with the glaze (Pb:  $E_{C(L3)} = 13.035$  keV) the 20 keV lens was used. Although the lens with a nominal energy of 33.2 keV would have been able to excite the medium-low range, the 20 keV lens was used for the measurements. This lens, due to its bigger aperture, provides more flux at the sample and the absorption efficiency is higher for this elemental range.



**Figure 3.21** – Scheme of the BAMline. X-ray source is a 7T WLS (Wave Length Shifter) installed at the storage ring BESSY II. The optical elements are a Double Multilayer Monochromator, a Double Crystal Monochromator and the CRL (sketch by G. Buzanich [39, 67]).



**Figure 3.22** – (a) Layout of the  $\mu$ -XRF experiment at the BAMline; (b) a sketch of the sample composition (wall-tile) in terms of its layers. The scans were performed up to a maximum of 500  $\mu\text{m}$  thickness of ceramic body [39].

## 3.2 X-ray Diffraction (XRD)

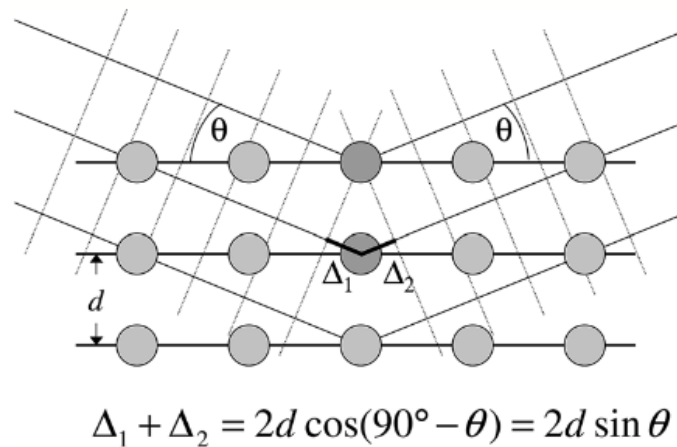
### 3.2.1 XRD principles

When a monochromatic incident X-ray beam interacts with a material in which a regular and periodic arrangement of atoms (or molecules) exists – crystalline structure – diffraction of the beam takes place in definite directions. This phenomenon can be seen as reflection of the incident beam by interior planes of a crystal (Bragg reflection) and it follows the Bragg equation, in first approximation [42]:

$$n\lambda = 2d \sin \theta_n \quad (3.24)$$

where  $n$  is the order of reflection,  $d$  is the interplanar spacing and  $\theta_n/2$  is the angle of reflection (Bragg's angle), which is defined by the angle between the reflecting plane of the crystal and incident or reflected beam (figure 3.23). The first order of reflection is the strongest and the reflected intensity decreases as  $n$  increases.

As previously described one of the types of interaction between X-rays and matter is elastic scattering of the X-rays (Rayleigh scattering). Diffraction is one example of elastic scattering – the wavelength  $\lambda$  of the diffracted X-ray beam is conserved. A detailed theoretical development of the scattering occurring in a group of atoms can be found elsewhere [69].



**Figure 3.23** – Visualization of the Bragg equation. Maximum scattered intensity is only observed when the phase shifts add to a multiple of the incident wavelength  $\lambda$  [69].

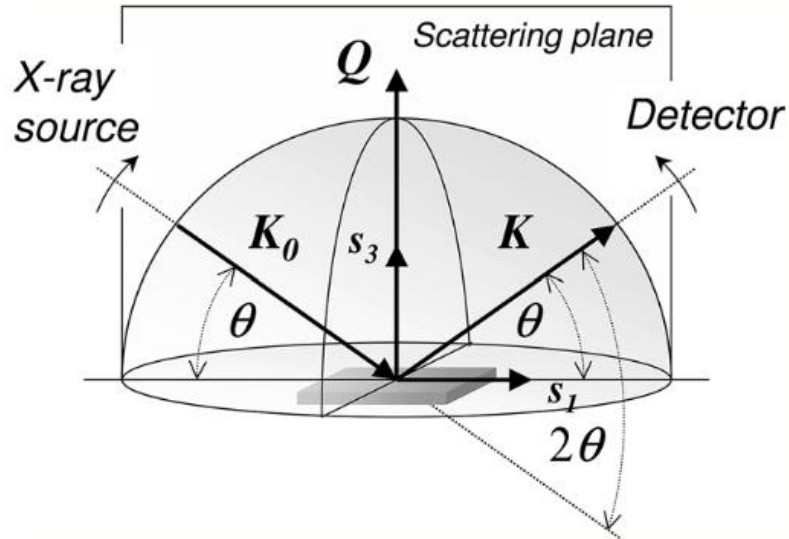
One obtains, therefore, information about the minerals that constitute the sample. However, due, the sample preparation process as well as instrumental background it can hinder some diffracted peaks – for example due to preferred crystallographic arrangement.

### The $\theta/2\theta$ scan

One is interested in the measurement of Bragg reflections, i.e. their position, shape, intensity, in order to derive microstructural information from them. The intensity variation that is associated with the reflection is included in the interference function developed in [69], while the scattered intensity depends on the distance from the sample to the detection system R. Therefore the instrument should be configured such that one can scan the space around the



sample by keeping the sample–detector distance  $R$  constant. This measure ensures that any intensity variation observed is due to the interference function and is not caused by a dependency on  $R$ . The detector should accordingly move on a sphere of constant radius  $R$  with the sample in the center of it – performed by a goniometer. In addition, the sphere reduces to a hemisphere above the sample, since we are only interested in the surface layer and data collection will be performed in reflection mode (figure 3.24).



**Figure 3.24** – Schematic representation of a  $\theta/2\theta$  scan from the point of view of the sample reference frame [69].

The sample is positioned in the center of the instrument and the probing X-ray beam is directed to the sample surface at an angle  $\theta$ . At the same angle the detector monitors the scattered radiation. The sample coordinate vectors  $S_1$  and  $S_3$  lie in the scattering plane defined by  $K_0$  and  $K$ . During the scan the angle of the incoming and exiting beam are continuously varied, but they remain equal throughout the whole scan:  $\theta_{in}=\theta_{out}$ . The  $\theta/2\theta$  scan can also be understood as a variation of the exit angle when this is determined with respect to the extended incoming beam and this angle is  $2\theta$  for all points in such a scan. The quantity measured throughout the scan is the intensity scattered into the detector. The results are typically presented as a function of  $I(2\theta)$  type [69].

### **3.2.2 Experimental setup and methodology**

XRD analyses were performed at the GeoBioTec from the University of Aveiro (Portugal). The equipment used was a Philips X'Pert PW 3040/60 goniometer, using Cu-K $\alpha$  radiation ( $\lambda = 1.5405$  Å), 50 kV and 30 mA, automatic divergent notch graphite monochromator and a step size of  $1^\circ/2\theta/\text{min}$  in the  $4\text{--}65^\circ$   $2\theta$  range, with data acquisition by Philips X'Pert-Pro Data Collector v1.2.

The sample preparation is the following: a small amount (6 – 8 grams) of sample is removed and dried at around  $40^\circ\text{C}$  and then grinded, which is then passed through a sieve of  $63\ \mu\text{m}$ . The obtained powder is mounted on a sample holder under a slight pressure – in order to minimize preferred crystallographic arrangement. This sample holder is then placed inside the diffractometer. Identification of crystalline phases by XRD was carried out using the International Centre for Diffraction Data Powder Diffraction Files (ICDD PDF).

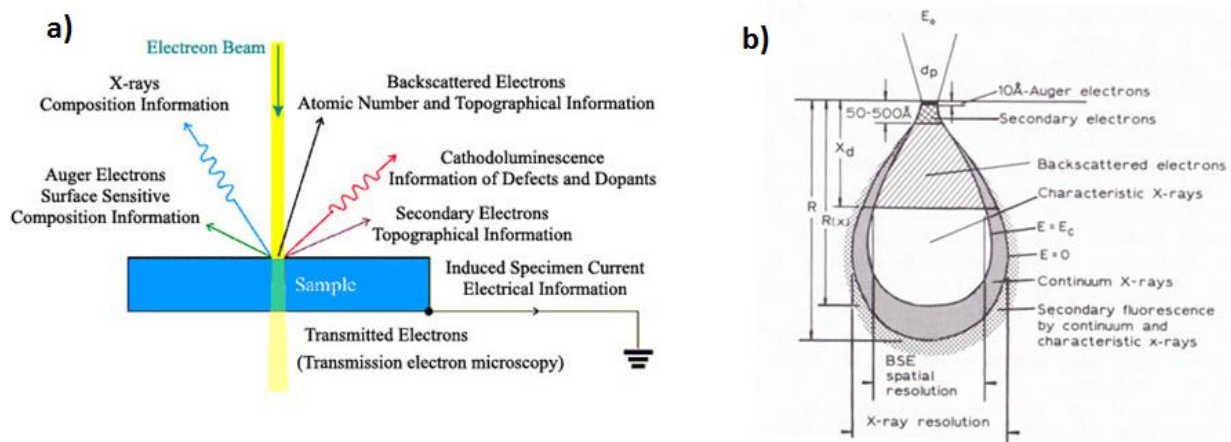
## **3.3 Scanning Electron Microscopy / Energy Dispersive X-ray System (SEM/EDX)**

### **3.3.1 SEM/EDX principles**

#### **Electron beam-specimen interaction**

This is a versatile technique, through which one obtains both morphological (SEM) and compositional (EDX) information about the sample. The latter has developed into an own field – so to say – often referred as Electron Probe Micro-Analysis (EPMA). The primary reason for SEM's usefulness is the high resolution that can be obtained when bulk objects are examined.

The principle of this method consists in bombarding target atoms (of a sample) with an electron beam. In figure 3.25a a scheme of the electron-beam solid interactions as well as the range and spatial resolutions for each one is shown (figure 3.25b).



**Figure 3.25** – (a) Electron beam solid interactions; (b) summary of range and spatial resolutions of electrons and X-rays produced in SEM [71].

The primary effects by impinging a high-voltage electron beam on the electrons of a target material are elastic scattering – change of direction with negligible energy loss – and inelastic scattering – energy loss with negligible change in direction. Elastic scattering is mainly caused by interactions with the nucleus, through which significant deviations from the incident direction occur. Inelastic scattering is caused by two mechanisms: (i) inelastic interaction with the atomic nucleus and (ii) inelastic interaction with the bound electrons. Inelastic scattering is mainly responsible for producing signals than backscattered electrons. Inelastic interactions with the nuclei of atoms are characterized by loss of energy in the Coulomb field of the nuclei and continuum X-radiation is emitted. Inelastic collisions between loosely bound outer electrons of the target atoms provoke the ejection of these. Typically these ejected electrons will have energy of about 50 eV and are called *secondary electrons (SE)*. If these secondary electrons are produced close to the surface and their energy is enough to overcome the surface barrier (2-6 eV) they have high probability of escaping. However, these electron will be strongly absorbed if they are produced much below the surface ( $\geq 100 \text{ \AA}$ ) and the probability of escape is lowered drastically [71]. One other result of inelastic collisions is the production of characteristic X-ray lines. The dissipation of energy from an impinging electron during inelastic scattering is quite complex to determine. From the quantum theory, Bethe obtained an

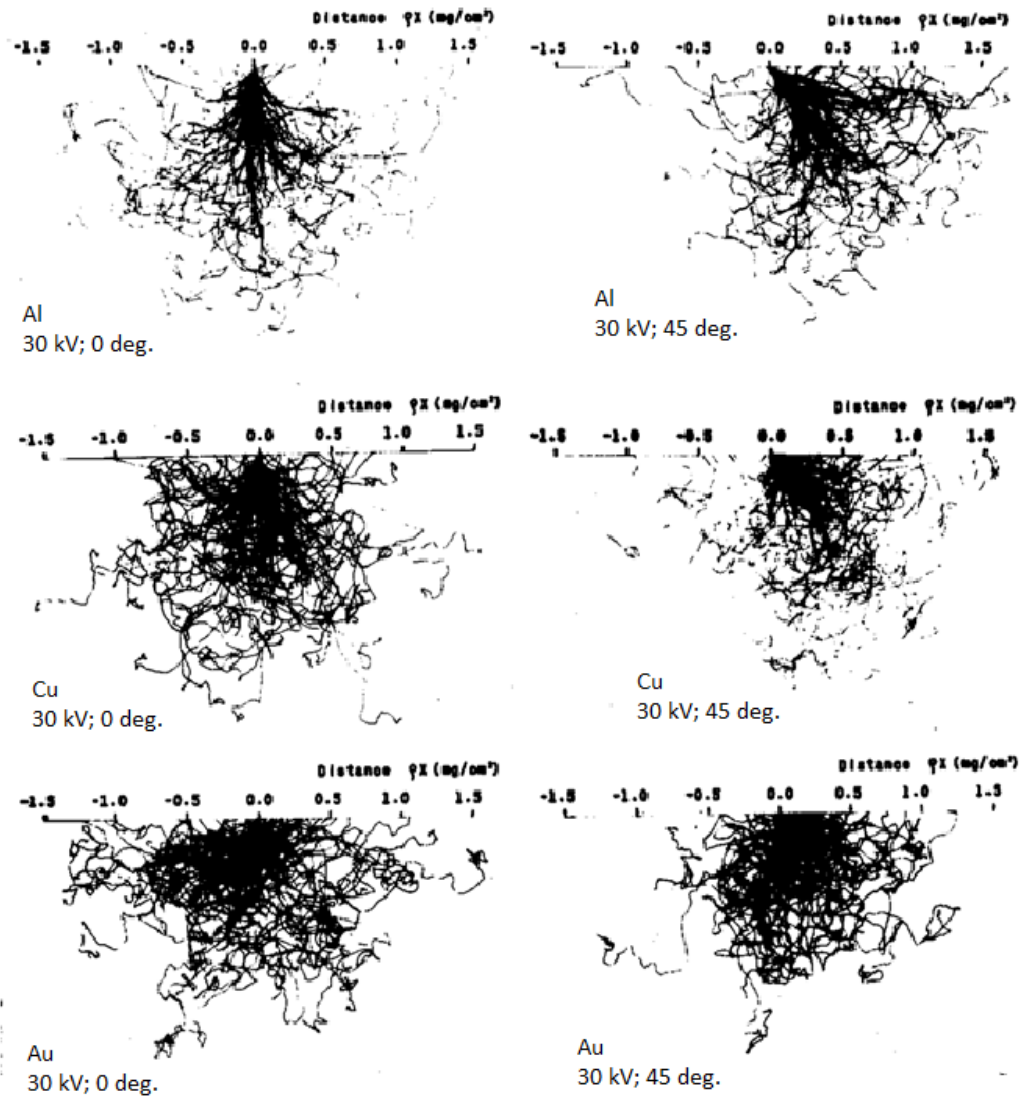
expression which described the stopping power of an electron (S) and can be simplified in the following form:

$$S = -\frac{1}{\rho} \frac{dE_m}{dX} \quad (3.25)$$

and indicates the energy loss per unit mass thickness.  $\rho$  is the physical density. S increases with decreasing Z, being about 50% greater for Al than for Au at 20 keV.

Elastic scattering – by the nucleus – is by far the most probable large-angle scattering mechanism. The cross-section for inelastic scattering into angles greater than  $10^{-2}$  rad is much smaller than for elastic scattering for all elements except for the ones of low-Z. Elastic scattering should be seen in two parts: (i) Rutherford scattering – which occurs in the Coulomb field of the nucleus and is characterized by a large change in direction (even greater than  $90^\circ$ ); and (ii) multiple scattering – composed of many small scattering events, in which in each of these events the electron passes through the electron cloud of the atom and act as a screening field for the nucleus. It may also results in large change of direction. In sum, beam electrons may change directions in a series of events, travel back to the surface and escape – process of backscattering (figure 3.25) [71]. Backscattered electrons (BSE) leave the sample with reduced energy due to inelastic processes. From a certain depth in the target material, the original direction of the electron beam is lost and the electrons diffuse through the material randomly. The depth from which this happens can be seen as the depth of complete diffusion ( $x_d$  – figure 3.25b).

The scattering cross-section at constant energy varies with  $Z^2$  and the probability of scattering through a given angle varies as  $Z^2/E^2$ . The mean free path between scattering events at 30 keV decreases with increasing Z from 528 Å for Al to 131 Å for Cu and to 50 Å for Au (figure 3.26) [71].



**Figure 3.26** – Electron trajectories calculated for Al, Cu and Au,  $E_0 = 30$  keV at normal ( $0^\circ$ ) and  $45^\circ$  incidence [71].

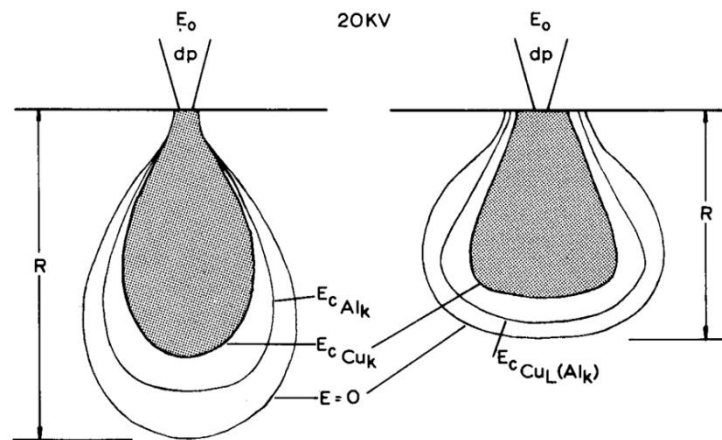
For low-Z samples, most electrons penetrate deeply into the target before changing direction by more than  $90^\circ$  and are absorbed in the sample. For high-Z samples the amount of scattering will increase and a state of complete diffusion will occur. In case of a heavy element, such as Au, diffusion happens much nearer the surface than for a light element, and most of the backscattered electrons are caused by multiple rather than single scattering [71]. From figure

3.26 it can be observed that, at the same energy, the electron appear to penetrate more deeply into the low-Z element and the electron distribution seems to be more pear-shaped.

There are two electron beam-solid interactions which lead to X-rays production: (i) core scattering – that results in the emission of continuous spectrum – and (ii) inner shell ionization – yielding characteristic lines. In (i) impinging electrons are inelastically scattered by the nucleus which results in a continuous spectrum of X-rays – similar to what happens in an X-ray tube, where *Bremsstrahlung* is produced. These X-rays assume a maximum energy value of incident electron  $E_0$ . The relationship between wavelength and energy of the X-ray photos is:

$$e.U = h.v_{max} = h.\frac{c}{\lambda_{min}} \Leftrightarrow \lambda_{min}(\text{\AA}) = \frac{h.c}{E [keV]} = \frac{12.4}{E [keV]} \quad (3.26)$$

The X-ray ranges can be summarized with the help of figure 3.27.



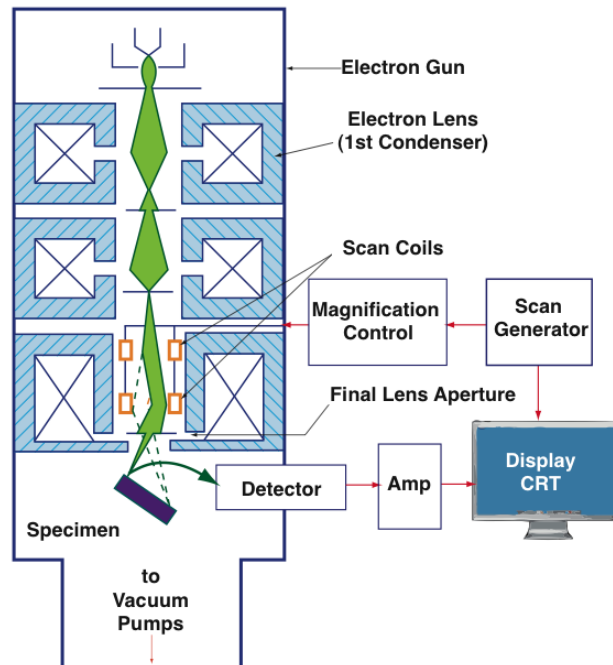
**Figure 3.27** – Comparison of X-ray production regions from specimen with densities of  $3 \text{ g/cm}^3$  (Al) (left) and  $10 \text{ g/cm}^3$  (Cu) (right) [71].

The X-ray range for Al- $K\alpha$  in Al is much greater than that for Cu- $K\alpha$  in Cu. Moreover, the Cu- $K\alpha$  in Al comes from a depth closer to the surface in Al than it does the Al- $K\alpha$ . However, Cu- $K\alpha$  radiation in Al comes from much deeper in the sample than it does the Cu- $K\alpha$  in Cu. For light elements measured in high-Z matrices, the beam size is larger.

Summarizing, electron-beam interactions are responsible for the signals that can be used to reveal the topography and the local chemistry of the sample.

## Image formation

The quality and resolution of SEM images are function of three major parameters: (i) Instrument performance, (ii) selection of imaging parameters, and (iii) nature of the specimen. One of the most surprising aspects of scanning electron microscopy is the apparent ease with which SEM images of three-dimensional objects can be interpreted by any observer with no prior knowledge of the instrument. The main components of a typical SEM are electron column, scanning system, detector(s), display, vacuum system and electronics controls (figure 3.28).



**Figure 3.28** – Main components of a typical SEM: electron column, scanning system, detector(s), display, vacuum system and electronics controls [72].

The electron gun generates free electrons and accelerates these electrons to energies in the range 1-40 keV in the SEM. The purpose of the electron lenses is to create a small, focused electron probe on the specimen. In order to produce images the electron beam is focused into a fine probe, which is scanned across the surface of the specimen with the help of scanning coils (figure 3.29). Each point on the specimen that is struck by the accelerated electrons emits signal in the form of electromagnetic radiation. Selected portions of this radiation, usually secondary (SE) and/or backscattered electrons (BSE), are collected by a detector and the resulting signal is amplified and displayed on a TV screen or computer monitor. The resulting

image is generally straightforward to interpret, at least for topographic imaging of objects at low magnifications. The electron beam interacts with the specimen to a depth approximately 1  $\mu\text{m}$  and complex interactions of the beam electrons with the atoms of the specimen produce wide variety of radiation – as previously explained.

Unlike optical or transmission electron microscopes no true image exists in the SEM. The particularity of SEM is that the image is generated and displayed electronically, where no optical transformation takes place, and no real or virtual optical images are produced.

The primary signal carriers in SEM used to form images are secondary (SE) and backscattered electrons (BSE). SE are low energy particles with typical energy of about 5 eV. BSE are high energy particles with energies approaching the energy of the incident electron beam, e.g. several thousand eV. Compositional contrast or atomic number contrast arises because the intensity of the signal generated from areas with different composition is proportional to the difference in the average atomic number of the respective areas. The most efficient way to image compositional contrast is by using backscattered electrons because of the nearly monotonic increase of the BSE coefficient  $\eta$  with atomic number [71, 72]. Regions of high average atomic number will appear bright relative to regions of low atomic number. The magnitude of the atomic number contrast can be predicted. If a detector sensitive to the number of BSE is used, then the detected signal is proportional to the backscatter coefficient. The contrast between two regions 1 and 2 can be calculated as the difference between the backscatter coefficients ( $\eta_1$  and  $\eta_2$ ):

$$C = \frac{\eta_1 - \eta_2}{\eta_2} \quad (3.27)$$

Elements separated by one unit of atomic number produce low contrast; for example, Al and Si yield contrast of only 6.7%. For elements widely separated in atomic number, the contrast is much larger; for example, Al and Au produce contrast of 69%. Contrast above 10% is relatively easy to image in the SEM, contrast in the range 1 –10% requires careful strategy, and contrast <1% requires extreme measures to successfully image it.

Topographic contrast includes all effects by which the shape and morphology of the specimen can be imaged. Most of applications of the SEM involve studying shapes. Topographic contrast is the most important imaging mechanism. Topographic contrast arises because the



number and trajectories of BSE and the number of SE depend on the angle of incidence between the beam and the specimen's surface. The angle of incidence varies because of the local inclination of the specimen. At each point the beam strikes, the number of BSE and SE detected gives direct information on the inclination of the specimen.

### **Sample requirements**

Since the SEM is operated under high vacuum the specimens that can be studied must be compatible with high vacuum ( $\sim 10^{-5}$  mbar). This means that liquids and materials containing water and other volatile components cannot be studied directly. Also fine powder samples need to be fixed firmly to a specimen holder substrate so that they will not contaminate the SEM specimen chamber. Non-conductive materials need to be attached to a conductive specimen holder and coated with a thin conductive film by sputtering or evaporation. Typical coating materials are Au, Pt, Pd, their alloys, as well as carbon.

### **3.3.4 Experimental setup and methodology**

The experiments have been carried out in two specialized institutions:

- A. At the GeoBioTec – University of Aveiro (Aveiro, Portugal);
- B. At BAM, Federal Institute for Materials Research and Testing, Division 6.8 Surface Analysis and Interfacial Chemistry (Berlin, Germany).

A – In this case, measurements were carried out with a Hitachi S4100 system, equipped with Quantax 400 EDS system of Bruker AXS (XFlash Silicon Drift Detector). A 15 kV acceleration voltage and a current intensity of 32  $\mu\text{A}$  were applied. The chemical information by EDS was taken from an area of  $300 \times 400 \mu\text{m}^2$  selected regarding its homogeneity and lack of voids, with spectrum acquisition times of minimum 60 s. The semi-quantitative results were based on a peak-to-background ZAF evaluation method (P/B-ZAF), being ZAF a matrix correction, mainly based on analytical expressions for atomic number (Z), X-ray yield, self-absorption (A) and secondary fluorescence enhancement (F), provided by the Esprit software.

B – In this case measurements were performed by a scanning electron microscope (SEM) Zeiss Supra 40 with a Schottky field emitter having attached a silicon drift detector energy

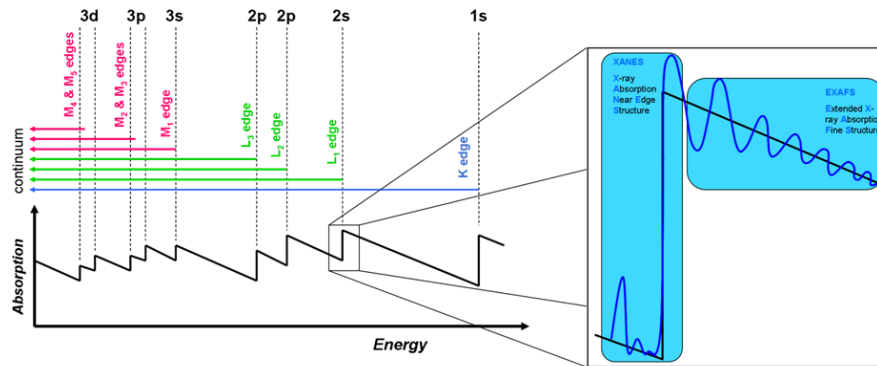
dispersive X-ray spectrometer (SDD-EDS) Quantax 400 from Bruker as well as a Si(Li)-EDS from Thermo Fisher Scientific (see [73-75] for more details). Various beam voltages from 5 to 30 kV have been applied. EDX spectra have been taken mostly in the “point and shoot” mode in order to pick up as much as possible information from representative structural features observed with the SEM.

Both “top” observations of the specimen surface and in the cross-section one through the thick coating(s) have been employed. Depending on the size of the structural features selected for investigation various magnifications have been used, for the real magnification (periodically calibrated) see the micrometer marker on each SEM micrograph. Note that some micrographs have been taken in the conventional (high-resolution) mode of the SEM and some micrographs having associated selected areas for EDX “point and shoot” analyses have been taken over the EDS system in the low-resolution mode. This lies in the need of increasing the efficiency of analysis for the rather high number of samples and investigated areas of interest.

### **3.4 X-ray Absorption Fine Structure (XAFS)**

#### **3.4.1 XAFS principles**

XAFS settles under the physical principle of X-ray Absorption, which is a consequence of the photoelectric effect. One obtains variations of the absorption coefficient of a certain element while the energy of the incident photons is tuned around the absorption edge of that element. XAFS can be divided in two parts, X-ray Absorption Near Edge (XANES) and Extended X-ray Absorption Fine Structure (EXAFS) (figure 3.29).



**Figure 3.29** – Scheme enhancing XANES and EXAFS regions of an absorption edge.

XANES or NEXAFS is related to transitions from core levels to unoccupied levels of the probed atom, which correspond to the edge fine structure. The interpretation of XANES is extremely complicated as there is no simple physical description for it. However, the features of absorption at this region are governed by the density of final states (DOS). Hence, measurements at the XANES region allow the determination of the oxidation state and local coordination number (related to the crystal structure) of the analyzed element.

EXAFS is related to the interference between the outgoing wave (transition from core level to the continuum) and the incoming wave (backscattered from neighboring atoms) (figure 3.30). The variations in the absorption coefficient,  $\mu(E)$ , emerge from the interference between these waves in a probabilistic way and because of this it can only be described quantum-mechanically. As the absorption process represents the transition between two quantum states, one can describe  $\mu(E)$  with Fermi's Golden Rule:

$$\mu(E) \propto |\langle i|H|f\rangle|^2 \quad (3.28)$$

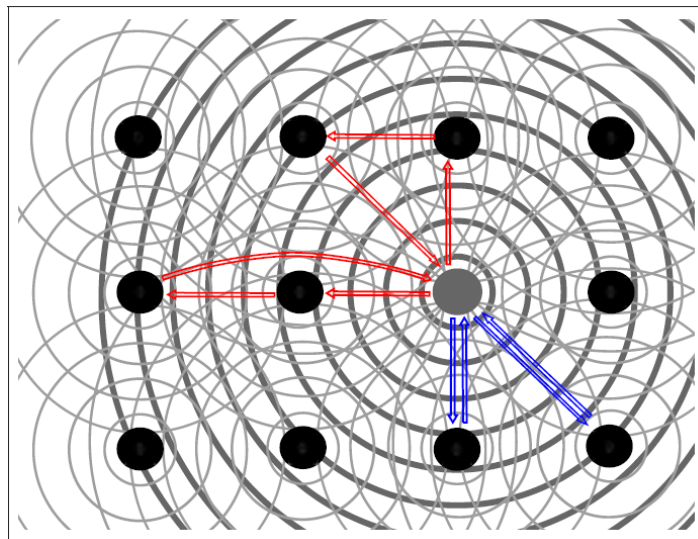
with  $\langle i|$  and  $|f\rangle$  being the initial and final states, respectively and  $H$  is the operator that describes the process of changing between two energy and momentum states. By the presence of a neighboring atom, the photoelectron can be scattered by the electrons of the neighboring atom and return to the absorbing atom, hence the final state will carry this contribution as well [76]. Based on the considerations for the quantum wave theory, the equation for EXAFS can be written as:

$$\chi(k) = \sum_j \frac{N_j e^{-2k^2 \sigma_j^2} \cdot e^{-2R_j/\lambda(k)} \cdot f_j(k)}{kR_j^2} \sin[2kR_j + \delta_j(k)] \quad (3.29)$$

As in real samples more than one neighbor atom is found, equation (3.29) comprises the sum of the contribution of each scattering atom type (also denominated *coordination shell*). Hence,  $j$  corresponds to the individual coordination shells at approximate distance from the probed atom;  $N$  is the coordination number;  $\sigma^2$  is the mean square displacement within the inter-atomic distance ( $R$ );  $\lambda$  is the mean free path of the photo-electron and  $k$  the wave-number.

Some remarks about equation (3.29) are for example: from the terms  $\lambda(k)$  and  $R^{-2}$  the information obtained is local, in the range of 5 Angstroms away from the absorber atom [76]; the amplitude of the EXAFS signal is proportional to the coordination number; the  $\sigma^2$  dampens exponentially and the *sine* factor implies that longer inter-atomic distances result in higher frequency oscillations; this equation breaks down at low- $k$ , which makes it complicated to interpret XANES. In sum, measurements at the EXAFS region provide information about the local surrounding environment (neighbors) of the probed atom.

Examples for further insight on the XAFS theory and properties are given by Rehr et al. [77] and by Yano et al. [78].



**Figure 3.30** – Scheme for single scattering (in blue) and multiple scattering (in red) in the EXAFS region [79].

### 3.4.2 Data handling

Once the spectra are recorded, column ASCII raw data files have to be stored in order to be processed by proper developed software that handle XAFS data. All data were prior normalized to the Ionization Chamber (IC), so that variations in the primary beam intensity are taken into account. For processing the experimental XAFS data ATHENA (v. 0.8.056) was used [80]. This GUI program belongs to the main package IFEFFIT (v. 1.2.11) [80].

The first step for treating a XAFS spectrum is to perform background subtraction by normalization to the edge step, which was carried out automatically using ATHENA. This comprises the pre-edge normalization range (at the very beginning) and post-edge normalization region (at the far energy region). After normalization the pre-edge and post-edge regions become parallel and the automatic background subtraction takes into account the regions previously defined.

For the XANES measurements, the use of materials with known crystal structures is most of the time the best approach to infer about the unknown samples. XANES scans were performed on the original samples as well as on reference materials (known valence and coordination) and prepared replicas. Using the ATHENA program a linear combination fitting routine was performed taking all reference spectra into account in order to compare with the 'unknown' spectra. A weight of the contribution that each reference has on the 'unknown' spectrum gives, therefore, a hint of the possible valences and coordinations.

Regarding the EXFAS region, measurements were performed on original samples, reference materials and replicas. With ATHENA one can plot  $\chi(k)$  against  $R(\text{\AA})$  and the oscillations represent different frequencies, which correspond to the different distances for each coordination shell. Hence, Fourier transforms (FT) are necessary for the analysis process. The FT from the k-space to R-space was performed with a Hanning-type window with a range of 2  $\text{\AA}$  to 14  $\text{\AA}$ . However, if one keeps just comparing the oscillations between spectra, the reliable knowledge obtained is limited, since accurate results are given for the first two or three neighbor shells only. Software codes such as FEFF [81] provide accurate scattering factors which

are taken into account for multiple scattering phenomena and assist the conclusions about the neighboring environment of the probed atom.

### 3.4.3 Experimental setup and methodology

XAFS measurements at the Sb-K edge and at the Pb-L3 edge were performed, and for this case two beamlines with different experimental specifications were used:  $\mu$ Spot beamline and BAMline. Even if both beamlines – at the BESSY-II storage ring (Berlin, Germany) – use the same 7 T wavelength shifter as insertion device, they have very different qualities. The advantage of the  $\mu$ Spot beamline is the higher photon flux – due to a focusing mirror – in the energy region from 1 keV to about 25 keV ( $>10^{11}$  ph/s), while at the BAMline the flux in this energy range is about two orders of magnitude lower. Above 25 keV the photon flux of the  $\mu$ Spot drops rapidly under  $10^8$  ph/s, while at the BAMline this mark is only reached at about 75 keV. Furthermore,  $\mu$ Spot beamline allows a depth resolved speciation of a certain chemical state of a given element (by means of 3D Micro-XAFS), with a reliable reconstruction procedure recently developed by Lühl et al. [82]. This beamline uses a seven-element Si(Li) detector (from e2v, Sirius model, UK) with an active area of  $30\text{ mm}^2$  each, and a polycapillary half-lens was placed in front of one of them. At the excitation channel, a polycapillary half-lens was also used, having a FWHM  $18\text{ }\mu\text{m}$  for Cu-K $\alpha$  ( $\sim 9\text{ keV}$ ). Furthermore, the transmission function of this lens has a maximum at around 15 keV.

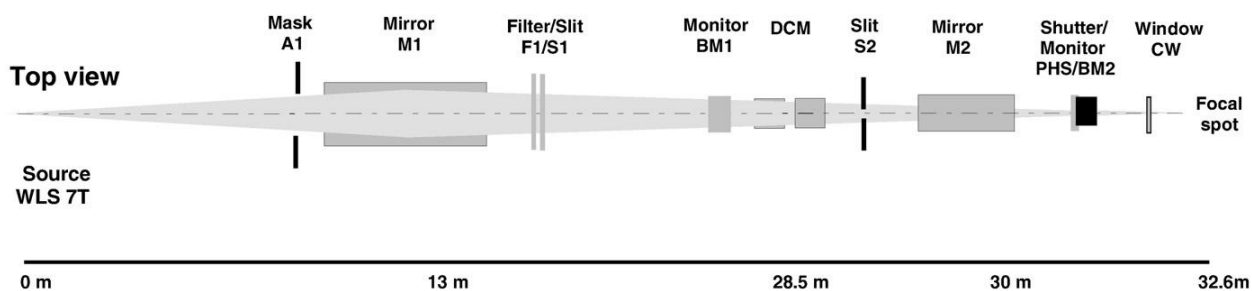
Both beamlines use a double crystal monochromator (DCM) with Si (311) crystals at the  $\mu$ Spot (energy resolution  $E/\Delta E \approx 25000$ ) and Si (111) crystals at the BAMline ( $E/\Delta E \approx 5000$ ). Further detailed descriptions of the  $\mu$ Spot beamline can be found in [83] and further technical data for the BAMline can be found in [84]. Furthermore, the radiation detection at the BAMline was carried out by means of a Si(Li) detector from e2v as well but this one is a single-element detector with an active area of  $30\text{ mm}^2$ .

Both conventional and confocal measurements were performed in order to evaluate the usefulness of the latter geometry for the samples hereby described. It was proven that given the thickness and high-Z matrix of the samples, no significant alteration of the signal was obtained by measuring in conventional mode. At the  $\mu$ Spot conventional Pb-L3 XANES

measurements were performed on both yellow and glaze surfaces, while at the *BAMline* both conventional Pb-L3 EXAFS and Sb-K XANES and Sb-K EXAFS measurements were performed.

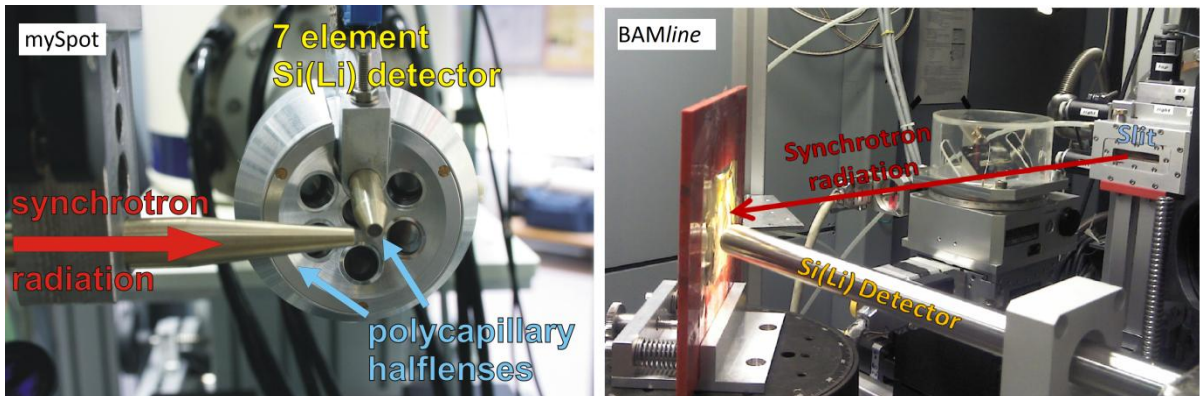
All measurements were performed in fluorescence mode, as the samples are thick and contain high Z matrix. Furthermore, thin sections could not have been obtained because one is dealing with Cultural Heritage (CH) related objects and a non-destructive approximation is a requisite for this investigation.

The experimental setup at the *BAMline* is the same as shown before (*cf.* figure 3.22), except that instead of the CRL lenses, a slit with an aperture of 3x1 mm, was used. The experimental setup at the  $\mu$ Spot is depicted in figure 3.31.



**Figure 3.31** – Optical layout of the MySpot beamline. Energy range of 4.5 keV–30 keV. Angular acceptance of 1.5 mrad (h)  $\times$  0.2 mrad (v) [83].

Pictures of both setups are shown in figure 3.32a (for the  $\mu$ Spot) and 3.32b (for the *BAMline*).



**Figure 3.32** – left-hand side: setup at the  $\mu$ Spot beamline with possibility of 3D Micro-XRF and –XAFS by the lenses mounted on the upper detector element (picture by I. Mantouvalou [61] ; right-hand side: setup at the BAMline for XAFS measurements (picture by A. Guilherme).

### 3.5 Statistical data handling

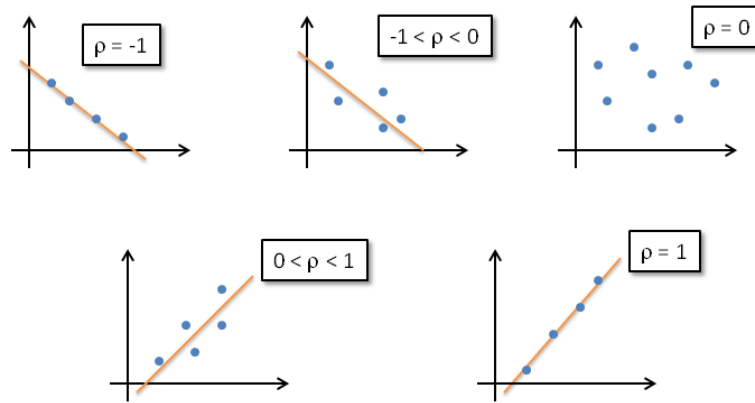
When performing scientific studies, the search for patterns among the analytical data becomes necessary to assist the conclusions. For this purpose, statistical data handling is essential. The only remaining question is what kind of treatment is suitable for the present study.

Statistical studies can be separated into two big groups: parametric and nonparametric methods. Parametric studies follow well-known distributions, such as the *Gaussian* distribution where individual data are specified by assigning constant values to two parameters (normally these are the mean -  $\mu$  - and the variance -  $\sigma^2$ ). However, to perform a parametric inference on any population of data is most of the times unreasonable, even if one has precise measurements, as one is implying a certain normality within the data (mean, median and mode) that may not exist [85].

Based on the aims of this investigation, finding correlations can be quite useful to determine relationships between the data and aid the conclusions. Correlation is a measure of the relationship between two variables. This can be performed using the Pearson correlation coefficient, denoted by  $\rho$  (rho), which – in the parametric context – estimates the degree of linearity between two variables. This coefficient can assume values between -1 and +1. When  $\rho = -1$ , there is a negative correlation between the variables (they are inversely proportional),



when  $\rho = +1$  there is a positive correlation (they are directly proportional), and when  $\rho = 0$  there is no linear correlation (they are either independent or there is a non-linear relationship between them) [85]. In figure 3.33 a representation of the different correlation values of  $\rho$  is given.



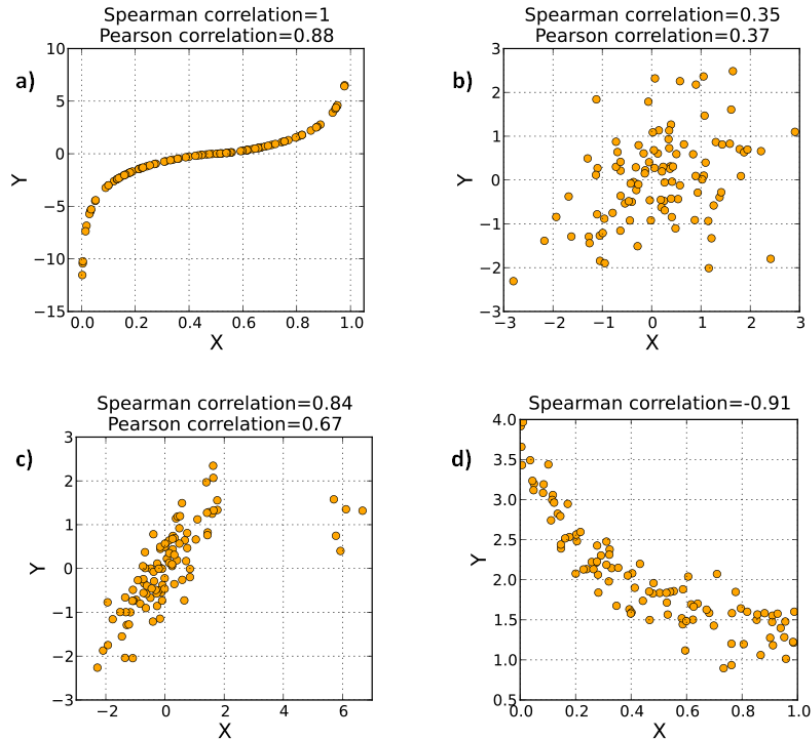
**Figure 3.33** – Examples of different Pearson correlation coefficient values ( $\rho$ ) [86].

However, the limitation of this method is being sensitive to linear dependence only. Other more robust correlation coefficients have been developed, which are sensitive to nonlinear relationships as well, such as the Spearman rank correlation coefficient. This coefficient denoted by  $r_s$ , is a nonparametric measure of the statistical dependence between two variables, inferring on how well the relationship between these variables can be described using an order function (monotonicity) [85]. The Spearman's coefficient can be calculated by equation 3.25:

$$r_s = 1 - \frac{6[\sum_i(r_i - s_i)^2]}{n(n^2 - 1)} \quad (3.30),$$

where  $\sum_i(r_i - s_i)^2$  represents the sum of the squares of the difference between the ranks of each sample pair and  $n$  is the number of individuals for the sample. Here the raw data variables  $(x_i, y_i)$  are replaced by their ranks  $(r_i, s_i)$ . If the x and y ranks are all equal for each individual one obtains  $r_i = s_i$ , then the sum term becomes zero and  $r_s = 1$ . For the opposite situation one obtains  $r_s = -1$ . If there is no correlation between ranks,  $r_s = 0$  [85]. Figure 3.34

shows some examples of possible correlations obtained with the Spearman correlation coefficient [87].



**Figure 3.34** – Examples of different Spearman correlation coefficient values ( $r_s$ ): a)  $r_s = 1$  when two variables are monotonically related, even when their relationship is not exactly linear (proven by the Pearson coefficient ( $\rho$ ) as well); b) there is not an obvious relationship between the variables and the coefficients assume values close to zero (also from  $\rho$ ); c) there seems to exist a linear correlation between the variables but  $r_s$  is not so sensitive to outliers than the  $\rho$ ; d) in this case a negative  $r_s$  corresponds to a decreasing monotonic tendency between the two variables [87].

When using such methods one should determine its significance – that is, how stable the relationship found between the data is. This is provided by the  $p$ -value – the probability of error that is involved in accepting the observed result as valid. This directs to a statistical hypothesis test that consists in two hypotheses: the null hypothesis ( $H_0$ ), which is going to be tested and the alternative hypothesis ( $H_1$ ) that corresponds to the sample observations. For the present case, the used test was the so-called two-tailed test, which means that  $H_0$  is equal a certain value and  $H_1$  assumes any other value different from  $H_0$  [85]. In the presented studies, using the

Spearman correlation method,  $H_0$  – represents no correlation and  $H_1$  – represents a correlation.  $H_0$  will be rejected if  $p \leq 0.05$  and for these cases a correlation between variables is found.

Another important tool for the present investigation is cluster analysis (CA). CA provides meaningful taxonomies, groups or clusters of data based on combinations of instrumental variables (IV), which maximizes the similarity of cases within each cluster while maximizing the dissimilarity between groups that are initially unknown [88]. As the number of groups or clusters that will emerge is unknown, this technique follows two stages:

- 1) Carry out a hierarchical cluster analysis using the *Ward's* method applying squared Euclidean Distance as the distance or similarity measure;
- 2) Rerun the hierarchical cluster analysis with a selected number of clusters, which enables to allocate every case in ones sample to a particular cluster.

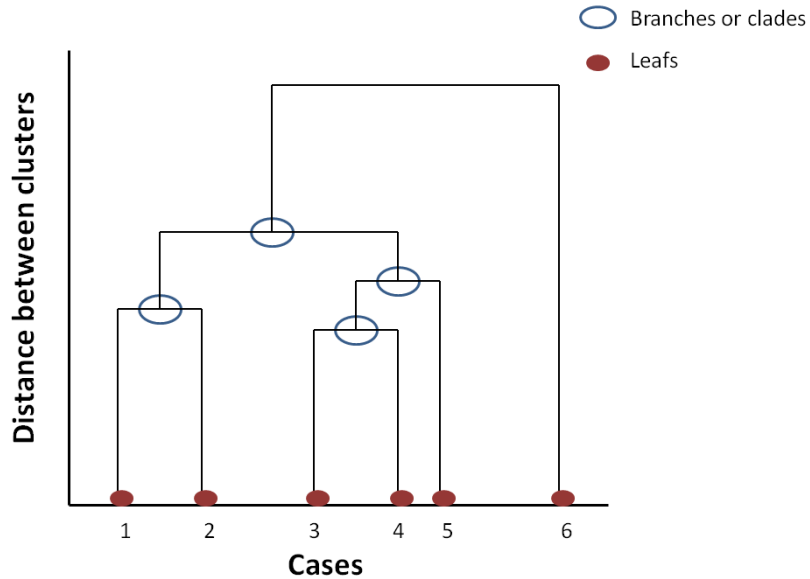
Euclidean distance is an ordinary distance between two points that can be measured with a ruler, which is the simpler way of computing distances between objects in a multi-dimensional space, as they represent an extension of the Pythagoras' theorem. Moreover, the squared Euclidean distance is used more often than the simple Euclidean distance in order to place progressively greater weight on objects that are further apart [88].

The next important topic is to choose the clustering algorithm, i.e. the rules that govern between which points distances are measured to determine cluster membership. Among all the possible clustering methods, the *Ward's* method will be used. This method uses an analysis of variance<sup>5</sup> approach to evaluate the distances between clusters. Cluster membership is evaluated by calculating the total sum of squared deviations from the mean of a cluster. The cluster criterion should produce the smallest possible increase in the error sum of squares.

A dendrogram is a graphical representation of hierarchical cluster analyses. It is a branching diagram that represents the relationships of similarity among a group of entities. Figure 3.35 shows an example a dendrogram in horizontal display.

---

<sup>5</sup> A measure of how far the set of numbers is spread out.



**Figure 3.35** – Example of a dendrogram. The blue circles represent the branches (or *clades*) and the dark red filled circles mark the so called *leaves*.

The height of the vertical lines indicates the degree of difference between branches – the longer the line, the larger the difference. For example, cases 3 and 4 are more similar to each other than cases 1 and 2 because the height of the vertical lines of the former is smaller than the latter. One can find clusters at any height of the dendrogram, as at each clade a new cluster appears. It is just a matter of choosing a distance between clusters.

The software used for the statistical data handling was SPSS (Statistical Package for Social Sciences), version 20.0.

## CHAPTER 4 – RESULTS

### 4.1 – Suitability of XRF for glazed ceramics analyses

Due to high heterogeneity among glazed ceramic objects, one must primarily distinguish the scale at which differences in the composition occur especially if the chosen techniques are providing reliable information at that scale. This is intrinsically related to the resolution and the sensitivity of the technique and in order to evaluate this and other crucial technical features, the suitability of the XRF setup for the present case study was evaluated. The following topics were considered:

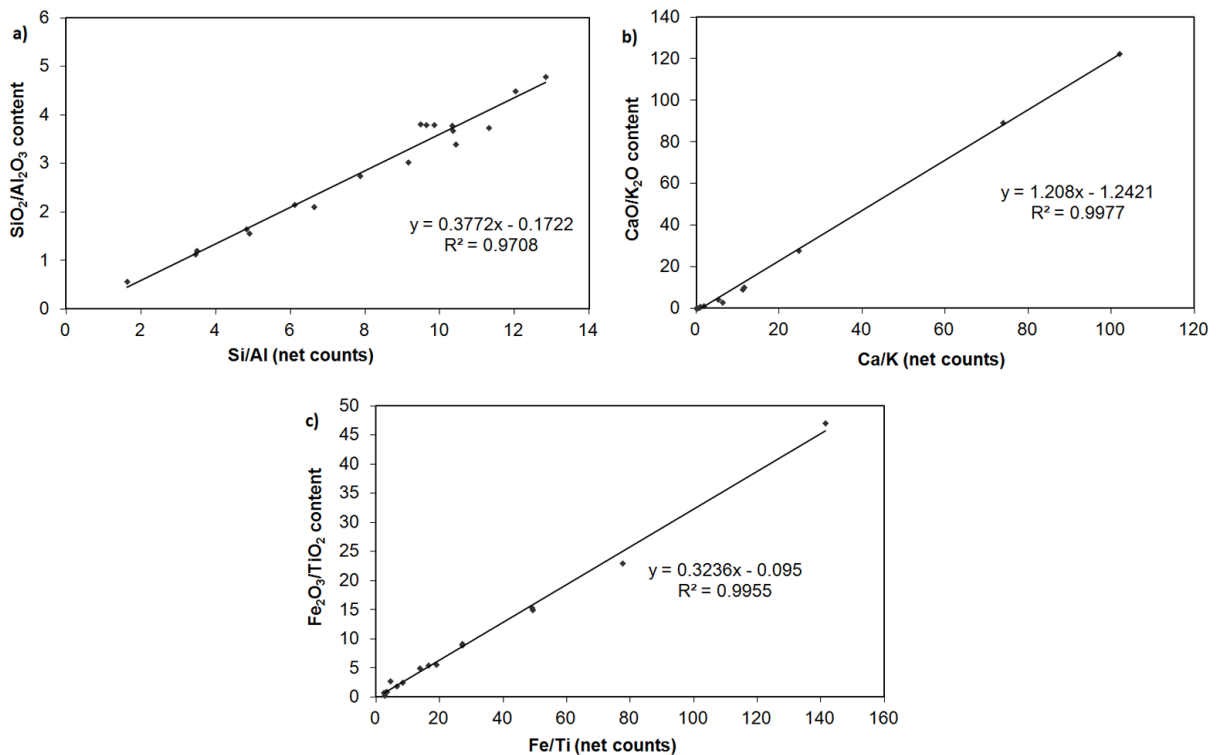
- i) Analysis of standard reference materials with two emission modes: polycapillary lens and collimator;
- ii) Performance tests: linearity through calibration curves;
- iii) Estimation of the mass attenuation coefficient of the specimen based on the Compton peak intensity.

Two groups of standard reference materials are presented: the silicates group to infer on the ceramic body and the glasses group to infer on the glaze.

The silicates group was provided by I. Queralt from the Spanish National Research Council (CSIC) in Barcelona, Spain. All of them are Geochemical Certified Reference Materials (CRM's), with data reported in the Govindaraju's compilation [89]: Basalt (BE-N), Diorite (DR-N), Granite (GS-N), Anorthosite (AN-G), Granite (MA-N), Granite (AC-E), Dolerite (WS-E), Microgabbro (PM-S); Potash Feldspar (BCS-376), Firebrick (BCS-315) and Sillimanite (BCS-309). The glasses group belongs to CFAUL and the CRM's are: SRM-612 (from NIST – National Institute of Standards and Technology), Fluoride Opal Glass SGT-4, Soda-Lime-Magnesia-Silica Glass SGT-5, Soda-Lime-Silica Glass SGT-7, Lead-Oxide-Potassium Oxide-Silica Glass SGT-8 (Standard Glass Technology).

The silicates group represents prepared pressed powder pellets with a nominal mass of 5 g. In the glasses group only the SRM-612 is a pressed pellet. SGT-4 was supplied as white pieces; SGT-5, SGT-7 and SGT-8 as colorless glass pieces.

Some characteristics and distinctive features of different ceramics can be found among relationships between chemical elements playing similar roles in the structure (network formers, modifiers, nucleating agents, etc.) in ceramic production process. Hence, the linearity between several elemental ratios was checked and is displayed in figure 4.1. The x-axis represents the net peak area ratios between neighbor elements and the y-axis represents oxide composition found in the sheets from the certifying company. Through this relationship one is able to retrieve directly the ratio between the respective oxides (usual form in ceramic chemical assemblages).



**Figure 4.1** – Linearity response with net peak area ratios of neighboring elements and respective tabled oxide composition for all the silicate standard reference materials.

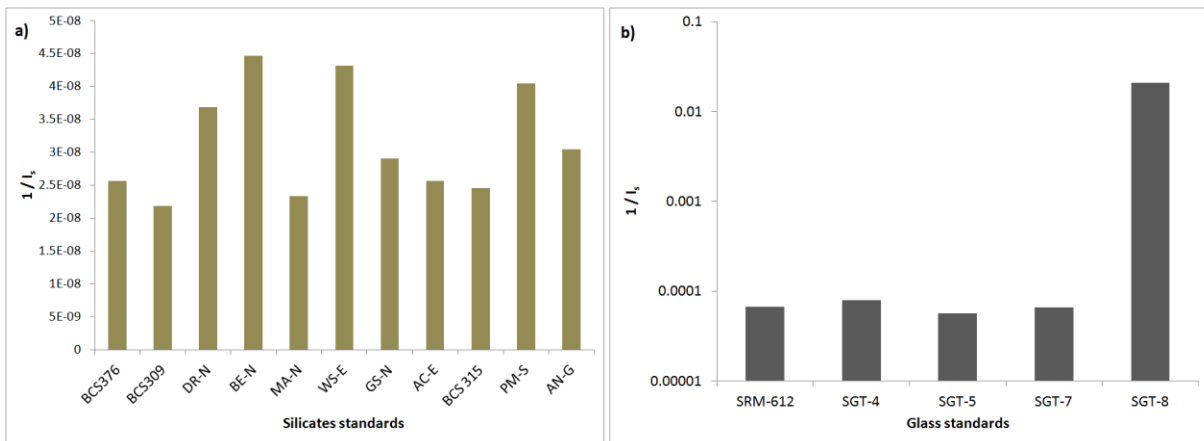
Since Compton scattering increases with decreasing average atomic number (*cf.* chapter 3, sub-section 3.1.2), a way of estimating the matrix effects is to evaluate the Compton scatter peak from the characteristic X-ray lines of the tube anode material (*cf.* chapter 3, section 3.2).

Since the intensity of the Compton peak ( $I_s$ ) is inversely proportional to the mass attenuation coefficient ( $\mu_s$ ) of the specimen,

$$I_s(\lambda_s) \sim \frac{1}{\mu_s(\lambda_s)} \quad (4.1)$$

it can be used to estimate the absorption coefficient of the sample at the wavelength (or energy) of the scattered photons [90].

The analyzed spectra of the silicates and glass standards were fitted and the Compton net peak areas were used to estimate the mass attenuation coefficient ( $\mu_s$ ) in the specimen, using (4.1). Figure 4.2 shows the order of magnitude for the  $\mu_s$  in each standard. In figure 4.2a one sees that the values for  $\mu_s$  are of the same order of magnitude for the different standards, which means that the matrix average atomic number (Z) does not vary significantly among the different silicates. Conversely, in figure 4.2b a difference of two orders of magnitude for the  $\mu_s$  between the glass standard SGT-8 and the rest is observed. This can be explained by the high lead oxide (PbO) content present in the SGT-8 standard (about 31%), while in the other glass standards PbO is a minor or trace compound.



**Figure 4.2** – Mass attenuation coefficient ( $\mu_s$ ) estimation by calculating the inverse of the Compton scatter intensity ( $I_s$ ) at the wavelength of Mo- $K\alpha$ , for a) silicates standards and b) glass standards.

Since  $\mu_s$  and  $I_s$  are inversely proportional, it becomes clear that the higher the average atomic number (Z) of the sample the lower the Compton peak and the stronger the mass attenuation coefficient.

One of the most important aspects is the fact that the features hereby presented are at a qualitative level and can provide significant information about the samples by comparing elemental ratios. Quantification was not performed in this investigation, due to compositional heterogeneities and irregularities in the thickness of layers.

## **4.2 – Original samples: fragments**

The structure of this section is based on the comparison between the two ceramic production centers to enhance differences and/or similarities between the technological aspects of these objects. This study corresponds to analyses performed on fragments from faiences from Coimbra and wall-tiles both from Coimbra and Lisbon (*cf.* Annex 1.3). A shorter version of this study for whole museum objects is presented further in section 4.4 – *In situ analysis of whole Museum objects*.

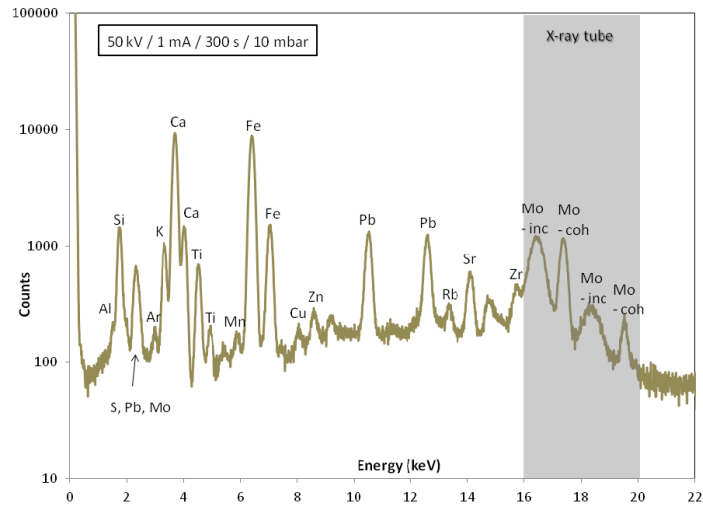
As previously described (*cf.* chapter 1, section 1.2) these objects are composed by three main zones: body, glaze and surface decoration. Hence, a subsection focused on each part of the samples is created in order to compare their features.

### **4.2.1 – Ceramic body**

#### ***X-ray Fluorescence (XRF)***

Conventional XRF measurements were performed in the ceramic body of all available pieces. In figure 4.3 an example of the elemental variability found in the ceramic support is shown.

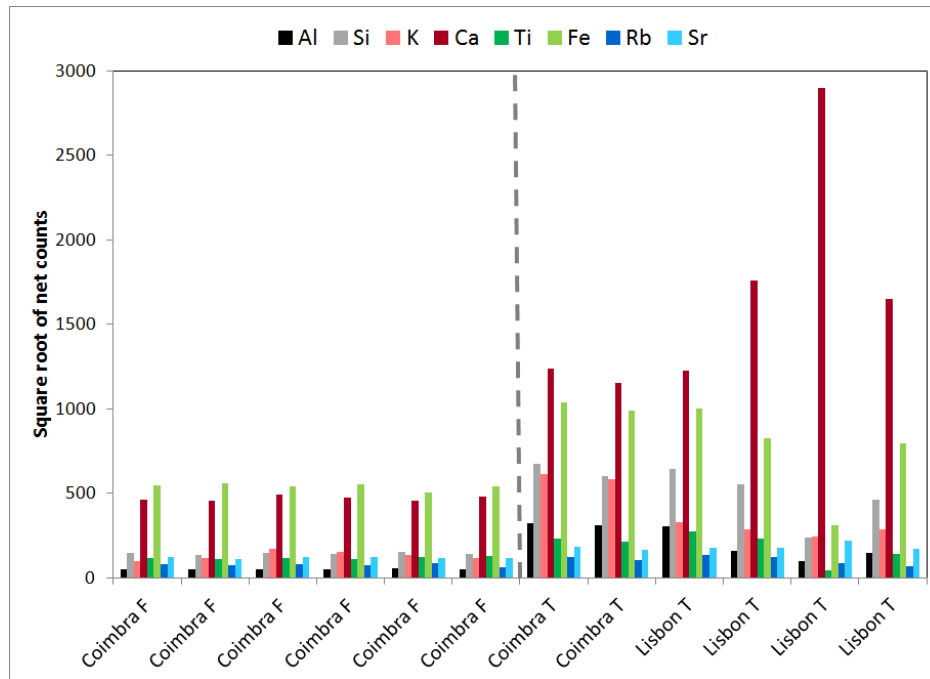




**Figure 4.3** – XRF spectrum of the ceramic body of faience from Coimbra, obtained in conventional mode.

From the spectrum depicted in figure 4.3 one sees that apart from the expected (main) presence of Al and Si, the major elements are K, Ca and Fe. These are a hint for the (expected, as well) presence of feldspars, more precisely potash-feldspar (microcline or orthoclase) and calcium plagioclase (Anorthite). Another important element, which comes normally in association to feldspars, is sodium (Na). This, however, could not be detected by the used spectrometer, as its quantity lies below the detection limit.

Another important aspect to discuss about is the thickness of the samples. The fragments from faience samples are all thin (max. 2 mm thick body). XRF analyses on the ceramic body were performed on the back side (non-glazed). As previously described (*cf.* chapter 1, subsection 1.2.1) the elemental variability within the ceramic support is strongly dependent on the geological resources of the region as well as the manufacturing techniques employed. For this reason, a comparison of the most significant elements within the ceramic body composition between the different samples (faiences from Coimbra, wall-tiles from Coimbra and from Lisbon) was carried out (figure 4.4).

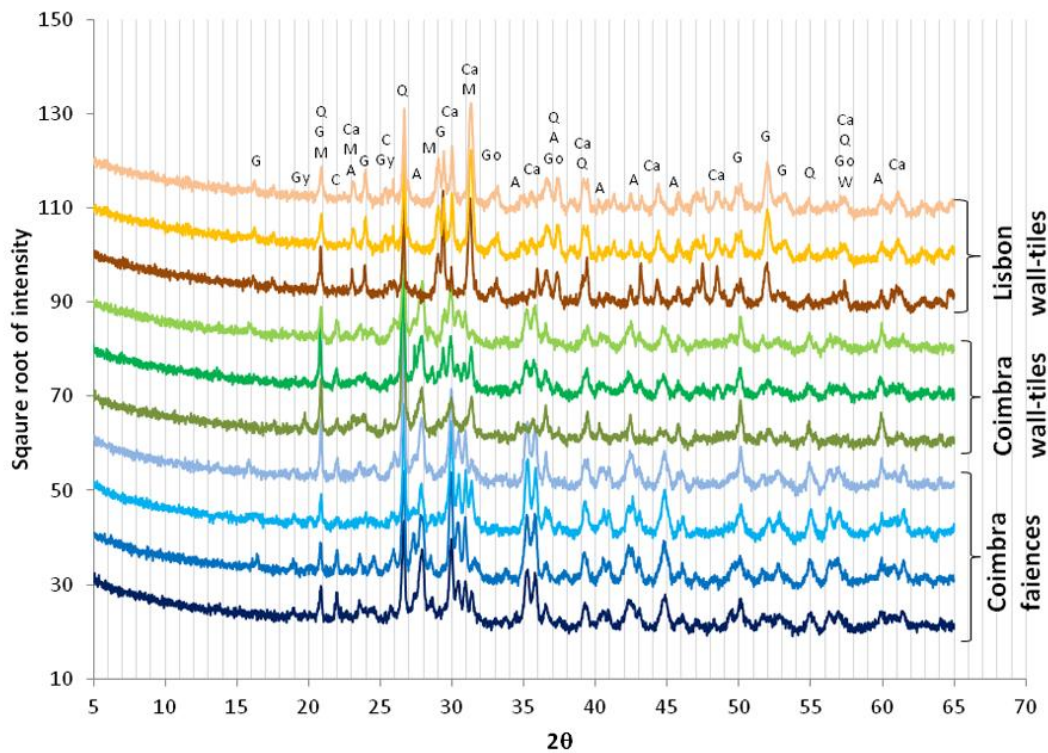


**Figure 4.4** – Comparison of most significant elements that constitute the ceramic body (Al, Si, K, Ca, Ti, Fe, Rb, Sr) between faiences from Coimbra (Coimbra F), wall-tiles from Coimbra (Coimbra T) and wall-tiles from Lisbon (Lisbon T).

From figure 4.4 one extracts that a difference between some elements, such as Ca and Fe, exists. Faiences from Coimbra (Coimbra F) show higher Fe count rate than Ca, which does not happen for the wall-tiles from Coimbra (Coimbra T) and Lisbon (Lisbon T). Moreover, there is a one order of magnitude difference for the Fe count rate between wall-tiles and faiences. In general, the elemental variability is much more constant for the faience samples, than for the wall-tile samples, which is intrinsic to the manufacturing process (*cf.* chapter 5).

### ***X-ray Diffraction (XRD)***

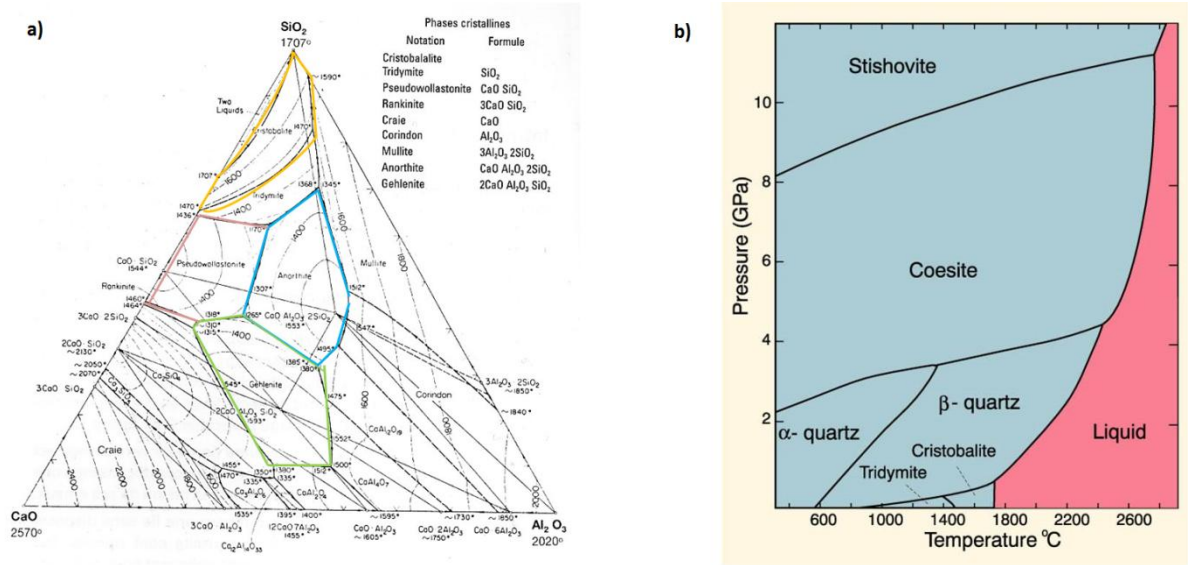
As complementary information to the so far presented results, XRD measurements were also performed on the ceramic support of some of the samples (figure 4.5). At this point it is important to highlight that this is a destructive procedure and, therefore, just some pieces were able to be analyzed. To these results, specifically the ones from faiences from Coimbra, the work developed by M. J. Fonseca [91] was taken into account.



**Figure 4.5** – Diffractograms of the ceramic bodies of 4 faiences from Coimbra (blues), 3 wall-tiles from Coimbra (greens) and 3 wall-tiles from Lisbon (red-oranges). The crystalline phases are marked on the top, assigned with initials: G – Gehlenite; Gy – Gypsum; Q – Quartz; M – Microcline; C – Cristobalite; Ca – Calcite; A – Anorthite; Go – Goethite; W – Wollastonite.

In general, quartz ( $\text{SiO}_2$ ) and alkali feldspars (Microcline (**M**):  $\text{KAlSi}_3\text{O}_8$  - K-rich) are the crystalline phases identified among all samples, as well as Gypsum ( $\text{CaSO}_4 \cdot 2\text{H}_2\text{O}$ , denoted as **Gy**) but with a much lower significance. Other feldspars that are Ca-rich, such as Anorthite:  $\text{CaAl}_2\text{Si}_2\text{O}_8$  (denoted as **A**) are identified with higher significance among the samples from Coimbra – faiences and wall-tiles – with more intense diffraction peaks for faiences. Calcite ( $\text{CaCO}_3$ , denoted as **Ca**) and Gehlenite ( $\text{Ca}_2\text{Al}(\text{AlSiO}_7)$ , denoted as **G**) are identified with higher significance among the wall-tiles from Lisbon. In addition, Wollastonite ( $\text{CaSiO}_3$ , denoted as **W**) and Goethite ( $\text{FeO}(\text{OH})$ , denoted as **Go**) are identified only in the wall-tiles from Lisbon. At last, Cristobalite (denoted as **C**) – which is a high-temperature polymorph of silica (same chemical

formula but different crystal structure) – is pronounced among the samples from Coimbra (faïences and wall-tiles) only, at around  $2\theta = 22^\circ$ .



**Figure 4.6** – a) Phase equilibrium diagram of CaO-Al<sub>2</sub>O<sub>3</sub>-SiO<sub>2</sub> [92]. Cristobalite (in yellow), Anorthite (in blue) and Gehlenite (in green) are some of the crystalline phases identified by the diffractograms; b) Phase-diagram of SiO<sub>2</sub> [93].

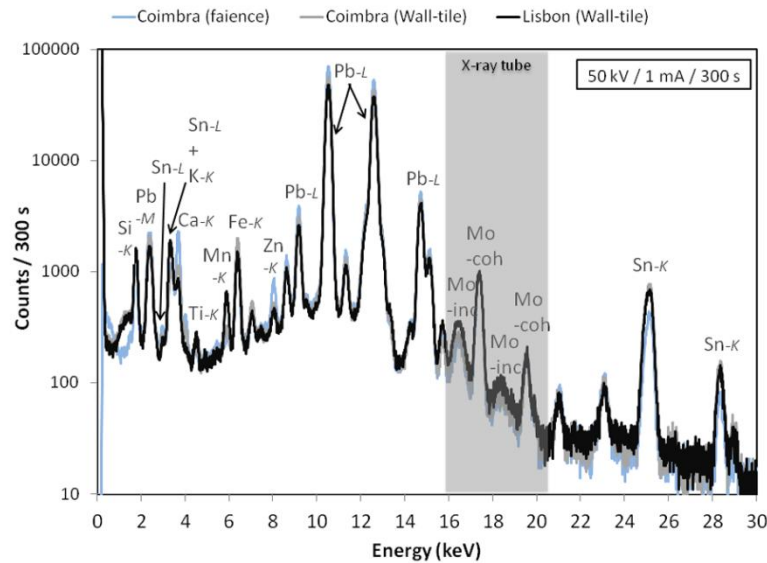
Regarding Cristobalite, its presence in XRD diagrams is a strong hint of the cooling process occurred. As the firing temperature increases, silica undergoes the so-called “quartz inversion” – from quartz- $\alpha$  to quartz- $\beta$  - and when the pressure increases, polymorph phases such as Tridymite and Cristobalite are formed (figure 4.6b). If the cooling process is made rapidly enough, typical high-temperature phases keep in the structure along with some thermal tensions, which leads to a more fragile object.

## 4.2.2 – Glaze

### X-ray Fluorescence (XRF)

Conventional XRF measurements were performed on the glazed surfaces (white areas) of all samples in order to compare the elemental content. In this case, the incident beam was

conducted through the collimator and the analyzed areas of about 1.2 mm<sup>2</sup> give reliable information of the whole glazed white parts of the samples, due to their intrinsic heterogeneity. Yet, three measurements on each sample in different spots were carried out and averaged for each sample. Figure 4.7 is an example of the elemental diversity found in such glazes, and in this case it corresponds to a faience and a wall-tile from Coimbra as well as a wall-tile from Lisbon.

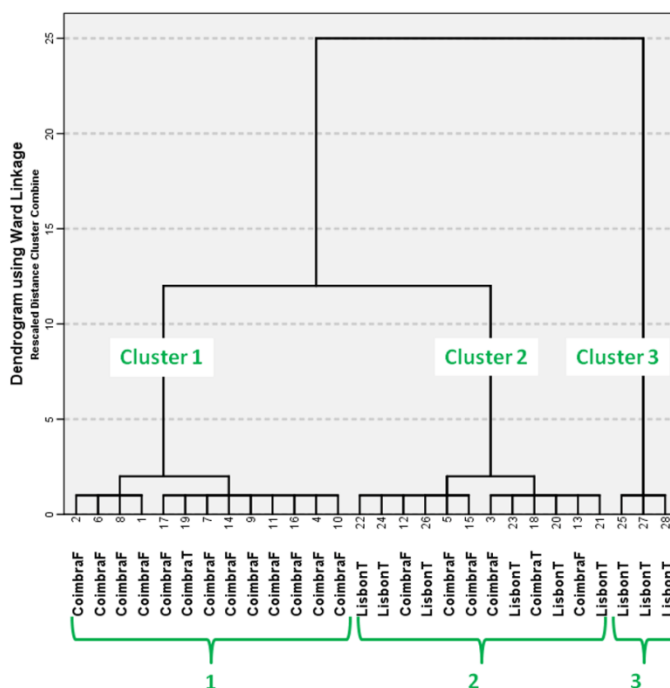


**Figure 4.7** – XRF spectra of the glaze of a faience and a wall-tile from Coimbra and wall-tile from Lisbon, obtained in conventional mode. Elemental recognition indicates a lead-tin-based glaze.

From figure 4.7 one sees that the elemental distribution of the glazes is quite similar among the three different groups of samples. From the spectra the only differences identified are higher concentrations of Ca, Zn and Pb and lower of Sn in the faience sample in comparison to the wall-tiles from Coimbra and Lisbon. The four peaks assigned as “Mo-inc” and “Mo-coh” correspond to the incoherent (Compton) and coherent (Rayleigh) lines characteristic from the anode material (Mo) of the X-ray tube, respectively.

The elemental variability in these samples is broad and it is important to mention here that there are elements present, such as B, Na and Mg, which cannot be detected by this experimental system.

In order to assign possible groups regarding the chemical information of the different types of ceramic objects here investigated, statistical clustering methods were a choice for such purposes. The input data for the dendrogram in figure 4.9 are the net peak areas of the elements that mostly characterize the glazes: Al, Si, K, Ca, Ti, Mn, Fe, Cu, Zn, Sn and Pb.

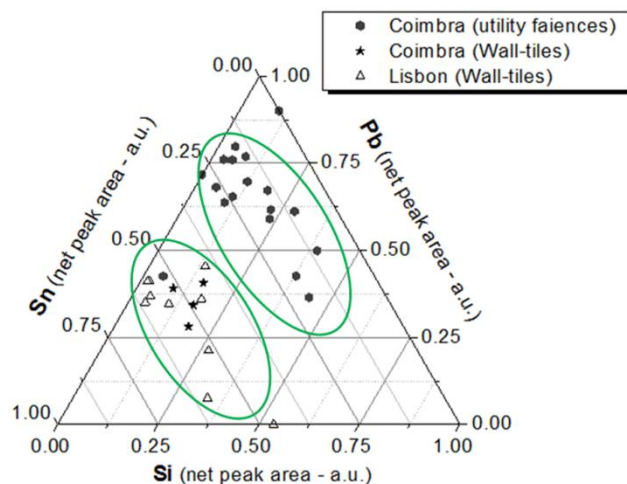


**Figure 4.8** – Dendrogram representing the clusters formed with the elemental data obtained from conventional XRF. Three clusters are unambiguously formed.

From the dendrogram (figure 4.8) one sees that three clusters can be clearly identified. Cluster 1 comprises Coimbra samples only, cluster 2 has a mixture of both Coimbra and Lisbon samples and cluster 3 includes samples from Lisbon only.

One of the most characteristic features of the presented samples is opacifying character of the glazes, owed to introduction of cassiterite ( $\text{SnO}_2$ ) in the chemical composition. A ternary diagram between silicon (Si), lead (Pb) and tin (Sn) is plotted in figure 4.9. The data points correspond to net peak areas from the fitted XRF spectra (in conventional mode). These elements were chosen due to their role in glazes, as previously described (*cf.* chapter 1). Si has a structural role in the glaze as is a network-forming agent; Pb has a network-modifier nature and Sn was introduced as an opacifier agent. Differences between these three elements (or

compounds) will provide a first-approach confirmation about the use of these raw materials and, hence, about the manufacturing processes.



**Figure 4.9** – Ternary diagram Si-Sn-Pb with net peak areas obtained by conventional XRF on glazes of all analyzed samples: utility faiences from Coimbra (●), wall-tiles from Coimbra (★) and wall-tiles from Lisbon (△).

From figure 4.9 one can identify two distinct groups of data. The faience samples (Coimbra) are emphasized by lower counts of Sn and higher counts of Pb in comparison to the wall-tile samples (Coimbra and Lisbon). At this point finding correlations between elemental data will be useful to trace the choice of raw materials for both manufacturing centers as well as different types of objects (faiences and tiles). For this purpose, Spearman correlation tests were performed for the different groups of samples (faiences and tiles). Table 4.1 shows the correlation coefficients between the elements that constitute the glazes of faiences from Coimbra.

**Table 4.1** – Spearman correlation coefficient ( $\rho$ ) for net peak areas of the elements that most characterize the glazes of faiences from Coimbra (N = 18). ‘\*\*\*’ indicates that the correlations are significant at the  $p < 0.01$  level; ‘\*’ indicates that the correlations are significant at the  $p < 0.05$  level.

		Al	Si	S	K	Ca	Ti	Mn	Fe	Cu	Zn	Sn	Pb
<b>Al</b>	$\rho$		-.440	.293	-.688**	.435	-.034	-.071	-.150	.243	.160	-.209	-.244
	Sig. (2-tailed)		.077	.254	.002	.081	.896	.788	.567	.348	.541	.420	.344
<b>Si</b>	$\rho$	-.440		-.490*	.625**	-.162	.136	.071	.107	-.134	.060	.328	-.051
	Sig. (2-tailed)	.077		.046	.007	.535	.604	.786	.684	.609	.819	.199	.846
<b>S</b>	$\rho$	.293	-.490*		-.392	-.044	-.356	-.461	-.439	-.309	-.389	-.339	.123
	Sig. (2-tailed)	.254	.046		.119	.866	.161	.062	.078	.228	.123	.184	.639
<b>K</b>	$\rho$	-.688**	.625**	-.392		-.248	.245	.015	.248	-.284	.009	.329	-.135
	Sig. (2-tailed)	.002	.007	.119		.338	.343	.955	.338	.269	.974	.197	.605
<b>Ca</b>	$\rho$	.435	-.162	-.044	-.248		.272	.499*	.412	.588*	.195	.114	-.023
	Sig. (2-tailed)	.081	.535	.866	.338		.290	.041	.101	.013	.453	.663	.929
<b>Ti</b>	$\rho$	-.034	.136	-.356	.245	.272		.342	.560*	-.170	-.343	.094	-.224
	Sig. (2-tailed)	.896	.604	.161	.343	.290		.179	.019	.513	.178	.720	.387
<b>Mn</b>	$\rho$	-.071	.071	-.461	.015	.499*	.342		.671**	.660**	.331	.346	.114
	Sig. (2-tailed)	.788	.786	.062	.955	.041	.179		.003	.004	.194	.173	.662
<b>Fe</b>	$\rho$	-.150	.107	-.439	.248	.412	.560*	.671**		.225	.239	.189	-.179
	Sig. (2-tailed)	.567	.684	.078	.338	.101	.019	.003		.384	.355	.468	.491
<b>Cu</b>	$\rho$	.243	-.134	-.309	-.284	.588*	-.170	.660**	.225		.598*	.485*	.284
	Sig. (2-tailed)	.348	.609	.228	.269	.013	.513	.004	.384		.011	.049	.270
<b>Zn</b>	$\rho$	.160	.060	-.389	.009	.195	-.343	.331	.239	.598*		.257	.156
	Sig. (2-tailed)	.541	.819	.123	.974	.453	.178	.194	.355	.011		.319	.550
<b>Sn</b>	$\rho$	-.209	.328	-.339	.329	.114	.094	.346	.189	.485*	.257		.277
	Sig. (2-tailed)	.420	.199	.184	.197	.663	.720	.173	.468	.049	.319		.283
<b>Pb</b>	$\rho$	-.244	-.051	.123	-.135	-.023	-.224	.114	-.179	.284	.156	.277	
	Sig. (2-tailed)	.344	.846	.639	.605	.929	.387	.662	.491	.270	.550	.283	

\*\* . Correlation is significant at the 0.01 level (2-tailed).

\* . Correlation is significant at the 0.05 level (2-tailed).

Both  $\rho$  and  $p$  are important to conclude about the existent correlation between two elements.  $\rho$  indicates the strength and direction ( $\pm$ ) of correlation – the bigger the absolute value the better and  $p$  indicates the tendency for the given correlation if one would add more data to group (i.e. its significance).

Given the particular case presented by table 4.1, one realizes that there is a negative correlation between Al-K with a significance at the  $p < 0.01$  level and a positive correlation between Si-K with a significance at the  $p < 0.01$  level. Furthermore there is a positive correlation between Mn-Fe and Mn-Cu with a significance at the  $p < 0.01$  level.



**Table 4.2** – Spearman correlation coefficient ( $\rho$ ) for net peak areas of the elements that most characterize the glazes of tiles from Lisbon (N = 16). ‘\*\*\*’ indicates that the correlations are significant at the  $p < 0.01$  level; ‘\*\*’ indicates that the correlations are significant at the  $p < 0.05$  level.

		Al	Si	S	K	Ca	Ti	Mn	Fe	Cu	Zn	Sn	Pb
<b>Al</b>	$\rho$		.467	.418	.297	.539	.445	.321	.347	.333	.261	-.091	.115
	Sig. (2-tailed)		.174	.229	.405	.108	.197	.365	.327	.347	.466	.802	.751
<b>Si</b>	$\rho$	.467		-.200	.867***	.588	.823***	.055	.632*	.139	-.261	.182	-.273
	Sig. (2-tailed)	.174		.580	.001	.074	.003	.881	.050	.701	.466	.614	.446
<b>S</b>	$\rho$	.418	-.200		-.030	.261	-.262	.612	.055	.248	.505	.146	.430
	Sig. (2-tailed)	.229	.580		.934	.467	.464	.060	.881	.489	.137	.688	.214
<b>K</b>	$\rho$	.297	.867***	-.030		.661*	.451	.212	.723*	-.127	-.444	.170	-.382
	Sig. (2-tailed)	.405	.001	.934		.038	.191	.556	.018	.726	.199	.638	.276
<b>Ca</b>	$\rho$	.539	.588	.261	.661*		.287	.224	.863***	-.055	-.249	-.219	-.321
	Sig. (2-tailed)	.108	.074	.467	.038		.422	.533	.001	.881	.487	.544	.365
<b>Ti</b>	$\rho$	.445	.823***	-.262	.451	.287		-.067	.257	.482	.113	.183	.006
	Sig. (2-tailed)	.197	.003	.464	.191	.422		.854	.474	.159	.756	.612	.987
<b>Mn</b>	$\rho$	.321	.055	.612	.212	.224	-.067		.231	.515	.511	.511	.345
	Sig. (2-tailed)	.365	.881	.060	.556	.533	.854		.521	.128	.132	.132	.328
<b>Fe</b>	$\rho$	.347	.632*	.055	.723*	.863***	.257	.231		-.188	-.354	.116	-.365
	Sig. (2-tailed)	.327	.050	.881	.018	.001	.474	.521		.602	.316	.750	.300
<b>Cu</b>	$\rho$	.333	.139	.248	-.127	-.055	.482	.515	-.188		.729*	.413	.564
	Sig. (2-tailed)	.347	.701	.489	.726	.881	.159	.128	.602		.017	.235	.090
<b>Zn</b>	$\rho$	.261	-.261	.505	-.444	-.249	.113	.511	-.354	.729*		.409	.875***
	Sig. (2-tailed)	.466	.466	.137	.199	.487	.756	.132	.316	.017		.241	.001
<b>Sn</b>	$\rho$	-.091	.182	.146	.170	-.219	.183	.511	.116	.413	.409		.505
	Sig. (2-tailed)	.802	.614	.688	.638	.544	.612	.132	.750	.235	.241		.137
<b>Pb</b>	$\rho$	.115	-.273	.430	-.382	-.321	.006	.345	-.365	.564	.875***	.505	
	Sig. (2-tailed)	.751	.446	.214	.276	.365	.987	.328	.300	.090	.001	.137	

\*\*\*. Correlation is significant at the 0.01 level (2-tailed).

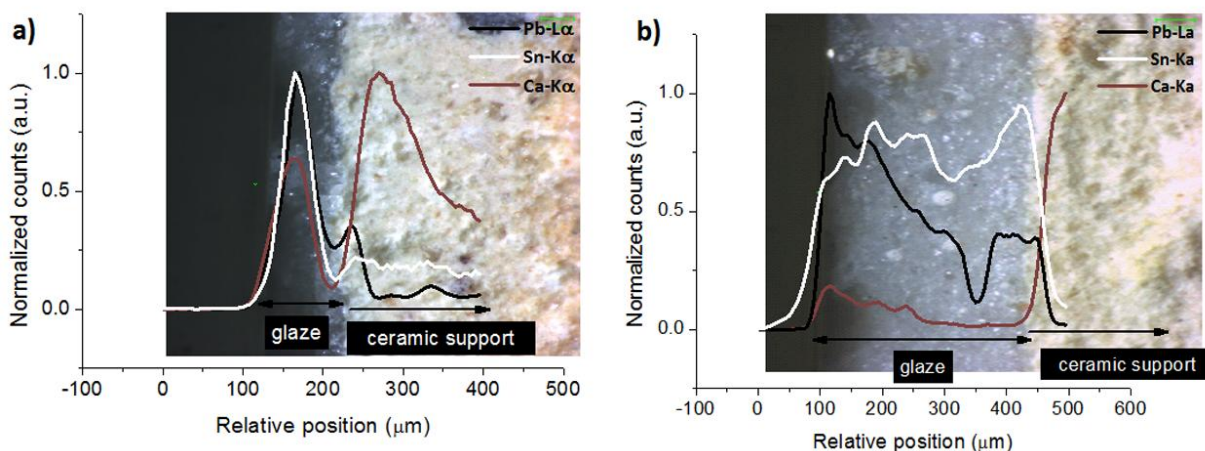
\*. Correlation is significant at the 0.05 level (2-tailed).

From table 4.2, there is a positive correlation between Si-K, Si-Ti, Ca-Fe and Zn-Pb with a significance at the  $p < 0.01$  level.

The color application as well a possible third firing stage (for the decoration only) may have taken place is still an open question (*cf.* figure 1.6). Further developments on this part will be given further on (*cf.* section 4.2.3).

As complementary information, it is important to investigate the stratigraphy of the samples for estimating the thickness of each layer and especially the elemental distribution in depth. Therefore, 3D Micro-XRF analyses were performed (*cf.* chapter 3, sub-section 3.1.3).

Three cross-section scans on glaze + body were carried out for each sample. Figures 4.10a and 4.10b shows the elemental profiles for a faience from Coimbra and a wall-tile from Lisbon, respectively. A key element for each important region in the stratigraphy of the samples was inspected – Pb and Sn for the glaze and Ca for the ceramic body.



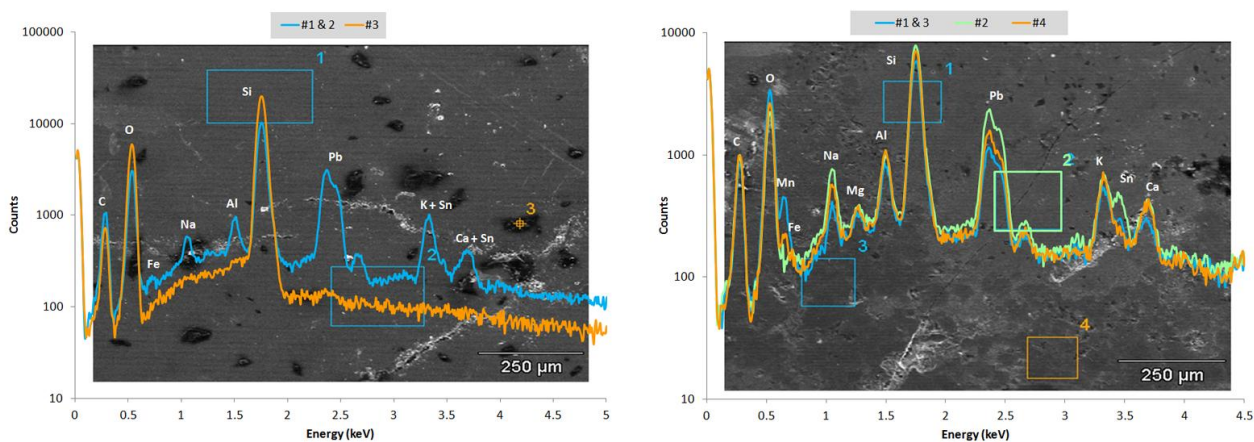
**Figure 4.10** – 3D Micro-XRF cross section scans performed on glaze + ceramic support on: a) a faience from Coimbra and b) a wall-tile from Lisbon [37].

Following the Pb-L $\alpha$  profiles for all analyzed sample it was realized that faiences have glaze thickness between 150 – 250  $\mu\text{m}$ , while the glaze of wall-tiles (both from Coimbra and Lisbon) is between 300 – 400  $\mu\text{m}$  thick. Although glazes also contain Ca, this element is mostly characteristic for the ceramic body as it is depicted in figure 4.10. A very interesting point is the region where the connection between two main parts of the sample occurs (what it will be called '*interface area*' from this point forth). Comparing the profiles between figure 4.10a and 4.10b (plotted over the images obtained by the microscope inside the confocal setup) one sees that at the glaze/body interface the elemental exchange for the faience samples from Coimbra happens in a smoother way (approximately 50  $\mu\text{m}$ ) than for the wall-tiles from Lisbon (less than 30  $\mu\text{m}$ ).

### Scanning Electron Microscopy/Energy Dispersive X-ray Spectrometry (SEM/EDX)

In order to prove the assumptions above, the use of techniques that provide compositional and morphological information is a requirement. Hence, SEM/EDX analyses were performed onto the glazes of some samples. At this point it is important to emphasize that given the heterogeneity among these objects, quantitative results obtained with EDX will be here presented just as an estimation of the content at a specific area. Hence, these will not be considered as providing representative quantitative information of the whole piece/area.

Figure 4.11 shows two examples of the elemental distribution on the glaze surfaces of one faience form Coimbra (a) and one wall-tile form Lisbon (b). The image contrast provides information about the atomic number (Z) of a certain area/spot. Dark spots/areas correspond to low-Z compounds and bright ones to high-Z compounds.



**Figure 4.11** – SEM micrographs taken on the glaze surface of a faience sample from Coimbra (a) and a wall-tile sample from Lisbon (b).

Observing figure 4.11a one can identify quartz phases (dark spots) confirmed by the EDX spectrum (#3, in orange) due the presence of Si and O only. Areas #1 and #2 represent a more uniform contribution of all compounds present in the glaze, where Na, Al, Si, K, Ca, Fe, Sn and Pb are identified by the EDX spectrum.

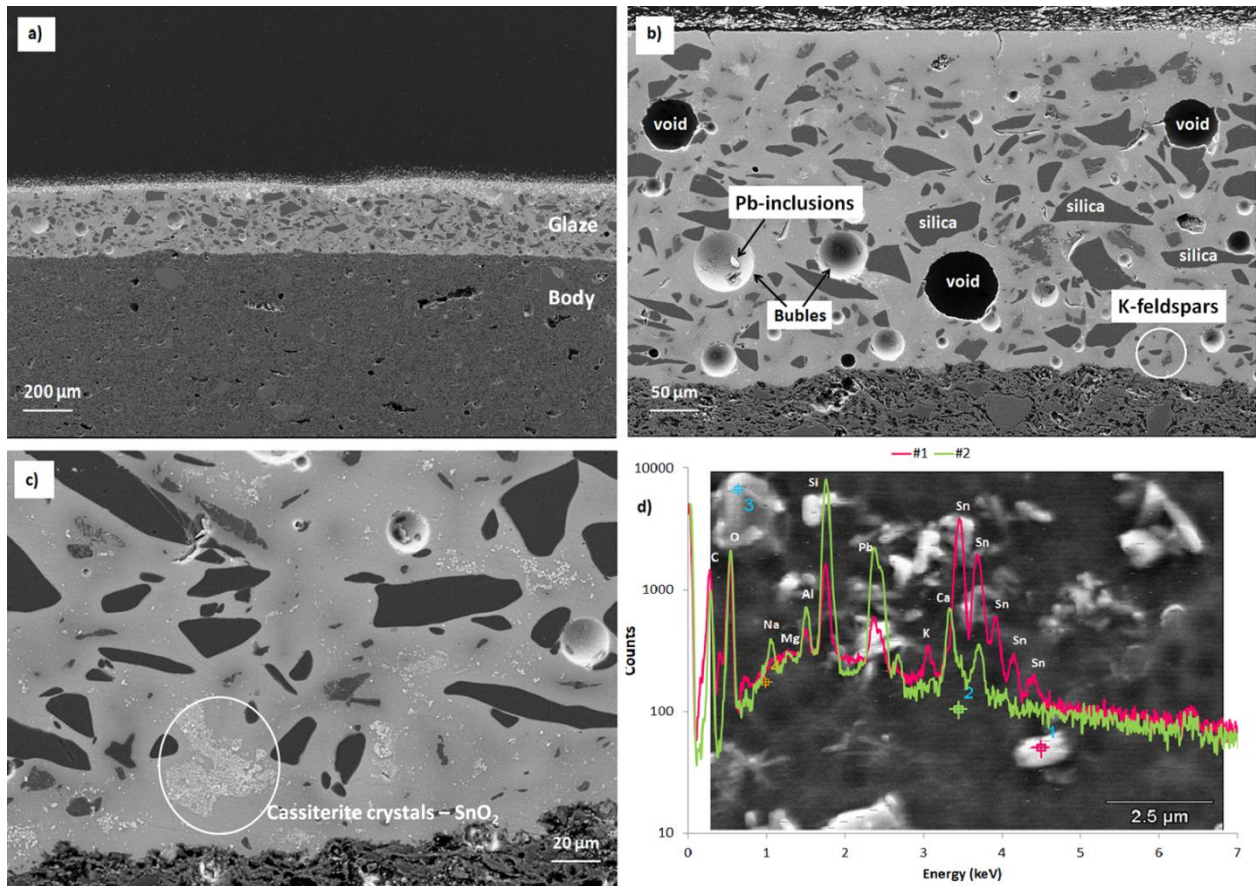
Sodium is a key element for glaze characterization, which could not be detected by XRF. In table 4.3, quantities for the elements in glaze surfaces detected by EDX for all analyzed samples

are presented. These measurements were taken under a low magnification (wide-area) and the morphology of the cross-section was taken into account in order to better estimate the concentrations.

**Table 4.3** – Elemental composition of glazes of the samples (*N* is the number of samples analyzed) from Coimbra and Lisbon (in wt-%) obtained with standardless EDX (wide-area). Note the need of careful dealing with the values as rough estimates serving primarily to distinguish between the various types of samples.

Samples	Na <sub>2</sub> O	MgO	Al <sub>2</sub> O <sub>3</sub>	SiO <sub>2</sub>	K <sub>2</sub> O	CaO	Fe <sub>2</sub> O <sub>3</sub>	PbO	SnO <sub>2</sub>
<b>Coimbra faïences (N = 11)</b>	≤ 1	< 1	2 – 3	31 – 32	8 – 9	3	4	40 – 41	10 – 11
<b>Coimbra &amp; Lisbon Wall-tiles (N = 9)</b>	3 – 4	< 1	3 – 4	29 – 30	4 – 6	≤ 1	2 – 3	45 – 46	9 – 10

Glazes from faïences (Coimbra) reveal relatively higher amounts of CaO (3 wt%) than the ones from wall-tiles from Coimbra and Lisbon (CaO: ≤ 1 wt%). Although faïences show higher content of K<sub>2</sub>O (8 – 9 wt%) and lower content of Na<sub>2</sub>O (≤ 1 wt%) when compared to the wall-tiles from Coimbra and Lisbon (4 – 6 wt% of K<sub>2</sub>O and 3 – 4 wt% of Na<sub>2</sub>O) the total alkali content is practically the same (~10 wt%). In addition, the PbO content is lower in the glazes from faïences than from wall-tiles. In order to evaluate the morphology of the glazes, a series of micrographs is presented in figure 4.12.



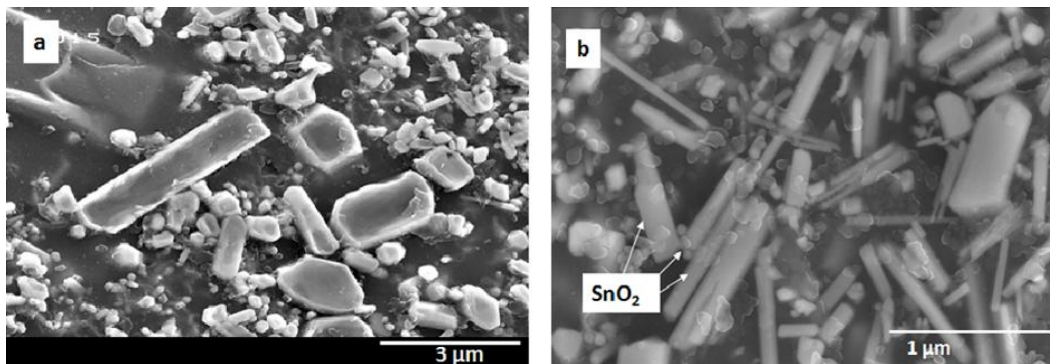
**Figure 4.12** – SEM micrographs: a) cross-section of a faience from Coimbra (low-mag.); b) cross-section of a faience (interface glaze/body is observed at the bottom); c) enhancement of the same sample, where the deposition of cassiterite crystals is observed; d) high magnification on the cassiterite crystals, supported by the EDX results.

#### General features of the glazes:

- From the micrograph in figure 4.12a one realizes how smooth the interface glaze/body is, meaning that there was a good adhesion between glaze and ceramic support;
- The brightness of the glaze (also confirmed by figure 4.12b) indicates that the matrix average atomic number is medium-high.
- The quartz grains are observable as dark spots, which shape varies from sphere-like to more oblong, with sizes up to around 60 µm (figures 4.12b and 4.12c);
- Feldspars are identified with sizes up to 5 µm;

- Cassiterite ( $\text{SnO}_2$ ) crystals are typically found in this type of ceramic glazes and the crystals size is around  $1\ \mu\text{m}$  and less; With a high magnification (figures 4.12c and 4.12d) one can see that these crystals form agglomerates and are well distributed in the glaze.

As a last example of the morphology of the glazes figure 4.13 exhibits two micrographs, one from a faience form Coimbra (a) and one from a wall-tile from Lisbon (b). One can see how well distributed the tin oxide crystals are within the glassy matrix. Their length varies between for 1 and  $2\ \mu\text{m}$  for the former (a) and between  $0.5$  and  $0.8\ \mu\text{m}$  for the latter (b).

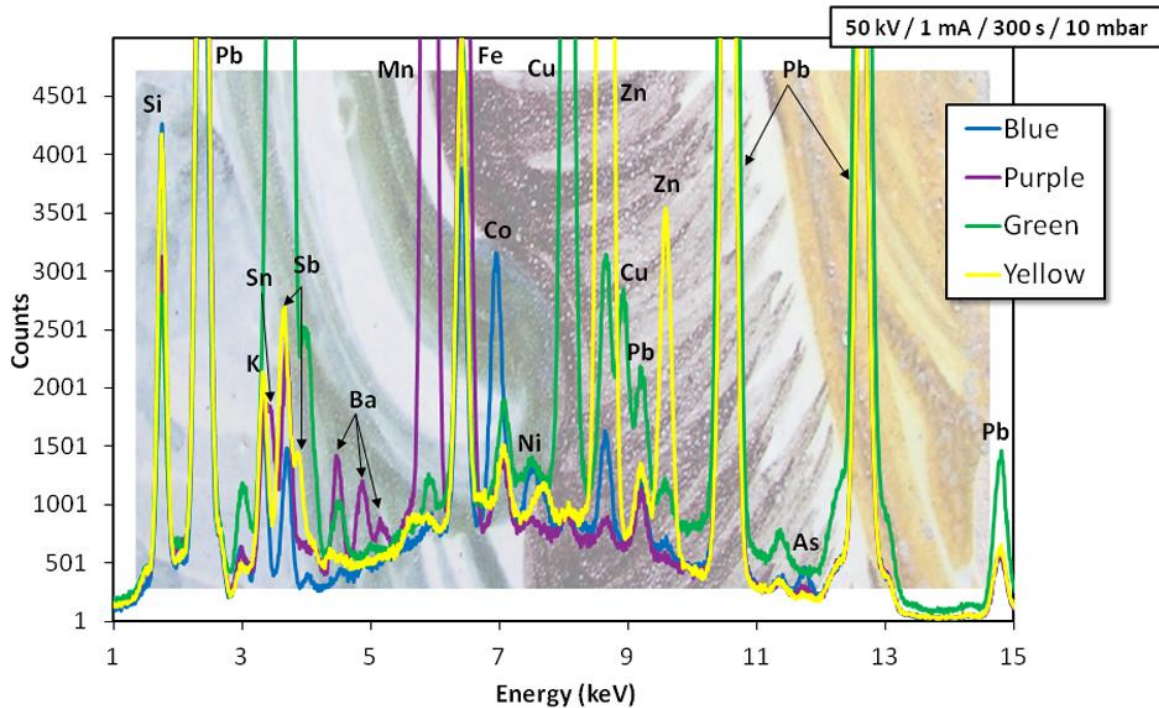


**Figure 4.13** – SEM micrographs taken on the glaze surface of a faience sample from Coimbra (a) and a wall-tile sample from Lisbon (b), with high magnification [37].

#### 4.2.3 – Surface decoration

Concerning polychrome glazed ceramics, some facts must be taken into account. The colors employed on the pieces were usually obtained from metallic oxides, which could have been used in a “raw” state or in a mixture called frit, which is a pre-melting of the pigment together with fluxes, such as Pb, Na, and sometimes even Sn (to make it more opaque). After cooling down, this mixture (frit) was grinded until a powder was obtained and then applied over the “base glaze” (*cf.* figure 1.7). The brilliance or opacity and the migration ability of the elements, which grant the color, are some factors that help assign the way the pigment was applied onto/within the glaze [33, 37].

In figure 4.14 XRF spectra from the four most used colors (blue, purple, green and yellow) are plotted.



**Figure 4.14** – XRF spectra – obtained in conventional mode – correspondent to blue, purple, green and yellow colors respectively.

From these spectra key elements – that characterize each color – can be identified: Cobalt (Co) for blue, Manganese (Mn) (and possibly Barium (Ba)) for purple, Copper (Co) for green and Antimony (Sb) for yellow.

#### 4.2.3.1 – Blue pigment

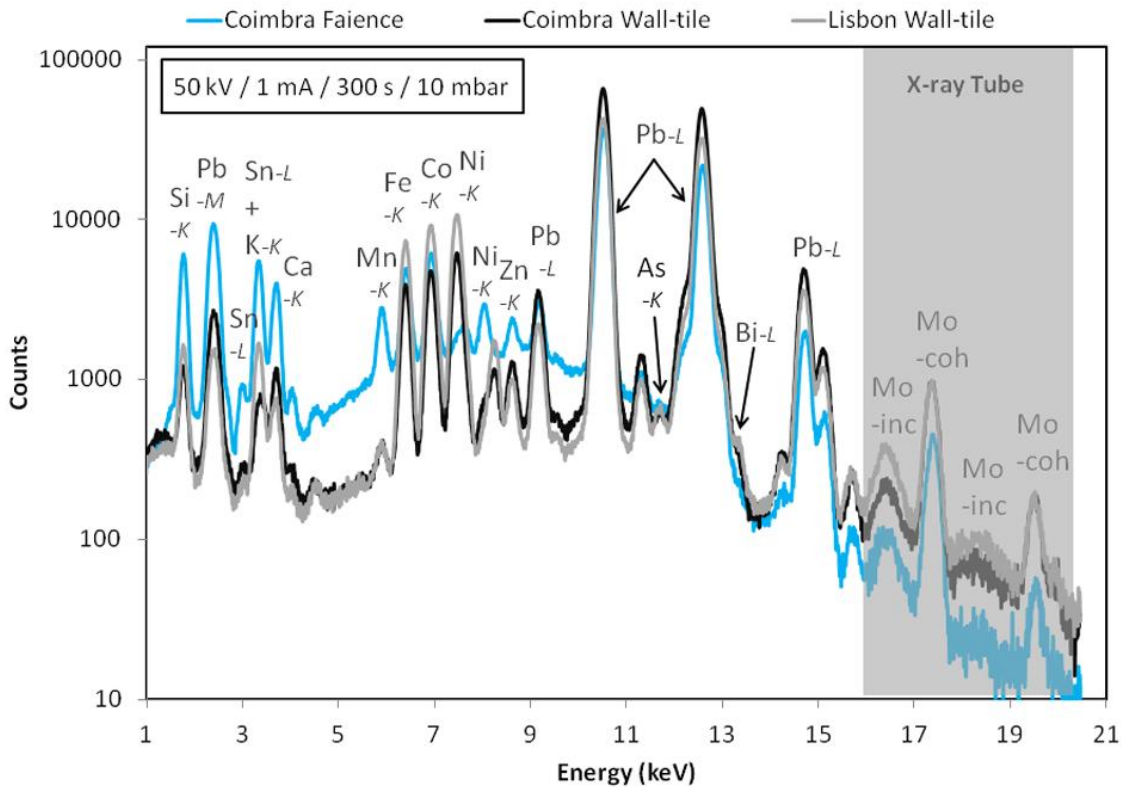
##### *X-ray Fluorescence (XRF)*

Blue is without a doubt the most common color for (Portuguese) glazed ceramic decoration. Its common association with majesty made it the most required color for this purpose.

From figure 4.14 the typical elements detected are Fe, Co, Ni and As (Smalt). According to the literature [27], the use of Co-pigments until about the 12<sup>th</sup> century AD is related to two mineral ores only: i) *Qamsar* and *Anarak* in Persia and ii) the *Erzgebirge* – Ore Mountains – at

the border between Saxony (Germany) and Bohemia (Czech Republic). These were geologically rich enough to support a trade route over Europe, North Africa and the East (till China). The main mining industry in the *Erzgebirge* was Silver (Ag), whose minerals were found admixed in the so-called 'five-element' veins (Ni-Co-As-Ag-Bi). Since then, the *Erzgebirge* has supplied the Co-pigment market to a large extent.

The decorative motives as well as the hues used, make the difference. Measurements with the conventional XRF setup were performed on blue areas, and in order to identify the elements from the color a spectra from the glaze next to these areas was subtracted. In figure 4.15, spectra – obtained by conventional XRF – from blue areas in faiences from Coimbra and wall-tiles from Coimbra and Lisbon are presented.



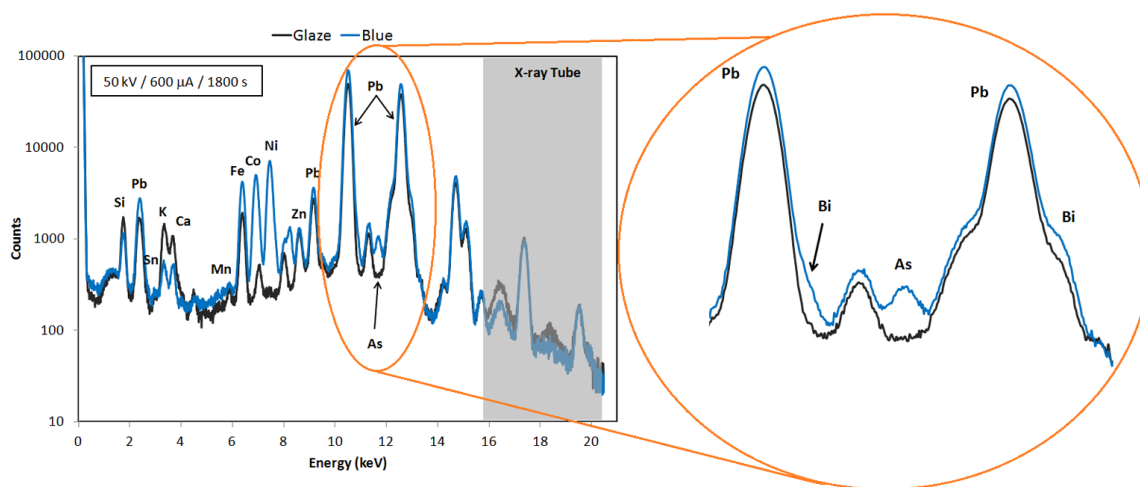
**Figure 4.15** – XRF spectra from blue regions from faiences from Coimbra and wall-tiles from Coimbra and Lisbon.

From figure 4.15 a difference in the shape of the spectra between faiences and wall-tiles is observed. Since blue painted regions were much smaller in faiences than in wall-tiles, X-ray



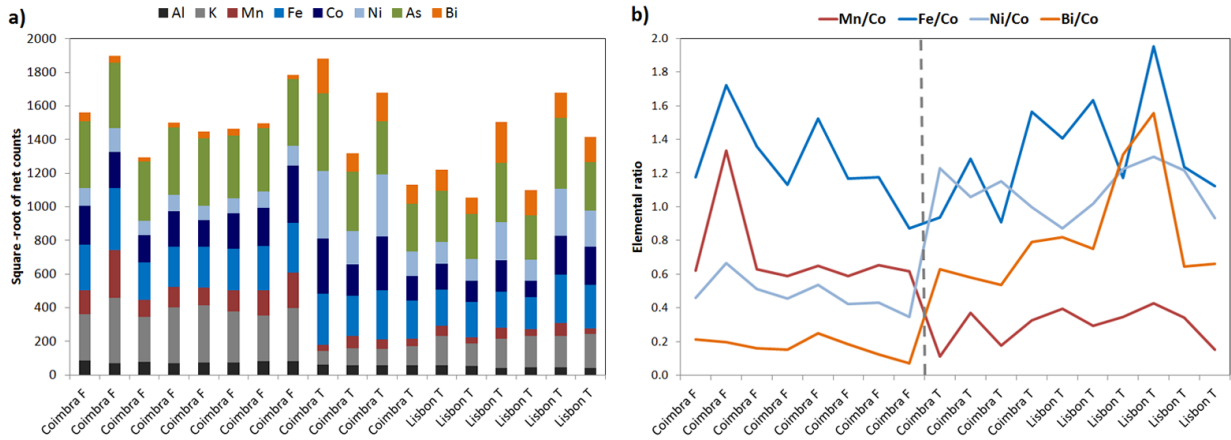
excitation was performed using the polycapillary lens for faïences. This way one restrains the desired analyzed and has no overlap with adjacent colors. The shape of the background in the spectrum corresponding to the faïence in figure 4.15 is in agreement with the theory of polycapillary lenses (*cf.* chapter 3, sub-section 3.1.2)

An interesting feature detected on these spectra is that there seems to appear a peak on the right side of the Pb-L $\beta$  line, which energy would correspond to Bismuth (Bi-L $\beta$ ). Given the inherent instrumental limitations in terms of energy resolution, long measurements (of 30 min.) were carried out on the blue areas of each sample. For this purpose (and to assure that the upper layer is selected), 3D Micro-XRF measurements were performed placing the probing volume on the upper layer (blue).



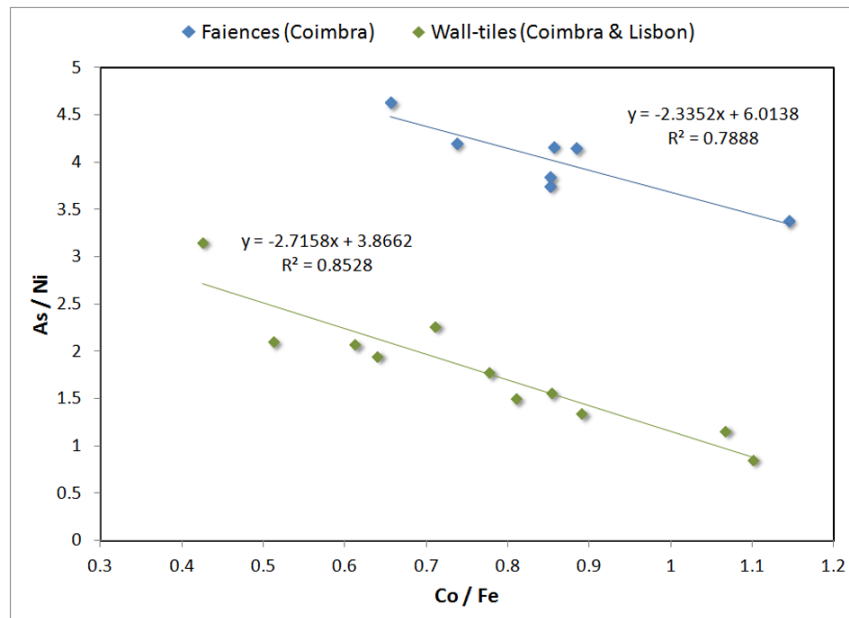
**Figure 4.16** – Comparison between blue and glaze spectra, performed with 3D Micro-XRF on the upper layer of each area. The shoulder appearing on the right side of both Pb-L $\alpha$  and Pb-L $\beta$  indicates the presence of Bismuth (Bi) in the blue.

Figure 4.16 shows that with long measuring time, both lines of Bismuth (L $\alpha$  and L $\beta$ ) become emphasized, when compared with respective glaze. In order to evaluate whether the presence of the elements that are “linked” to Cobalt is found in all samples or not, net counts for these elements were compared between the different kinds of samples.



**Figure 4.17** – a) Plot of the elemental net counts for Al, K, Mn, Fe, Co, Ni, As, Bi for faiences from Coimbra (Coimbra F), wall-tiles from Coimbra (Coimbra T) and wall-tiles from Lisbon (Lisbon T); b) comparison elemental ratios (Mn/Co, Fe/Co, Ni/Co, Bi/Co) between faiences from Coimbra (Coimbra F), wall-tiles from Coimbra (Coimbra T) and wall-tiles from Lisbon (Lisbon T).

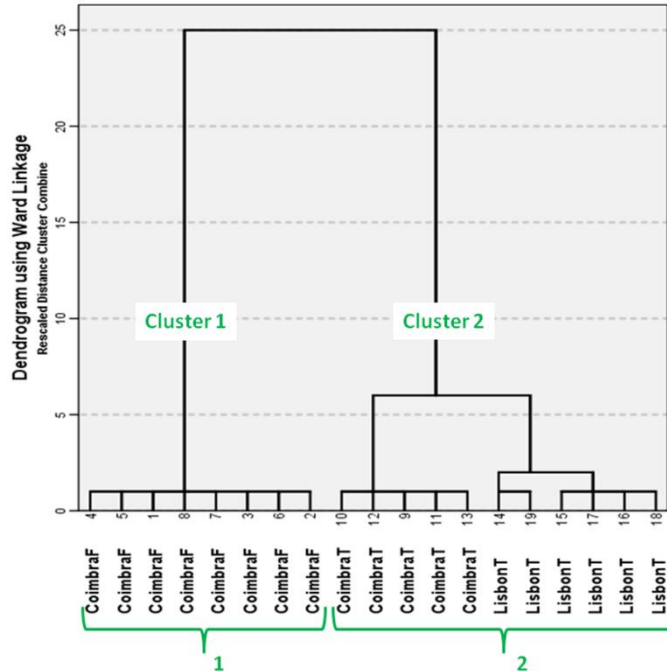
From figure 4.17a one sees that the wall-tiles (Coimbra T and Lisbon T) show higher count rates for Ni and Bi and lower count rates for Mn in comparison to the faiences (Coimbra F). This is easier to observe by the ratio plot in figure 4.17b, where an increase of the Ni/Co (light-blue line) and Bi/Co (orange line) and a drop of the Mn/Co (red line) for the wall-tiles are observed (right hand-side of the grey dashed line). The ratio Fe/Co (blue line) keeps more or less unchanged between faiences and wall-tiles. Furthermore, the fact that the source of Co has “contaminant” elements such as Fe, Ni, As and Bi, allows inferring about the time at which these objects were manufactures. According to Van der Linden et al. [28], the more recent the object is, the higher the “purity” of the Co-source that was employed is. In figure 4.18, the As/Ni ratio is plotted against the Co/Fe ratio.



**Figure 4.18** – As/Ni square-root net counts ratio plotted against Co/Fe square-root net counts ratio, for both faïences (Coimbra) and wall-tiles (Coimbra & Lisbon).

From figure 4.18 one sees a negative linear relationship between As/Ni and Co/Fe for both faïences (Coimbra) and wall-tiles (Coimbra & Lisbon). However, looking at both scales, the difference with the Co/Fe and As/Ni ratio does not vary much, which means that the whole set of pieces belongs to the same period.

In order to assign possible groups regarding the chemical information of the blue used in the different pieces, statistical clustering methods were chosen (*cf.* chapter 3, section 3.5 – statistical data handling). The input data for the dendrogram in figure 4.19 are the net peak areas of the elements that mostly characterize the **blue** color together with the respective glaze: Al, Si, K, Ca, Ti, Mn, **Fe, Co, Ni, As**, Sn, **Bi** and Pb.



**Figure 4.19** – Dendrogram showing the clusters formed with the elemental data of the blue. Two clusters are unambiguously formed: cluster 1 – faiences from Coimbra (Coimbra F); cluster 2 – wall-tiles from Coimbra and Lisbon (Coimbra T and Lisbon T).

From figure 4.19 one realizes two distinct clusters – one for faiences from Coimbra (Coimbra F) and one for wall-tiles (Coimbra T and Lisbon T) – with a big distance. However, cluster 2 could be sub-divided into two clusters, as there is a smaller distinct division between wall-tiles from Coimbra (Coimbra T) and wall-tiles from Lisbon (Lisbon T).

Spearman correlation tests were performed for the different groups of samples (faiences and tiles). Table 4.4 shows the correlation coefficients between the elements that characterize the blue of faiences from Coimbra, table 4.5 the blue of wall-tiles from Coimbra and table 4.6 the blue of wall-tiles from Lisbon. For further insight on this statistical treatment, see please chapter 3, section 3.5 – statistical data handling.

**Table 4.4** – Spearman correlation coefficient ( $\rho$ ) for net peak areas of the elements that most characterize the blue in faiences from Coimbra (N = 16). ‘\*\*\*’ indicates that the correlations are significant at the  $p < 0.01$  level; ‘\*’ indicates that the correlations are significant at the  $p < 0.05$  level.

		<b>Mn</b>	<b>Fe</b>	<b>Co</b>	<b>Ni</b>	<b>As</b>	<b>Bi</b>
<b>Mn</b>	$\rho$		.916**	.819*	.964**	.042	.060
	Sig. (2-tailed)		.001	.013	.000	.921	.887
<b>Fe</b>	$\rho$	.916**		.786*	.929**	.084	.286
	Sig. (2-tailed)	.001		.021	.001	.844	.493
<b>Co</b>	$\rho$	.819*	.786*		.810*	.048	-.071
	Sig. (2-tailed)	.013	.021		.015	.910	.867
<b>Ni</b>	$\rho$	.964**	.929**	.810*		.263	.214
	Sig. (2-tailed)	.000	.001	.015		.528	.610
<b>As</b>	$\rho$	.042	.084	.048	.263		.359
	Sig. (2-tailed)	.921	.844	.910	.528		.382
<b>Bi</b>	$\rho$	.060	.286	-.071	.214	.359	
	Sig. (2-tailed)	.887	.493	.867	.610	.382	

\*\* - Correlation is significant at the 0.01 level (2-tailed).

\* - Correlation is significant at the 0.05 level (2-tailed).

From the results in table 4.4 it becomes clear that there is a significant positive correlation among the elements Mn-Fe-Co-Ni. The correlation between Mn-Fe, Mn-Ni and Fe-Ni is positive significant at a  $p < 0.01$  level and the Co shows a positive significant correlation at the  $p < 0.05$  level with Mn, Fe and Ni. As has a tendency for positive correlation with all elements (higher with Bi) but not very consistent (proved by the high  $p$ -values). Moreover, Bi and Co have no consistent correlation ( $p = 0.867$ ).

**Table 4.5** – Spearman correlation coefficient ( $\rho$ ) for net peak areas of the elements that most characterize the blue in Wall-tiles from Coimbra (N = 12). ‘\*\*’ indicates that the correlations are significant at the  $p < 0.01$  level; ‘\*’ indicates that the correlations are significant at the  $p < 0.05$  level.

		<b>Mn</b>	<b>Fe</b>	<b>Co</b>	<b>Ni</b>	<b>As</b>	<b>Bi</b>
<b>Mn</b>	$\rho$		-.500	-.500	-.500	-.300	-.800
	Sig. (2-tailed)		.391	.391	.391	.624	.104
<b>Fe</b>	$\rho$	-.500		1.000**	1.000**	.900*	.900*
	Sig. (2-tailed)	.391		.	.	.037	.037
<b>Co</b>	$\rho$	-.500	1.000**		1.000**	.900*	.900*
	Sig. (2-tailed)	.391	.		.	.037	.037
<b>Ni</b>	$\rho$	-.500	1.000**	1.000**		.900*	.900*
	Sig. (2-tailed)	.391	.	.		.037	.037
<b>As</b>	$\rho$	-.300	.900*	.900*	.900*		.700
	Sig. (2-tailed)	.624	.037	.037	.037		.188
<b>Bi</b>	$\rho$	-.800	.900*	.900*	.900*	.700	
	Sig. (2-tailed)	.104	.037	.037	.037	.188	

\*\* - Correlation is significant at the 0.01 level (2-tailed).

\* - Correlation is significant at the 0.05 level (2-tailed).

From the results in table 4.5 it becomes clear that there is a positive significant correlation between Fe-Co-Ni at the  $p < 0.01$  level. As and Bi have a positive significant correlation with all elements (except with Mn) at the  $p < 0.05$  level. Mn has a tendency for a negative correlation with all elements, but not very consistent – proved by the  $p$ -values.

**Table 4.6** – Spearman correlation coefficient ( $\rho$ ) for net peak areas of the elements that most characterize the blue in Wall-tiles from Lisbon (N = 14). ‘\*\*\*’ indicates that the correlations are significant at the  $p < 0.01$  level; ‘\*’ indicates that the correlations are significant at the  $p < 0.05$  level.

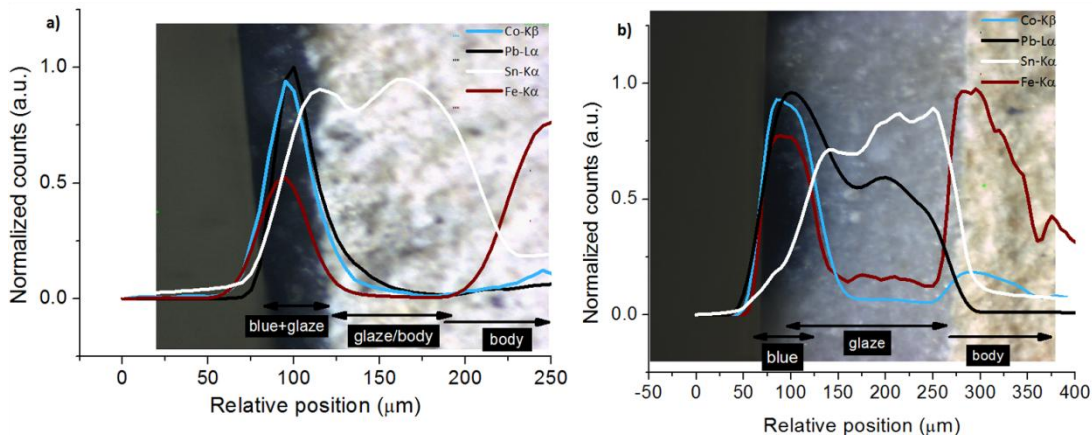
		Mn	Fe	Co	Ni	As	Bi
<b>Mn</b>	$\rho$		-.086	-.086	.086	-.086	-.200
	Sig. (2-tailed)		.872	.872	.872	.872	.704
<b>Fe</b>	$\rho$	-.086		1.000**	.943**	.886*	.257
	Sig. (2-tailed)	.872		.	.005	.019	.623
<b>Co</b>	$\rho$	-.086	1.000**		.943**	.886*	.257
	Sig. (2-tailed)	.872	.		.005	.019	.623
<b>Ni</b>	$\rho$	.086	.943**	.943**		.943**	.314
	Sig. (2-tailed)	.872	.005	.005		.005	.544
<b>As</b>	$\rho$	-.086	.886*	.886*	.943**		.429
	Sig. (2-tailed)	.872	.019	.019	.005		.397
<b>Bi</b>	$\rho$	-.200	.257	.257	.314	.429	
	Sig. (2-tailed)	.704	.623	.623	.544	.397	

\*\* - Correlation is significant at the 0.01 level (2-tailed).

\* - Correlation is significant at the 0.05 level (2-tailed).

From the results in table 4.6 it becomes clear that there is a positive significant correlation between Fe-Co-Ni and Ni-As at the  $p < 0.01$  level, and a positive correlation between Fe-As and Co-As at the  $p < 0.05$  level. Bi has a tendency for a positive correlation with all elements (except with Mn), but not very consistent – proved by the  $p$ -values. Mn has a tendency for a negative correlation with all elements, but not very consistent – proved by the  $p$ -values.

In order to check the elemental distribution in depth, specifically the pigment dissemination throughout the glaze, 3D Micro-XRF scans on the cross-section were carried out. The results reported here correspond to an average of three measurements per analyzed cross-section.



**Figure 4.20** – 3D Micro-XRF cross section scans performed on blue + glaze + ceramic support on: a) a faience from Coimbra and b) a wall-tile from Lisbon [37].

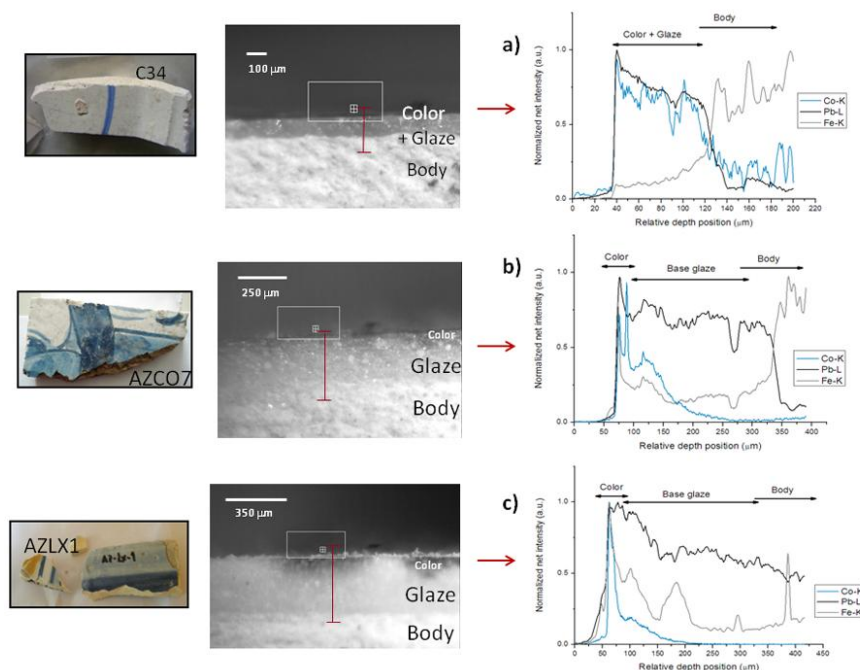
Figure 4.20 shows an example of the elemental dispersion in depth for a faience from Coimbra (a) and wall-tile from Lisbon (b).

From the elemental profile two main differences are observed: i) the glaze of the faience from Coimbra is thinner (ca. 150  $\mu\text{m}$ ) than the one from the wall-tile from Lisbon (ca. 400  $\mu\text{m}$ ), as previously shown; ii) by monitoring the Co K-line, the pigment is distributed throughout the whole glaze in the faience sample (figure 4.20a) while in the wall-tile the pigment dissemination is about 100  $\mu\text{m}$  in depth. On one hand, either there is no interface between color/glaze in the sample from Coimbra or is less than the resolution allowed for the 3D Micro-XRF. This may indicate that glaze and pigment were applied together, as it is also proved by the Co-K and Pb-L $\alpha$  profiles (figure 4.20a). On the other hand, there is an interface color/glaze in the sample from Lisbon (figure 4.20b). However, the pigment disseminates quite well through the glaze, which is also proved by the profiles obtained for Co-K and Pb-L $\alpha$ . In both cases Sn is more abundant in the lower part of the glaze, being dominant in the sample from Coimbra (figure 4.20a). This is in agreement with the assumption that tin crystals are very dense and deposit on the lower part of the glaze.

In order to complement the information above, these scans were performed with high lateral resolution (1  $\mu\text{m}$ ) at the BAMline @ BESSY-II (Berlin, Germany) [39]. For focusing the incident X-ray beam Compound Refractive Lenses (CRLs) were used. Further technical details of the experiment are previously described (*cf.* chapter 3, sub-section 3.1.4). The scans were



performed, in the same way as the ones for 3D Micro-XRF. The results reported here correspond to an average of three measurements per analyzed cross-section.



**Figure 4.21** – Cross-section scans were performed through the blue/glaze/body of two samples from Coimbra – (a) faience and (b) wall-tile – and a wall-tile from Lisbon (c) [39].

Pictures taken with the incorporated microscope, in which the different areas of each sample are easy to observe, are also displayed in figure 4.21. The red line in these pictures gives an idea of how the scans were accomplished, from the top of the surface down to the ceramic body.

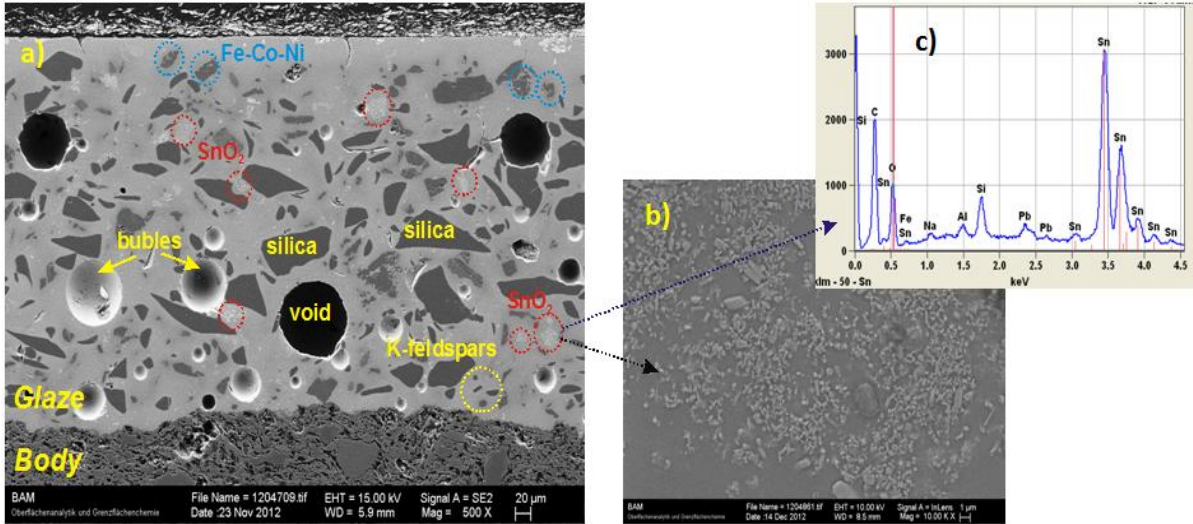
The scans compare the Co-K, Pb-L and Fe-K signals, which characterize blue, glaze and body, respectively. Tracing the Co signal in the faience sample, one sees that the glaze and surface decoration exist as one layer together. The glaze is thin and the pigment was applied together with the glaze in one firing stage. Comparison of the Co-signal between the two tiles shows that its maximum is broader in the sample from Coimbra (ca. 150 µm – figure 4.21b) than in the one from Lisbon (ca. 125 µm – figure 4.21c). Another point is that the Pb-signal in the wall-tiles from Coimbra (figure 4.21b) has an abrupt drop in the interface glaze/body. There is a smooth drop

of the Pb-signal when reaching the body of the sample from Lisbon (figure 4.21c), allowing a higher intake of the glaze throughout the body. In addition, the Fe-signal (mainly characteristic of the ceramic body) is higher at the interface glaze/body in the sample from Lisbon than in the sample from Coimbra.

### ***Scanning Electron Microscopy/Energy Dispersive X-ray Spectrometry (SEM/EDX)***

It is known that in addition to the choice and preparation of the materials, the firing and cooling conditions play an important role in the granularity and differences in the spatial distributions of the finished composition [27]. Therefore, it is crucial to infer about the stratigraphy of these objects, as there is no typical expected layered-system in such items. Hence, it becomes necessary to gain knowledge about the morphology not only of the glazes but also of the pigments. In the case of blue pigments although Co is the color-carrier, a linkage between several elements exists: Fe-Co-Ni-As-Bi, as mentioned above. Moreover, tracing the Co-signal throughout the glaze one realizes how diffused this pigment is.

In figure 4.22a a cross-section of the blue-colored glaze from a faience sample from Coimbra is presented. Several Cassiterite ( $\text{SnO}_2$ ) agglomerates throughout the whole glaze – from top to bottom (marked by white circles) - are observed. Figure 4.22b represents an enlargement of one of the areas containing  $\text{SnO}_2$  agglomerates.

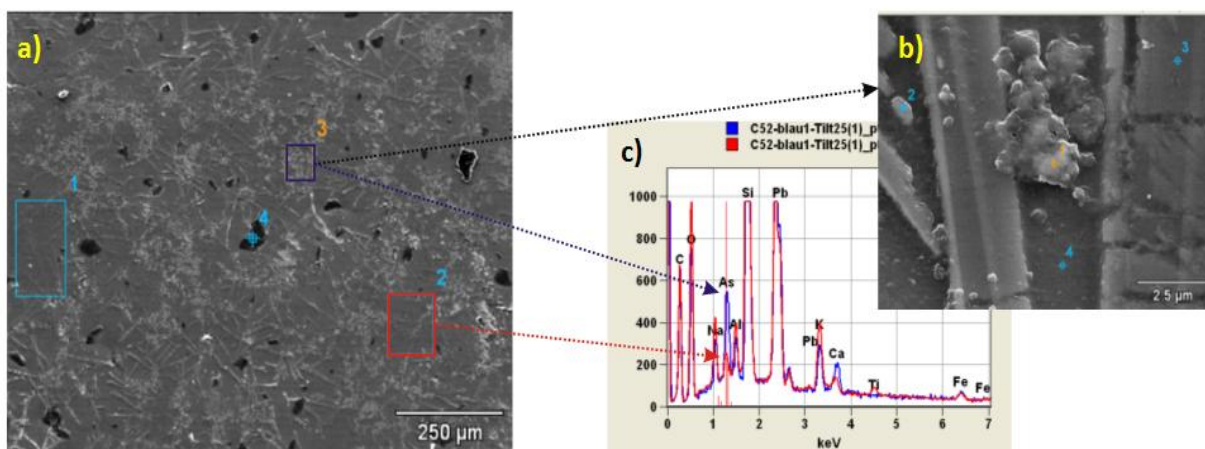


**Figure 4.22** – SEM micrographs on the “blue” sample areas: a) cross-section of a faience sample from Coimbra (low magnification) with visualization of Cassiterite ( $\text{SnO}_2$ ) agglomerates (white marks) and Fe-Co-Ni structures (blue marks); b) enlargement of one area of the  $\text{SnO}_2$  agglomerates and c) EDX spectrum taken from the area shown in (b) demonstrating the massive presence of Sn. 239x87mm (150 x 150 DPI) [94].

The presence of Sn in the agglomerates as those in figure 4.22b is clearly proven by the EDX spectrum shown in figure 4.22c. The Fe-Co-Ni structures (marked by blue circles) are rather scarce in the whole region, plus they are found somewhat “buried” in the glaze (around 100  $\mu\text{m}$  in depth according to figure 4.22a), in agreement with Zucchiatti et al. [27]. This means that given the heterogeneity in these objects, together with the fact that the excitation volume of the X-ray electron probe microanalysis in such matrices (at the high-voltages employed) is about 1-3  $\mu\text{m}$  (*cf.* chapter 3, sub-section 3.3.1), the EDX analyses of the Fe-Co-Ni structures become a real challenge in this case.

From the structures found in figure 4.22, the amount of Sn-agglomerates in the blue regions is a hint for a particular manufacturing process. Co-blue is in its natural state a very strong and dark blue, which is not the hue in the blue surface motifs, by naked-eye observation. So, since Sn is a natural white-opacifier, one can deduce that the potter added it intentionally to the pigment in order to obtain a lighter blue hue.

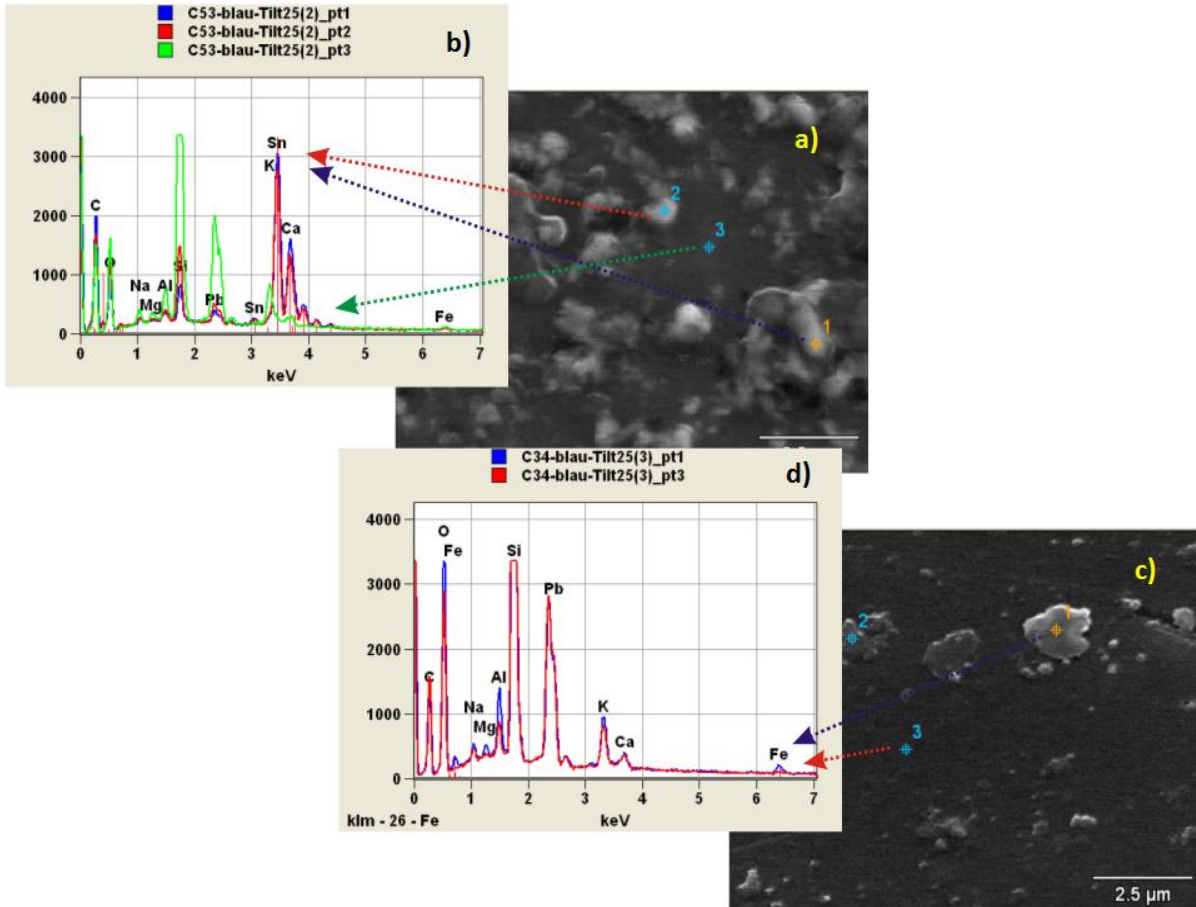
The micrograph in Figure 4.23a corresponds to a blue-painted surface of a faience sample from Coimbra. Some needle-like structures (figure 4.23b) correspond to As-compounds, which markedly were found in blue regions only.



**Figure 4.23** – SEM micrographs of a surface area of a faience from Coimbra (low magnification (a) and high magnification (b)) with visualization of Arsenic needle-like structure; c) EDX spectra correspondent to the areas marked in a) demonstrating the presence of As in the bright needle-like structures; Note that a Fe-Ni-rich structure could be also identified (see point #1 in c) by EDX. 238x80mm (150 x 150 DPI) [94].

The EDX spectra from figure 4.23c correspond to the areas marked in figure 4.23a. The analytical challenges described above are here demonstrated. The EDX spectra taken from the area #1 and area #2 in figure 4.23a show no significant Co peaks ( $K\alpha$  @ 6.93 keV and  $L\alpha$  @ 0.77 keV). However, the presence of other elements that are linked with the Co-structure, such as Fe, are observed. Moreover, the L-line of As is well detected, especially in the spectrum corresponding to area #3. This is easily observed by the higher concentration of “bright” As-structures (needle-like). Figure 4.23b corresponds to an enlargement of area #3 from figure 4.23a. Point #1 in figure 4.24c is obviously rich in Fe – shown by the correspondent EDX spectrum. Furthermore, this structure is presumably rather thin in comparison to the needle-like structures, as one can see by the “shade” it provokes on the As-structure in figure 4.23b. The EDX spectra of points #2, 3 and 4 show the presence of As-L line (1.28 keV), while for point #1 the line which partially overlaps this one is Mg-K (1.25 keV).

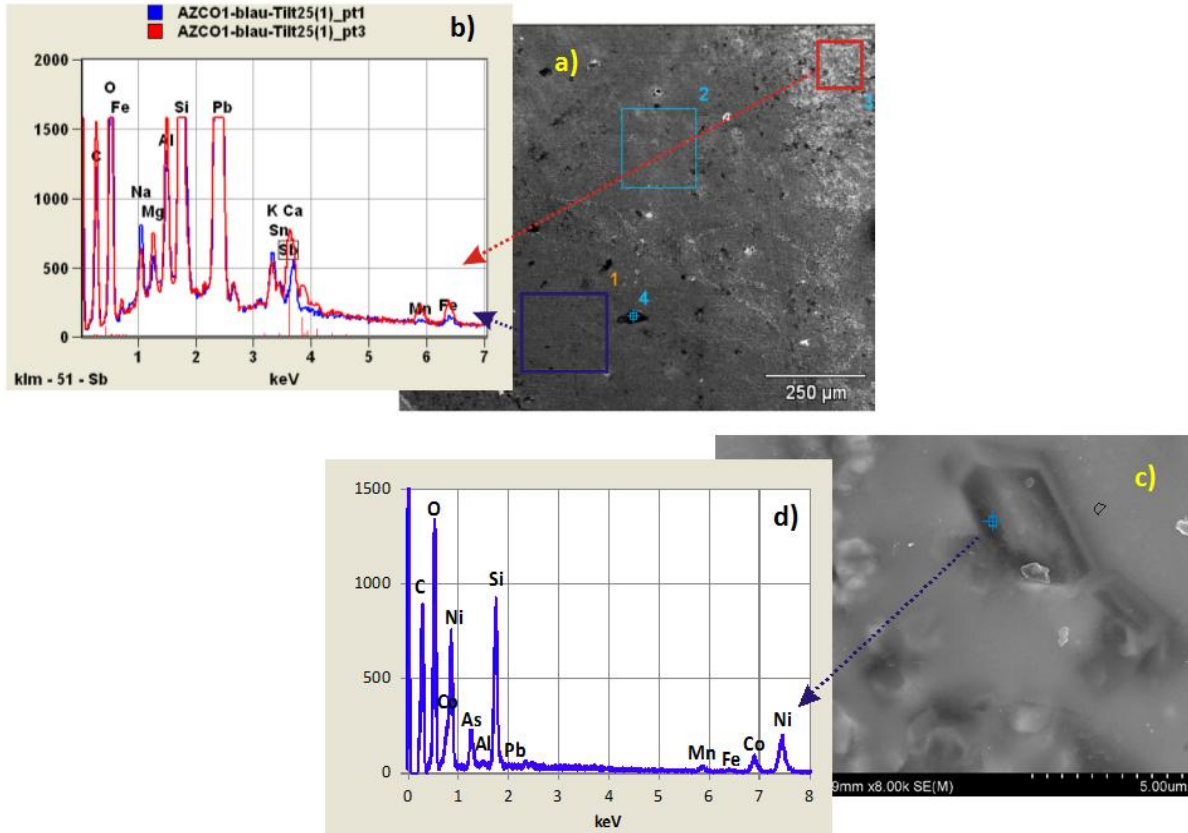
A comparison between micrographs taken with high magnification on blue painted regions from samples from the two locations, Coimbra and Lisbon, is made. Figure 4.24 shows examples of blue surfaces from two faiences from Coimbra.



**Figure 4.24** – SEM micrographs: a) surface of a faience from Coimbra with visualization of the mixture between Sn-crystals and Fe-Ni-rich structures; b) EDX spectra correspondent to the point analysis marked in a); c) surface of a faience from Coimbra with visualization of Fe-Ni-rich structures, dispersed throughout the whole colored area; d) EDX spectra corresponding to the points marked in c). 168x90mm (150 x 150 DPI) [94].

In figure 4.24a a smooth mixture of dark and bright zones is observable, which corresponds to the Fe-containing structures and Sn-crystals, respectively (figure 4.24b). Figure 4.24c corresponds to another Coimbra faience sample and in this case, the Fe-containing structures are more dispersed at the surface level.

Regarding wall-tile samples, figure 4.25 shows a micrograph taken onto the surface of a wall-tile from Lisbon, at a low magnification.



**Figure 4.25** – SEM micrographs of two Lisbon wall-tile samples in the blue painted areas together with EDX spectra (b and d) on selected spots demonstrating the presence of Fe-Mn-rich or Ni-rich micro-structures. 175x80mm (150 x 150 DPI) [94].

In figure 4.25a darker and brighter relatively large regions are observed. Comparing this surface micrograph with the one from figures 4.23a and b (faience from Coimbra), As-structures (needle-like) are not observable in the wall-tile sample at similar magnifications. This is also confirmed by the EDX spectra in figure 4.25b, where As-lines were not detected. According to Zucchiatti et al. [27], As is found in the glaze with connection to Ca and Pb only and in fact there is a lower intensity for Pb-M and Ca-K lines in the spectrum of figure 4.25b. There is, however, a higher areal concentration of Sb-compounds – see e. g. area #3 in figure 4.23a and the respective EDX spectrum in red (figure 4.25b) – in comparison to the faience surface in figures

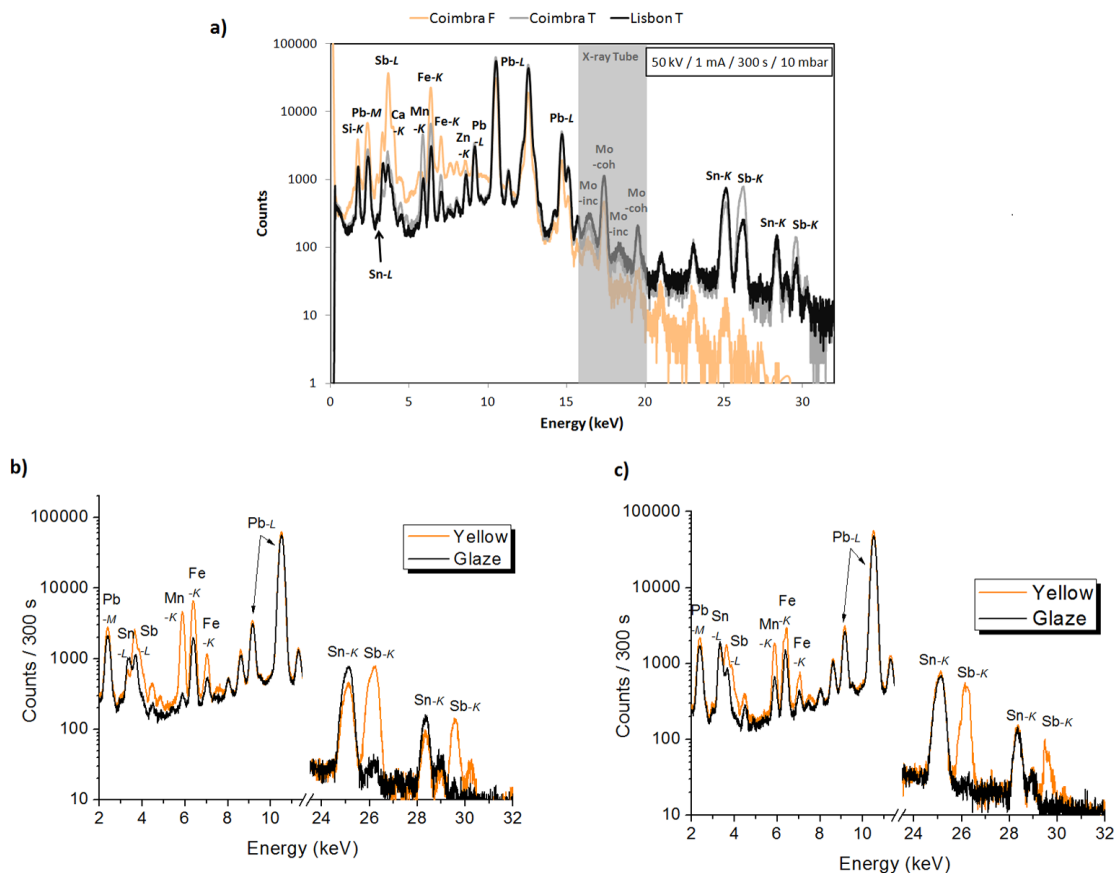
4.23a and b, which indicates the presence of yellow painted regions close to the blue regions. Figure 4.25c is an enlargement of area #3 in figure 4.25a. Some micro- and submicro-structures are observed and the blurry appearance indicates that these are somewhat “buried” in the depth of the blue-glaze. However, one of these structures seems to “touch” the surface (blue point in figure 4.25c), see the respective EDX spectrum in figure 4.25d. Ni, Co and Mn were clearly detected in this structure. By the count rate ratio between these elements, a Ni-rich structure encloses the Co-blue pigment, in comparison to the ones from Coimbra, where a Fe-rich environment is found.

#### **4.2.3.2 – Yellow pigment**

##### ***X-ray Fluorescence (XRF)***

By naked eye observation, faiences from Coimbra exhibit bright yellow decoration (except one sample); the wall-tiles from Coimbra show a mate yellow-orange hue and the wall-tiles from Lisbon have relatively bright yellow decorations (*cf.* Annex 1.3).

Surface analyses with conventional XRF were performed on all yellow regions on the samples and in figure 4.26 spectra from: one faience (Coimbra) and wall-tiles (one from Coimbra and one from Lisbon) are plotted.

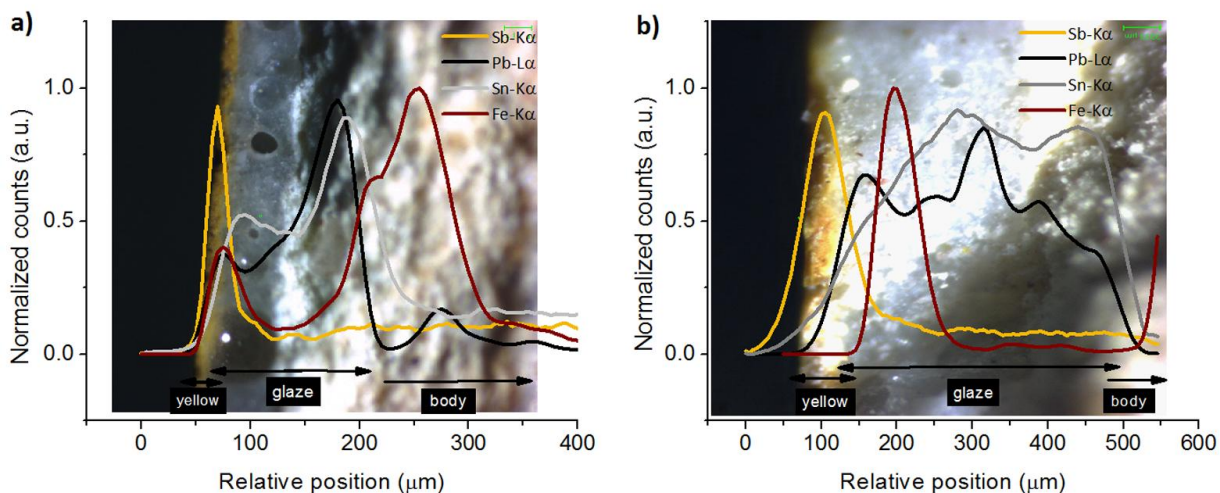


**Figure 4.26** – XRF spectra: a) yellow regions from faiences from Coimbra (Coimbra F) and wall-tiles from Coimbra (Coimbra T) and Lisbon (Lisbon T); b) comparison between yellow and glaze of a faience from Coimbra; c) comparison between yellow and glaze of a wall-tile from Lisbon.

From the spectra in figure 4.26a one sees that the color yellow is owed to the presence of Antimony (Sb). Along with this element, Pb and Sn seem to be in strong association – by the strong count rate in both Coimbra and Lisbon samples (figures 4.26b and 4.26c). The lead-antimonate pigment – also known as Naples Yellow ( $Pb_2Sb_2O_7$ ) – was commonly used for the yellow motifs [22]. Samples from Coimbra show higher count rates for Mn and Fe than the ones from Lisbon (figure 4.26a), which may justify the more orange hue in the former. Additional considerations about the chemical environment related to the yellow pigment are presented further on.



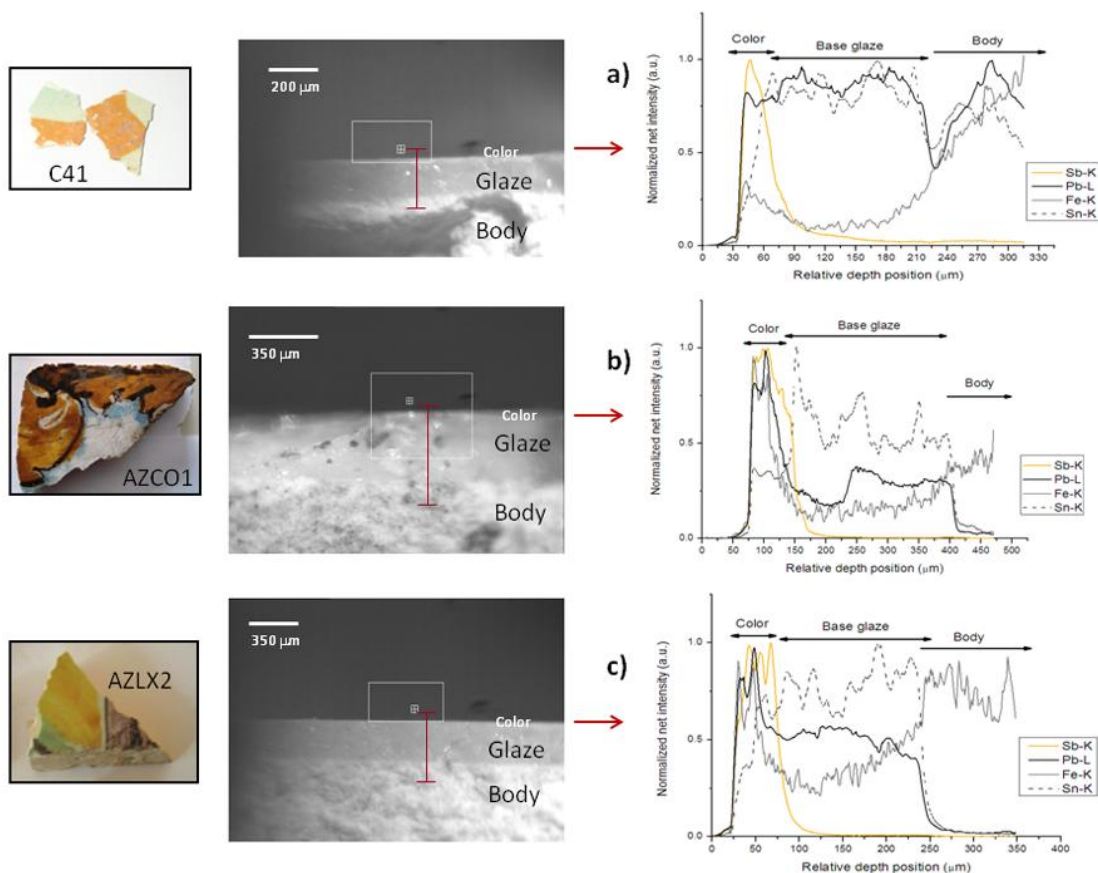
On a first approach to complement the consideration so far made, 3D Micro-XRF scans on the cross-section of samples from Coimbra and Lisbon are presented. The results here reported correspond to an average of three measurements per analyzed cross-section.



**Figure 4.27** – 3D Micro-XRF cross section scans performed on yellow + glaze + ceramic support on: a) a faience from Coimbra and b) a wall-tile from Lisbon [37].

From figure 4.27 one realizes that the yellow pigment is distinguished from the base glaze, whether in Coimbra or in Lisbon samples. Tracing the Sb-K $\alpha$  line, a thickness of about 30  $\mu\text{m}$  is obtained for the yellow layer in the faience from Coimbra (figure 4.27a) and about 80  $\mu\text{m}$  for the yellow layer in the wall-tile from Lisbon. Tracing the Pb-La line, a thickness of about 150  $\mu\text{m}$  is obtained for the glaze of the faience from Coimbra (figure 4.27a) and a thickness of ca. 300  $\mu\text{m}$  is obtained for the wall-tile from Lisbon (figure 4.27b) [37]. In agreement to the results above, the Fe-signal was detected in the yellow layer from the sample from Coimbra (red line in figure 4.27a) while in the sample from Lisbon it starts just at the base glaze (red line in figure 4.27b). Furthermore, in the sample from Coimbra both Pb- and Sn-signal start approximately at the same place as the Sb-signal (figure 4.27a) and in the sample from Lisbon the Pb-signal starts just about 30  $\mu\text{m}$  after the Sb-signal, while the Sn-signal accompanies the Sb-signal (figure 4.27b).

In order to complement the information above, these scans were performed with high lateral resolution (1  $\mu\text{m}$ ), again at the BAMline @ BESSY-II (Berlin, Germany) [39]. The scans were performed, in the same way as the ones for 3D Micro-XRF. The results reported here correspond to an average of three measurements per analyzed cross-section.



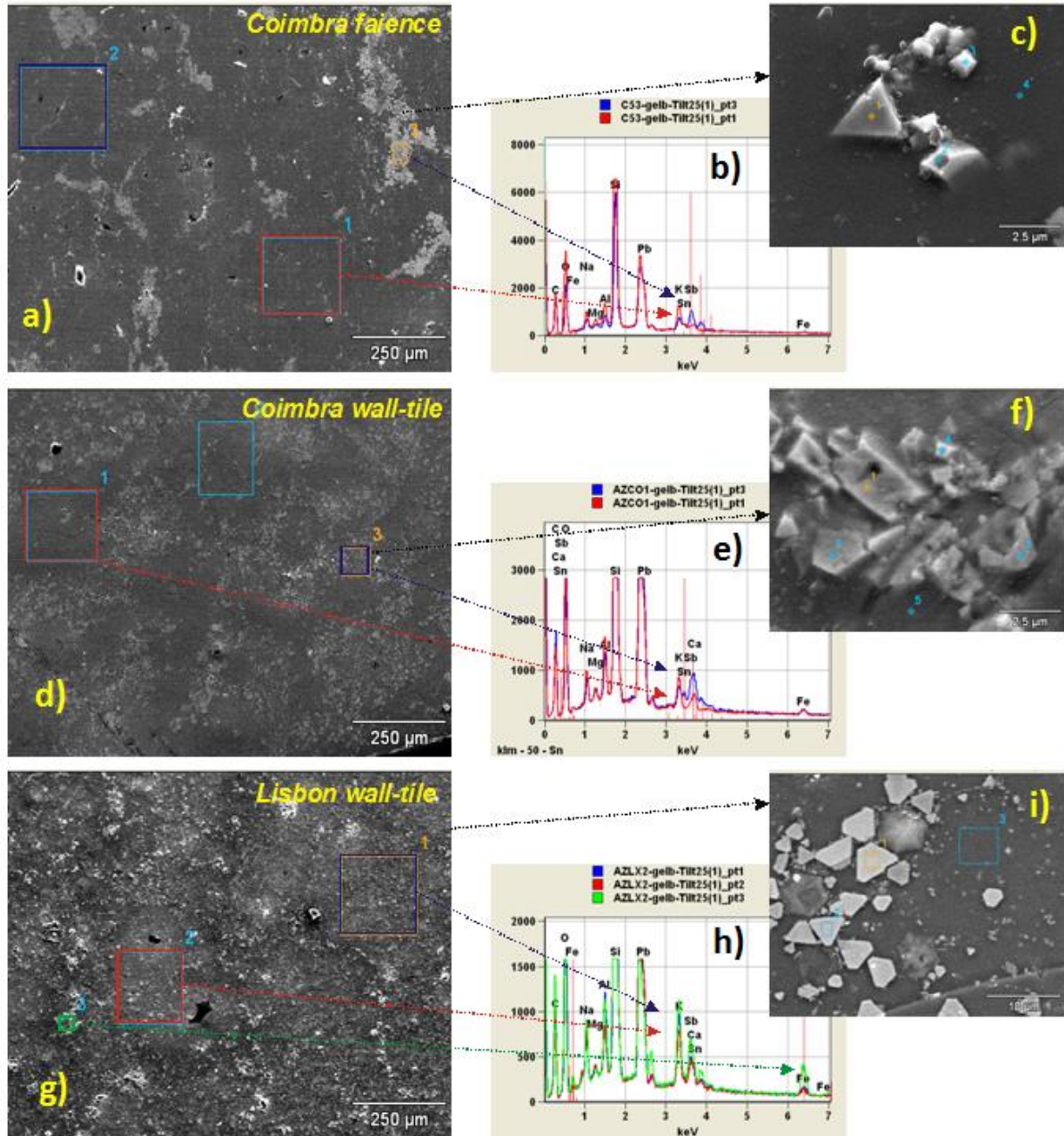
**Figure 4.28** – Cross-section scans were performed through the blue/glaze/body of two samples from Coimbra – (a) faience and (b) wall-tile – and a wall-tile from Lisbon (c) [39].

In figure 4.28a one sees that the pigment layer (30  $\mu\text{m}$ ) is not completely dispersed into the glaze (ca. 180  $\mu\text{m}$ ). One can also see that Pb keeps throughout the whole glaze until the first tens of micrometers of the body. Comparing the profiles of figures 4.28b and 4.28c, it is obvious that the pigment layers of both samples have about the same thickness (about 100  $\mu\text{m}$ ); Conversely to what happens in figure 4.28a, the Pb signal accompanying the pigment in wall-tiles from Coimbra and Lisbon drops (figures 4.28b and 4.28c), being more abruptly for the

former. Moreover, the Pb-signal does not observed in the first tens of micrometers of the body [39].

### Scanning Electron Microscopy/Energy Dispersive X-ray Spectrometry (SEM/EDX)

Representative SEM micrographs taken on the “yellow” surface of one of each type of object are displayed in figure 4.29.



**Figure 4.29** – SEM micrographs of yellow painted areas of the surface of (a) a Coimbra faience sample, (d) a Coimbra wall-tile sample, and (g) a Lisbon wall-tile sample. On the right side EDX spectra on selected spots and further high-mag micrographs are shown. 153x160mm (150 x 150 DPI) [94].

The faiences from Coimbra exhibit localized very bright areas (for example area #3 in figure 4.29a), which correspond to the local higher density of Sb-crystals – as shown by the respective EDX spectra in figure 4.29b. The wall-tiles from Coimbra appear in figure 4.29d relatively darker in general with lower local density of Sb-compounds – as indicated by the EDX spectra (figure 4.29e). The wall-tiles from Lisbon shows, in figure 4.29g, a more uniform mixture of bright and darker regions, which indicates a quite homogeneous distribution of the Sb-crystals – shown by the EDX spectra of all marked regions on the micrograph (figure 4.29h). High-magnification micrographs (figures 4.29c, 4.29f and 4.29i) were also taken onto the yellow surface areas from the samples together with the respective EDX spectra.

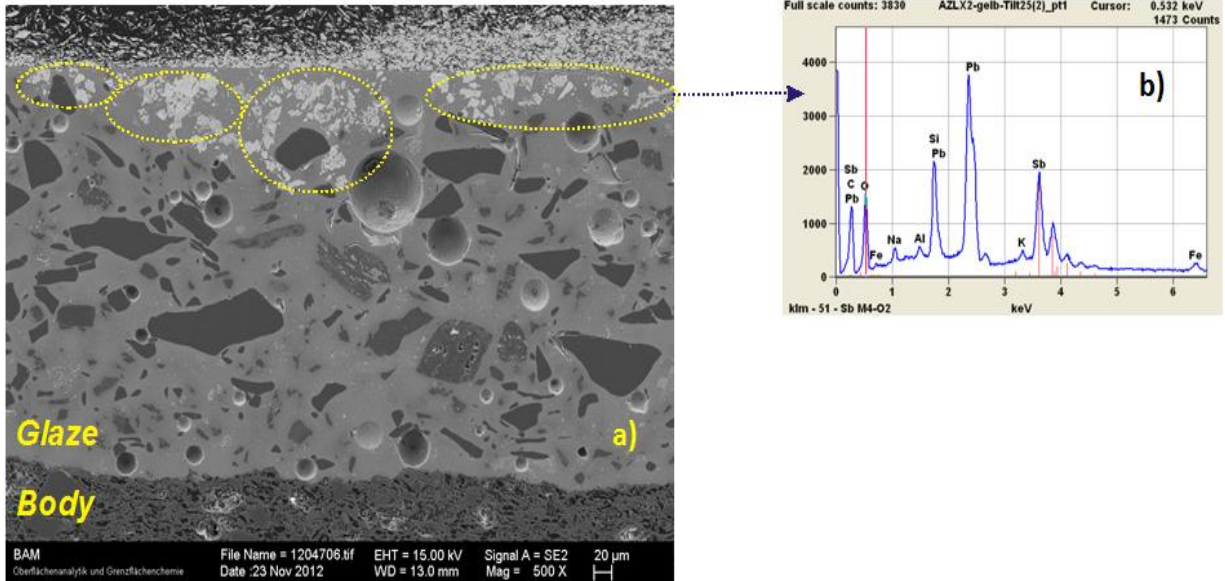
The rough concentration of the elements present in yellow regions as detected by EDX for all analyzed samples were calculated by using the commercial standardless quantification routines offered by one of the EDS systems employed (NSS 300 Thermo Fisher Scientific). The corresponding measurements were taken at a low magnification, *i. e.* integrating over larger areas, and the morphology of the cross-section was checked as well in order to better evaluate the concentrations.

**Table 4.7** – Elemental composition of the yellow regions of the samples (*N* is the number of samples analyzed) from Coimbra and Lisbon (in wt-%) obtained with standardless EDX (wide-area). Note the need of careful dealing with the values as rough estimates serving primarily to distinguish between the various types of samples [94].

<b>Samples</b>	Na	Mg	Si	K	Ca	Fe	Sn	<b>Sb</b>	<b>Pb</b>	<b>O</b>
<b>Coimbra</b>										
<b>faiences</b> ( <b>N = 4</b> )	1 – 3	≤ 1	13 – 15	2 – 4	1 – 2	2 – 4	2 – 4	<b>11 – 14</b>	<b>36 – 39</b>	25 – 27
<b>Coimbra</b>										
<b>Wall-tiles</b> ( <b>N = 2</b> )	1 – 2	< 1	16 – 17	1 – 3	2 – 3	1 – 3	3 – 4	<b>6 – 8</b>	<b>35 – 37</b>	25 – 27
<b>Lisbon</b>										
<b>Wall-tiles</b> ( <b>N = 4</b> )	1 – 2	< 1	12 – 16	3 – 4	≤ 1	4 – 6	1 – 2	<b>4 – 6</b>	<b>12 – 15</b>	45 – 48

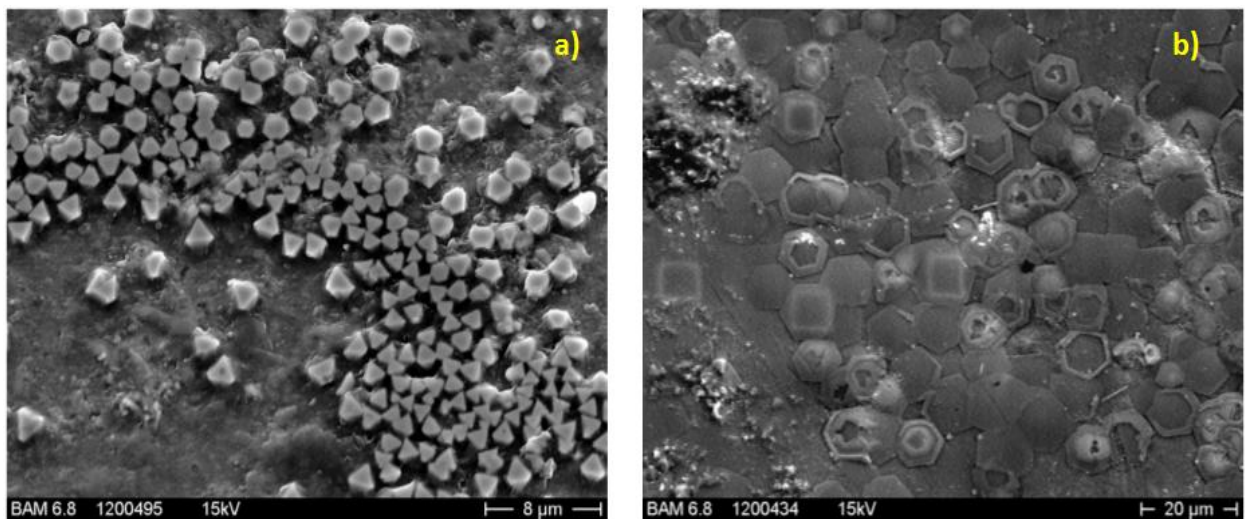
The analyses with wide-area mode on yellow decorations (table 4.7) reveal that the wall-tiles have a lower content of Sb, in comparison to faiences. Furthermore, the presence of Sn indicates that the Sn-ions may participate in the crystalline structure that forms the yellow pigment – possibly by replacing Sb [95]. Other elements, which are embedded in the glaze matrix, such as Si, are also identified in these spectra due to the rather large analyzed volume.

Another interesting perspective to observe the way the Sb-crystals are spread through the glaze is shown in figure 4.30. Clearly the Sb-crystals keep at the first tens of micrometers beneath the surface – marked in yellow circles.



**Figure 4.30** – a) SEM micrograph of a cross-sectioned Coimbra faience sample in an yellow painted area; b) EDX spectrum corresponding to the areas marked with yellow in a) demonstrating the presence of Sb. 219x91mm (150 x 150 DPI) [94].

Figure 4.31 shows the differences between the morphology of the Sb-crystals between wall tiles from Coimbra and Lisbon.



**Figure 4.31** – a) SEM micrographs showing Sb-crystals at the surface a wall tile from Coimbra (a) and a wall tile from Lisbon (b) 234x91mm (150 x 150 DPI) [94].

The size of the crystals is smaller in the sample from Coimbra (faïences and wall-tiles – figures 4.30a and 4.30b) than in the samples from Lisbon (figure 4.30c). The crystal size is about 1-2  $\mu\text{m}$  for the former and about 5-10  $\mu\text{m}$  for the latter. Furthermore the crystal-shape is different: in faïences and wall-tiles from Coimbra they are triangular-like while in wall-tiles from Lisbon they have a well-formed hexagonal shape (figures 4.31a and 4.31b).

### ***X-ray Absorption Fine Structure (XAFS)***

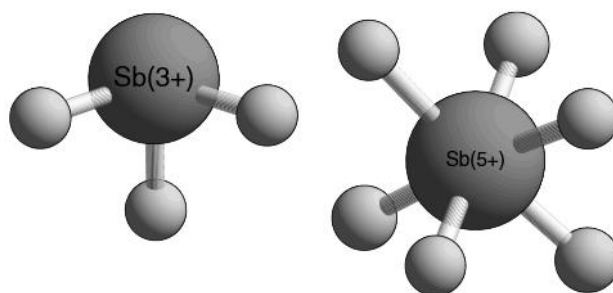
Regarding the yellow pigment used for decoration in glazed ceramic objects, questions about the structural nature of the most common yellow pigment – Naples Yellow ( $\text{Pb}_2\text{Sb}_2\text{O}_7$ ) – emerged. This lead-antimonate yellow pigment is a synthetic pigment, normally obtained by calcination of a mixture of ore compounds. This is a thermal treatment process in which the compounds are heated below their fusing point, causing decomposition of carbonates, among others. In order to obtain Naples yellow, lead compounds (metallic lead, lead monoxide and lead white) were calcinated together with antimony compounds (metallic antimony, antimony trioxide and potassium antimonate or antimony sulfide). A more detailed description about the used compounds for calcination as well as their possible ratios is presented by Dik et al. [96]. During the calcination process other elements, such as Al, Si or Zn, were added and therefore they serve as hint for the recipes used.

The pyrochlore-type lead-antimonate was commonly used as pigment for the yellow hues, however previous investigations on the yellow decorated parts have indicated the presence of other elements such as Sn or Zn [37]. This suggests either the use of other compounds or changes in the original pyrochlore-type. Four distinct yellow components were mostly used in paintings and glass manufacture: 1) the orthorhombic lead-tin yellow I ( $\text{Pb}_2\text{SnO}_4$ ); 2) the cubic pyrochlore lead-tin yellow II ( $\text{PbSn}_{1-x}\text{Si}_x\text{O}_3$ ); 3) the cubic pyrochlore lead-antimonate ( $\text{Pb}_2\text{Sb}_2\text{O}_7$ ); 4) the cubic pyrochlore lead-tin antimonate yellow ( $\text{Pb}_2\text{Sb}_{2-x}\text{Sn}_x\text{O}_{6.5}$ ) [18, 19, 22]. A detailed description about recipes used to obtain these pigments as well as the crystal structure characterization is given by Clark et al. [97].

In order to distinguish such fine details, a chemically-sensitive technique is required. Information about the coordination geometry and local environment of the investigated

element are sought and therefore X-ray Absorption Fine Structure (XAFS) analyses were carried out on both Pb-L3 and Sb-K edges. For this purpose, a set of original samples, some prepared replica and reference materials were analyzed. In addition, theoretical simulations (modulations) of the Pb and Sb XAFS spectra, assuming different valences, were performed.

With the aim of finding differences in manufacturing techniques of the two main glazed ceramic production centers in Portugal (Coimbra and Lisbon), it is of great importance to learn about the Sb and Pb chemical environment and understand the role of these cations within the pigment and the glassy matrix [98]. The electron configuration of Sb:  $[\text{Kr}2 4d^{10}5s^25p^3]$  allows the formal valences of (+3) and (+5). The electron pair  $5s^2$  of Sb(III) is strongly localized and induces an asymmetric coordination and the three bonds point away from this lone electron pair, forming a trigonal pyramidal coordination (figure 4.32). Conversely, Sb(V) is octahedral coordinated to 6 oxygen atoms, in line with the symmetric  $4d^{10}$  electron configuration (figure 4.32) [99].



**Figure 4.32** – Coordination of Sb(III) and Sb(V) in oxide minerals. Oxygen atoms are indicated by the smaller balls. For both oxidation states Sb-O distances largely overlap ( $1.92\text{-}2.04 \text{ \AA}$  for Sb(III) and  $1.98\text{-}2.10 \text{ \AA}$  for Sb(V)) [99].

The same happens for Pb, with an electron configuration:  $[\text{Xe}] 4f^{14}5d^{10}6s^26p^2$  and formal valences of (+2) and (+4). The electron pair  $6s^2$  in Pb(II) induces the coordination asymmetry and the  $5d^{10}$  electrons in Pb(IV) will account for the energy perturbation [100]. It is of great importance to raster these structural differences in order to provide answers about the raw materials used as well as hints for firing processes used.



Sample preparation:

- A set of thirteen original samples from both production centers (Coimbra and Lisbon) was gathered. Six faience samples from the *Museu Machado de Castro* (MMC), in Coimbra, and five wall tile samples (originally produced in Lisbon) as well as two wall tile samples (originally produced in Coimbra) from the *Museu Nacional do Azulejo* (MNAz), in Lisbon, were granted for non-destructive analysis. The limited number of samples is due to the fact that yellow surface decorations are quite 'rare' and difficult to find.

- A set of reference lead- and antimony-based compounds were purchased from Kremer Pigmente©: PbO (litharge); Pb<sub>2</sub>Sb<sub>2</sub>O<sub>7</sub> (Naples yellow); Pb<sub>3</sub>(SbO<sub>4</sub>) (lead antimonate); Pb(SbSn)O<sub>3</sub> (lead tin antimony from Paris). PbO<sub>2</sub> (lead dioxide), Pb<sub>3</sub>O<sub>4</sub> (lead tetroxide, Red lead) and PbCO<sub>3</sub> (lead carbonate, White lead) were provided by BAM. Furthermore, XAFS spectra from several Sb-based compounds were kindly provided by Andreas C. Scheinost (Beamline BM20 at the ESRF, Grenoble, France): Sb<sub>2</sub>O<sub>5</sub> Fluka, Sb<sub>2</sub>O<sub>3</sub> (Senarmonite), Sb<sub>2</sub>O<sub>3</sub> (Valentinite), Sb<sub>3</sub>O<sub>6</sub>(OH) (Stibiconite), SbSbO<sub>4</sub> (Cervantite) and Sb<sub>2</sub>O<sub>5</sub> synth [99].

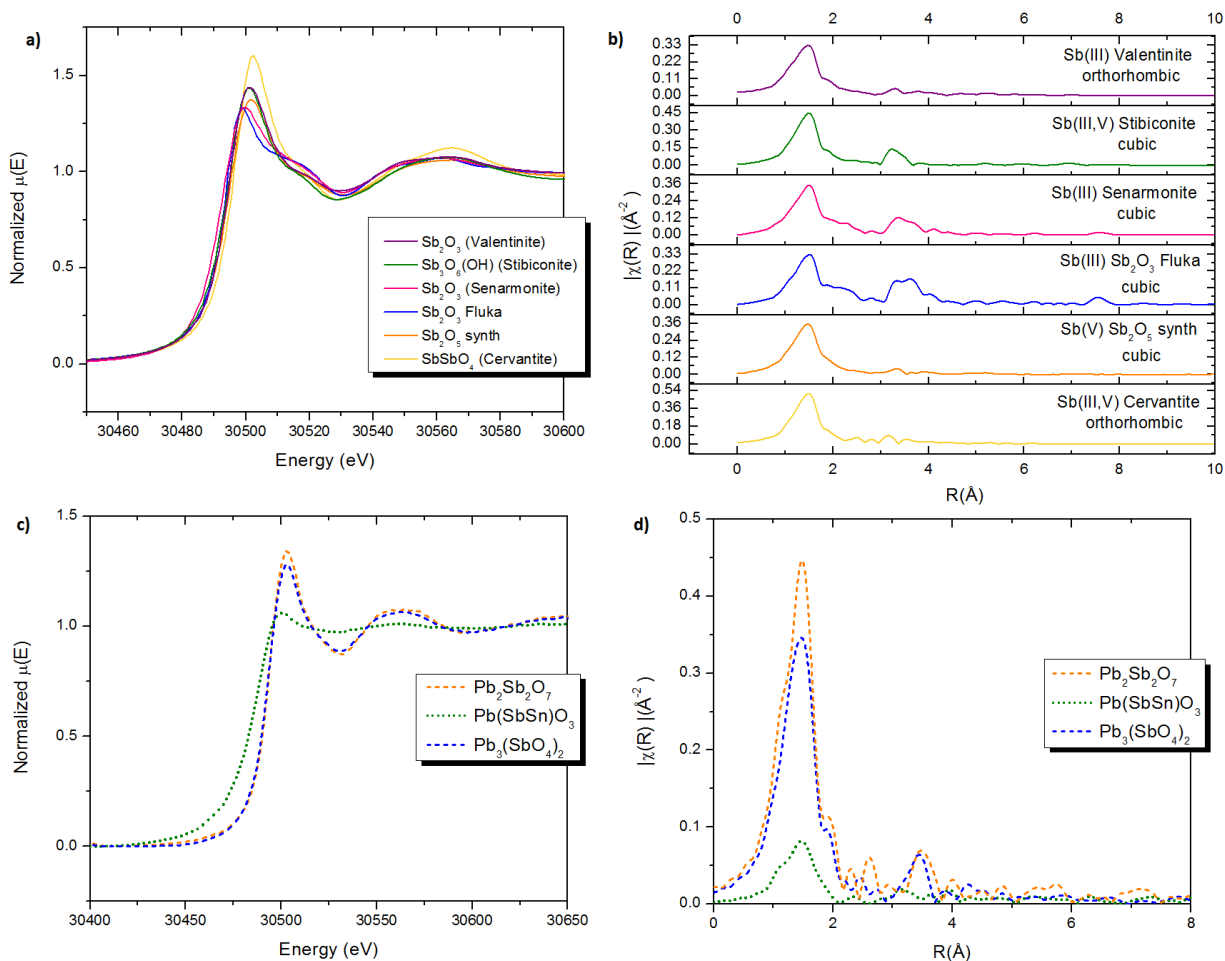
- Aside from the list above, some replicas were produced at the Department of Arts, Conservation & Restoration from the Polytechnic Institute of Tomar (Portugal). The manufacturing procedure for the replicas is described further in detail (*cf.* section 4.3, sub-section 4.3.1.2 – Surface decoration: yellow).

**Note:** Self-absorption (SA) effects were not taken into account in the following results. SA effects should be considered, especially when measuring in fluorescent mode (which is the present case). Although one would expect different SA for standards and original samples, the amount of Pb or Sb present in the latter reaches almost 40 % in most of the cases. This assigns the samples with high-Z matrix and theoretically not much difference between SA-effects on standards and originals should be expected. However, further investigations are in course, considering this aspect. The results here presented serve as comparative basis between oxidations states and post-edge features between standards and unknown only.

### **Sb-K speciation: standards**

In order to investigate the absorption behavior of Sb at the K-edge (30491 eV), the XAFS spectra were measured with a step width of 10 eV in the pre-edge region (from 30391 eV to 30461 eV) and from there over the edge in 2 eV steps until 30595 eV. From 30595 eV until 31488 eV in 220 equidistant steps in the k-space. All measurements were performed in fluorescence mode, as the samples are thick and have high-Z matrix. A Sb-foil was used to calibrate the monochromator for the energy of the atomic Sb-K absorption edge, at 30491 eV.

In figures 4.33a and 4.33c, the XANES region for the Sb-K edge from all reference materials is plotted. Apart from  $\text{Pb}(\text{SbSn})\text{O}_3$  compound, the white lines are broad and the oscillations on the post-edge region reveal that multiple scattering at low kinetic energies takes place. The transition in the case of a K-edge (1s) occurs between  $s \rightarrow p$  orbitals and the final state may have mixing with other orbitals (hybridization) that change the absorption profile.



**Figure 4.33** – a) & c) XANES spectra of Sb-based reference materials @ Sb-K edge. Differences in the edge positions as well as on the post-edge oscillations can be observed, owed to the contribution of different electronic shells; b) & d) Fourier transform of  $\chi(R)$  of experimental Sb-K edge EXAFS  $\chi(k)$  for different reference compounds.

The absorption features at the XANES region (figures 4.33a and 4.33c) reveal that the edge position for cubic crystalline compounds with just one valence state ( $\text{Sb}_2\text{O}_5$ ,  $\text{Sb}_2\text{O}_3$  Fluka,  $\text{Pb}_2\text{Sb}_2\text{O}_7$  and  $\text{Pb}_3(\text{SbO}_4)_2$ ) is at 30494 eV. Moreover, the absorption edge of compounds with orthorhombic crystalline structure (Cervantite, Stibiconite and Valentinite) is at 30496 eV. Senarmonite (a cubic crystalline phase of  $\text{Sb}_2\text{O}_3$ ) assumes the lowest edge position at 30493 eV.

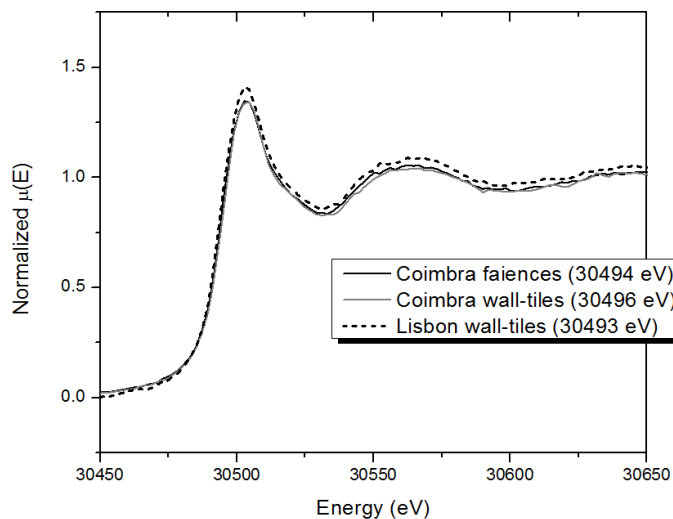
XANES spectroscopy is extremely sensitive to the local coordination chemistry and the differences in the post-edge features suggest that the  $4d^{10}$  electrons in the SbV state are responsible for these perturbations.

Figures 4.33b and 4.33d show the Fourier transform of  $\chi(R)$  of experimental Sb-K edge EXAFS  $\chi(k)$  for the reference compounds. With EXAFS one is able to identify differences at other levels (environment of the probed atom), such as coordination and symmetry – that cannot be attained by the XANES region. Here, the peaks represent resonant frequencies – resulting from the interference between the outgoing and the incoming scattered waves (*cf.* chapter 3, section 3.4). The higher the amplitude of these peaks, the higher the coordination number (CN) and the structural symmetry. From figures 4.33b and 4.33d, one can observe several differences between the EXAFS spectra of the Sb-reference compounds. First of all, differences arise between compounds with the same molecular formula but different crystalline structures (Valentinite and Senarmonite – figure 4.33b). This is owed mainly to symmetry issues: the cubic arrangement reveals higher symmetry – higher amplitude – while the opposite happens for orthorhombic crystallographic arrangements.

Looking at figure 4.33d, a large difference between the  $\text{Pb}(\text{SbSn})\text{O}_3$  and the rest exists. The small amplitude peaks from this compound reveal that there is a low CN – low number of neighbors – and also low symmetry. The first neighbor in all Sb-reference compounds is at about 1.7 Å and it corresponds to the Sb-O1 path of interference. Then at about 2.8 Å another Sb-O2 happens, which is just observable for the  $\text{Pb}_2\text{Sb}_2\text{O}_7$  compound. At about 3.4 Å and 3.8 Å the interference paths Sb-Sb1 and Sb-Sb2 occur, which are observed for all compounds except  $\text{Pb}(\text{SbSn})\text{O}_3$ .

#### **Sb-K speciation: original samples**

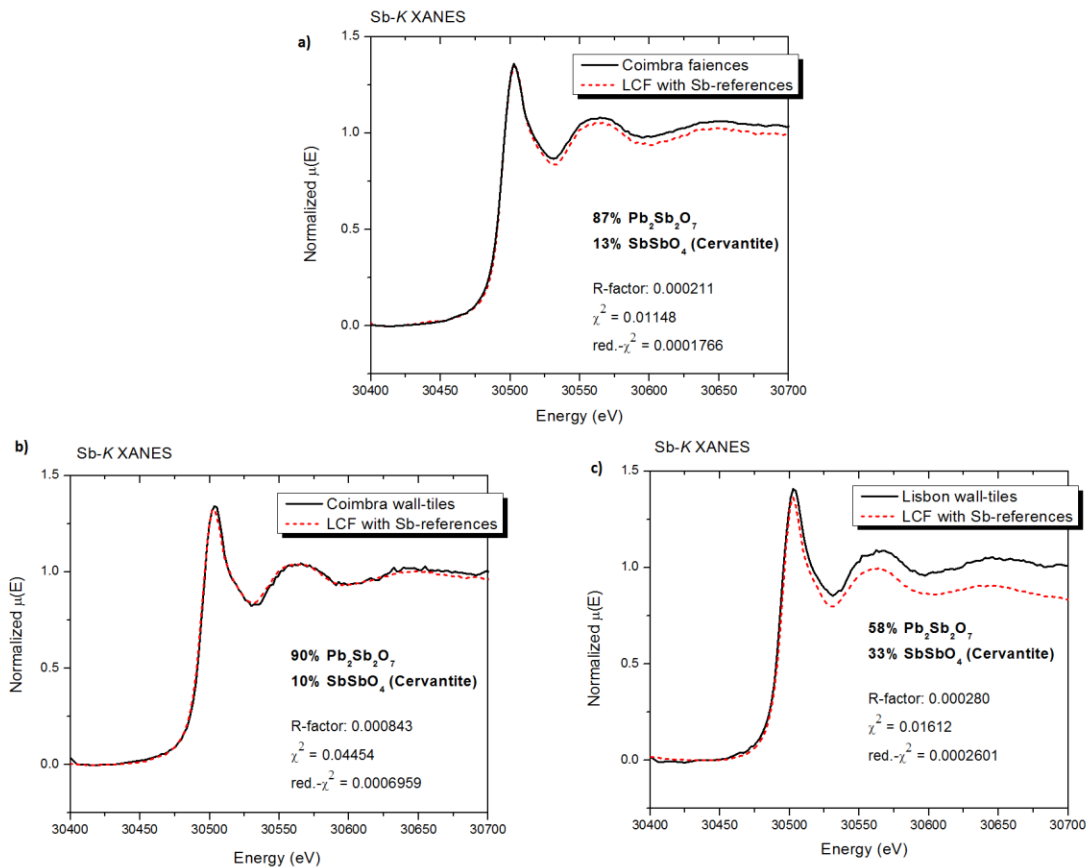
XANES measurements were performed onto the yellow surface decorations from original samples and in figure 4.34, a spectrum of each type of sample is plotted .



**Figure 4.34** – XANES spectra of some of the original samples @ Sb-K edge.

From figure 4.34 one sees that the edge position of all Sb-K XANES spectra is slightly shifted. Faiences from Coimbra reveal Sb-K edge @ 30494 eV, wall-tiles from Coimbra @ 30496 eV and wall-tiles from Lisbon @ 30493 eV. The post-edge features seem quite similar among all spectra from original samples but the shift in energy suggests differences in the crystalline structure. According to figures 4.33a and 4.33c, edges @ 30494 eV can represent different oxidations states but a cubic crystalline structure is expected. If the edge is at 30496 eV an orthorhombic crystallographic arrangement is present and the edge position at 30493 eV is in agreement with the Sb(III) state in Senarmonite.

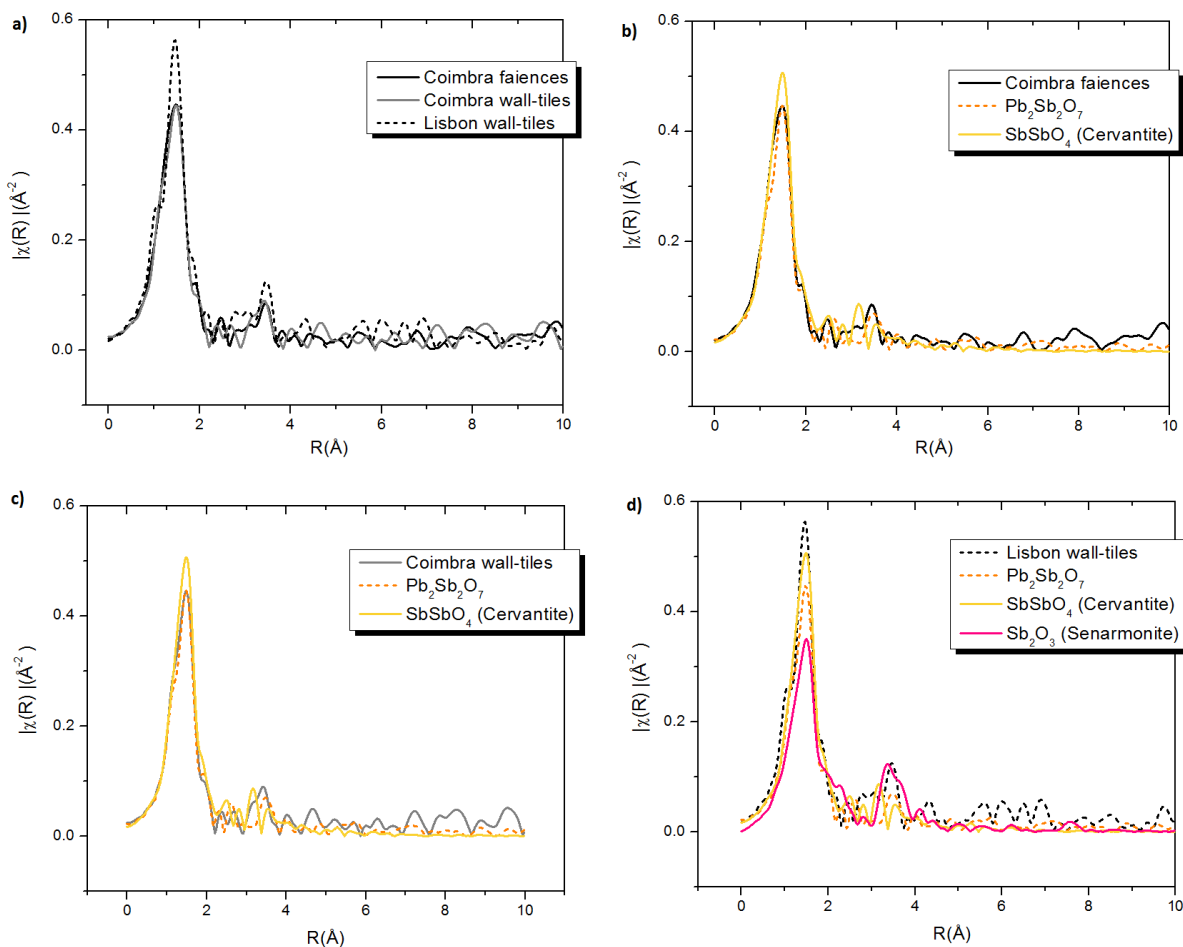
A linear combination fitting (LCF) procedure was performed for each spectrum with all the Sb-reference compounds, in order to find similarities in the composition of the unknown spectra from the original samples. In figure 4.35 spectra from the three different types of samples are shown together with the spectra obtained by LCF with standards.



**Figure 4.35** – Linear combination fitting (LCF) with Sb-reference compounds adjusted to the unknown XANES spectra of yellow of a) faiences from Coimbra, b) wall-tiles from Coimbra and c) wall-tiles from Lisbon. (Note: the difference in height between original (black) and LCF (dashed-red) in c) is merely due to an exportation fault from ATHENA.)

From figure 4.35 one realizes that  $\text{Pb}_2\text{Sb}_2\text{O}_7$  adjusts practically entirely to the features of the XANES spectra of all samples. However, the yellow from the samples from Lisbon (figure 4.35c) reveals a mixture of valences for Sb, where 58% adjusts to  $\text{Pb}_2\text{Sb}_2\text{O}_7$  and 33% to  $\text{SbSbO}_4$ . It is important to realize that this process of LCF does not necessarily mean that, when a result of 100% suitability with a certain compounds arises, the unknown spectrum corresponds exactly to that compound. For the edge position and post-edge features it is in good approximation a valid result but one must (if possible) always confirm with the EXAFS region.

Figure 4.36a shows the EXAFS spectra of each type of original samples: faiences from Coimbra and wall-tiles from Coimbra and Lisbon. Figures 4.36b, 4.36c and 4.36d show overlap between EXAFS spectra of each original sample and all the Sb-reference compounds.



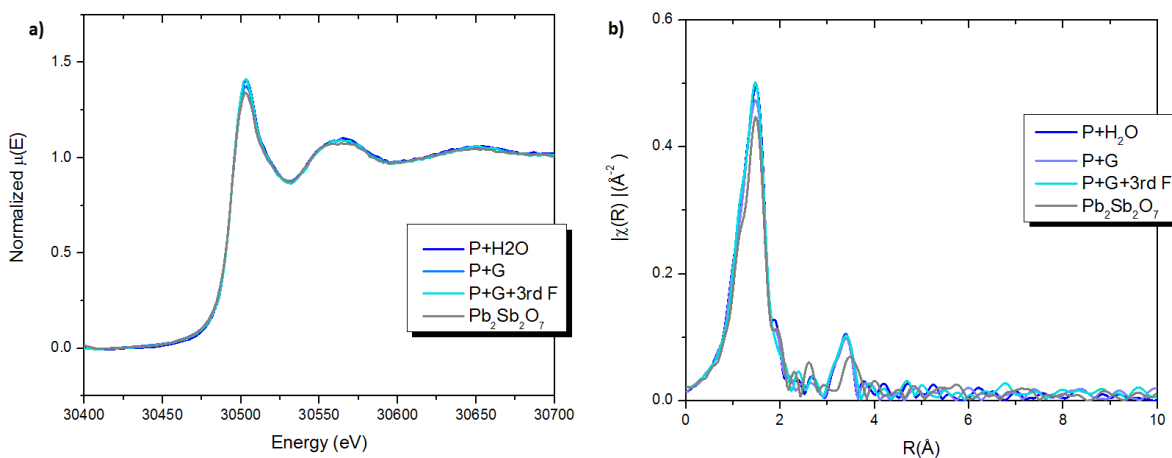
**Figure 4.36** – Fourier transform of  $\chi(R)$  of experimental Sb-K edge EXAFS  $\chi(k)$  for different types of original samples: a) Faiences and Wall-tiles (Coimbra) and Wall-tiles (Lisbon); together with the reference compounds: b) Faiences from Coimbra, c) Wall-tiles from Coimbra, d) Wall-tiles form Lisbon.

From figure 4.36a one realizes clear differences between the EXAFS profiles of different samples. For both faiences and wall-tiles from Coimbra, EXAFS signals adjust quite well to Naples Yellow ( $\text{Pb}_2\text{Sb}_2\text{O}_7$ ) and Cervantite ( $\text{SbSbO}_4$ ) compounds (figures 4.36b and 4.36c). The wall-tiles from Lisbon have shown further details, in which the shape of the frequencies seems to distinguish from any other Sb-compound (figure 4.36c). For example the first peak reveals an

overlap of three different interference paths – by the presence of “shoulders” on the left- and right-side of the peak (at about 1.8 Å). Furthermore, the succession of peaks around 3 Å does not have a match with any of the Sb-reference compounds. Probably a mixture of other Sb-based compounds exists and the available reference materials are not enough to testify this assumption.

Between the different samples one can observe a higher symmetry and CN among the wall-tiles from Lisbon (figure 4.36a) – owed to the higher amplitude of the first peak. Further information obtained by EXAFS is how far the closest neighbors from Sb are found at about 1.5 Å and 3.5 Å.

The next step was to verify if there are differences in the molecular structure on the yellow pigment depending on the manufacturing process used. For this purpose replicas were manufactured in laboratory according to procedure explained ahead in section 4.3, sub-section 4.3.1.2. The pigment used was the so-called “conventional” Naples Yellow ( $\text{Pb}_2\text{Sb}_2\text{O}_7$ ). Figure 4.37 shows XANES (a) and EXAFS (b) spectra for the three replicas together with the  $\text{Pb}_2\text{Sb}_2\text{O}_7$  in powder.



**Figure 4.37** – a) XANES and b) spectra of the three replicas together with the  $\text{Pb}_2\text{Sb}_2\text{O}_7$  in powder.

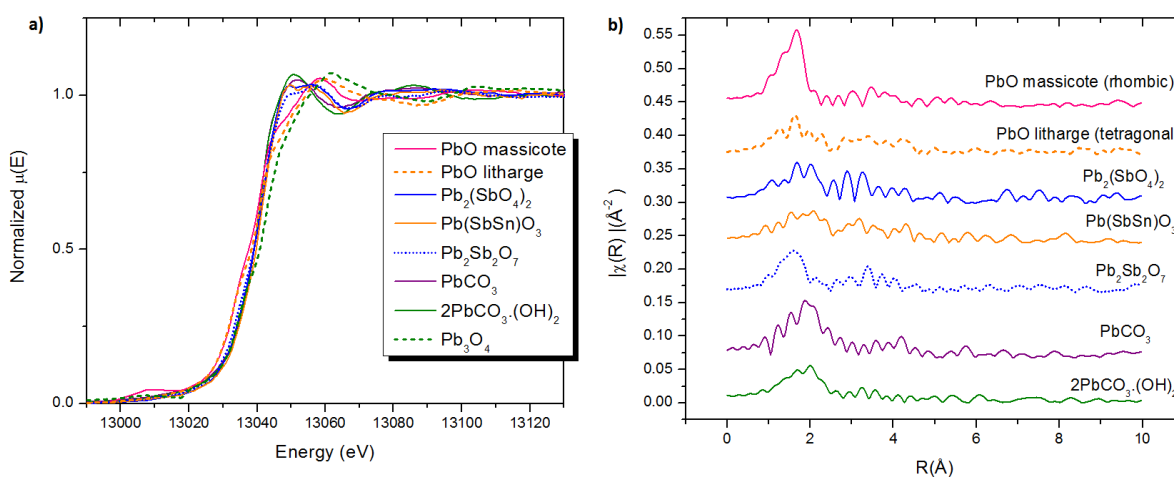
Whether the pigment was applied mixed with water (P+H<sub>2</sub>O) or with glaze (P+G) or with glaze and submitted to a third firing stage (P+G+3<sup>rd</sup> F) does not affect the structural role of Sb –



as one can observe by the strong resemblance between all spectra in the XANES region (figure 4.37a) and EXAFS region (figure 4.37b).

### **Pb-L<sub>3</sub> speciation: standards**

Since the yellow pigments are also Pb-based, a similar approach was also carried out for lead. The chemical speciation was performed at the Pb-L<sub>3</sub> edge. In figure 4.38a an overlap of the XANES spectra collected for all the reference materials is presented in order to evaluate the differences in absorption.



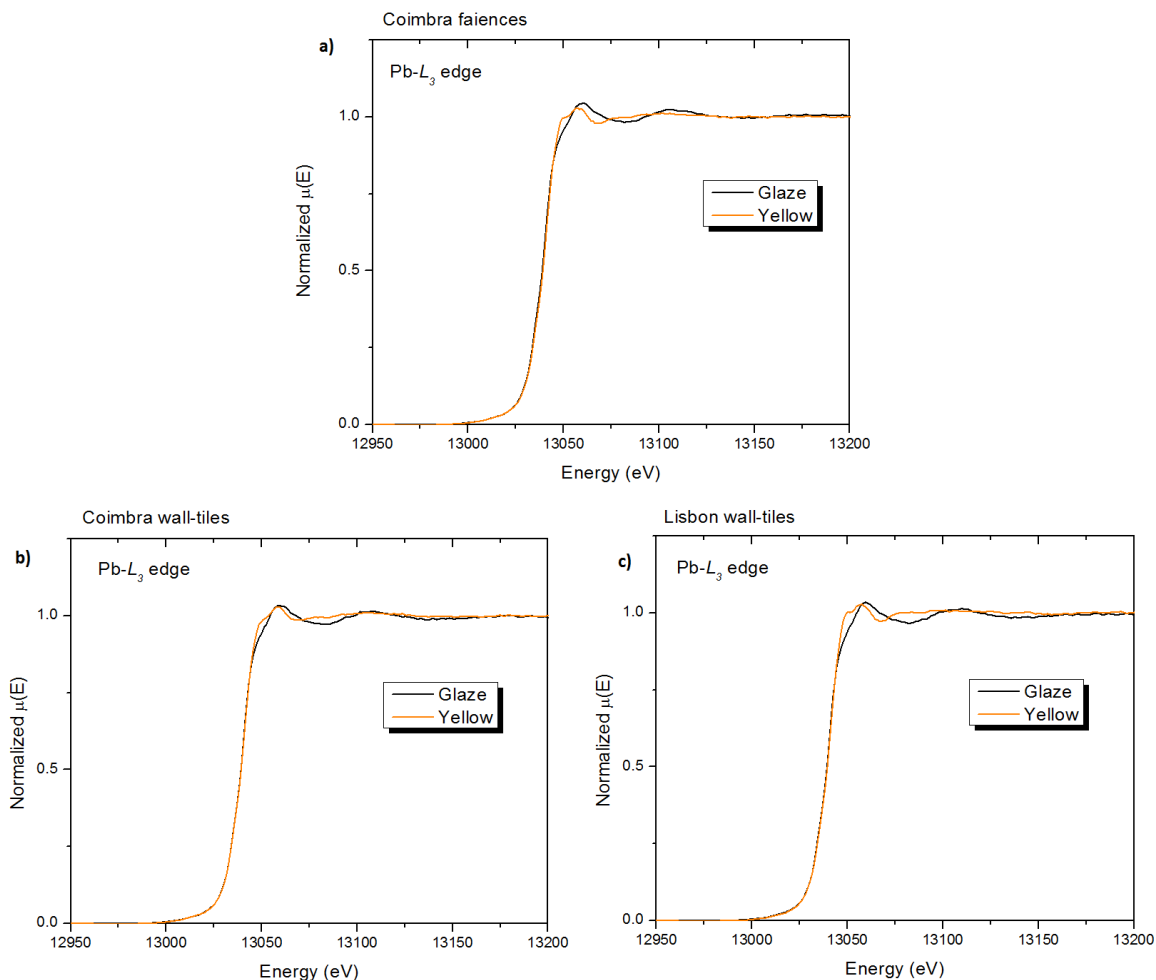
**Figure 4.38** – a) XANES spectra of Pb-based reference materials @ Pb-L<sub>3</sub> edge. Differences in the edge positions as well as on the post-edge oscillations can be observed, owed to the contribution of different electronic shells; b) Fourier transform of  $\chi(R)$  of experimental Pb-L<sub>3</sub> edge EXAFS  $\chi(k)$  for different reference compounds.

According to what was already mentioned (at the beginning of this section) the electronic configuration of Pb allows formally the +2 and +4 valences. The atomic absorption edge for Pb-L<sub>3</sub> is 13035 eV. According to the XANES spectra in figure 4.38a, the differences in the edge position are not significant in comparison to the clear differences in the pre- and post-edge details. The edge positions range between 13040 – 13041.5 eV for all compounds except for  $Pb_3O_4$  (13043.8 eV), owed to the fact that it comprised both Pb(II) and Pb(IV) oxidation states. The energy perturbation of the 5d<sup>10</sup> electrons due to the chemical bonding in Pb(IV) induces intensity variations in the XANES post-edge [101].

In contrast to the Sb-K EXAFS spectra, the Pb-L3 EXAFS region revealed huge differences in the frequencies domain which can be observed in figure 4.39b. Comparing the EXAFS signals emerging from PbO massicot and litharge, the difference between the crystalline structures (orthorhombic and tetragonal) is translated in huge differences. The former shows higher CN number and symmetry (by the higher peaks), while the low-amplitude peaks in the latter indicate the opposite. In general, probing Pb-L3 at the EXAFS regions revealed a lower CN and symmetry.

### **Pb-L<sub>3</sub> speciation: original samples**

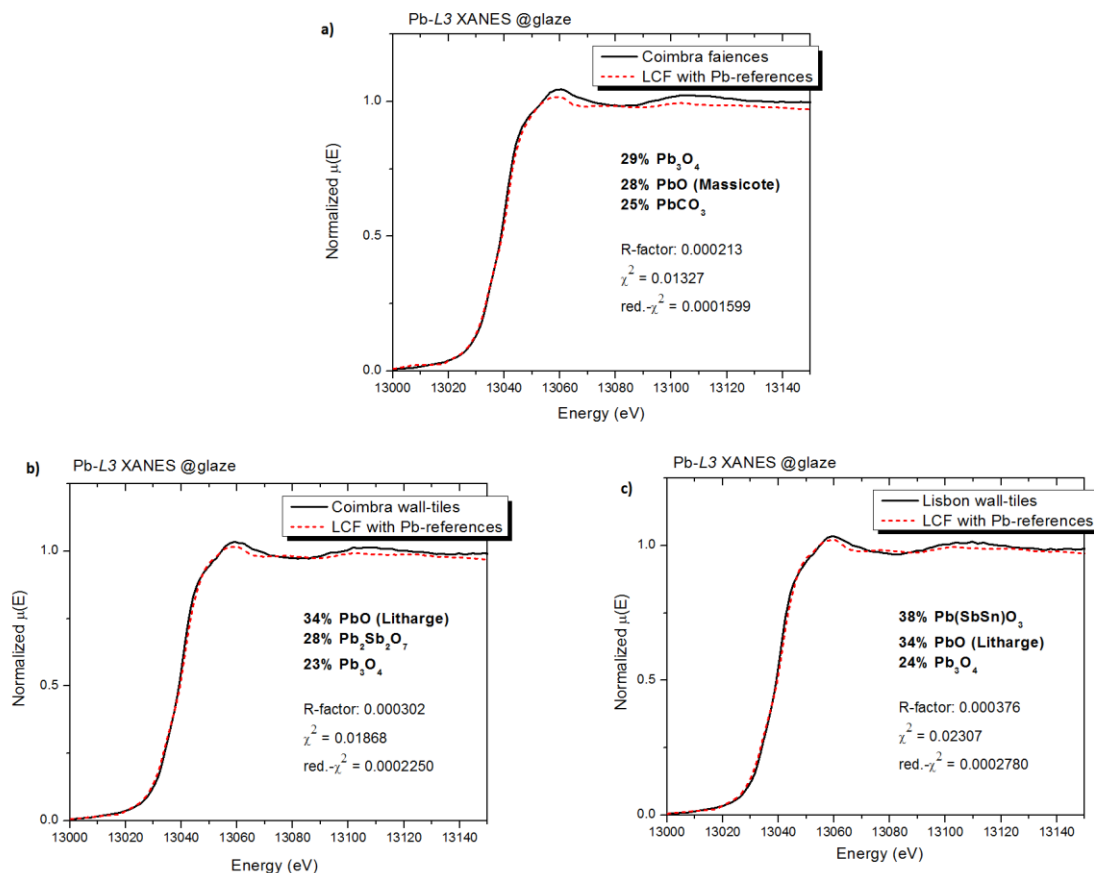
XANES measurements were performed on both glaze and yellow surfaces of each sample and, at first approach, a comparison between the two XANES spectra is made. Figure 4.39 shows spectra from Coimbra (faïences and wall-tiles) and from Lisbon samples (wall-tiles).



**Figure 4.39** – XANES spectra of some of the original samples @ Pb-L3 edge on both glaze (black) and yellow surfaces (orange) from faiences from Coimbra (a), wall-tiles from Coimbra (b) and wall-tiles from Lisbon (c).

In all cases, a 1 eV difference between the edges of glaze and yellow spectra was identified – with higher edge energy for the yellow spectra. The glazes have an absorption edge at 13040 eV and the yellows at 13041 eV – which represents a 5 eV shift for the former and 6 eV for the latter in comparison to the atomic value (13035 eV). Most noticeable are the post-edge differences existing between glaze and yellow absorption spectra, where two maxima are observed for the latter as well as opposite absorption coefficients for the energy range of 13070 – 13100 eV.

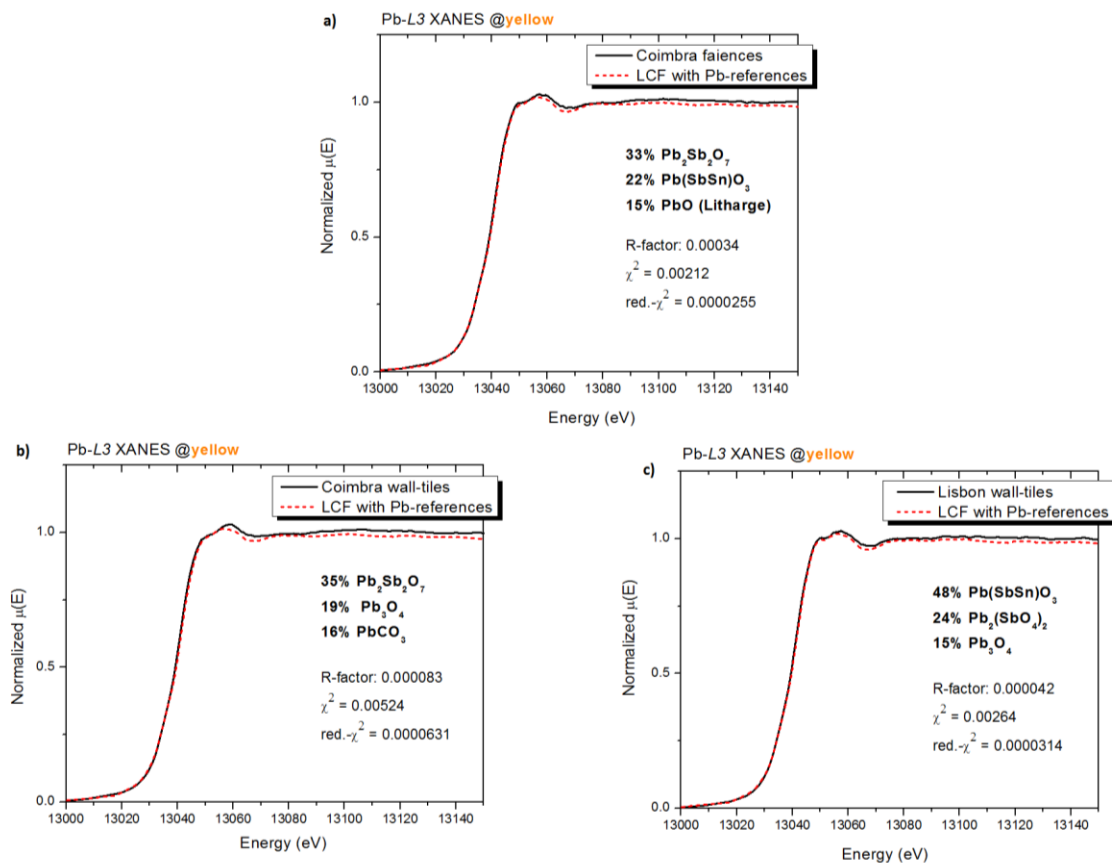
A linear combination fitting (LCF) procedure was performed for each spectrum with all the Pb-reference compounds, in order to find similarities in the composition of the unknown spectra from the original samples. In figure 4.40 spectra from the three different types of samples (on glaze) are shown together with the spectra obtained by LCF with Pb-standards.



**Figure 4.40** – Linear combination fitting (LCF) with Pb-reference compounds adjusted to the unknown XANES spectra of glazes of a) faiences from Coimbra, b) wall-tiles from Coimbra and c) wall-tiles from Lisbon.

From figure 4.40 one realizes different contributions from different Pb-reference materials emerge for each type of sample. In glazes from faiences from Coimbra  $\text{Pb}_3\text{O}_4$ ,  $\text{PbO}$  (massicot) and  $\text{PbCO}_3$  are the main compounds found with higher affinity from the LCF procedure (figure 4.40a). In wall-tiles from Coimbra a contribution from  $\text{Pb}_2\text{Sb}_2\text{O}_7$  (with 28%, figure 4.40b) and in wall-tiles from Lisbon a contribution of the  $\text{Pb}(\text{SbSn})\text{O}_3$  (with 38% - figure 4.40c) was found, both significant, which could suggest a mixture of yellow to the glaze to look yellowish.  $\text{PbO}$  (litharge) is the main component in the glazes from wall-tiles from Coimbra (figure 4.40b) and the second main in glazes from wall-tiles from Lisbon (figure 4.40c). The main conclusion from these LCFs is that Pb coexists in several forms within the glazes, intentionally added by the potter.

The same treatment was performed for the yellow regions and spectra from the three different types of samples (on glaze) are shown together with the spectra obtained by LCF with Pb-standards (figure 4.41).

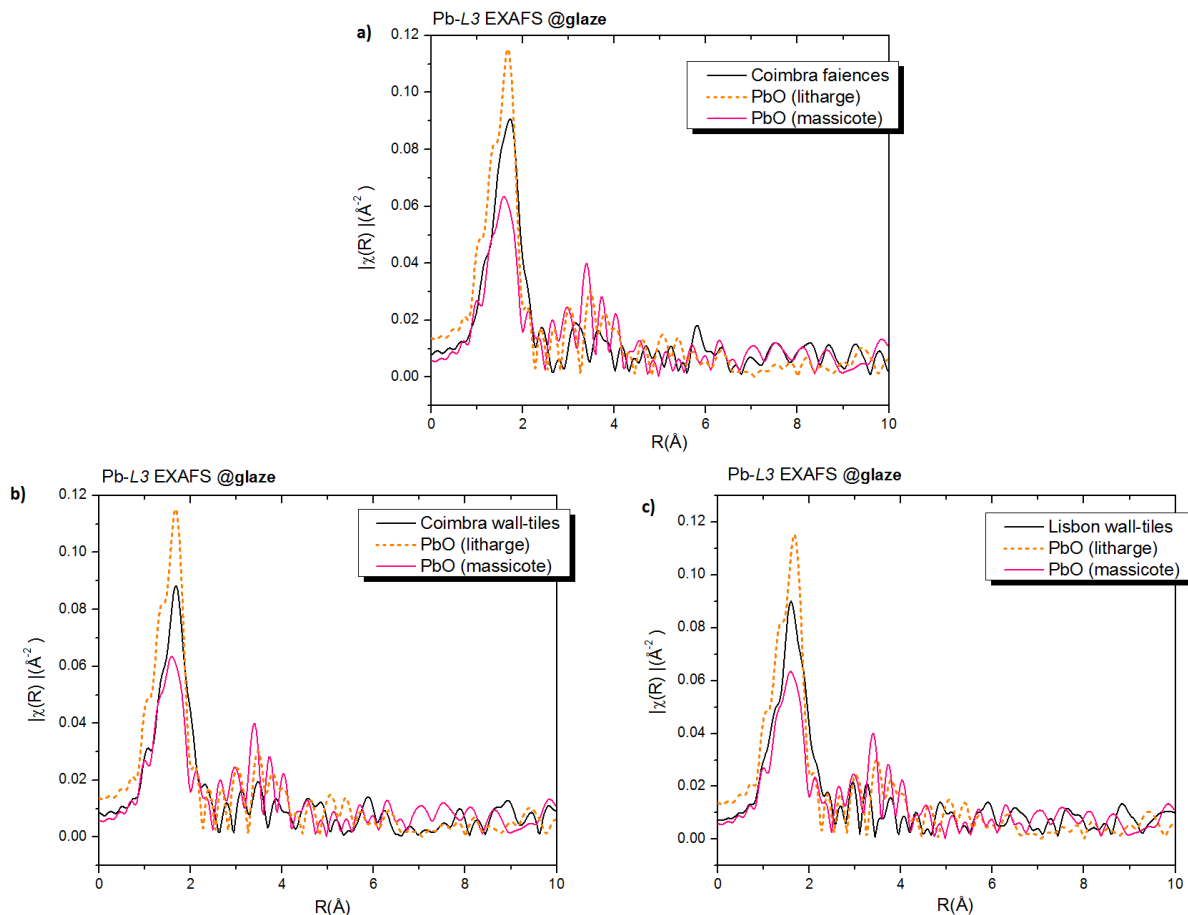


**Figure 4.41** – Linear combination fitting (LCF) with Pb-reference compounds adjusted to the unknown XANES spectra of yellow of a) faiences from Coimbra, b) wall-tiles from Coimbra and c) wall-tiles from Lisbon.

From figure 4.41 one realizes that the results obtained from the LCF for Sb-K (*cf.* figure 4.35) are in agreement with these ones. In samples from Coimbra (faiences and wall-tiles) the yellow pigment is mainly characterized by the Naples Yellow ( $\text{Pb}_2\text{Sb}_2\text{O}_7$ ) with percentages of 33% for faiences (figure 4.41a) and 35% for wall-tiles (figure 4.41b). Furthermore, in faiences from Coimbra the form  $\text{Pb}(\text{SbSn})\text{O}_3$  is the second most significant (with 22%), while for wall-tiles from Coimbra other Pb-based forms are the next most significant (19%  $\text{Pb}_3\text{O}_4$  and 16%  $\text{PbCO}_3$ ). The yellows from Lisbon are different (as shown before for the Sb-K speciation), since the most

significant compound is  $\text{Pb}(\text{SbSn})\text{O}_3$  (with 48%), followed by  $\text{Pb}_2(\text{SbO}_4)_2$  (with 24% - figure 4.41c). According to both Sb-K and Pb-L3 speciation Lisbon yellows revealed different composition, which suggests different manufacturing recipes and even different raw-materials used.

At last, EXAFS spectra were also acquired on both glaze and yellow from all samples and are presented below.

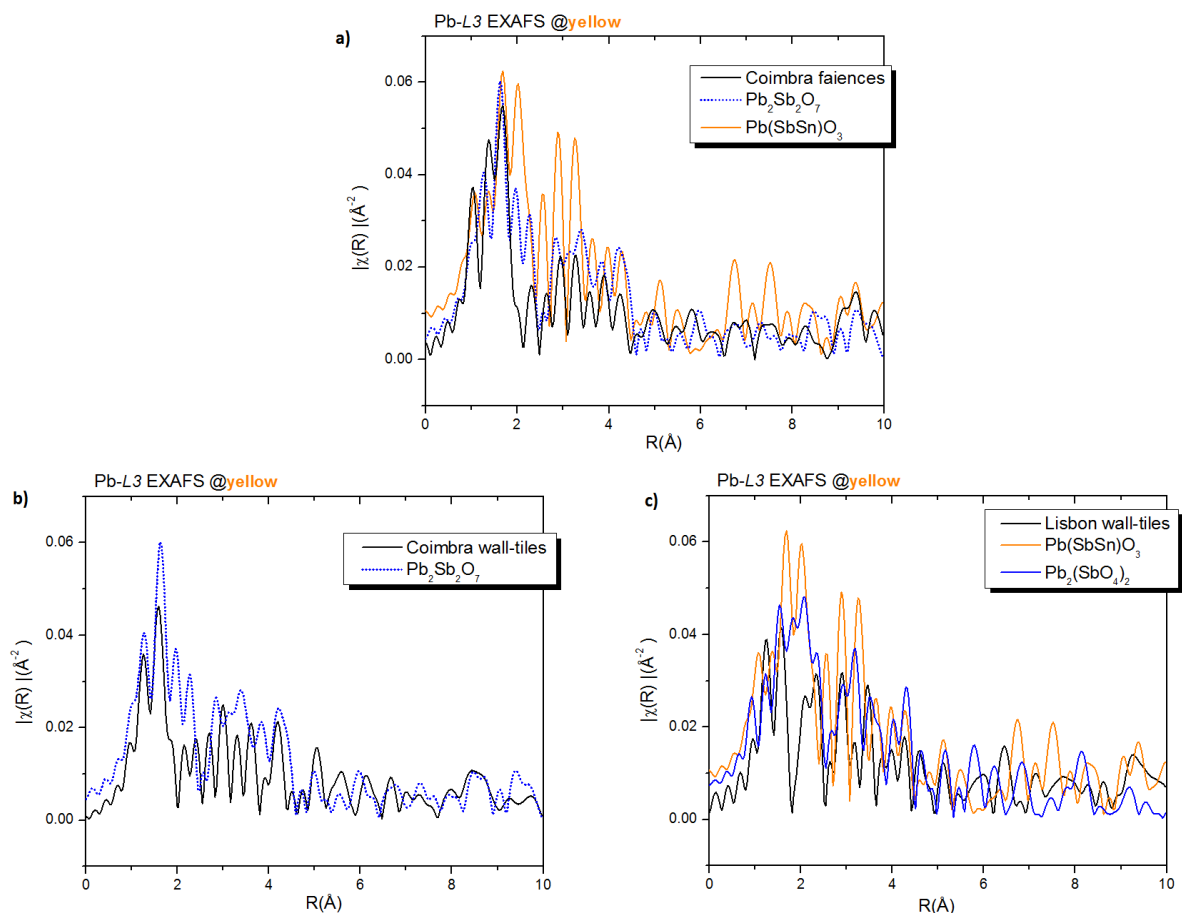


**Figure 4.42** – Fourier transform of  $\chi(R)$  of experimental Pb-L3 edge EXAFS  $\chi(k)$  of the glazes of different types of original samples: a) Faiences from Coimbra, b) Wall-tiles from Coimbra, c) Wall-tiles from Lisbon, all together with the two most compatible compounds (PbO litharge and massicot).

From figure 4.42 one sees a huge resemblance from the composition among the glazes from all samples. In the case of Pb-compounds, all glazes show high compatibility with the PbO compounds in both arrangements (tetragonal in litharge and orthorhombic in massicot).

However, the glazes in faïences from Coimbra show higher compatibility with PbO massicot (figure 4.42a), while wall-tiles from Coimbra show higher compatibility with PbO litharge (figure 4.42b).

Further EXAFS measurements were performed onto yellow decorated regions on the three types of samples and are plotted in figure 4.43.



**Figure 4.43** – Fourier transform of  $\chi(R)$  of experimental Pb-L3 edge EXAFS  $\chi(k)$  of the yellow regions for different types of original samples: a) Faïences from Coimbra, b) Wall-tiles from Coimbra, c) Wall-tiles from Lisbon.

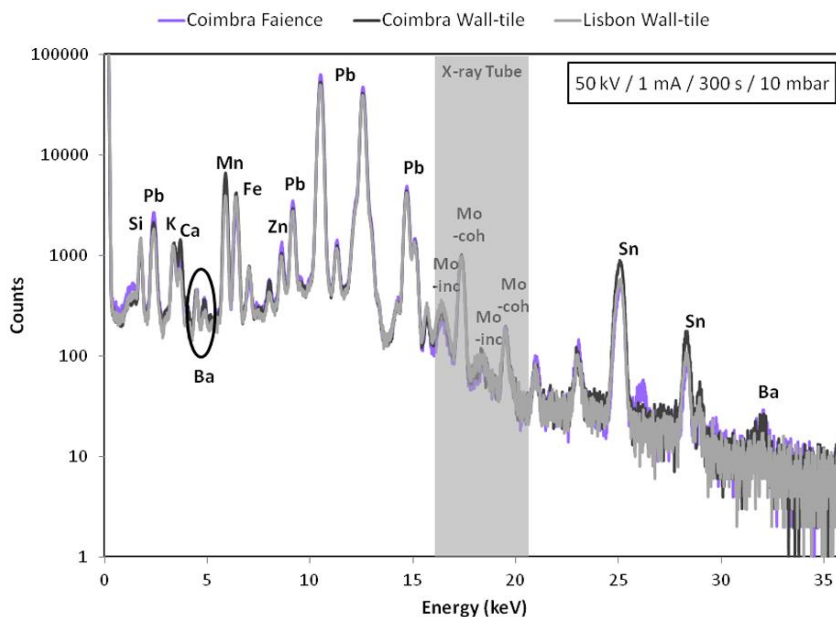
By evaluation of the EXAFS profiles, the results are in agreement with the LCF performed for the XANES region (*cf.* figure 4.41). The yellow pigment on both faïences and wall-tiles from Coimbra are compatible with the Naples Yellow pigment ( $\text{Pb}_2\text{Sb}_2\text{O}_7$ ) (figures 4.43a and 4.43b), while the yellow pigment on wall-tiles from Lisbon showed practically no resemblance to the

conventional Naples Yellow pigment. Instead a compatibility between the EXAFS profiles of two other Sb-compounds ( $\text{Pb}(\text{SbSn})\text{O}_3$  and  $\text{Pb}_2(\text{SbO}_4)_2$ ) is found for the yellow in wall-tiles from Lisbon (figure 4.43c).

#### 4.2.3.3 – Purple pigment

##### *X-ray Fluorescence*

Analyses performed with conventional XRF showed similar chemical composition in all purple colors from both production centers (figure 4.44).

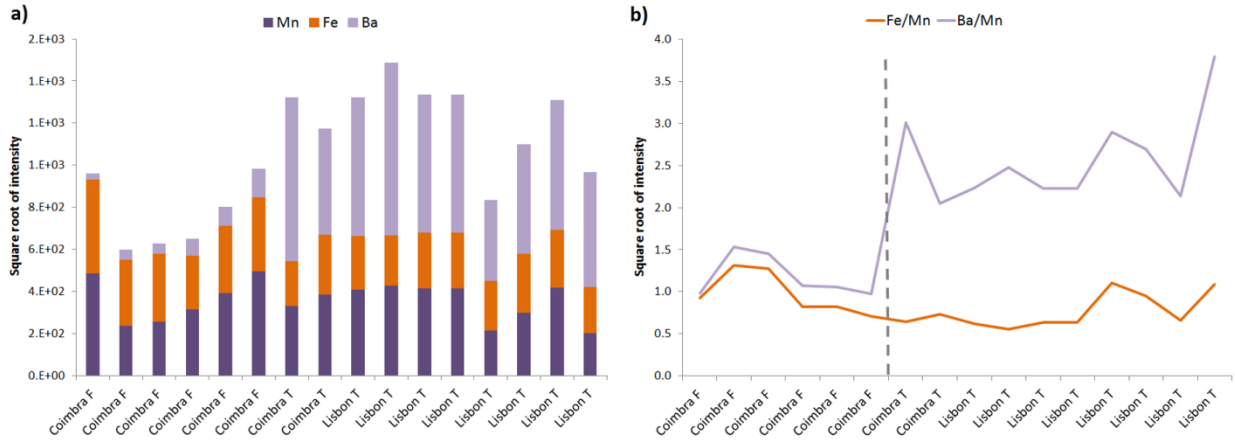


**Figure 4.44** – XRF spectra – obtained in conventional mode – from purple regions from faiences from Coimbra and wall-tiles from Coimbra and Lisbon.

The dominant element that confers the purple color is Manganese (Mn), and the presence of Barium (Ba) in the spectra indicates that the mineral Psilomelane  $[(\text{Ba},\text{H}_2\text{O})_2\text{Mn}_5\text{O}_{10}]$  may have been used as source of Mn. It is known that in Portugal (specifically in the *Alentejo* region) Psilomelane is quite abundant and this means that the source for Manganese may be local [102].



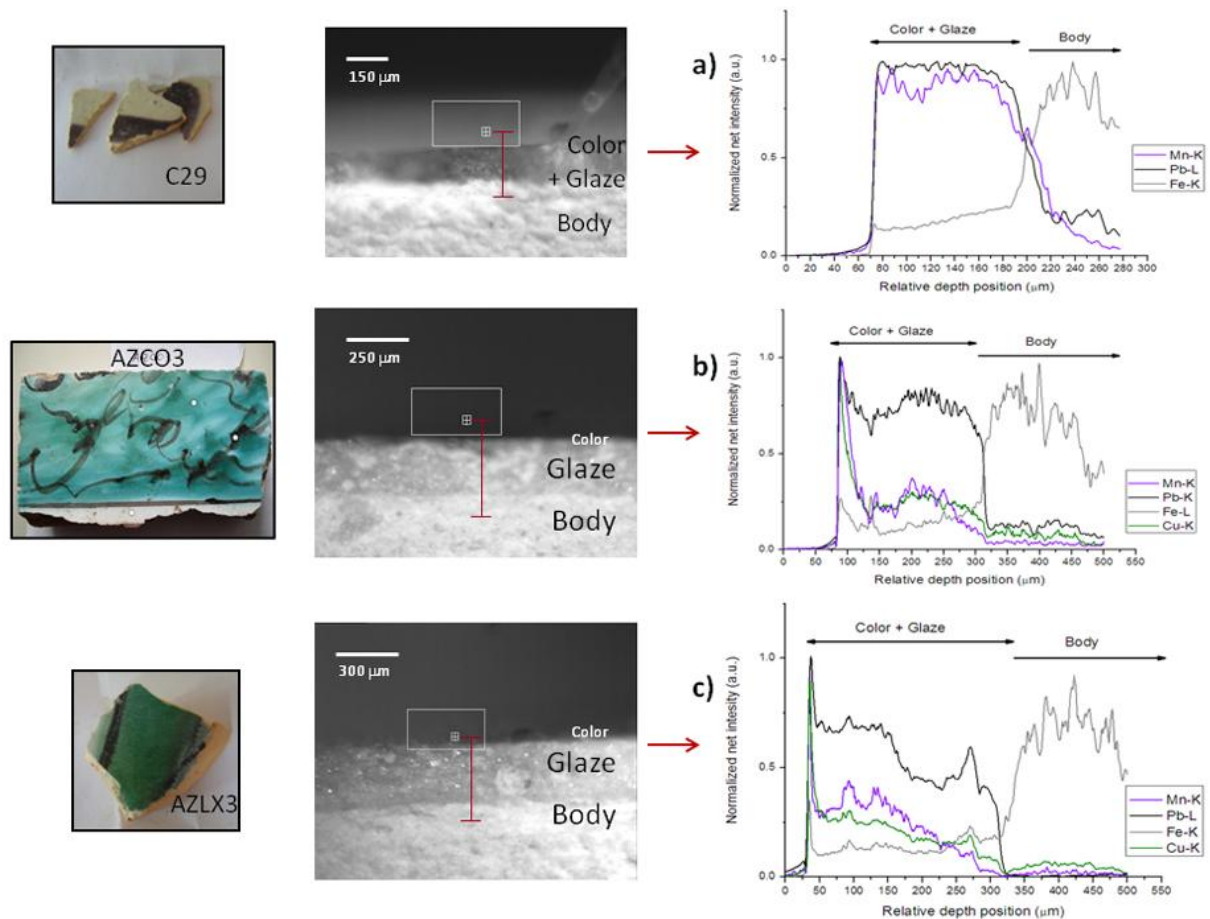
In order to evaluate the consistence of the presence of Barium connected to Manganese, net counts for these elements was taken into account and compared between faiences and wall-tiles (from Coimbra and Lisbon) (figure 4.45).



**Figure 4.45** – Plot of the elemental net counts for Mn, Fe and Ba for faiences from Coimbra (Coimbra F), wall-tiles from Coimbra (Coimbra T) and wall-tiles from Lisbon (Lisbon T); b) comparison of elemental ratios (Fe/Mn, Ba/Mn) between faiences from Coimbra (Coimbra F), wall-tiles from Coimbra (Coimbra T) and wall-tiles from Lisbon (Lisbon T).

From figure 4.45a one sees that the wall-tiles (Coimbra T and Lisbon T) show higher count rates for Ba-L lines and in comparison to the faiences (Coimbra F). This is proved by the ratio plot in figure 4.45b, where an increase of the Ba/Mn (light-purple line) is observed (right hand-side of the grey dashed line). The ratio Fe/Mn (orange line) keeps more or less unchanged between faiences and wall-tiles.

In order to check the elemental distribution in depth, specifically the pigment dissemination throughout the glaze, high-resolved Micro-XRF scans on the cross-section were carried out.



**Figure 4.46** – Cross-section scans performed through purple/glaze/body of a) a faience from Coimbra, b) a wall-tile from Coimbra, and c) a wall-tile from Lisbon [39].

In figure 4.46 the elemental profiles of samples containing purple decorative motifs are compared. Cross-section scans were performed through purple/glaze/body from a faience from Coimbra (figure 4.46a) a wall-tile from Coimbra (figure 4.46b) and a wall-tile from Lisbon (figure 4.46c).

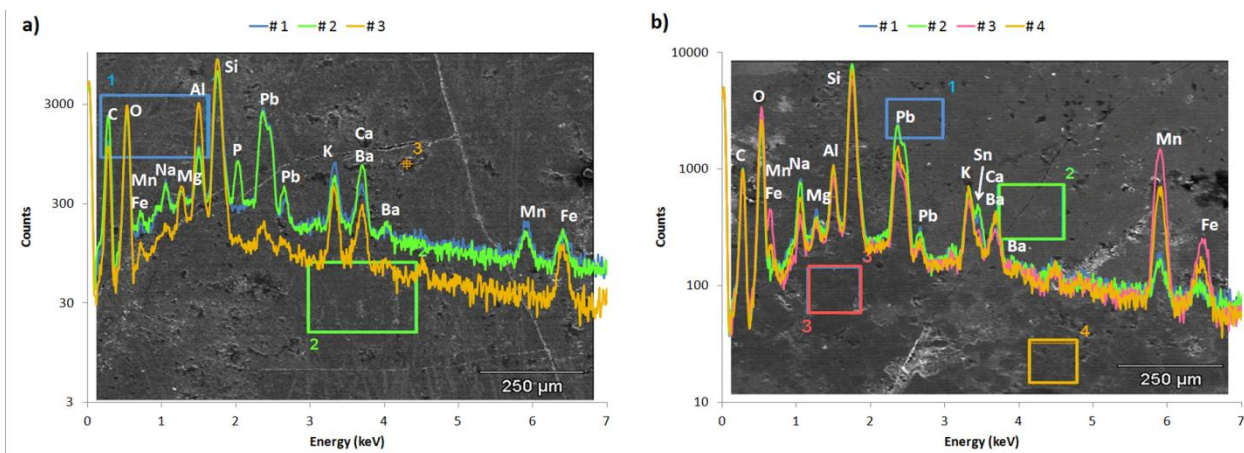
Again, in the pictures taken with the microscope it is indicated how the scans were performed. The scans compare the Mn-K, Pb-L and Fe-K signals, which characterize purple, glaze and body, respectively. Once again one can see that the faience sample (figure 4.46a) reveals no interface between color/glaze. The glaze thickness is approximately 150  $\mu\text{m}$  and the pigment was applied to the glaze and both have been submitted to one firing stage. There is, however, a moderate connection between glaze and body in this sample, to observe by the

smoothly decreasing and increasing of the Pb and Fe profiles, respectively. Comparing the tiles from Coimbra and Lisbon it is to see that the pigment (Mn) is equally well dispersed through the glaze in both samples (figures 4.46b and 4.46c). However, the Mn profile in the sample from Coimbra (figure 4.46b) reveals a broader maximum at the surface ( $\sim 50 \mu\text{m}$ ) than in the sample from Lisbon ( $< 25 \mu\text{m}$  – figure 4.46c). The Copper (Cu) signal was also plotted because the purple motifs were applied together with a green colored layer (observable on the picture). The glazes from both tiles have thicknesses of about 250 and 300  $\mu\text{m}$  for the Coimbra and Lisbon cases, respectively. Again one observes a smoother elemental exchange at the interface glaze/body in the sample from Lisbon (figure 4.46c) than in the sample from Coimbra (figure 4.46b).

#### ***Scanning Electron Microscopy/Energy Dispersive X-ray Spectrometry (SEM/EDX)***

At this point, knowledge about the morphological properties of this pigment is also a requirement in order to complement and support the data so far presented. Hence, SEM/EDX analyses were performed on the purple areas of some samples (from both production centers). Again, it is important to emphasize the heterogeneity among these objects. Therefore, quantitative results obtained with EDX will be here presented just as an estimation of the content at a specific area. Hence, these will not be considered as providing representative quantitative information of the whole piece/area.

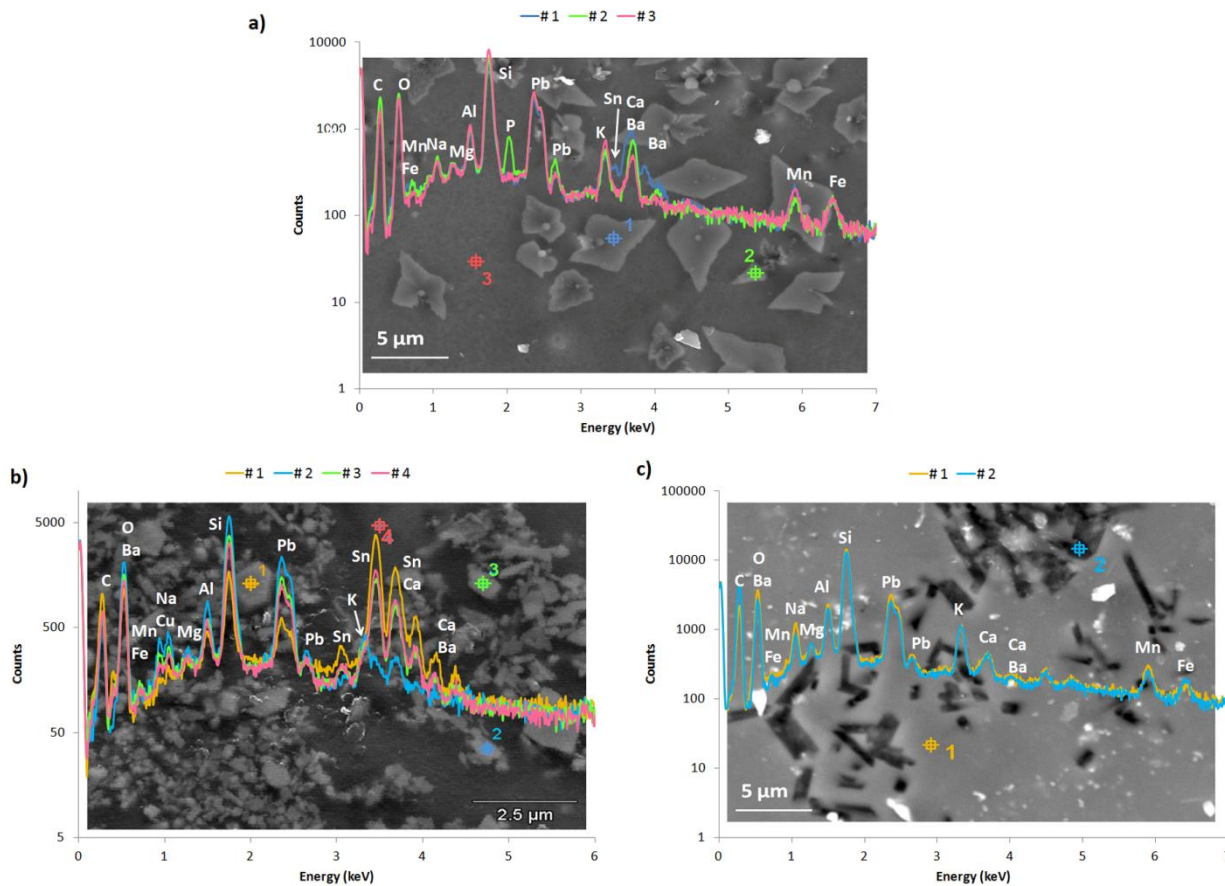
EDX results were obtained by wide-area analyses onto the purple surfaces (figure 4.47 and table 4.8).



**Figure 4.47** – SEM micrographs taken on the purple surface of a faience from Coimbra (a) and a wall-tile from Lisbon (b).

**Table 4.8** – Elemental composition of the purple regions of the samples (*N* is the number of samples analyzed) from Coimbra and Lisbon (in wt-%) obtained with standardless EDX (wide-area). Note the need of careful dealing with the values as rough estimates serving primarily to distinguish between the various types of samples.

Samples	Na	Mg	Al	Si	K	Ca	Mn	Fe	Sn	Ba	Pb	O
<b>Coimbra faiences</b> ( <i>N</i> = 4)	≤ 1	< 1	2–3	15–17	3–4	2–3	7–9	1–2	1–2	≤ 1	30–32	33–34
<b>Coimbra &amp; Lisbon</b> <b>Wall-tiles</b> ( <i>N</i> = 3)	≤ 1	< 1	1–2	11–13	1–2	≤ 1	19–20	1–2	1–2	≤ 1	9–11	43–44



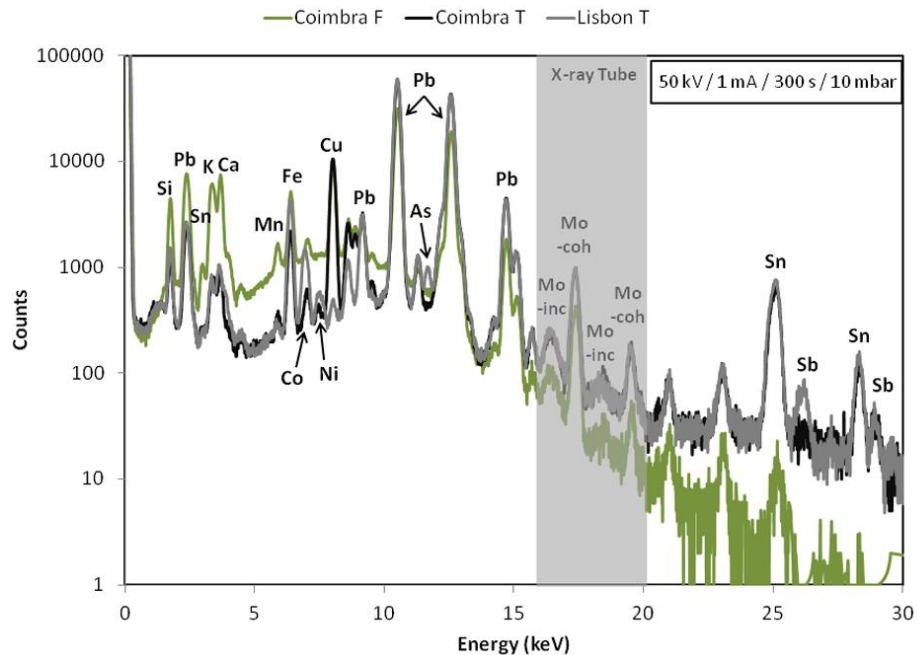
**Figure 4.48** – SEM micrographs (high magnification), with visualization of purple pigment crystals and the respective EDX spectra. a) Faience from Coimbra; b) wall-tile from Coimbra; c) wall-tile from Lisbon.

Interesting to observe is the difference in the amount of glaze components such as Pb, Si, K and Ca which is higher in the faiences than in wall-tiles. Particularly Pb which is much higher in faiences (ca. 30 wt%) than in wall-tiles (ca. 10 wt%). Furthermore, for the analyzed the amount of Mn is lower in faiences (ca. 10 wt%) than in wall-tiles (ca. 20 wt%). High magnification analyses have revealed that the crystals in the purple layer could be observed from both centers of production (figure 4.48).

#### 4.2.3.4 – Green pigment

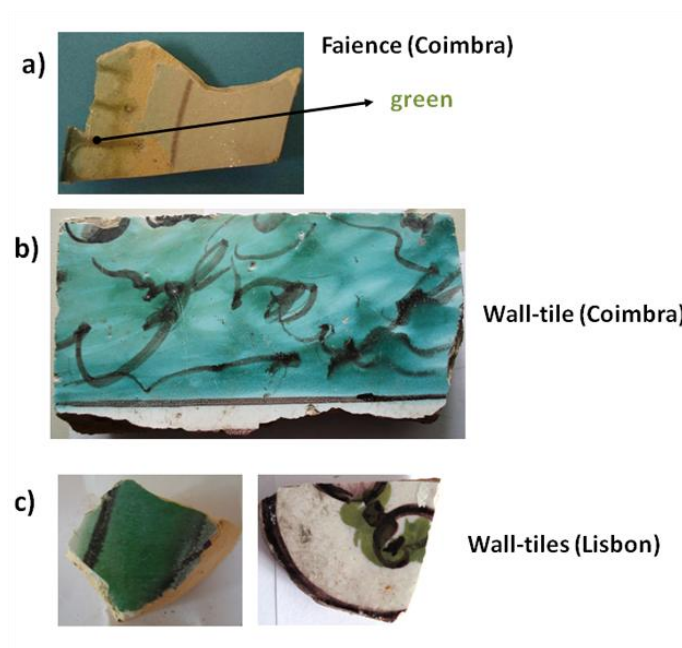
##### *X-ray Fluorescence*

Green was found to be rather scarce as color used for decoration purposes, among this type of objects. Within all analyzed samples, green was found in 2 faiences, 2 wall-tiles from Coimbra and 3 wall-tiles from Lisbon. Analyses performed with conventional XRF showed similar chemical composition in all green colors from both production centers, except for one wall-tile from Lisbon (figure 4.49).



**Figure 4.49** – XRF spectra – obtained in conventional mode – from green regions from faiences from Coimbra and wall-tiles from Coimbra and Lisbon.

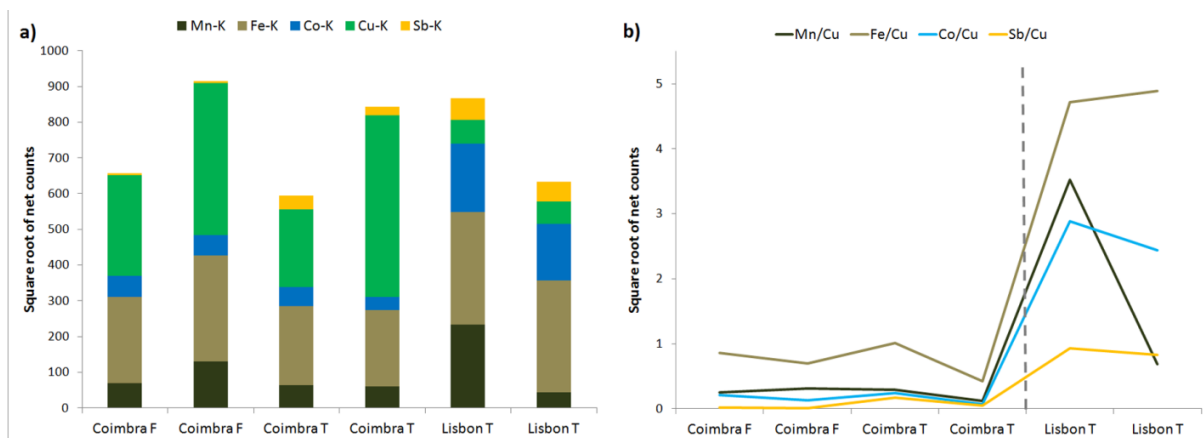
First of all the difference in the shape of the background between the spectrum of the faience (green) and the spectra from both wall-tiles (grey and black) is due to the fact that the former was obtained by means of a polycapillary lens and the latter by means of a collimator. This choice was due to the fact that the green areas in the faiences from Coimbra were much smaller than in the ones from the wall-tiles (figure 4.49), and in order to avoid overlap of information from adjacent areas, the polycapillary was more suitable.



**Figure 4.50** – Samples in which green was found for the decoration: a) faience from Coimbra (green stripes with ca. 1 mm thickness), b) wall-tile from Coimbra, c) wall-tiles from Lisbon (two different hues).

One can see – from figure 4.49 – that the dominant element is Copper (Cu). However, for one the wall-tiles from Lisbon the green hue is obtained by an intentional mixture between blue (Co-Ni-As) and yellow (Sb), seen in the light green spectrum in figure 4.49. This spectrum corresponds to the sample AZLX6, exhibited in figure 4.50c (right-hand side) and in fact a particular green hue is noticeable, when observing the other green hues from the other samples in the same figure.

In order to evaluate the consistence of the presence of Copper within the green decorated regions, net counts for these elements used and compared between faiences and wall-tiles (from Coimbra and Lisbon) (figure 4.51).

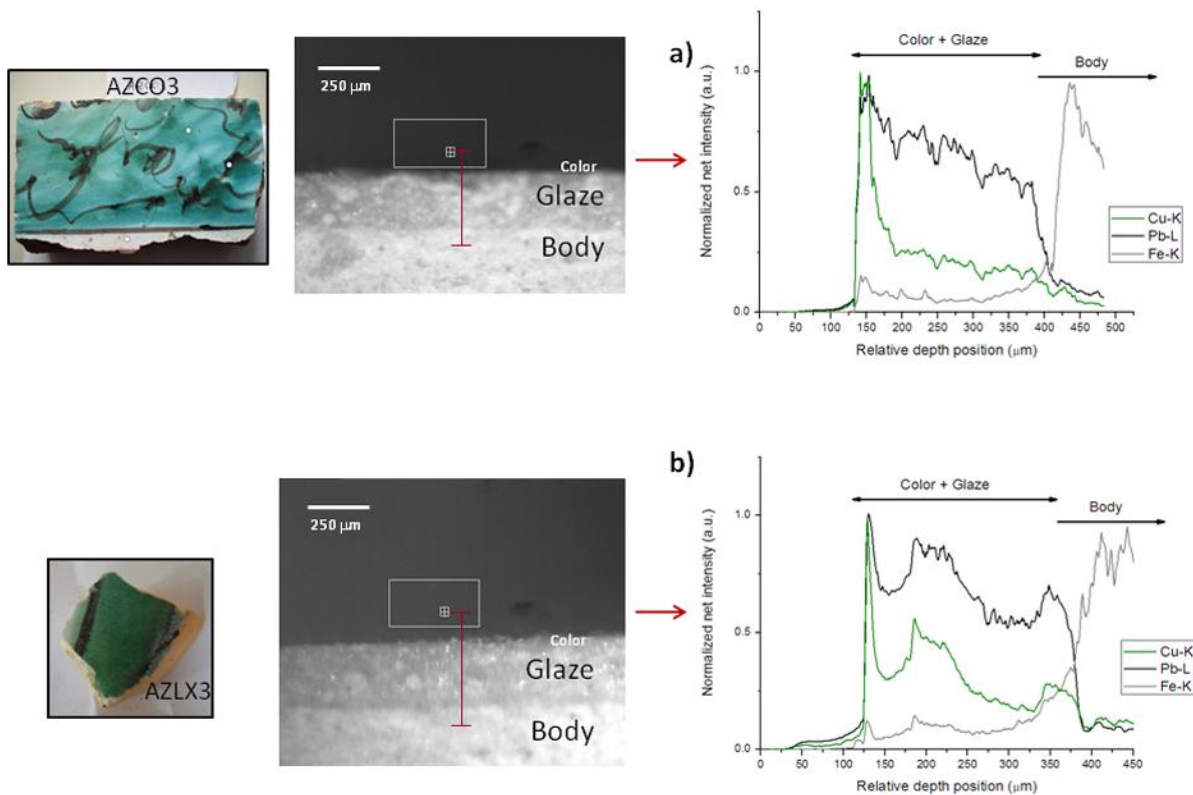


**Figure 4.51** – Plot of the elemental net counts for Mn, Fe, Co, Cu and Sb, for faiences from Coimbra (Coimbra F), wall-tiles from Coimbra (Coimbra T) and wall-tiles from Lisbon (Lisbon T); b) comparison elemental ratios (Mn/Cu, Fe/Cu, Co/Cu and Sb/Cu) between faiences from Coimbra (Coimbra F), wall-tiles from Coimbra (Coimbra T) and wall-tiles from Lisbon (Lisbon T).

From figure 4.51a one sees that in faiences and wall-tiles from Coimbra (Coimbra F and Coimbra T) the green color is due to a Cu-based pigment, while in wall-tiles from Lisbon (Lisbon T) the color green emerges from the mixture of a Co-based pigment (blue) and a Sb-based pigment (yellow). This is confirmed by the ratios plot in figure 4.51b. The Mn/Cu, Fe/Cu and Co/Cu ratio is relatively low in faience and wall-tiles from Coimbra (Coimbra F and Coimbra T), which means that Copper is the key-element for the green color. Conversely, the same ratios are relatively high in wall-tiles from Lisbon (Lisbon T), together with the Sb/Cu ratio, which indicated that the green color is mainly due to the overlap of blue and yellow.

In order to check the elemental distribution in depth, specifically the pigment dissemination throughout the glaze, high-resolved Micro-XRF scans on the cross-section were carried out [39].





**Figure 4.52** – Cross-section scans performed through green/glaze/body of a) a wall-tile from Coimbra, and b) a wall-tile from Lisbon [39].

Cross-section scans were performed through the green/glaze/body of a wall-tile from Coimbra (figure 4.52a), and a wall-tile from Lisbon (figure 4.52b). Evaluating the Cu-signal, the intake of pigment into the glaze seems to be higher in the sample from Lisbon than in the sample from Coimbra. However, a broader maximum of the Cu-signal at the surface from the sample from Coimbra (ca. 50  $\mu\text{m}$  – figure 4.52a) than in the sample from Lisbon (ca. 25  $\mu\text{m}$  – figure 4.52b) is observed [39]. Also, the elemental exchange between the glaze and the body seems to be more pronounced in the sample from Lisbon than in the sample from Coimbra. The justification is the same as previously explained (*cf.* 4.2.3.3 – Purple).

## **4.3 – Replicas**

One of the goals of this investigation was trying to carry out a non-destructive approach, as one is dealing with CH-related objects. The samples used for this work are fragments – and there is quite considerable available amount of such fragments in Portugal – so, some of these objects could undergo minor physical invasion. For example, an application of Carbon-layer to perform SEM measurements and also a small amount of ceramic body removal was allowed in order to perform XRD analyses. The ceramic body is not so crucial to keep intact, as it is quite easy to remove part of it while keeping the integrity of the whole piece.

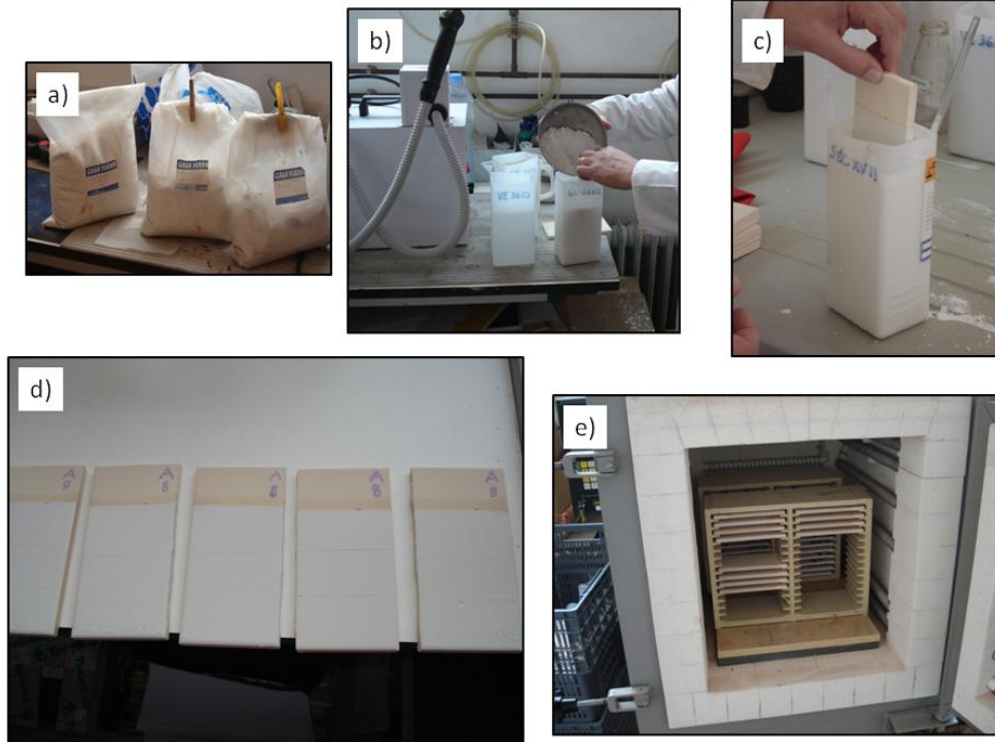
For all these “difficulties” the need of recreating analogues to the original samples became necessary in order to understand some features obtained by the experimental analyses.

All replicas were produced by Ricardo Triães from the Department of Arts, Conservation & Restoration from the Polytechnic Institute of Tomar (Portugal).

### **4.3.1 – Manufacturing processes**

#### **4.3.1.1 – Glaze**

It is important to know the mineralogical features of glazes and possibly to estimate the firing temperature to which they were submitted. For this purpose, three different types of glazed surfaces were produced. Using these glazes – with known chemical and mineralogical composition – one can observe the phase differences and mineralogical changes after each thermal transformation. Following the identification of the mineralogical changes in the prepared samples, one can correlate the obtained results for the original glazes, allowing estimating the production firing temperature [36]. The manufacturing procedure is explained in the following steps, with the help of figure 4.53:



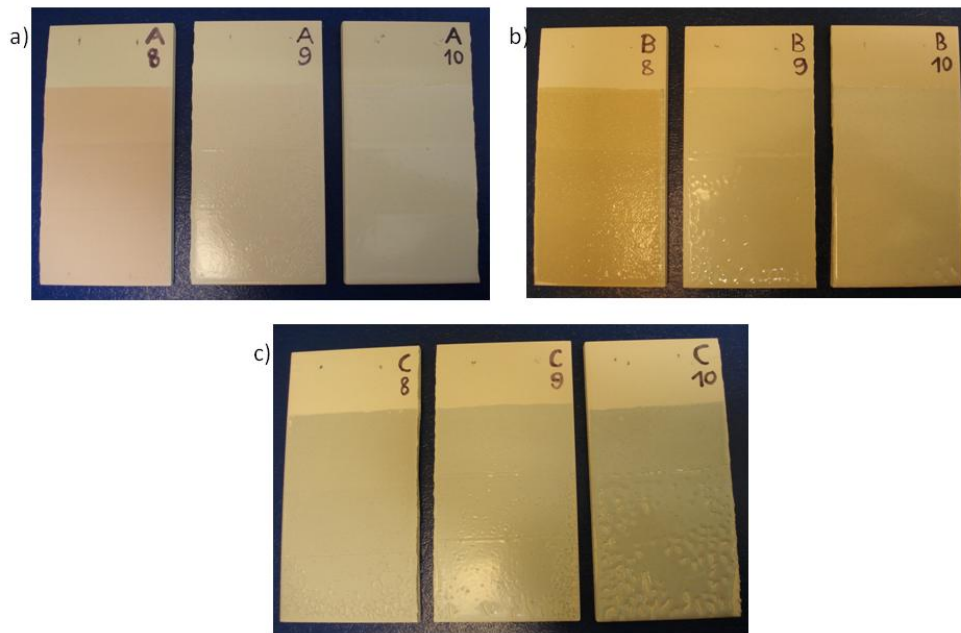
**Figure 4.53** – Manufacturing procedure for the glazed surfaces.

- 1) Industrial ceramic support was used as base;
- 2) Three different glazes (frit) – in powder – were used. Glaze A and B are two types of ancient glaze (XVII century) and Glaze C is a rustic glaze (figure 4.53a);
- 3) Each powder was diluted in water on a proportion of 1:3 (figure 4.53b);
- 4) The ceramic support was then submersed for 5 seconds in the glaze (figure 4.53c).
- 5) The pieces were put to “rest” just shortly in order for them to dry (figure 4.53d); they were marked with a designation which corresponds to the type of glaze (A, B or C) and to the temperature to which they were submitted (8 – 800 °C, 9 – 900 °C and 10 – 1000 °C). A total of four pieces were prepared for each glaze and temperature.
- 6) At last they were placed in the oven (figure 4.53e) and the firing sequence was the following:
  - i. 15 min. until 110 °C;

- ii. 15 min. at the 110 °C stage;
- iii. 90 min. until 550 °C;
- iv. 30 min. until 600 °C;
- v. 90 min. until maximum temperature (800, 900 or 1000 °C)

7) After the pieces are fired, the oven has to cool down to a temperature below 100 °C in order to open it.

In figure 4.54 a picture of how the pieces look like after fired is presented.



**Figure 4.54** – Three different types of glazes (A, B and C) submitted to three different firing temperatures (800 °C, 900 °C and 1000 °C) [36].

From figure 4.54 some aspects are noticeable by naked-eye observation. Features like color, brightness and integrity are obviously susceptible to changes according to the chemical composition and firing temperature used. Glaze A (figure 4.54a) has a matte appearance and it has experienced a change in the hue for higher firing temperature (from pinkish to grayish). Moreover, it has kept its integrity and smoothness under different firing temperatures. Glaze B (figure 4.54b) has a shiny appearance and the color has changed from yellow to light-yellow (from 800 °C to 1000 °C); plus, it has kept its integrity under different firing temperatures but it

shows a certain surface roughness with increasing temperature. Glaze C (figure 4.54c) has a shiny appearance as well and it has not changed its color. However, it has not kept its integrity with increasing firing temperatures: at 900 °C it has began to crack and for 1000 °C one sees quite high amount of holes in the glaze surface.

All these differences were mainly due to the glaze composition. Glaze A is more similar in composition to the ones used at the time the original pieces were manufactures, and one sees it kept intact even when submitted to 1000 °C. Glaze C is more modern and therefore, has less lead content which promotes the loss of integrity under “extreme” firing conditions.

#### **4.3.1.2 – Surface decoration – yellow**

Further replicas were prepared in laboratory in order to understand how the decorative motifs were applied to the glaze. This was especially investigated for the yellow pigments. As shown before, this pigment is a combination of Sb and Pb and it forms a quite compact “layer” on the upper part without much diffusion throughout the glaze (*cf.* sub-section 4.2.3.2 – yellow). In order to better evaluate whether the pigment was applied over the base glaze and the whole piece was submitted to a third firing stage (for the surface decoration), replicas with variable parameters were produced in laboratory.

The manufacturing procedure of these replicas is explained in the following steps:

- 1) Industrial ceramic support was used as base;
- 2) Glaze A (ancient-like, XVII century) was used and applied in the same way as described above, for the previous replicas (figure 4.53);
- 3) Naples Yellow ( $Pb_2Sb_2O_7$ ) – NY – purchased at the Kremer Pigmente© was used in all the variations of manufacture:
  - a. NY mixed with water and applied onto the base glaze – both fired at the same time;
  - b. NY mixed with water and applied onto the previously fired base glaze – third firing stage for the whole piece (which means, own firing stage for NY+water mixture);

c. NY mixed with glaze and applied onto the previously fired base glaze – third firing stage for the whole piece (which means, own firing stage for the NY+glaze mixture).

All replicas were then cut along the painted areas in order to have polished cross-sections having color/base glaze/body.

### 4.3.2 – Chemical and mineralogical characterization

#### 4.3.2.1 – Glaze

The use of raw glazes on traditionally fired products is a well-established practice. However, documental facts of the ceramic production in Coimbra report both raw and fritted applications on the bisque [9]. During the firing process of raw glazes, different processes can occur, such as: decomposition of raw materials, chemical reactions giving either crystalline or glassy products, and melting followed by nucleation and crystallization of the melt [103]. The glazes used for the replicas are commercially obtained frits.

XRF analyses on each type of glaze were performed and in figure 4.55 the respective spectra are shown.

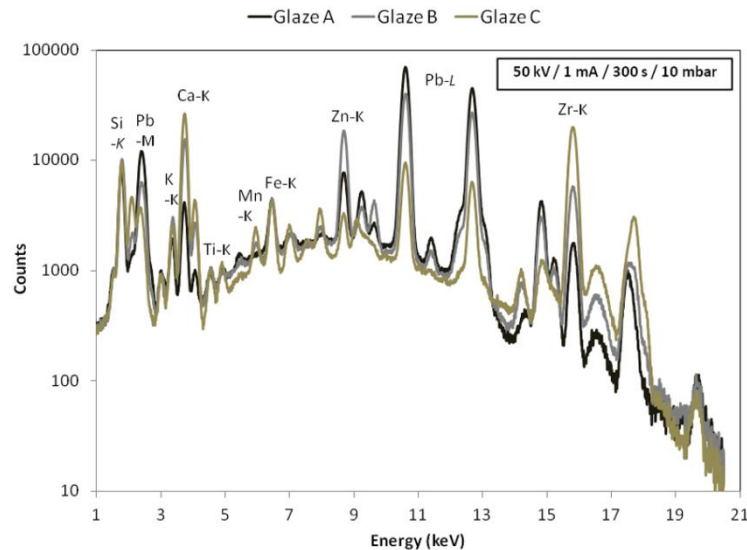


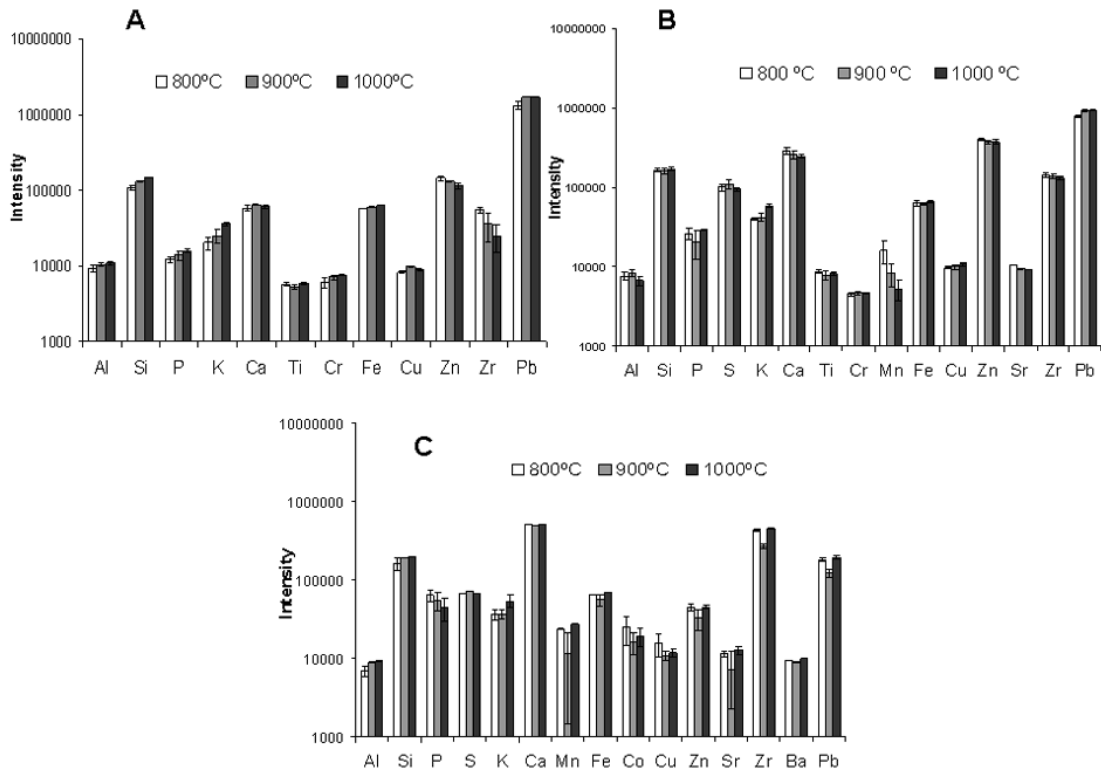
Figure 4.55 – XRF spectra of the three types of glaze used for the replicas.

From figure 4.55, differences between the glazes elemental variability are observed. Glaze A corresponds to a more ancient type and Glaze C corresponds to a rustic modern one. This difference is mainly realized by the much lower count rate for Pb-lines in Glaze C, when compared with Glaze A. This decrease in Pb must be compensated by another flux agent, which in this case is Zirconium (Zr) – with higher contribution – and Titanium (Ti) – with lower contribution, to obtain similar glaze properties.

Glaze B – assuming an intermediary-age position between Glaze A and C – shows lower Pb and higher Zn concentration, when compared with Glaze A.

It is known that Pb is an excellent flux-acting agent in the glassy matrix conferring properties that no other element can offer (*cf.* chapter 1, section 1.2.2). However, it has a huge drawback: it is highly toxic. Therefore, the use of other fluxes in the glazes became necessary.

After submitting all three types of glaze to the above firing conditions – for three different temperatures – XRF analyses were performed on the three pieces and for the three different temperatures, ten points were studied. The obtained results are displayed in figure 4.56 and correspond to an average of all measurements.



**Figure 4.56** – Net counts plot of the elements that compose the three glazes for three different firing temperatures: 800, 900 and 1000 °C [36].

As expected, no elemental changes occurred for the three glazes having different firing temperatures. More interesting is to observe whether there are or not changes in the mineralogical composition depending on the firing temperature used. For this purpose, XRD analyses were carried out and tables 4.9, 4.10 and 4.11 exhibit the mineralogical content of Glazes A, B, C, respectively for the three firing temperatures used together with the mineralogy of the glaze in powder before applied to the ceramic body.



**Table 4.9** – Mineralogical firing temperature dependence obtained by XRD for the glaze A, submitted to 800 °C, 900 °C and 1000 °C, respectively.

Compound	Kaolinite [Al <sub>2</sub> Si <sub>2</sub> O <sub>5</sub> (OH) <sub>4</sub> ]	Zircon (ZrSiO <sub>4</sub> )	Sodium Alumino-trisilicate (NaAlSi <sub>3</sub> O <sub>8</sub> )	Quartz (SiO <sub>2</sub> )	Cristobalite (polymorph of SiO <sub>2</sub> )	Skutterudite (CoAs <sub>3</sub> )	Illite (K,H <sub>3</sub> O)(Al,Mg,Fe) <sub>2</sub> (Si,Al) <sub>4</sub> O <sub>10</sub> [(OH) <sub>2</sub> ,(H <sub>2</sub> O)]
Powder	✓	✓		✓			✓
800		✓	✓	✓			
900		✓	✓	✓		✓	
1000		✓	✓	✓	✓		

**Table 4.10** – Mineralogical firing temperature dependence obtained by XRD for the glaze B, submitted to 800 °C, 900 °C and 1000 °C, respectively.

Compound	Kaolinite [Al <sub>2</sub> Si <sub>2</sub> O <sub>5</sub> (OH) <sub>4</sub> ]	Zircon (ZrSiO <sub>4</sub> )	Cassiterite (SnO <sub>2</sub> )	Quartz-low (SiO <sub>2</sub> )	Cristobalite (polymorph of SiO <sub>2</sub> )	Anorthite (CaAl <sub>2</sub> Si <sub>2</sub> O <sub>8</sub> )
Powder	✓					
800		✓	✓	✓	✓	
900		✓		✓	✓	✓
1000		✓		✓		✓

**Table 4.11** – Mineralogical firing temperature dependence obtained by XRD for the glaze C, submitted to 800 °C, 900 °C and 1000 °C, respectively.

Compound ----- Firing temperature (°C)	Cristobalite (polymorph of SiO <sub>2</sub> )	Zircon (ZrSiO <sub>4</sub> )
<b>Powder</b>		✓
<b>800</b>		✓
<b>900</b>	✓	✓
<b>1000</b>	✓	✓

All glazes (A, B and C) were obtained by commercial frits and the similarity with old glazes elemental content is decreasing from A to C (Tables 4.9, 4.10 and 4.11). The simulation of old-like glazes production is performed by introducing Quartz and clay minerals to the frit, as it is exhibited in the XRD profile of glazes A and B. Moreover, in glazes A and B, kaolinite becomes amorphous at 550 °C and vanishes after the firing process is finished and at 1000 °C the changes are basically due to mineral orientation, rather than thermal modifications (Tables 4.9 and 4.10). Additional important aspects are the fact that Glaze A exhibits more Kaolinite and Illite than the other two and after the firing process is finished, it reveals a more matte appearance than glaze C (figure 4.54). Glaze C is mainly composed by zircon (ZrSiO<sub>4</sub>), which assigns it as a modern one. In its profile is also shown a peak of Cristobalite, characteristic from a high-temperature polymorph of Quartz—this means that it has the same chemistry as Quartz but a different structure (Table 4.11). Some of the compounds are only formed after the glaze reaches the so called “working point”. This is the stage where all components have melted and this liquid matrix state of the glaze originates the formation of some mineralogical components such as Skutterudite (CoAs<sub>3</sub>), Anorthite (CaAl<sub>2</sub>Si<sub>2</sub>O<sub>8</sub>) and sodium aluminium-trisilicate (NaAlSi<sub>3</sub>O<sub>8</sub>). Furthermore, Cassiterite (SnO<sub>2</sub>) crystallizes from 800 °C. Depending on the amount and on the original components from the raw frit, the “working point” can be reached at

different temperatures for each kind of glaze [104]. Another interesting fact is that Skuterrudite appears only due to the initial presence of cobalt oxide in the raw frit. This compound causes an interesting optic effect on the glaze and it was commonly used to confer some bluish-hue to the glaze in order to reduce the typical commercial yellowish nature from the glazes. From an esthetical point of view, in general people tended to prefer the less yellowish glazes. One can even prove this fact by observation of the three different glazes applied on the ceramic pieces (figure 4.54), where glaze A is less yellow than the other two.

#### **4.4 – In *situ* analysis of whole Museum objects**

A set of forty-seven (47) glazed ceramic objects – faiences –, originally produced in Coimbra (Portugal), were submitted to elemental analysis, having as premise the manufacture production recognition. According to the literature [9] these objects are marked with the potters labels and a correct date assignation was possible. Objects from the XVII, XVIII and XIX centuries were analyzed.

Although having been produced in Coimbra, their location changed as time passed due to historical reasons. An exhibition celebrating the glazed ceramics production in Coimbra took place at the *Museu Machado de Castro* (Coimbra) in 2008, and shortly after – before the objects were deported to their current locations – in situ XRF analyses were able to be carried out. Annex 1.4 resumes a description of all analyzed objects and figure 4.58 an example of some objects.

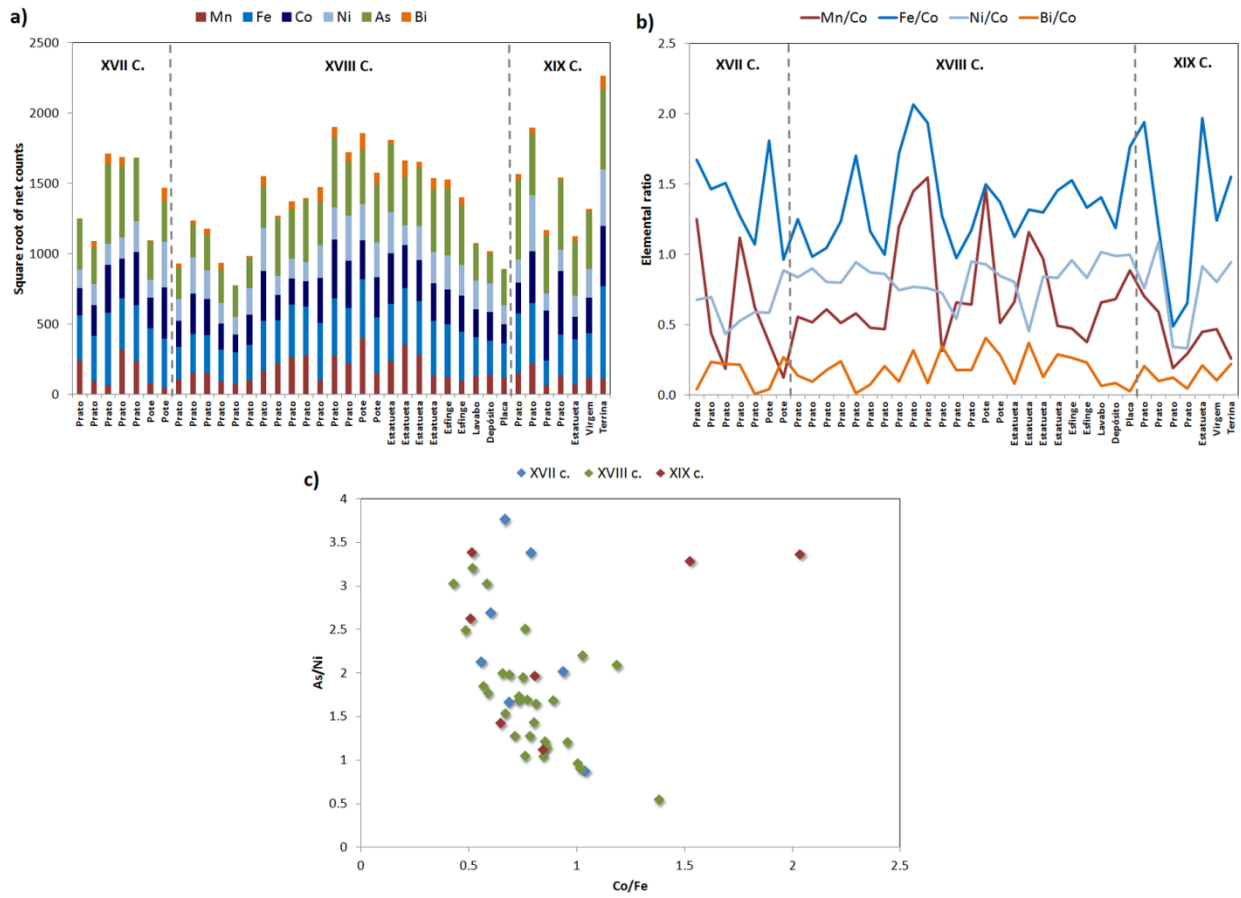
With the aim of tracing differences between objects from different centuries, Micro-XRF analyses on whole Museum ceramic objects were performed. Of course the only viable methods of analyses are in *situ* and therefore information on the elemental level only was possible.



**Figure 4.57** – Examples of faiences from Coimbra: (a) polychrome piece “Prato Vascomselos”: 6×Ø27 cm (b) the use of purples in “Prato Mulher Pássaro”: 4.8×Ø27.4 cm; (c) plate: decorative motives used in these pieces only in blue, such as laces (marked in the picture), typical from Coimbra “Prato Flôr”: 5.3×Ø33.6 cm; (d) Micro-XRF *in situ* analysis of a barrel (“Pote”) from Coimbra: 14.5×24×Ø15 cm [9, 38].

#### 4.4.1 – Blue pigment

The XRF spectra of the blue regions in all objects were deconvoluted, fitted and the net peak areas of the characteristic elements were considered for comparison between the different dates. In figure 4.58 net peak areas for Mn, Fe, Co, Ni, As and Bi are presented, together with the ratios Mn/Co, Fe/Co, Ni/Co and Bi/As.



**Figure 4.58** – a) Plot of the elemental net counts of Mn, Fe, Co, Ni, As, Bi for faiences from Coimbra from the XVII, XVIII and XIX centuries; b) comparison elemental ratios (Mn/Co, Fe/Co, Ni/Co, Bi/Co) of faiences from Coimbra from the XVII, XVIII and XIX centuries; c) As/Ni square-root net counts ratio plotted against Co/Fe square-root net counts ratio, for faiences objects (Coimbra).

From figure 4.58a one sees that there is no significant elemental variability between objects from the XVII, XVIII and XIX. This is also confirmed by the ratios depicted in figure 4.58b. Bismuth has a weak presence among the blue in faiences from Coimbra (also previously confirmed by the plots in figure 4.17 for the fragments). Although the ratio changes are more or less stable Ni/Co and Bi/Co have the lowest change among all objects, while Fe/Co and Ni/Co show sharper changes – though in a small scale ( $\pm 0.5$ ). Furthermore – as already mentioned before (*cf.* figure 4.17) – there is no significant difference between objects from the XVII, XVIII and XIX centuries regarding the contaminant association to the Co-ore. In figure 4.58c the As/Ni ratio against Co/Fe ratio is plotted and one sees no distinguished groups for the different

production dates. One could assume a possible separation for the objects from the XIX century in terms of Co-purity, as two of the samples reveal higher values for Co.

In addition, Spearman correlation test was performed and table 4.12 shows the correlation coefficients between the elements that characterize the blue of faiences from Coimbra.

**Table 4.12** – Spearman correlation coefficient ( $\rho$ ) for net peak areas of the elements that most characterize the blue in faiences from Coimbra – museum objects (N = 37). ‘\*\*\*’ indicates that the correlations are significant at the  $p < 0.01$  level; ‘\*\*’ indicates that the correlations are significant at the  $p < 0.05$  level.

		Mn	Fe	Co	Ni	As	Bi
<b>Mn</b>	$\rho$		.337*	.134	.178	.264	.059
	Sig. (2-tailed)		.041	.428	.293	.114	.730
<b>Fe</b>	$\rho$	.337*		.552**	.504*	.660**	.568**
	Sig. (2-tailed)	.041		.000	.001	.000	.000
<b>Co</b>	$\rho$	.134	.552**		.630**	.519**	.483**
	Sig. (2-tailed)	.428	.000		.000	.001	.002
<b>Ni</b>	$\rho$	.178	.504*	.630**		.236	.491**
	Sig. (2-tailed)	.293	.001	.000		.159	.002
<b>As</b>	$\rho$	.264	.660**	.519**	.236		.297
	Sig. (2-tailed)	.114	.000	.001	.159		.075
<b>Bi</b>	$\rho$	.059	.568**	.483**	.491**	.297	
	Sig. (2-tailed)	.730	.000	.002	.002	.075	

\*\* - Correlation is significant at the 0.01 level (2-tailed).

\* - Correlation is significant at the 0.05 level (2-tailed).

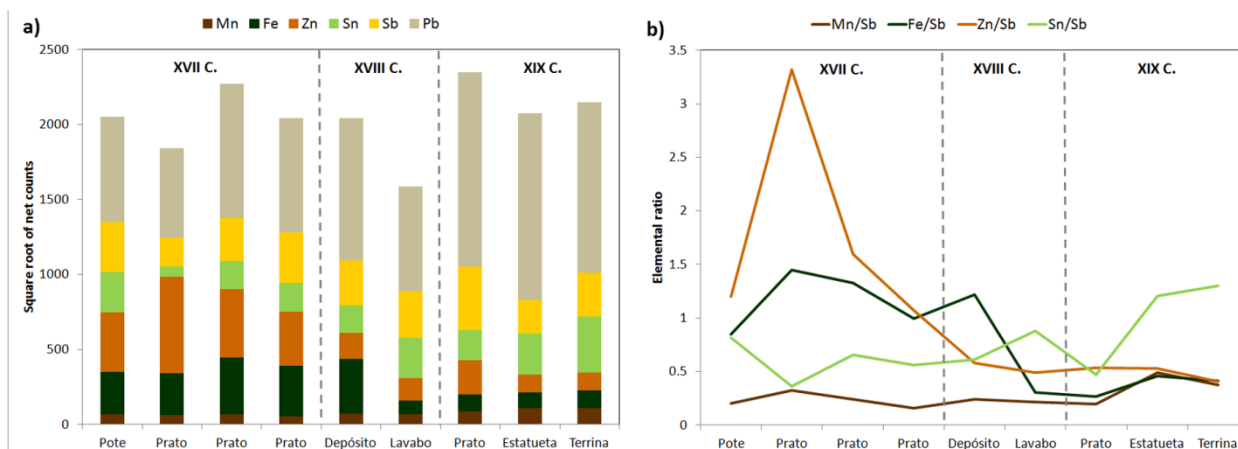
From the results in table 4.12 it becomes clear that there is a significant positive correlation among the elements Fe-Co-Ni-As-Bi. Co-Fe, Co-Ni Co-As and Co-Bi show a positive significant correlation at the  $p < 0.01$  level.

Taking all the above into account, no significant differences are observed with respect to the source of Co for the blue. There is definitely a connection to the five element vein related to Co itself (Fe-Co-Ni-As-Bi), as it was previously identified.

#### 4.4.2 – Yellow pigment

XRF measurements on the yellow regions revealed the presence of Sb together with strong peaks of Pb, which is in agreement with the use of Naples Yellow pigment – as previously explained.

Although Pb is connected to the structure of the yellow pigment, conventional in situ Micro-XRF measurements carry the uncertainty from how deep the fluorescent signal comes and therefore, one cannot estimate whether Pb is owed to the yellow “layer” only or to the base glaze as well. The same is valid for Sn – which is possible to be part of the crystal structure as well (*cf.* 4.2.3.2 – Yellow). However, the ratios of the elements that mostly characterize the yellow pigment are displayed in figure 4.59.

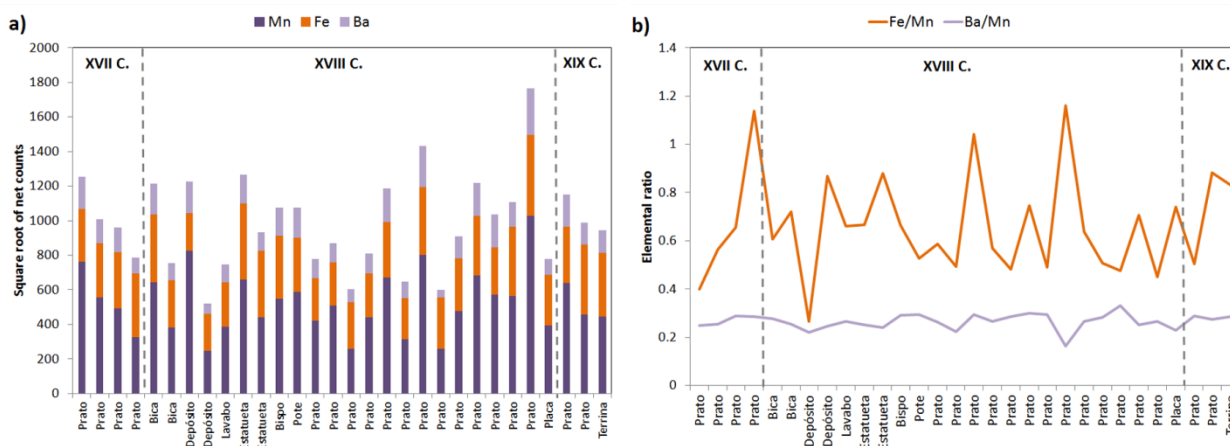


**Figure 4.59** – a) Plot of the elemental net counts of Mn, Fe, Zn, Sn, Sb and Pb of yellow regions of faïences from Coimbra from the XVII, XVIII and XIX centuries; b) comparison elemental ratios (Mn/Sb, Fe/Sb, Zn/Sb and Sn/Sb) of faïences from Coimbra from the XVII, XVIII and XIX centuries.

Other hues such as orange-like and brownish were also analyzed and in these cases the obtained spectra show mainly Mn and Fe. This suggests the use of ochres of these elements mixed with Naples yellow. These results are in agreement with the documented hypothesis that manganese oxides and iron oxides and hydroxides were responsible for the orange and brown colors [38]. From figure 4.59b one sees for example a decrease in the Fe/Sb and Zn/Sb from the XVII to the XIX centuries, which indicates a less use of other ochres in the yellow regions in the more recent objects.

#### 4.4.3 – Purple pigment

As previously described (*cf.* 4.2.3.3 – Purple), Mn is the dominant element for conferring the purple hue. The source of Mn is highly probable to be Portuguese as the mineral Psilomelane  $[(Ba,H_2O)_2Mn_5O_{10}]$  is quite abundant in the country [102]. Once again the connection between Mn and Ba is observed for known faïences from Coimbra. In figure 4.60 the ratios of the characteristic elements conferring this hue is presented as well as the Fe/Mn and Ba/Mn ratios.

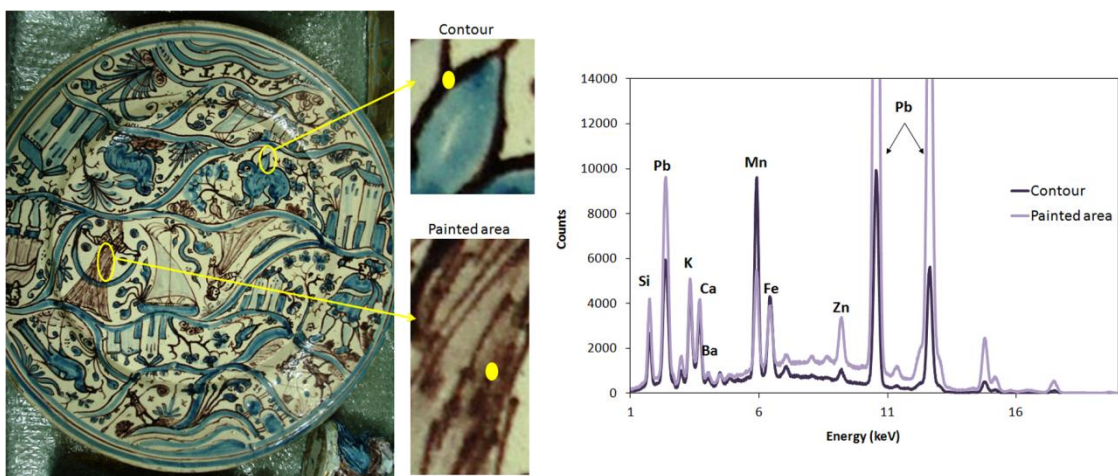


**Figure 4.60** – Plot of the elemental net counts for Mn, Fe and Ba for faïences from Coimbra; b) comparison of elemental ratios (Fe/Mn, Ba/Mn).

From figure 4.60a one realizes little change in the Mn net counts. The possible changes are due to a denser painted area, in which more pigment was used. Observing the ratios in figure 4.60b a very constant Ba/Mn relationship is kept which indicates a strong association between Mn and Ba – this was also observed for the analyzed purple regions in faïence fragments (*cf.* figure 4.45). Fe – although constant in all spectra – seems to have little participation in the purple color, as there is not a strong association between Mn and Fe (figure 4.60b).

The ceramic production in Coimbra is also distinguished by another feature, which is the fine and detailed contours between the painted areas, usually in purple. In figure 4.61 one can observe that the contours are more dense colored areas and this is evidenced by the increase in Mn and the decrease of Pb (characteristic from the glaze), due to a thicker layer of purple color [38].



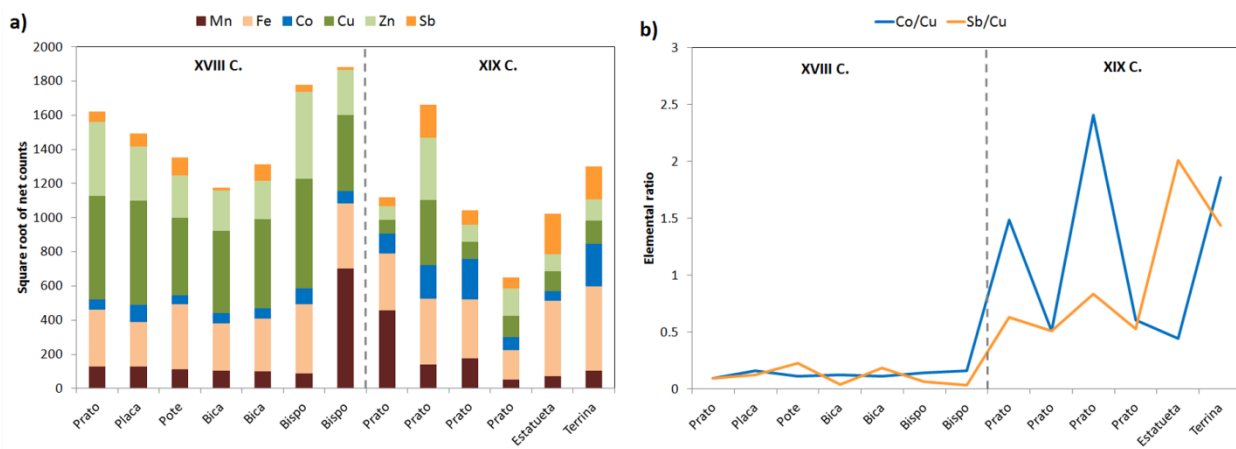


**Figure 4.61** – Left-hand side: Faience from Coimbra “Prato” with two marked regions (yellow) enhancing purple contour and painted area; right-hand side: XRF spectra correspondent to purple contour and painted area, respectively [38].

#### 4.4.4 – Green pigment

According to the literature, green was just started to appear as decoration in faiences from mid. XVIII century [9]. Moreover it was not a very common color to find in such applications. It has been seen before (*cf.* 4.2.3.4 – Green), that differences in the green pigments from faiences and wall-tiles exist. In faiences the pigment used is Cu-based while in wall-tiles from Lisbon a mixture between blue and yellow was made in order to obtain the desired green hue. In this case, no original green pigment was used.

In figure 4.62 ROIs of the possible green-conferring elements are presented as well as useful ratios for the case.



**Figure 4.62** – Plot of the elemental net counts for Mn, Fe, Co, Cu, Zn and Sb of green regions of faïences from Coimbra; b) comparison of elemental ratios (Co/Cu, Sb/Cu).

A difference between the elemental recognition in green regions is observed between objects from the XVIII and XIX centuries. Clearly, the ones from the XVIII century are Cu-based – with little contribution of blue or yellow components– while the ones from the XIX century reveal higher contribution of blue and yellow elements (figure 4.62a). The Co/Cu and Sb/Cu ratios are relatively low for the XVIII objects (left-hand side from the dashed-grey line in figure 4.62b), justified by the higher count rates of Cu. On the other hand these ratios are rather unstable for objects from the XIX century (right-hand side from the dashed-grey line in figure 4.62b), which means that Cu is no longer the only color-giving element but rather a mixture between blue (Co) and yellow (Sb).

These results are in agreement with the ones obtained for the faïence fragment (*cf.* figure 4.51), which indicated that the whole analyzed fragments belong to the period until the XVIII century.

## CHAPTER 5 – DISCUSSION, CONCLUSIONS and OUTLOOK

In this chapter a discussion about the results presented in the previous chapter is made. General features obtained by various analytical methods are summarized and conclusions are withdrawn. Differences between Coimbra and Lisbon arose, regarding the ceramic body, glaze, blue and yellow regions. The discussion is, therefore, presented according to this division.

At the end perspectives for future work are presented.

### 5.1 Ceramic body

Information obtained by XRF has shown that elemental variability is less for faiences than for wall-tiles. This is in agreement with the manufacturing process behind faiences and wall-tiles. Faiences are formed using potter's wheel – which confers higher uniformity among the raw-materials – while wall-tiles are made in plaques (which induce a higher material heterogeneity).

Together with the results obtained by XRD, wall-tiles from Lisbon revealed several Ca-based compounds – which justify the higher Ca count rate from XRF data. Conversely, faience samples revealed two types of feldspars (Microcline and Anorthite), while wall-tiles (both from Coimbra and Lisbon) have revealed just K-rich feldspars (Microcline). Although they are both feldspars, there are some differences between the presence of Microcline and Anorthite in the pastes. Microcline belongs to the raw materials, while Anorthite is a mineral that emerges from a thermal transformation.

Gehlenite is found mainly in wall-tiles, from Coimbra and Lisbon, being Fe its main element and it is mostly used in wall-tiles, as it confers a darker-reddish hue to the body. This is not desired in faiences – where whitish pastes are required.

Furthermore, the presence of Cristobalite in the samples from Coimbra and not in the samples from Lisbon is a hint of different cooling processes used for the ceramic support. The ones from Coimbra have undergone rapid cooling processes, allowing keeping phases such as Cristobalite in the structure, as well as thermal tensions which lead to a more fragile body.

The presence of Pb in all spectra from the body has to do with a capillarity effect that occurs during the drying process. According to [105], lead is water-soluble and when applied over the

ceramic body – together with other glaze components – the solution penetrates into the porous body allowing lead migration until the bottom of the body, favored by its high porosity. This effect happens for both types of samples, being more pronounced in wall-tiles from Lisbon due to their higher porosity in comparison with faiences (Coimbra).

## 5.2 Glaze

Glazes in all samples are characterized by similar compound-groups: network-forming agent (Silica), network-modifiers or fluxes (Pb, Zn, Ca, K, Na) and opacifiers (Sn, Ti). Further coloring agents were added to the glaze (Mn, Fe, Cu). However the strong presence of Pb and Sn confers the designation *lead-tin-based glazes*. The addition of Pb was a very important step in glazes manufacture, as it lowers the melting point of the whole glassy structure and therefore it can be formed at lower firing temperatures. However, differences in the proportions of these and other important elements provide hints for manufacturing techniques.

The positive correlation between Si-K for both faiences and wall-tiles suggests that the higher the network-forming agents the higher the need for fluxes addition (such as K). Moreover, the positive correlation between Pb-Zn in wall-tiles from Lisbon suggests the use of more fluxes than in faiences (Coimbra), which implies then a lower melting point for the glazes in samples from Lisbon than from Coimbra. This was also supported by the SEM/EDX analyses, in which the glazes from wall-tiles have more fusibility (higher content in network modifiers – fluxes) than the ones from faiences. Pb and Na act as dominant fluxes within the glassy matrix and lower the melting temperature [37].

By the inspection of original documents that contain some recipes used to produce glazes, they were applied as frits. This process comprises at least two stages: i) roasting a mixture of lead and tin, which is mixed further with sand and then melted. In accordance with this step, analyses of medieval frits always yielded a PbO–SiO<sub>2</sub> melt with SnO<sub>2</sub> particles. ii) The frit is ground down and applied in a water suspension or mixed with a gum on the ceramic surface. However, regarding the inclusion of Sn-crystals not much is found. Previous investigations reported by Molera et al. [34] have shown that SnO<sub>2</sub> particles react during the glaze formation. This study has revealed that SnO<sub>2</sub> particles are in the order of several hundred nanometers in

size that show crystallization faces in tin-opacified glazes. Several reference materials with varying amounts of  $\text{SiO}_2$ ,  $\text{PbO}$  and  $\text{SnO}_2$  were prepared and the heating and cooling processes were monitored by means of High-temperature XRD (XRD-HT). Results have shown that  $\text{SnO}_2$  reacts with  $\text{Pb}$  at temperatures  $> 600\text{ }^\circ\text{C}$  and a metastable phase is formed ( $\text{PbSnO}_3$ ). As the temperature increases this and other  $\text{Pb}$ -phases melt and, as the liquid phase starts forming,  $\text{SnO}_2$  re-crystallizes [34]. Furthermore, higher numbers of larger-sized particles were observed as the annealing temperature is increased.

Taking the above into account, SEM micrographs shown in the previous chapter reveal the presence of higher amount of slightly larger  $\text{Sn}$ -crystals in glazes from Lisbon which suggests higher firing temperature for Lisbon samples.

The fact that glazes in faiences are thinner (about  $150 - 250\text{ }\mu\text{m}$ ) than glazes from wall-tiles ( $300 - 400\text{ }\mu\text{m}$ ) is in agreement with the nature of these objects. Faiences are technologically “finer” and one of the reasons is the fact that a thinner piece is desired, as most of their utility is at home both for decoration and functional purposes. Wall-tiles are more robust as they are used as outer decoration for buildings, which are then subject to all atmospheric conditions. Furthermore, the cross-section scans provided by 3D Micro-XRF have shown that a smoother connection between glaze and ceramic body exists for faiences (Coimbra), in comparison to the wall-tiles (Lisbon) – where an abrupt drop of  $\text{Pb}$  occurs between glaze and body. This is due to the capillary effect – described above – that transfers  $\text{Pb}$  into lower parts of the ceramic body. Higher porosity in bodies promotes lead diffusion, which consequently induces a stronger elemental separation at the interface glaze/body.

### **5.3 Surface decoration**

According to documental proofs [9] Coimbra was a less wealthy center of production, when compared to Lisbon and, hence, the expensive raw materials were spared as much as possible. Therefore, one would find a broader range of elements used to confer the intended color.

### 5.3.1 Blue

A higher Mn/Co ratio found in faiences (Coimbra) than in wall-tiles reinforces the hypothesis that Mn was intentionally added by the potter in order to spare the expensive Co-source. On the other hand, a higher purity in Co-content was found for faiences by the lower Ni/Co and Bi/Co ratios, in comparison to wall-tiles. Still, the slight increase in both Co/Fe and As/Ni ratios for faiences (Coimbra) indicates that there was an intention of preparing the pigments with a higher level of purity. Moreover, there are positive correlations between Mn-Fe, Mn-Ni, Fe-Ni, Mn-Co, Fe-Co and Co-Ni for the blue in faiences. These correlations were also obtained for wall-tiles but no correlation between Co and Mn exists, which support the theory of the intentionally added Mn to the blue pigment used in faiences (Coimbra) but not in wall-tiles.

Cluster analyses have shown that regarding the blue pigment composition, two distinct groups are formed: one for faiences and one for wall-tiles. In this case the difference is made between types of object rather than between production centers.

Regarding the cross-section scans performed by high-resolved XRF, some differences in the pigment diffusion throughout the glaze appeared. A higher intake of the blue pigment was observed for samples from Coimbra than for samples from Lisbon. There are several factors that allow a higher intake of the pigment particles through the glaze: (i) a higher content of fluxes in the glaze; (ii) a higher firing temperature of the glaze; and (iii) more refractory pigment particles, meaning that particles do not undergo physical changes when they are submitted to a higher temperature [106]. Since the pigment sources used should be the same, the factors which can promote a higher penetration of the pigment in the glaze are (i) and (ii).

Concerning SEM/EDX measurements, one was able to identify Sn-agglomerates throughout the whole blue+glaze cross-section among all samples, which is a hint for a certain manufacturing process. Co-blue is in its natural state a very strong and dark blue, which is not the hue one sees in the blue surface motifs. So, since Sn is a natural opacifier the potter intentionally added it to the pigment in order to obtain a lighter blue hue. By inspection of the

The expected connection between Fe-Co-Ni-As-Bi was not easy to investigate. Co was difficult to observe but the other elements that participate on the pigment structure were investigated. Co was found in Fe- or Ni-rich structures but with no structural connection to As

or Bi. However, the As-needle-like structures were always identified in blue regions. A difference between faiences and wall-tiles was observed: in faiences Co is found in Fe-rich structures while in wall-tiles Co is found in Ni-rich structures [94].

### 5.3.1 Yellow

Yellow pigments used in the analyzed samples are Sb-based with connection to Pb as well.

SEM micrographs have shown that the Sb-crystals are mainly concentrated at the surface of the samples (only going deep over the first tens of micrometers in depth). Moreover, differences noticed in the crystal shape and size are indicative for the same firing cycle the use of different firing temperatures used [22]. The rather hexagonal shape found for the microstructures in the wall-tiles from Lisbon indicates that, in this context, a higher firing temperature was used ( $\geq 1100$  °C), in comparison to the samples from Coimbra (from 950 °C) (faiences and wall-tiles), whose micro-structure shape is rather irregular and triangular-like. Thus, one can conclude that the firing cycle plays an important role in this simple linear model, which means that similar crystal-morphologies could be obtained for both short-firing cycles at high temperatures and for long-firing cycles at lower temperatures [94].

Further information obtained by XAFS revealed differences between manufacturing centers (at a first approximation) regarding the yellow pigment. By Sb-K speciation, it has been shown that the yellow compound is different between Coimbra and Lisbon. In samples from Coimbra, the yellow fits quite well to the Naples Yellow ( $\text{Pb}_2\text{Sb}_2\text{O}_7$ ), while in samples from Lisbon a mixture of Sb-based compounds has been used. It is important to stress again that these results are merely in a comparative basis and no definite conclusion should be withdrawn. Further investigations are already in course in order to conclude more accurately about the chemical environment of Pb and Sb. For this purpose, tests that involve inclusion of self-absorption (SA) effects are being developed in order to evaluate their influence in this kind of samples – or better said, matrices.

**Table 5.1** – Summary of the properties of Lisbon and Coimbra productions, from this investigation.

Faiences are a unique type of glazed ceramics.

	Coimbra		Lisbon
	Faiences	Wall-tiles	Wall-tiles
<b>Glaze</b>	Thickness: max. 180 $\mu\text{m}$	Thickness: max. 400 $\mu\text{m}$	Thickness: max. 400 $\mu\text{m}$
<b>Blue</b>	Pigment (Co) completely dispersed into the glaze; Positive correlation between Mn and Co; Presence of Sn-agglomerates; Co-structures are in Fe-rich environment.	Pigment (Co) diffused down $\sim 150$ $\mu\text{m}$ into the glaze; No correlation between Mn and Co; Presence of Sn-agglomerates; Co-structures are in Ni-rich environment.	Pigment (Co) diffused down $\sim 125$ $\mu\text{m}$ into the glaze; No correlation between Mn and Co; Presence of Sn-agglomerates; Co-structures are in Ni-rich environment.
<b>Yellow</b>	Pigment (Sb) thickness: $\sim 30$ $\mu\text{m}$ ; Sb-crystals rather irregular shaped (triangular-like) $\Rightarrow$ $< 1000$ $^{\circ}\text{C}$ firing temperature; Naples Yellow ( $\text{Pb}_2\text{Sb}_2\text{O}_7$ ) confirmed by XAFS.	Pigment (Sb) thickness: $\sim 100$ $\mu\text{m}$ ; Pb signal strong drop together with Sb signal; Sb-crystals rather irregular shaped (triangular-like) $\Rightarrow$ $< 1000$ $^{\circ}\text{C}$ firing temperature; Naples Yellow ( $\text{Pb}_2\text{Sb}_2\text{O}_7$ ) confirmed by XAFS.	Pigment (Sb) thickness: $\sim 100$ $\mu\text{m}$ ; Pb signal slight drop after the pigment layer (Sb); Sb-crystals more regular shaped (hexagonal) $\Rightarrow$ $\geq 1100$ $^{\circ}\text{C}$ firing temperature; Mixture of Sb-based compounds confirmed by XAFS.
<b>Purple</b>	Pigment (Mn) completely dispersed into the glaze; Presence of Ba indicates the use of $(\text{Ba},\text{H}_2\text{O})_2\text{Mn}_5\text{O}_{10}$ as source – high abundance in Portugal; relatively low Ba/Mn ratio $\Rightarrow$ pureness of the source.	Pigment (Mn) completely diffused into the glaze; Mn maximum at the surface $\sim 50$ $\mu\text{m}$ broad; Presence of Ba indicates the use of $(\text{Ba},\text{H}_2\text{O})_2\text{Mn}_5\text{O}_{10}$ as source – high abundance in Portugal; relatively high Ba/Mn ratio.	Pigment (Mn) completely diffused into the glaze; Mn maximum at the surface $< 25$ $\mu\text{m}$ broad; Presence of Ba indicates the use of $(\text{Ba},\text{H}_2\text{O})_2\text{Mn}_5\text{O}_{10}$ as source – high abundance in Portugal; relatively high Ba/Mn ratio.
<b>Green</b>	Pigment (Cu) completely dispersed into the glaze;	Pigment (Cu) well diffused into the glaze; Cu maximum at the surface $\sim 50$ $\mu\text{m}$ broad.	Higher pigment (Cu) intake into the glaze; Cu maximum at the surface $\sim 25$ $\mu\text{m}$ broad; two



			samples in which green was obtained by mixing blue (Co) and yellow (Sb).
<b>General features</b>	No color/glaze interface, except for yellow decorations; Smoother elemental exchange at the glaze/body interface ⇒ less porous bodies; Pigments analysis: Constant elemental ratios ⇒ manufactured in potter's wheel (more refined manufacturing process)	Broader maximum of the pigment signal. Slightly lower intake of the pigment through the glaze; Pigments analysis: Irregular elemental ratios ⇒ rougher manufacturing process.	Slightly higher intake of the pigment into the glaze. Sharper elemental exchange at the glaze/body interface ⇒ higher porous bodies; Pigments analysis: Irregular elemental ratios ⇒ rougher manufacturing process.

## Outlook

This investigation (including the methodology) was pioneer regarding Portuguese glazed ceramics, especially the information obtained for faïences from Coimbra. With the hypothesis that the productions from Coimbra are unique, this has been confirmed by scientific data. In the field of Cultural Heritage it is important to understand the complexity of the objects in order to use the proper analytical tools for the sought answers. With the released scientific data, answers about raw materials and compositional features, at a mineralogical and morphological level, are provided. This has enriched the field of Arts in Portugal and can be used as basis for developing conservation and restoration methodologies.

This work has not only provided new information about ceramic productions from Coimbra and Lisbon but has also brought the need for carrying out further investigations. The sample universe available for this work was good in order to have a comparison basis between these two main ceramic manufacturing centers but analyses on samples from other centers are now required. Although Coimbra and Lisbon were considered the main centers, other centers such as Porto or Alcobaça have played an important role as routes for raw materials and this could

be a connection string for enriching the knowledge about Portuguese ceramic productions.  
New doors are open for further investigations.

## BIBLIOGRAPHY

1. Frahme, C.E., *Fundamentals of Ceramics Technology*. 1988: American Ceramic Society.
2. M. Rice, P., *Pottery Analysis: A Sourcebook*. 1987, Chicago, USA: The University of Chicago.
3. Weiß, G. *The Origins of Glazes*. 2010.
4. Tite, M.S., *Ceramic Production, Provenance and Use - a Review*. *Archaeometry*, 2008. **50**(2): p. 216-231.
5. *A Arte Do Azulejo Em Portugal*.
6. *MNAz Cronologia Do Azulejo Em Portugal*.
7. *Azulejo*.; Available from: <http://en.wikipedia.org/wiki/Azulejo>.
8. Pais, A., "Fabricado No Reino Lusitano - O Que Antes Nos Vendeu Tão Caro a China", a *Produção De Faiança Em Lisboa, Entre Os Reinados De Filipe li E D. João V.*, in *Escola das Artes2012*, Universidade Católica do Porto: Porto, Portugal.
9. Pais, A.N., Pacheco, A., Coroado, J., *Cerâmica De Coimbra*. 2007, Lisboa: INAPA.
10. Worth, W.-W.I.s. *Ceramics in Portugal*. [cited 2012 15 November 2012]; Available from: [http://www.wiw.net/pages.php?CDpath=3\\_5\\_633\\_2748\\_3208](http://www.wiw.net/pages.php?CDpath=3_5_633_2748_3208).
11. Smith, W.F., *Principles of Materials Science and Engineering*. 1996: McGraw-Hill.
12. Padilla, R., *Compositional Classification of Archaeological Ceramics Based in Non-Destructive Xrf Analysis.*, in *Faculty of Sciences2005*, University of Antwerp: Antwerp, Belgium.
13. Coroado, J., *Propriedades Cerâmicas Das Argilas Das Unidades Litoestratigráficas "Argilas De Aveiro" E "Argilas De Tomar"*. in *Geosciences department 2000*, University of Aveiro: Aveiro, Portugal.
14. Navarro, J.E.E., Albaro, J.L.A., Fuster, M.M., *Ecnologia Cerâmica, Vol. Iv, Tecnología De La Fabricación Cerámica. Secado Y Cocción*. 1985, Universidade de Valencia.: Instituto de Química Técnica. (Tecnología Ceramica).
15. Navarro, J.E.E., Albaro, J.L.A., Fuster, M.M., *Tecnología Ceramica, Vol. I, Introducción a La Tecnología Ceramica. Matérias Primas Ceramicas*. 1985, Universidade de Valencia: Instituto de Química Técnica (Tecnología Ceramica).
16. Navarro, J.M.F., *El Vidrio*. 2003, Madrid: CSIC.
17. Rhodes, D., *Clay and Glazes for the Potter*. 1973, London: A&C Balck.
18. Hradil, D., Grygar, T., Hradilová, J., Bezdička, P., Grúnwaldová, V., Fogaš, I., Miliani, C., *Microanalytical Identification of Pb-Sb-Sn Yellow Pigment in Historical European Paintings and Its Differentiation from Lead Tin and Naples Yellows*. *Journal of Cultural Heritage*, 2007. **8**: p. 377-386.
19. Maggetti, M., Neururer, C., *Antimonate Opaque Glaze Colours from the Faience Manufacture on Le Bois D'Epense (19th Century, Northeastern France)*. *Archaeometry*, 2009. **51**(2): p. 791-807.
20. Dik, J., Hermens, E., Peschar, R., Schenk, H., *Early Production Recipes for Lead Antimonate Yellow in Italian Art\**. *Archaeometry*, 2005. **47**(3): p. 593-607.

21. Padilla, R., Schalm, O., Janssens, K., Arrazcaeta, R., Van Espen, P., *Microanalytical Characterization of Surface Decoration in Majolica Pottery*. *Analytica Chimica Acta*, 2005. **535**(1–2): p. 201–211.
22. Sakellariou, K., Miliani, C., Morresi, A., Ombelli, M., *Spectroscopic Investigation of Yellow Majolica Glazes*. *Journal of Raman Spectroscopy*, 2004. **35**(1): p. 61–67.
23. Cotte, M., Susini, J., Dik, J., Janssens, K., *Synchrotron-Based X-Ray Absorption Spectroscopy for Art Conservation: Looking Back and Looking Forward*. *Accounts of Chemical Research*, 2010. **43**(6): p. 705–714.
24. Mangone, A., De Benedetto, G.E., Fico, D., Giannossa, L.C., Laviano, R., Sabbatini, L., van der Werf, I.D., Traini, A., *A Multianalytical Study of Archaeological Faience from the Vesuvian Area as a Valid Tool to Investigate Provenance and Technological Features*. *New J. Chem*, 2011. **35**: p. 2860–2868.
25. Nuevo, M.J., Martín-Sánchez, A., *Application of Xrf Spectrometry to the Study of Pigments in Glazed Ceramic Pots*. *Applied Radiation and Isotopes*, 2011. **69**: p. 574–579.
26. Sciau, P., Salles, P., Roucau, C., Mehta, A., Benassayag, G., *Applications of Focused Ion Beam for Preparation of Specimens of Ancient Ceramic for Electron Microscopy and Synchrotron X-Ray Studies*. *Micron*, 2009. **40**: p. 597–604.
27. Zucchiatti, A., Bouquillon, A., Katona, I., D'Alessandro, A., *The 'Della Robbia Blue': A Case Study for the Use of Cobalt Pigments in Ceramics During the Italian Renaissance*. *Archaeometry*, 2006. **48**: p. 131–152.
28. Van der Linden, V., Schalm, O., Houbraken, J., Thomas, M., Meesdom, E., Devos, A., Van Dooren, R., Nieuwdorp, H., Janssen, E., Janssens, K., *Chemical Analysis of the 16th to 19th Century Limoges School 'Painted Enamel' Objects in Three Museums of the Low Countries*. *X-Ray Spectrometry*, 2009. **39**: p. 112–121.
29. Pérez-Arantequí, J., Montull, B., Resano, M., Ortega, J.M., *Materials and Technological Evolution of Ancient Cobalt-Blue-Decorated Ceramics: Pigments and Work Patterns in Tin-Glazed Objects from Aragon (Spain) from the 15th to the 18th Century Ad*. *Journal of the European Ceramic Society*, 2009. **29** p. 2499–2509.
30. Aloupi, E., Karydas, A.G., Paradellis, T., *Pigment Analysis of Wall Paintings and Ceramics from Greece and Cyprus. The Optimum Use of X-Ray Spectrometry on Specific Archaeological Issues*. *X-Ray Spectrom.*, 2000. **29**: p. 18–24.
31. Coentro, S., Mimoso, J.M., Lima, A.M., Silva, A.S., Pais, A.N., Muralha, V.S.F., *Multianalytical Identification of Pigments and Pigment Mixtures Used in 17th Century Portuguese Azulejos*. *Journal of the European Ceramic Society*, 2012. **32**(1): p. 37–48.
32. Comodi, P., Bernardi, M., Bentivoglio, A., Gatta, G.D., Zanazzi, P.F., *The Production and Technology of Glazed Ceramics from the Middle Ages, Found in the Saepinum Territory (Italy): A Multimethodic Approach*. *Archaeometry* 2004. **46**(3): p. 405–419.
33. Tite, M.S., *The Production Technology of Italian Maiolica: A Reassessment*. *Journal of Archaeological Science*, 2009. **36**(10): p. 2065–2080.
34. Molera, J., Pradell, T., Salvado, Vendrell-Saz, M., *Evidence of Tin Oxide Recrystallization in Opacified Lead Glazes*. *Journal of American Ceramic Society*, 1999. **82**(10): p. 2871–2875.
35. Bultrini, G., Fragala, I., Ingo, G.M., Lanza, G., *Characterisation and Reproduction of Yellow Pigments Used in Central Italy for Decorating Ceramics During Renaissance*. *Appl. Phys. A* 2006. **83**: p. 557–565.

36. Guilherme, A., Coroado, J., Carvalho, M.L., *Chemical and Mineralogical Characterization on Glazes of Ceramics from Coimbra (Portugal) from the Sixteenth to Nineteenth Centuries*. Analytical and Bioanalytical Chemistry, 2009. **395**: p. 2051-2059.
37. Guilherme, A., Coroado, J., dos Santos, J.M.F., Lühl, L., Wolff, T., Kanngießer, B., Carvalho, M.L., *X-Ray Fluorescence (Conventional and 3d) and Scanning Electron Microscopy for the Investigation of Portuguese Polychrome Glazed Ceramics: Advances in the Knowledge of the Manufacturing Techniques*. Spectrochimica Acta Part B: Atomic Spectroscopy, 2011. **66**(5): p. 297-307.
38. Guilherme, A., Pessanha, S., Carvalho, M.L., dos Santos, J.M.F., Coroado, J., *Micro Energy Dispersive X-Ray Fluorescence Analysis of Polychrome Lead-Glazed Portuguese Faiences*. Spectrochimica Acta Part B: Atomic Spectroscopy, 2010. **65**(4): p. 328-333.
39. Guilherme, A., Buzanich, G., Radtke, M., Reinholz, U., Coroado, J., Dos Santos, J.M.F., Carvalho, M.L., *Synchrotron Micro-Xrf with Compound Refractive Lenses (Crls) for Tracing Key Elements on Portuguese Glazed Ceramics*. Journal of Analytical Atomic Spectrometry, 2012. **27**(6): p. 966-974.
40. Janssens, K., Van Grieken, R., *Non-Destructive Microanalysis of Cultural Heritage Materials*, ed. R.V.G. K Janssens. 2004, Netherlands: Elsevier.
41. Tsuji, K., Nakano, K., Takahashi, Y., Hayashi, K., Ro, C.-U., *X-Ray Spectrometry*. Analytical Chemistry, 2011. **84**: p. 636-668.
42. *Handbook of X-Ray Spectrometry*, ed. R. Van Grieken, A. Markowicz. 1993: Marcel Dekker, Inc.
43. *Handbook of Practical X-Ray Fluorescence Analysis*, ed. B. Beckhoff, B. Kanngießer, N. Langhoff, R. Wedell, H. Wolff. 2006, Germany: Springer-Verlag.
44. Tertian, R., Claisse, F., *Principles of Quantitative X-Ray Fluorescence Analysis*. 1982: Heyden & Son Ltd.
45. Mantler, M., *Basic Interactions between Photons and Atoms*, in *Handbook of Practical X-Ray Fluorescence Analysis*, B.K.e. B. Beckhoff, N. Langhoff, R. Wedell, H. Wolff, Editor. 2006, Springer-Verlag: Germany.
46. Salgueiro, L., Ferreira, J.G., *Introdução Á Física Atómica E Nuclear: Vol I*. 1974, Lisbon: Tip. Matemática.
47. Amptek *X-Ray Fluorescence (Xrf): Understanding Characteristic X-Rays*.
48. Hubbell, J.H., Seltzer, M., *Tables of X-Ray Mass Attenuation Coefficients and Mass Energy-Absorption Coefficients from 1 Kev to 20 Mev for Elements Z = 1 to 92 and 48 Additional Substances of Dosimetric Interest.*, in NISTIR 56321996, The National Institute of Standards and Technology (NIST).
49. Rao, D.V., Takeda, T., Itai, Y., Akatsuka, T., Cesareo, R., Brunetti, A., Gigante, G.E., *Doppler Broadening and Its Contribution to Compton Energy-Absorption Cross Sections: An Analysis of the Compton Component in Terms of Mass-Energy Absorption Coefficient*. J. Phys. Chem. Ref. Data, 2002. **31**: p. 769-818.
50. Buzanich, G., Wobrauschek, P., Strelci, C., Markowicz, A., Wegrzynek, D., Chinea-Cano, E., Bamford, S., *A Portable Micro-X-Ray Fluorescence Spectrometer with Polycapillary Optics and Vacuum Chamber for Archaeometric and Other Applications*. Spectrochimica Acta Part B: Atomic Spectroscopy, 2007. **62**(11): p. 1252–1256.

51. Solé, V.A., Papillon, E., Cotte, M., Walter, P., Susini, J., *A Multiplatform Code for the Analysis of Energy-Dispersive X-Ray Fluorescence Spectra*. Spectrochim. Acta Part B., 2007. **62**: p. 63-68.
52. Spieler, E., *Soft X-Ray Optics*. 1994: SPIE - The international Society for Optical Engineering.
53. Snigirev, A., Snigireva, I., *High Energy X-Ray Micro-Optics*. C. R. Phys., 2008. **9**: p. 507–516.
54. MacDonald, C.A., *Focusing Polycapillary Optics and Their Applications*. X-Ray Optics and Instrumentation, 2010: p. 17.
55. Guilherme, A., Buzanich, G., Carvalho, M.L., *Focusing Systems for the Generation of X-Ray Micro Beam: An Overview*. Spectrochimica Acta Part B: Atomic Spectroscopy, 2012. **77**(0): p. 1-8.
56. James, R.W., *The Optical Principles of the Diffraction of X-Rays*, ed. L. Bragg. 1962, London: G. BELL AND SONS LTD.
57. Vincze, L., Wei, F., Proost, K., Vekemans, B., Janssens, K., He, Y., Yan, Y., Falkenberg, G., *Suitability of Polycapillary Optics for Focusing of Monochromatic Synchrotron Radiation as Used in Trace Level Micro-Xanes Measurements*. J. Anal. At. Spectrom., 2002. **17**: p. 177-182.
58. Schields, P.J., Gibson, D.M., Gibson, W.M., Gao, N., Huang, H., Ponomarev, I.Y., *Overview of Polycapillary X-Ray Optics*. Powder Diffraction, 2002. **17**(2): p. 70-80.
59. Kanngiesser, B., Malzer, W., Reiche, I., *A New 3d Micro X-Ray Fluorescence Analysis Setup - First Archaeometric Applications*. Nucl. Instrum. Methods Phys. Res. Sect. B-Beam Interact. Mater. Atoms, 2003. **211**: p. 259-264.
60. Malzer, W., Kanngiesser, B., *A Model for the Confocal Volume of 3d Micro X-Ray Fluorescence Spectrometer*. Spectrochim Acta B, 2005. **60**: p. 1334-1341.
61. Mantouvalou, I., *Quantitative 3d Micro X-Ray Fluorescence Spectroscopy*, in Faculty of Mathematics and Natural Sciences 2009, Technical University.
62. Mantouvalou, I., Malzer, W., Kanngießner, B., *Quantification for 3d Micro X-Ray Fluorescence*. Spectrochimica Acta Part B: Atomic Spectroscopy, 2012. **77**: p. 9-18.
63. Seim, C., Laurenze-Landsberg, C., Schröder-Smeibidl, B., Mantouvalou, I., De Boer, C., Kanngiesser, B., *Old Traces, Read Anew - 'the Reading Hermit' in the Light of X-Ray Fluorescence*, 2013.
64. Duke, P.J., *Synchrotron Radiation: Production and Properties*, ed. J.R.H. J. Chikawa, S. W. Lovesey. 2009, United States of America: Oxford Science Publications.
65. *Helmholtz Zentrum Berlin (Hzb), Bessy-II*. [cited 2013; Available from: [http://www.helmholtz-berlin.de/angebote/arbeiten-lernen/info/beschleunigerphysik-fuer-anfaenger/der-speicherring\\_de.html](http://www.helmholtz-berlin.de/angebote/arbeiten-lernen/info/beschleunigerphysik-fuer-anfaenger/der-speicherring_de.html)].
66. Riken, J. *Spring-8 - Japanese Synchrotron Facility*. 2013; Available from: [http://www.spring8.or.jp/en/about\\_us/whats\\_sr/sp8\\_features/](http://www.spring8.or.jp/en/about_us/whats_sr/sp8_features/).
67. Buzanich, G., *Characterization of Compound Refractive Lenses for Synchrotron Micro-Xrf and Micro-Xas and Applications with High Spatial Resolution*, in Faculty of Physics 2013, Technical University of Vienna: Vienna, Austria.
68. *X-Ray Optical Systems; Refractive X-Ray Optics*. 2007 [cited 2013; Available from: [http://www.x-ray-optics.de/index.php?option=com\\_content&view=article&id=46&Itemid=54&lang=en](http://www.x-ray-optics.de/index.php?option=com_content&view=article&id=46&Itemid=54&lang=en)].

69. 2005.
70. *Scanning Electron Microscopy --- Principles*.
71. Goldstein, J.I., Yakowitz, H., Newbury, D.E., Lifshin, E., Colby, J.W., Coleman, J.R., *Practical Scanning Electron Microscopy - Electron and Ion Microprobe Analysis*, ed. H.Y. J. I. Goldstein. 1975, USA: Plenum Press, NY.
72. *Brief Introduction to Scanning Electron Microscopy (Sem)*. 2013.
73. Procop, M., Hodoroaba, V.-D., *X-Ray Fluorescence as an Additional Analytical Method for a Scanning Electron Microscope*. *Microchimica Acta*, 2008. **161**(3-4): p. 413-419.
74. Hodoroaba, V.-D., Radtke, M., Vincze, L., Rackwitz, V., Reuter, D., *X-Ray Scattering in X-Ray Fluorescence Spectra with X-Ray Tube Excitation – Modelling, Experiment, and Monte-Carlo Simulation*. *Nuclear Instruments & Methods in Physics Research Section B*, 2010. **268**(24): p. 3568-3575.
75. Rackwitz, V., Procop, M., Bjeoumikhova, S., Panne, U., Hodoroaba, V.-D., *A Routine Procedure for the Characterisation of Polycapillary X-Ray Semi-Lenses in Parallelising Mode with Sem/Eds*. *J. Anal. At. Spectrom.*, 2011. **26**: p. 499-504.
76. Newville, M. *Fundamentals of Xafs*. 2004.
77. Rehr, J.J., Albers, R.C., *Theoretical Approaches to X-Ray Absorption Fine Structure*. *Reviews of Modern Physics*, 2000. **72**(3): p. 621-654.
78. Yano, J., Yachandra, V., *X-Ray Absorption Spectroscopy*. *Photosynthesis Research*, 2009. **102**(2-3): p. 241-254.
79. Lühl, L., *Tiefenaufgelöste Röntgenabsorptionsspektroskopie*, in *Faculty of mathematics and Natural Sciences 2012*, Technical University in Berlin: Berlin, Germany.
80. Ravel, B., Newville, M., *Athena and Artemis: Interactive Graphical Data Analysis Using Ifeffit*. *Physica Scripta*, 2005. **2005**(T115): p. 1007.
81. Ankudinov, A., Ravel, B., Rehr, J.J. *The Feff Project*. 2000 [cited 2012; Available from: <http://leonardo.phys.washington.edu/feff/>].
82. Lühl, L., Mantouvalou, I., Malzer, W., Schaumann, I., Vogt, C., Hahn, O., Kanngiesser, B., *Reconstruction Procedure for 3d Micro X-Ray Absorption Fine Structure*. *Analytical Chemistry*, 2012. **84**(4): p. 1907-1914.
83. Erko, A., Zizak, I., *Hard X-Ray Micro-Spectroscopy at Berliner Elektronenspeicherring Für Synchrotronstrahlung II*. *Spectrochimica Acta Part B: Atomic Spectroscopy*, 2009. **64**(9): p. 833-848.
84. Riesemeier, H., Ecker, K., Görner, W., Müller, B.R., Radtke, M., Krumrey, M., *Layout and First Xrf Applications of the Bamline at Bessy II*. *X-Ray Spectrometry*, 2005. **34**(2): p. 160-163.
85. Sprent, J., Smeeton, N.C., *Applied Nonparametric Statistical Methods*, ed. C. Hall. 2001: CRC Press.
86. *Kiatdd Examples of Scatter Diagrams with Different Values of Correlation Coefficient (P)*. 2012.
87. Skbkekas *An Illustration of Spearman Correlation*. 2009.
88. *Cluster Analysis*.
89. Govindaraju, K., *1995 Working Values with Confidence Limits for Twenty-Six Crpg, Anrt and Iwg-Git Geostandards*. *Geostandards Newsletter*, 1995. **19**: p. 1-32.

90. Vrebos, B.A.R., *Compensation Methods - Scattered Radiation (Compton Scatter)*, in *Handbook of Practical X-Ray Fluorescence Analysis*, B.K.e. B. Beckhoff, N. Langhoff, R.Wedell, H.Wolff., Editor. 2006, Springer-Verlag: Germany.
91. Fonseca, M.J., *Estudo Composicional De Faiança Arqueológica Dos Séculos Xvi a Xvii Do Mosteiro De S. João De Tarouca E Santa Clara De Coimbra.*, 2010.
92. Franklin Osborn, E., *Phase Equilibrium Diagrams of Oxide Systems*. 1960.
93. Winter, J. *Teaching Phase Equilibria*. Available from: [http://serc.carleton.edu/research\\_education/equilibria/simplephasediagrams.html](http://serc.carleton.edu/research_education/equilibria/simplephasediagrams.html).
94. Guilherme, A., Hodoroaba, V.-D., Benemann, S., Coroado, J.,Carvalho, M.L., *Morphological and Compositional Features of Blue and Yellow Pigments Used in Portuguese Glazed Ceramics by Sem/Edx – Unraveling Manufacturing Differences*. Microscopy and Microanalysis, 2013.
95. Rosi, F., Manuali, V., Miliani, C., Brunetti, B.G., Sgamellotti, A., Grygar, T.,Hradil, D., *Raman Scattering Features of Lead Pyroantimonate Compounds. Part I: Xrd and Raman Characterization of Pb<sub>2</sub>Sb<sub>2</sub>O<sub>7</sub> Doped with Tin and Zinc*. Journal of Raman Spectroscopy, 2009. **40**: p. 107–111.
96. Dik, J., *Scientific Analysis of Historical Paint and the Implications for Art History and Art Conservation. The Case Studies of Naples Yellow and Discoloured Smalt.*, in *FNWI: Van 't Hoff Institute of molecular Sciences (HIMS)2003*, Faculty od Sciences: Amsterdam. p. 159.
97. Clark, R.J.H., Cridland, L., Kariuki, B.M., Harris, K.D.M.,Withnall, R., *Synthesis, Structural Characterisation and Raman Spectroscopy of the Inorganic Pigments Lead Tin Yellow Types I and II and Lead Antimonate Yellow: Their Identification on Medieval Paintings and Manuscripts*. Journal of the Chemical Society, Dalton Transactions, 1995(16): p. 2577-2582.
98. Figueiredo, M.O., Veiga, J.P., Silva, T.P., Mirão, J.P.,Pascarelli, S., *Chemistry Versus Phase Constitution of Yellow Ancient Tile Glazes: A Non-Destructive Insight through Xas*. Nuclear Instruments and Methods in Physics Research Section B: Beam Interactions with Materials and Atoms, 2005. **238**(1–4): p. 134-137.
99. Scheinost, A.C., Rossberg, A., Vantelon, D., Xifra, I., Kretzschmar, R., Leuz, A.-K., Funke, H.,Johnson, C.A., *Quantitative Antimony Speciation in Shooting-Range Soils by Exafs Spectroscopy*. Geochimica et Cosmochimica Acta 2006. **70**: p. 3299–3312.
100. Figueiredo, M.O. *Extended Vs. Local Structure in Sb-Pyrochlores: An Illustration of the Valuable Interplay between Crystallography and Xafs*. 2007. **882**, 205.
101. Figueiredo, M.O., Silva, T.P.,Veiga, J.P., *A Xanes Study of the Structural Role of Lead in Glazes from Decorated Tiles, Xvi to Xviii Century Manufacture*. Appl. Phys. A, 2006. **83**: p. 209–211.
102. de Jesus, A., Viana, A.,Cavaca, R., *Minerais De Portugal Continental*. Comm. Serv. Geol. Portugal., 1930. **16**.: p. 51-152.
103. Fröberg, L., Kronberg, T., Hupa, L.,Hupa, M., *Influence of Firing Parameters on Phase Composition of Raw Glazes*. Journal of the European Ceramic Society, 2007. **27**: p. 1671–1675.
104. Rasteiro, M.G., Gassman, T., Santos, R.,Antunes, E., *Crystalline Phase Characterization of Glass-Ceramic Glazes*. Ceramics International, 2007. **33**: p. 345–354.
105. Coroado, J.,Gomes, C. *Physical and Chemical Characterization of Ceramic Glazed Wall Tiles Dated of the 17th Century, from the "Convento De Cristo", in Tomar, Portugal*. in *7th*



*European Meeting of Ancient Ceramics (EMAC03)*. 2003. Lisbon, Portugal: Trabalhos de Arqueologia.

106. Coroado, J.,Gomes, C. *Physical and Chemical Characterisation of Ceramic Wall Tiles, Dated from the XVII Century, from the “Convento De Cristo”, in Tomar, Portugal*. in *7th European Meeting of Ancient Ceramics*. 2005. Lisbon, Portugal.

## ANNEX

### Annex 1.1 – Chronological development of *Azulejos* (Wall-tiles) in Portugal.

Period	Historical data	Style / Influences	Techniques / Chromatics
<b>XIII-XIV centuries</b>	First applications in <i>Al-Andalus</i> <sup>1</sup> (Seville, Valence, Malaga and Toledo)	<i>Hispano-Moresque-ware</i> : Islamic motifs (the Muslim star is frequent) that tangle themselves in repeated geometric schemes, forming a pattern.	<i>Cuerda-seca</i> – engraving the drawings on the ceramic plate still humid. The sulks were filled with manganese mixed with some fat, ensuring the separation of the different colored smalts during firing.
<b>XV-XVI centuries</b>	King D. Manuel I contacts Seville to order those <i>Azulejos</i> and decorate the <i>Sintra</i> Palace. The tiles from Seville start being used in Portugal.	More freedom: inspiration in Gothic decorative elements, such as vegetables. The use of <i>Azulejos</i> as architect support starts.	Embossing: graving of motifs on the bisque through wood or metal moulds.
<b>XVI century</b>	<i>Azulejos</i> start being produced in Portugal.	Italian Renaissance – grotesque: decorative painting based on motifs from Classic Rome in ruins. The appearance of humane figures, other beings, birds, flowers, fruits,	Maiolica (or faience): <i>Azulejos</i> covered with a white smalt. Painted motifs could be applied on the surface without having the colors mixed.

		pots, shells, etc., with no logic.	Technique introduced in Seville by Francesco Niculoso.
<b>XVII century</b>	Increase of the Portuguese production: Lisbon is the biggest production center. The big wall panels manufactured by craftsmen with typical patterns.	Oriental influence (fauna and flora) exotic figures of the oriental spirituality.	Most used colors: cobalt blue, yellow over white, brownish-orange, olive green, purple, blue contours.
<b>XVII-XVIII centuries</b>	The paintings on the surface of <i>Azulejos</i> become a task for masters in this field only. After the earthquake in 1755, tile factories are settled in Lisbon	Learning how to represent in perspective. Illusionism. New motifs appear: vases, birds, laces, ...	Influences from the Dutch tiles on which cobalt blue and purples with manganese are used. Brush strokes become fancy.
<b>XIX century</b>	Use of <i>Azulejos</i> in frontages. New factories are built in Lisbon, Aveiro and Oporto.		Mechanical stamping of the drawings.
<b>XX century</b>	Use of <i>Azulejos</i> in train stations, mercantiles, stores, housings.		Mechanical pressing of the clay.

<sup>1</sup>*Al-Andalus* - the territory occupied by the Muslim empire in Southern Iberian Peninsula.

## Annex 1.2 – Chronological development of faiences from Coimbra.

Period	Historical data	Style / Influences	Techniques / Chromatics
<b>XVI century</b>	In 1514 the fees for earthenwares became public; First reference to glazes.	Ceramic pastes obtained from two localities in Coimbra and the firing process was made under jury observation.	Two firing stages for lead glazes and one for the ones with lead sulphide.
<b>1<sup>st</sup> half of XVII century</b>	Confirmation of pottery-making prior to 1623;	Objects with simple decoration; circles and spirals	Developments in the technological aspects of manufacturing.
<b>2<sup>nd</sup> half of XVII century</b>	It becomes explicit three crafts: 1) white-ware (faience), 2) green- and yellow-ware, 3) unglazed earthenware.	The employed decoration characterizes the Coimbra products, like the dark purple contours in manganese; The colored curves as well as details to fill the decoration space; laces in blue with dark purple contours.	The embossed contoured areas reveal the possibility of a third firing stage; Glazes less bright and mate earthy tones; Blue tones tend to violet and yellow tones tend to orange.
<b>1<sup>st</sup> half of XVIII century</b>	Enormous increase of the registered potters – increase in the production; Some decorative models characteristic of the faiences from Coimbra were defined.	Acanthus leafs interspersed with vegetation motifs	<i>No information available</i>
<b>2<sup>nd</sup> half of XVIII century</b>	Ceramics from the <i>Brioso</i> family gain importance and the initials <b>C.B.</b> are found in some plates.	Scratches, grids and laces as decoration motifs; Dark purple and blue lines interspersed with each other	<i>No information available</i>

---

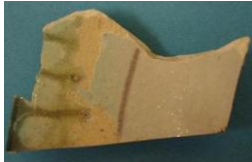
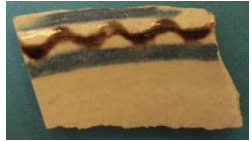

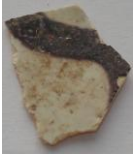
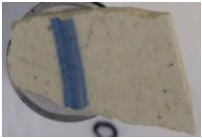
domain the decoration models.

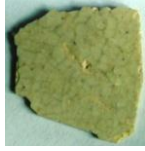
---

<b>1<sup>st</sup> half of XIX century</b>	Painting by stamping introduced by <i>Vandelli</i> becomes common but expensive; Less expensive style is developed, called " <i>Ratinha</i> "	Flowers and wreaths of flowers accompanied by a yellow strip, typical from <i>Vandelli</i> .	" <i>Ratinha</i> " should have lower amounts of Sn and colors always applied with brush and sponge.
<b>2<sup>nd</sup> half of XIX century</b>	First district ceramic exhibition.	Flowers and wreaths of flowers.	Modern kilns and new pastes are used.

---

### Annex 1.3 – Description of the analyzed fragments.

Sample	Type	Origin	Surface decoration <sup>1</sup>	Remarks
<p><b>C23</b></p> 	utility faience	Coimbra	G, B	Bright glaze and mate colors
<p><b>C24</b></p> 	utility faience	Coimbra	G, B, DP	Bright glaze and mate colors
<p><b>C26</b></p> 	utility faience	Coimbra	G, DP	Bright glaze and mate colors
<p><b>C29</b></p> 	utility faience	Coimbra	G, DP	Mate glaze and mate colors
<p><b>C34</b></p> 	utility faience	Coimbra	G, B	Mate glaze and mate colors
<p><b>C37</b></p>	utility faience	Coimbra	G	Mate glaze



**C41**



utility  
faience

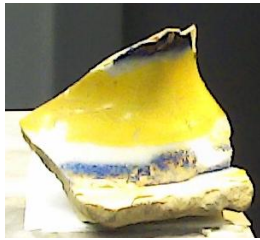
Coimbra

G, Y

Mate  
glaze and  
mate colors

---

**C50**



utility  
faience

Coimbra

G, B, Y

Bright  
glaze and  
bright  
colors

---

**C51**



utility  
faience

Coimbra

G, B, Y

Bright  
glaze and  
bright  
colors

---

**C52**



utility  
faience

Coimbra

G, B, Y

Bright  
glaze and  
bright  
colors

---

**C53**

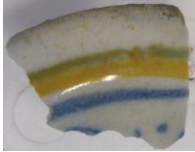

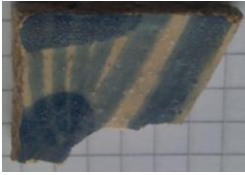


utility  
faience

Coimbra

G, B, Y

Bright  
glaze and


---

					bright colors
<b>C54</b>		utility faience	Coimbra	G, B, DP	Mate glaze and mate colors
<b>C55</b>		utility faience	Coimbra	G, B	Mate glaze and mate colors
<b>C56</b>		utility faience	Coimbra	G, B, DP	Mate glaze and mate colors
<b>C57</b>		utility faience	Coimbra	G, B	Bright glaze and mate colors
<b>C58</b>		utility	Coimbra	G, B	Bright

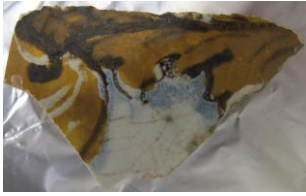


	faience			glaze and mate colors
---	---------	--	--	--------------------------

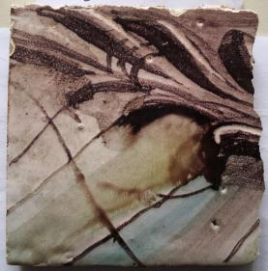
**C59**

	utility faience	Coimbra	G, B	Bright glaze and mate colors
---	--------------------	---------	------	------------------------------------

**AZCO1**

	Wall- tile	Coimbra	G, B, Y, Br	Mate glaze and mate colors
--	---------------	---------	-------------	----------------------------------

**AZCO2**

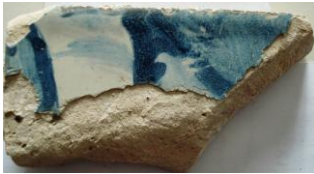
	Wall- tile	Coimbra	G, B, DP. Y	Partially bright colors
---	---------------	---------	-------------	-------------------------------

**AZCO3**

	Wall- tile	Coimbra	G, DP, G	Partially bright colors
--	---------------	---------	----------	-------------------------------



**AZCO4**



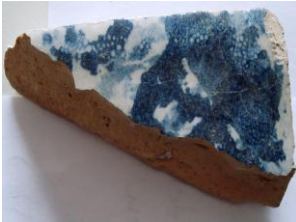
Wall-  
tile

Coimbra

G, B

Mate  
glaze and  
mate colors

**AZCO5**



Wall-  
tile

Coimbra

G, B

Mate  
glaze and  
mate colors

**AZCO6**



Wall-  
tile

Coimbra

G, DP

Mate  
glaze and  
mate colors

**AZCO7**



Wall-  
tile

Coimbra

G, B

Mate  
glaze and  
mate colors

---

---

<b>AZLX1</b>		Wall-tile	Lisbon	G, B, Y	Bright glaze and bright colors
<b>AZLX2</b>		Wall-tile	Lisbon	G, B, DP, Y, Gr	Bright glaze and bright colors
<b>AZLX3</b>		Wall-tile	Lisbon	DP, G	Bright colors
<b>AZLX4</b>		Wall-tile	Lisbon	G, B, DP, Y, Br	Bright glaze and bright colors
<b>AZLX5</b>		Wall-tile	Lisbon	G, B, DP, Y	Bright glaze and bright colors



**AZLX6**



Wall-  
tile

Lisbon

G, DP, Gr

Mate  
glaze and  
mate colors

---

**AZLX7a**



Wall-  
tile

Lisbon

G, B, DP, Y

Mate  
glaze and  
mate colors

---

**AZLX7b**



Wall-  
tile

Lisbon

G, DP

Mate  
glaze and  
mate colors

---

**AZLX8a**



Wall-  
tile

Lisbon

G, B

Bright  
glaze and  
bright  
colors

---

**AZLX8b**






Wall-

Lisbon

G, B

Bright

---

	tile			glaze and bright colors
<b>AZLX8c</b>				
	Wall-tile	Lisbon	G, B	Bright glaze and bright colors
<b>AZLX8d</b>				
	Wall-tile	Lisbon	G, B	Bright glaze and bright colors
<b>AZLX8e</b>				
	Wall-tile	Lisbon	G, B	Bright glaze and bright colors
<b>AZLX9</b>				
	Wall-tile	Lisbon	G, B, DP, Y, Gr	Partially bright glaze and colors

<sup>1</sup> Designation: **G** – Glaze; **B** – Blue; **DP** – Dark purple; **Y** – Yellow; **Gr** – Green; **Br** - Brown.

**Annex 1.4 – Description of the analyzed museum objects original from Coimbra.**

	Size (cm)	Date	Primary glaze	Decoration
	5.4 x Ø 32.5	XVIII	White	B, P
	15 x 24 x 14.5	XVIII	Light yellow	G, P
	30 x 18	XVIII	White	B, P



31.5 x 10.5 x 17.4

XVIII

White

B, G

---



36.8 x 24

XVIII

Light blue

B, G, Y,  
P

---



18.2 x 20.5 x 17

XVIII

Light yellow

B

---



17.3 x 16 x 15

XVIII

White

B

---



24 x 15.5

XIX

White

B, G, Y,  
O



36.8 x 24

XVIII

Light blue

B, G, Y,  
P



4 x Ø 34

XVIII

White

B, P



4.8 x Ø 27.7

XVIII

Light yellow

B, P





25 x 18.6

XVIII

Light blue

B, G, Y,  
BR



25.2 x Ø 16

XVIII

Light Yellow

B, G, P

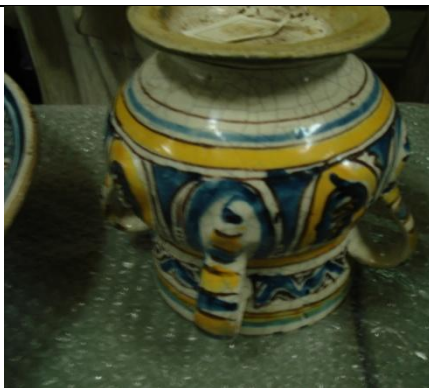


29.5 x 24

XIX

White

B



13.5 x Ø 10.5

XVII

White

B, Y, P

---



12.2 x 13.7

XVII

White

B



6 x Ø 26.6

XVII

White

B, Y, P



5.9 x Ø 40.3

XVII

Light yellow

B, Y, P



Ø 41

XVIII

White

B



3.8 x Ø 39

XVIII

White

B, P



4 x Ø 33.5

XVIII

White

B, P



4.3 x Ø 38

XVII

Light yellow

B, P



3.7 x Ø 42

XVIII

Light blue

B, BR



5.3 x Ø 33.6

XVII

White

B



5 x Ø 33.3

XVIII

White

B, P



32.5 x 41

XIX

White

B



Ø 29.3

XIX

Light blue

B, G, O



4 x Ø 33

XVII

White

B, P



5.5 x Ø 34.6

XVIII

White

B, P



4 x Ø 19.4

XVII

White

B, Y



6 x Ø 39

XVIII

White

B

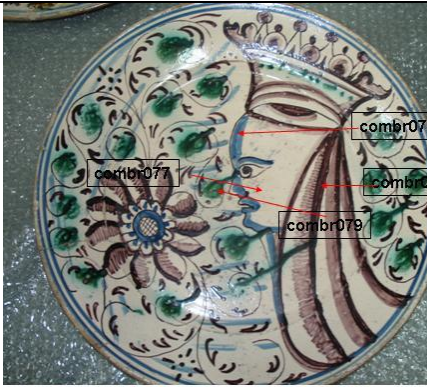


3.6 x Ø 34

XVIII

White

B



5 x Ø 35

XIX

White

B, G, P



5 x Ø 38.4

XVIII

White

B, P



5 x Ø 33.8

XVIII

White

B



32.5 x 39

XIX

White

B, G, BR

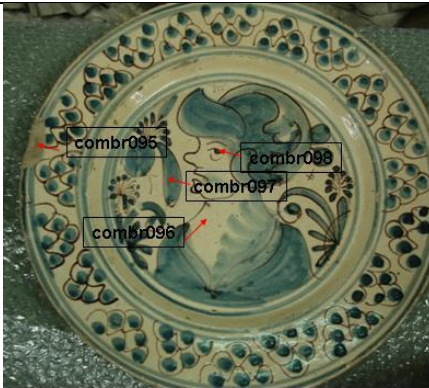


Ø 34.5

XIX

White

B, G, Y,  
P



26.5 x Ø 19

XVII

Light yellow

B, BR



26.5 x 8.7 x 9.5

XVIII

White

B, P



20 x 28

XIX

White

B, G, Y,  
P



19.5 x 10.5 x 9.8

XVIII

White

B, G

---

<sup>1</sup> Designation: **G** – Glaze; **B** – Blue; **DP** – Dark purple; **Y** – Yellow; **Gr** – Green; **Br** - Brown.



**Annex 1.5 – Papers published in peer reviewed international scientific journals in the framework of the present thesis.**

Cite this: *J. Anal. At. Spectrom.*, 2012, **27**, 966

www.rsc.org/jaas

PAPER

## Synchrotron micro-XRF with Compound Refractive Lenses (CRLs) for tracing key elements on Portuguese glazed ceramics

A. Guilherme,<sup>a</sup> G. Buzanich,<sup>bc</sup> M. Radtke,<sup>b</sup> U. Reinholz,<sup>b</sup> J. Coroado,<sup>d</sup> J. M. F. Dos Santos<sup>e</sup> and M. L. Carvalho<sup>\*a</sup>

Received 1st February 2012, Accepted 3rd April 2012

DOI: 10.1039/c2ja30030c

Several glazed ceramic fragments (XVI<sup>th</sup> to XVIII<sup>th</sup> centuries) from two production centers in Portugal (Coimbra and Lisbon) were the object of this study. The ones from Coimbra comprise two sets of samples: faiences and tiles. The ones from Lisbon are only tiles (*azulejos*, in Portuguese). The three main divisions of such pieces are the ceramic support (body), glaze and surface decoration. The system decoration/glaze is not easy to investigate, due to the high heterogeneity resulting from the mixing procedures and firing temperatures used. Moreover, the ability of the pigment to diffuse into the base glaze varies depending on the composition of both the pigment and the glaze in terms of fusibility. In order to raster these effects, high resolution techniques are required. In this work, synchrotron micro-X-ray fluorescence ( $\mu$ -XRF) analysis was performed to monitor the profiles of the characteristic elements from the colors used and the glaze in well prepared cross-sections of the samples. Key elements are: Co for blue, Mn for purple, Cu for green, Sb for yellow, Pb for the glaze and Fe for the body. The major difference observed is that faiences have glaze thicknesses between 150 and 200  $\mu\text{m}$  and tiles have glaze thicknesses between 350 and 400  $\mu\text{m}$ . Furthermore, in faiences all the pigments except the yellow ones are well dispersed into the glassy matrix, while in tiles, all of them are just partially diffused throughout the glaze. However, differences between the tiles from Coimbra and Lisbon were observed. In the samples from Lisbon, a higher intake from the pigment throughout the glaze is observed.

### 1. Introduction

To gain knowledge about Cultural Heritage (CH) objects, a physical–chemical characterization is required. A better understanding about the technologies used in the past is valuable for accurate object assignation as well as for conservation and restoration purposes.

For several years now there have been numerous references to different investigations bridging science and art. The use of different analytical techniques has been revealed to be the proper methodology for the study of CH. However, one must be aware of the advantages and limitations of each chosen method. This is the reason why one should always use a multianalytical approach in order to better characterize the given objects/samples.

With regard to ceramics studies (pigments, glazes, ceramic supports), several manuscripts can be found that describe the use of various analytical methods, for example, X-ray fluorescence (XRF),<sup>1–5</sup> X-ray diffraction (XRD),<sup>2,4,6</sup> Scanning Electron Microscopy (SEM),<sup>1,6–10</sup> Raman spectroscopy and Fourier Transform Infrared (FT-IR) spectroscopy<sup>4,11,12</sup> and also X-ray Absorption Fine Structure (XAFS).<sup>2,4,5,13,14</sup>

In the universe of CH studies, glazed ceramic objects are recognized by their high degree of complexity. In this case, fragments from the XVI<sup>th</sup> to XVIII<sup>th</sup> centuries were retrieved from two important production centers in Portugal, namely Coimbra and Lisbon.

When analyzing glazed ceramic pieces, one has to consider three important areas that comprise these objects: (1) the ceramic support (or body), (2) the glaze and (3) the surface decoration (color). The way these layers interfere with each other is strongly dependent on the raw materials chosen and on the manufacturing process used by the craftsman. Based on an ongoing investigation, this manuscript offers complementary information about the possible techniques used to produce such pieces. The analyzed glazed ceramic objects belong to a class called *Majolica*, produced mainly between the XIV<sup>th</sup> and XV<sup>th</sup> centuries in the Iberian Peninsula, based on Islamic traditions – the so-called *Hispano-Moresque* wares.<sup>15</sup> Previous investigations

<sup>a</sup>Atomic Physics Centre, University of Lisbon, 1649-003 Lisbon, Portugal. E-mail: luisa@cii.fc.ul.pt

<sup>b</sup>BAM Federal Institute for Materials Research and Testing, 12200 Berlin, Germany

<sup>c</sup>Institute of Atomic and Subatomic Physics, Vienna University of Technology, 1020 Vienna, Austria

<sup>d</sup>Dept. Arts, Conservation & Restoration, Polytechnic Institute of Tomar, 2300-313 Tomar, Portugal

<sup>e</sup>GIAN, Physics Department, University of Coimbra, 3004-516 Coimbra, Portugal

have revealed some information about these pieces.<sup>16–18</sup> They are polychrome lead-based glazed objects featuring tin-opacification. The aim of the craftsman was to have a white glaze as the base for surface decoration, and opacifying it with tin oxide inclusions was discovered to be the most favorable technique, even though opacification with other more ancient methods, such as inclusion of bubbles, is still found in these pieces.

An important piece of information for better understanding these objects is the amount of each compound present in the glazes. Previous analyses performed by Scanning Electron Microscopy with an Energy Dispersive System (SEM-EDS)<sup>16</sup> revealed that the glazes from the Coimbra pieces reveal relatively high amounts of K<sub>2</sub>O (8.1–9.3 wt%) and CaO (3.1–3.2 wt%) when compared with the ones from Lisbon (K<sub>2</sub>O: 4.3–5.8 wt% and CaO: 0.8–1.1 wt%). In addition, the amounts of Na<sub>2</sub>O (0.8–1 wt%) and PbO (40.1–40.5 wt%) in Coimbra are lower than the ones in Lisbon (Na<sub>2</sub>O: 3.5–4.2 wt%, and PbO: 45.5–45.9 wt%).

As for the pigment composition, by X-ray fluorescence techniques we were able to retrieve the basic elemental profiles from each color used.<sup>16</sup> Blue: the typical elements detected were Fe, Ni, Co and As (Smalt) with the presence of Mn and Ba in certain cases, mainly from Coimbra. Purple: the dominant element is Mn, and the presence of Ba indicates that the mineral Psilomelane [(Ba,H<sub>2</sub>O)<sub>2</sub>Mn<sub>5</sub>O<sub>10</sub>] was used as the raw material to obtain Mn. Green: Cu-based pigment. Yellow: the presence of Pb and Sb indicates the use of lead-antimonate (Pb(SbO<sub>3</sub>)<sub>2</sub>).

Knowing all these premises, monitoring the profiles of the characteristic elements from the three main “layers” is of interest: Co for blue, Mn for purple, Cu for green, Sb for yellow; Pb for the glaze; and Fe for the body. For clarifying the production techniques used in both centers (Coimbra and Lisbon), important issues to investigate are the system glaze/surface decoration and the ability of the pigment to diffuse into the base glaze. In order to understand these issues, we performed  $\mu$ -XRF analysis with a Compound Refractive Lens (CRL) on polished cross-sections. Synchrotron radiation together with exceptional optics allows us to have a 1  $\mu$ m beam, which provides information about the diffusion of the pigments throughout the glaze and the glaze throughout the ceramic support.

Given the fact that one of the major compounds forming the glaze is lead, strong absorption effects can always take place when one performs investigation with X-rays. However, as previously shown,<sup>16</sup> cross-section scans are one of the best methods to monitor the elemental profiles in depth. This brings valuable information about system color/glaze/body. The high lateral resolution offered by the experiment described here allowed us to obtain detailed elemental information, which is rarely achieved by most of the laboratory experimental techniques.

Furthermore, surface elemental mappings with a Color X-ray Camera (CXC) were also performed to get complementary information and knowledge about the pieces. With this technique it is easy to visualize the elements which characterize each color used as surface decoration.

## 2. Experimental methodology

Several fragments from each production site were analyzed and characterized. Table 1 summarizes the set of samples and their

main characteristics. The main division throughout the whole investigation is between Coimbra and Lisbon. Since for this study there are only tiles available for Lisbon, the differences between faiences and tiles are only considered as a subgroup of this work. The main goal of this study was to monitor the profiles of the characteristic elements from each part of the ceramic pieces. Since some lines of these elements overlap with each other,<sup>16</sup> after collecting the XRF data the spectra were fitted with PyMCA<sup>22</sup> and the fitted values were used for plotting the elemental profiles.

The capabilities for high resolution XRF analysis, provided at BAMline,<sup>19</sup> BESSY II electron storage ring, were the reason to perform this investigation there. The schematic of the BAMline @BESSY-II is shown in Fig. 1.

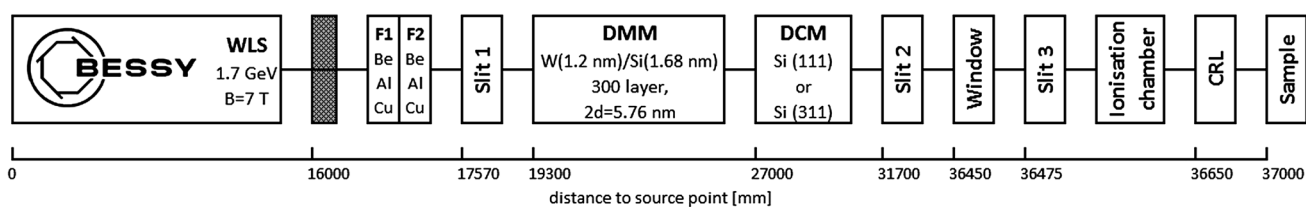
In the present work, two techniques were applied: (a)  $\mu$ -XRF analysis on the polished cross-sections of the samples and (b) surface elemental mappings obtained with a Color X-ray Camera (CXC).

To focus the incident X-ray beam for experiment (a), Compound Refractive Lenses (CRLs) were used. CRLs are one of several types of focusing X-ray optics devices and belong to the group of refractive optics, in which the X-rays undergo refraction at the surfaces between different materials. An example is displayed in Fig. 2. Since each lens only provokes a little change in the direction of the X-ray, an array of such lenses (*i.e.* Compound Refractive Lenses) is necessary to obtain acceptable focal sizes and distances.<sup>20</sup> Due to their simple design and alignment, CRLs are one of the most popular X-ray focusing devices. The important features are: (i) focusing in the region of 100 nm; and (ii) focusing of X-rays with energies in the range from 5–200 keV is possible. The energy bandwidth of these kinds of lenses (*ca.* 100 eV) is very small, meaning that for every energy value, a separate lens has to be manufactured. The fact that the CRLs require a monochromatic and parallel beam makes them suitable for synchrotron beamlines only.

An example of one CRL used @BAMline is shown in Fig. 3. For this beamline designed optics, a beam of 1  $\mu$ m diameter is feasible. In Fig. 4 the layout of the  $\mu$ -XRF experiment at the BAMline and a sketch of the sample composition (tile) in terms of its layers is shown to illustrate how the scans were performed. For these measurements two lenses were used: one with a nominal energy of

**Table 1** Set of significant analyzed samples from each production centre, their types and a summary of their characteristics, and the elemental composition obtained previously by XRF. The key elements correspond to the ones which were used as a tracer for each colour in the scans

Sample	Origin	Type	Colour	Detected elements	Key elements
C34	Coimbra	Faience	Blue	Fe, Co, Ni, As	Co
AZCO7	Coimbra	Tile	Blue	Fe, Co, Ni, As	Co
AZLX1	Lisbon	Tile	Blue	Fe, Co, Ni, As	Co
C29	Coimbra	Faience	Purple	Mn, Fe, Ba	Mn
AZCO3	Coimbra	Tile	Purple	Mn, Fe, Ba	Mn
			Green	Cu	Cu
AZLX3	Lisbon	Tile	Purple	Mn, Fe, Ba	Mn
			Green	Cu	Cu
C41	Coimbra	Faience	Yellow	Fe, Sb, Pb	Sb
AZCO1	Coimbra	Tile	Yellow	Fe, Sb, Pb	Sb
AZLX2	Lisbon	Tile	Yellow	Fe, Sb, Pb	Sb



**Fig. 1** Schematics of the BAMline @BESSY-II. The X-ray source is a 7T WLS (Wave Length Shifter) installed at the storage ring BESSY II. The optical elements are a Double Multilayer Monochromator, a Double Crystal and the CRL.

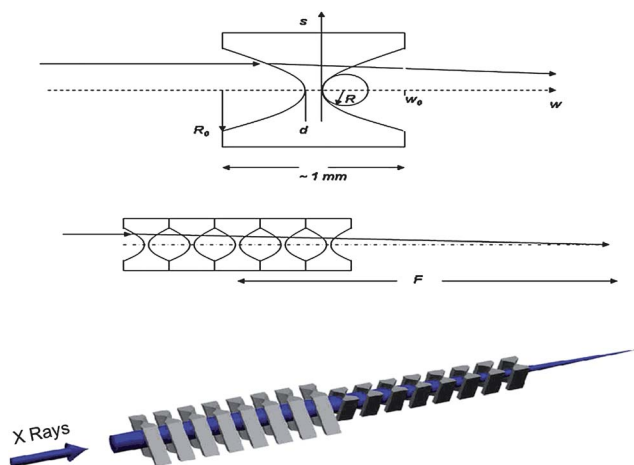
33.2 keV and another with a nominal energy of 20.0 keV. This choice was made due to the elemental variability present in the decorative motifs as well as in the glaze. For the pieces which had yellow (Sb:  $E_{c(K)} = 30.491$  keV) the 33.2 keV lens was ideal, and for the pieces which had blue (Co:  $E_{c(K)} = 7.709$  keV), green (Cu:  $E_{c(K)} = 8.979$  keV) and purple (Mn:  $E_{c(K)} = 6.539$  keV; Fe:  $E_{c(K)} = 7.112$  keV) colors together with the glaze (Pb:  $E_{c(L3)} = 13.035$  keV) the 20 keV lens was used. Although the lens with a nominal energy of 33.2 keV would have been able to excite the medium–low range, the 20 keV lens was used for the measurements. This lens, due to its bigger aperture, provides more flux at the sample and the absorption efficiency is higher for this elemental range. As a supplement to this investigation, surface elemental mappings were performed. For such data collection, a beam with a size of 20 mm  $\times$  5 mm was impinged onto the sample and a so-called Color X-ray Camera (CXC) together with 1 : 1 polycapillary optics was used. The CXC records 264  $\times$  264 spectra simultaneously with a spatial resolution of 50  $\mu$ m and an energy resolution of 152 eV @ Mn-K $\alpha$ .<sup>21</sup> The first prototype of the camera, the SLcam, was provided by the Institute for Scientific Instruments GmbH.

### 3. Results and discussion

#### 3.1. Micro-XRF cross-section scans

The results reported here correspond to an average of three measurements per analyzed area.

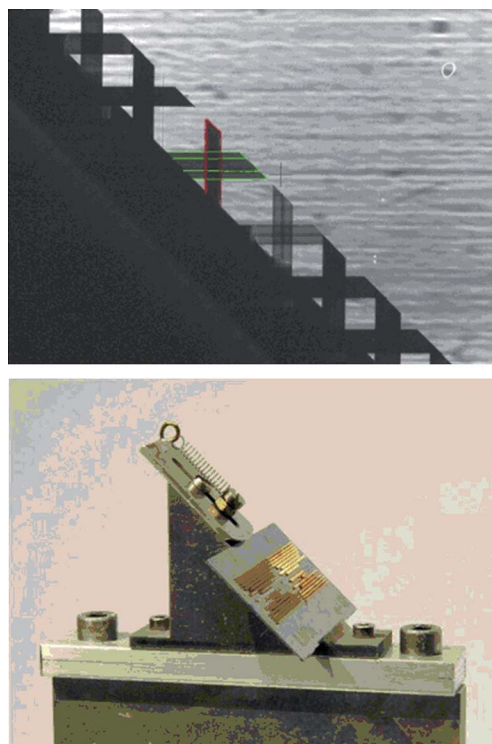
**3.1.1. Glazes with blue decorations.** In Fig. 5 the elemental profiles of samples containing blue decorative motifs are



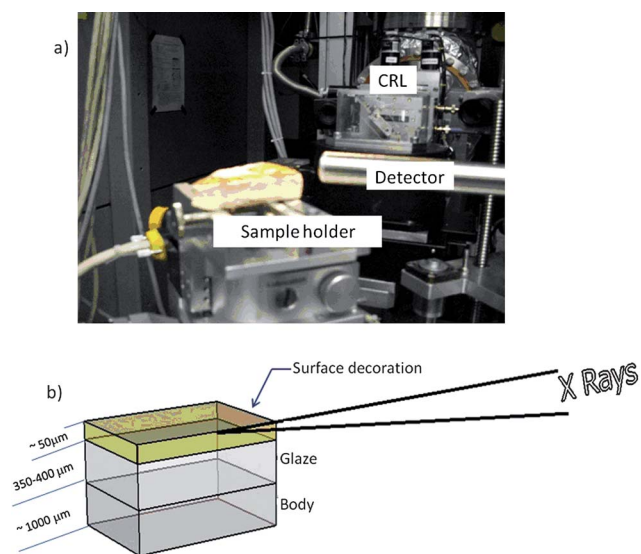
**Fig. 2** An example of a CRL and its working principle.

compared. Cross-section scans were performed through the blue/glaze/body of two samples from Coimbra, a faience (C34, Fig. 5a) and a tile (AZCO7, Fig. 5b), and one sample from Lisbon, a tile (AZLX1, Fig. 5c). Pictures taken with the incorporated microscope, in which the different areas of each sample are easy to observe, are also displayed in this figure. In red one can see how the line scans were accomplished from the top of the surface down to the ceramic body. These scans were repeated in three different regions of the cross-sections.

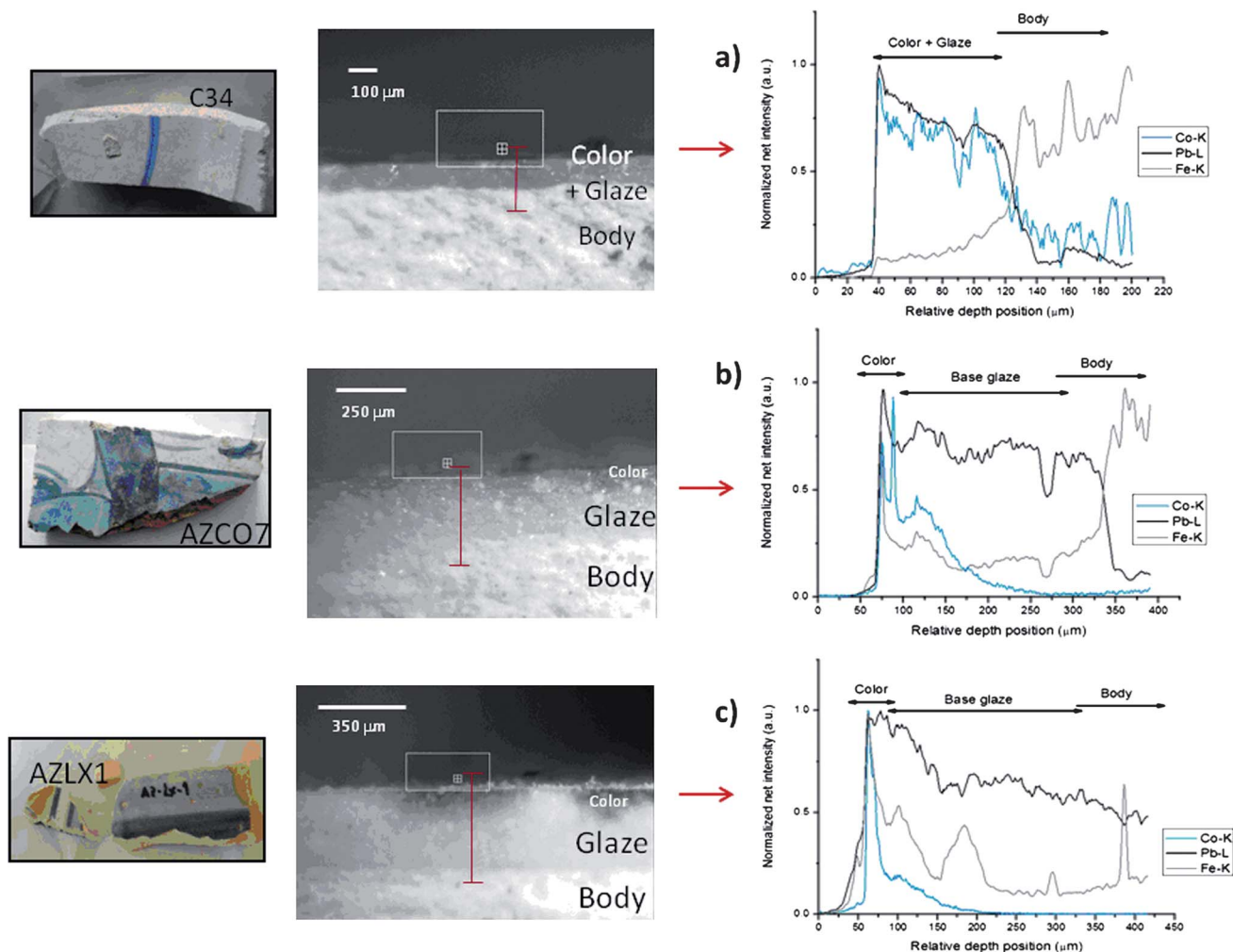
The scans compare the Co-K, Pb-L and Fe-K signals, which characterize blue, glaze and body, respectively. The first difference highlighted by these scans is the thickness of the glazes. With regard to the faience sample C34 (Fig. 5a), the glaze is approximately 120  $\mu$ m thick, while the tile samples (AZCO7 and AZLX1) have similar glaze thicknesses (between 350 and 400  $\mu$ m) (Fig. 5b and c). Tracking the Co signal in sample C34, one sees that the glaze and surface decoration exist as one layer together. The glaze is too thin and the pigment was applied together with the glaze in one firing stage. Comparison of the Co signal between the two tiles (AZCO7 and AZLX1) shows that its maximum is broader in the sample from



**Fig. 3** CRL @BAMline (from KIT: [www.x-ray-lenses.de](http://www.x-ray-lenses.de)).



**Fig. 4** (a) Layout of the  $\mu$ -XRF experiment at the BAMline; (b) a sketch of the sample composition (tile) in terms of its layers. The scans were performed up to a maximum of 500  $\mu\text{m}$  thickness of ceramic body.



**Fig. 5** Cross-section scans were performed through the blue/glaze/body of two samples from Coimbra – (a) a faience (C34) and (b) a tile (AZCO7) – and one sample from Lisbon, (c) a tile (AZLX1).

Coimbra ( $\sim 150\ \mu\text{m}$  – Fig. 5b) than in the one from Lisbon ( $\sim 125\ \mu\text{m}$  – Fig. 5c). There are several factors which allow a higher intake of the pigment particles through the glaze: (a) a higher content of fusible components in the glaze (lead oxides and alkaline compounds); (b) a higher firing temperature of the glaze; and (c) more refractory pigment particles, that is, the particles do not undergo physical changes when they are submitted to a higher temperature.<sup>23</sup> Since the pigment sources used should be the same, the factors which can promote a higher penetration of the pigment in the glaze are (a) and (b).

Another interesting fact is that the Pb signal in sample AZCO7 (Fig. 5b) has an abrupt drop in the interface glaze–body. This is not found to happen in sample AZLX1 (Fig. 5c). There is a smooth drop of the Pb signal when reaching the body of the sample from Lisbon, allowing a higher intake of the glaze throughout the body. In addition, the Fe signal (mainly characteristic of the ceramic body) is higher at the interface glaze/body in the sample from Lisbon than in the sample from Coimbra. These two aspects lead to the preliminary conclusion that the glaze and the ceramic body have undergone a higher chemical exchange in the interface during the firing procedure.

**3.1.2. Glazes with purple decorations.** In Fig. 6 the elemental profiles of samples containing purple decorative motifs are compared. Cross-section scans were performed through the purple/glaze/body of two samples from Coimbra, a faience (C29, Fig. 6a) and a tile (AZCO3, Fig. 6b), and one sample from Lisbon, a tile (AZLX3, Fig. 6c).

Again, in the pictures taken through the microscope, it is indicated how the scans were performed. Mn is the monitored element for the purple decoration since its source is a compound highly abundant in Portugal: *Psilomelane*  $[(Ba,H_2O)_2Mn_5O_{10}]$ . Once again one can see that the faience sample (Fig. 6a) reveals no interface between color and glaze. The glaze thickness is approximately 150  $\mu\text{m}$  and the pigment was applied to the glaze and both had been submitted to one firing stage. There is, however, a moderate connection between the glaze and the body in this sample, as observed from the smooth decrease and increase of the Pb and Fe profiles, respectively.

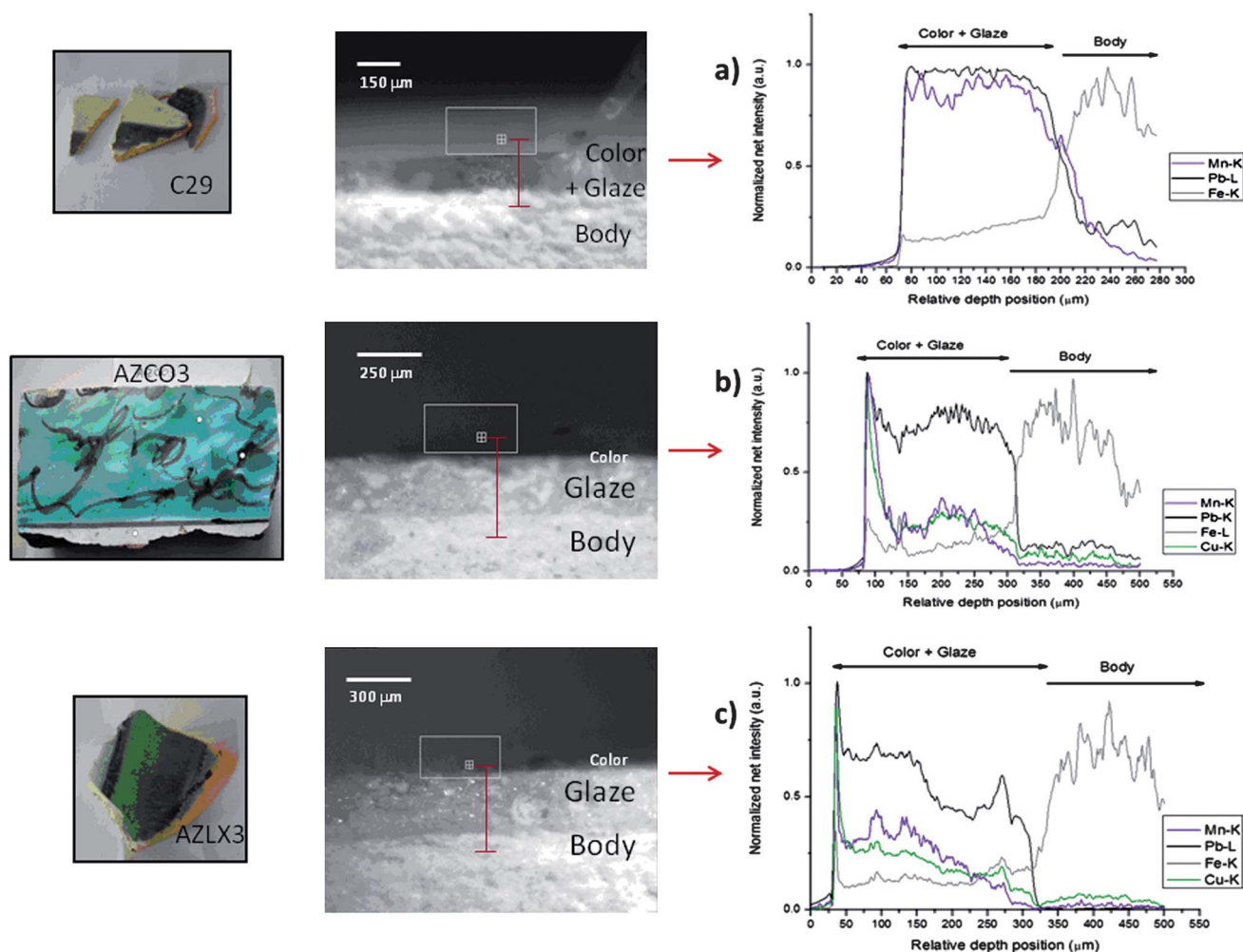
On comparing the tiles from Coimbra and Lisbon, it seems that the pigment (Mn) is equally well dispersed through the glaze in both the samples (Fig. 6b and c). However, the Mn profile in the sample from Coimbra (Fig. 6b) reveals a broader maximum at the surface ( $\sim 50 \mu\text{m}$ ) than in the sample from

Lisbon ( $<25 \mu\text{m}$  – Fig. 6c). The Cu signal was also plotted because the purple motifs were applied together with a green colored layer (as observed in this picture).

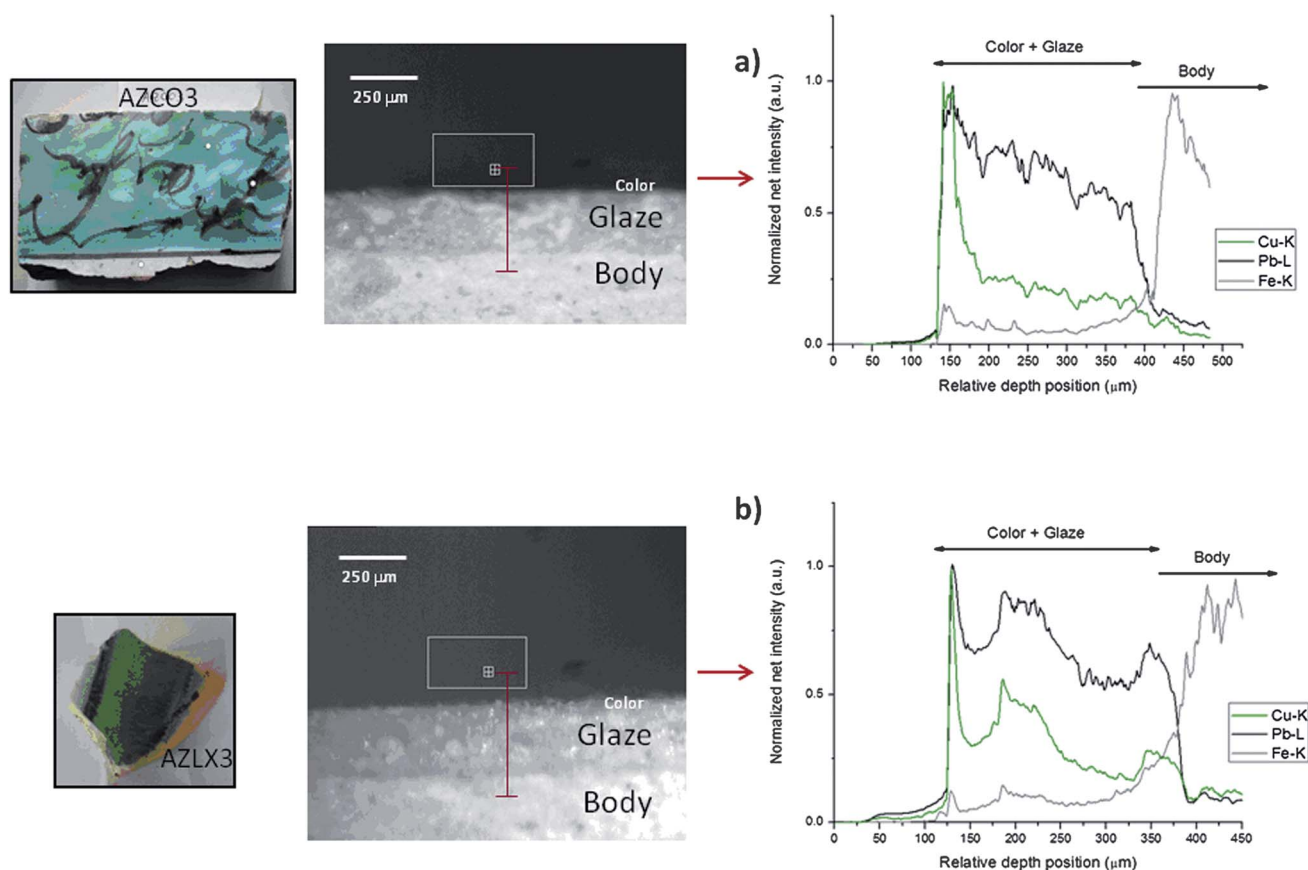
The glazes from both the tiles have thicknesses varying between 250 and 300  $\mu\text{m}$  for the Coimbra and Lisbon samples, respectively. Again one observes a smoother elemental exchange at the interface glaze–body in the sample from Lisbon (Fig. 6c) than in the sample from Coimbra (Fig. 6b).

**3.1.3. Glazes with green decorations.** In Fig. 7 the elemental profiles of samples containing green decorative motifs are compared. Cross-section scans were performed through the green/glaze/body of one sample from Coimbra, a tile (AZCO3, Fig. 7a), and one sample from Lisbon, a tile (AZLX3, Fig. 7b).

These samples are the same as the ones where Mn for the purple color was monitored, but here Cu for the green color was under investigation. On evaluating the Cu signal, the intake of pigment into the glaze seems to be higher in the sample from Lisbon than in the sample from Coimbra. However, a broader maximum of the Cu signal at the surface from the sample from Coimbra ( $\sim 50 \mu\text{m}$  – Fig. 7a) than in the sample from Lisbon ( $\sim 25 \mu\text{m}$  – Fig. 7b) is observed. Also, the chemical exchange



**Fig. 6** Cross-section scans were performed through the purple/glaze/body of two samples from Coimbra – (a) a faience (C29) and (b) a tile (AZCO3) – and one sample from Lisbon, (c) a tile (AZLX3).



**Fig. 7** Cross-section scans were performed through the green/glaze/body of one sample from Coimbra, (a) a tile (AZCO3), and one sample from Lisbon, (b) a tile (AZLX3).

between the glaze and the body seems to be more pronounced in the sample from Lisbon than in the sample from Coimbra. The justification is the same as previously explained.

**3.1.4. Glazes with yellow decorations.** In this section, the elemental profiles of samples containing yellow decorations are compared. Fig. 8 corresponds to the cross-section scans carried out through the yellow/glaze/body of two samples from Coimbra, a faience (C41, Fig. 8a) and a tile (AZCO1, Fig. 8b), and one sample from Lisbon, a tile (AZLX2, Fig. 8c).

Conversely to what has been said regarding the faïences' features, when one is dealing with yellow pigment, new aspects arise. The yellow pigment found in these ceramic objects is a lead–antimony composite. This has large sized crystals, which makes it difficult for the pigment itself to be dispersed throughout the glaze as a principle. Furthermore, a single firing stage just for the pigment (mixed with glaze) could have occurred. In Fig. 8a one sees that the pigment layer (30  $\mu\text{m}$ ) is not completely dispersed into the glaze ( $\sim 180 \mu\text{m}$ ). At the interface glaze–body, once again a smooth decrease of the Pb signal and a smooth increase of the Fe signal is observed.

Now, by comparing the profiles of Fig. 8b and c, some features are explained. The pigment layers of both samples appear to have the same thickness ( $\sim 100 \mu\text{m}$ ); however, the Pb signal accompanying the pigment (in Fig. 8b) has a high drop at the interface color–glaze, indicating the possibility of a separate firing stage just for the pigment. This effect is not observed in the sample

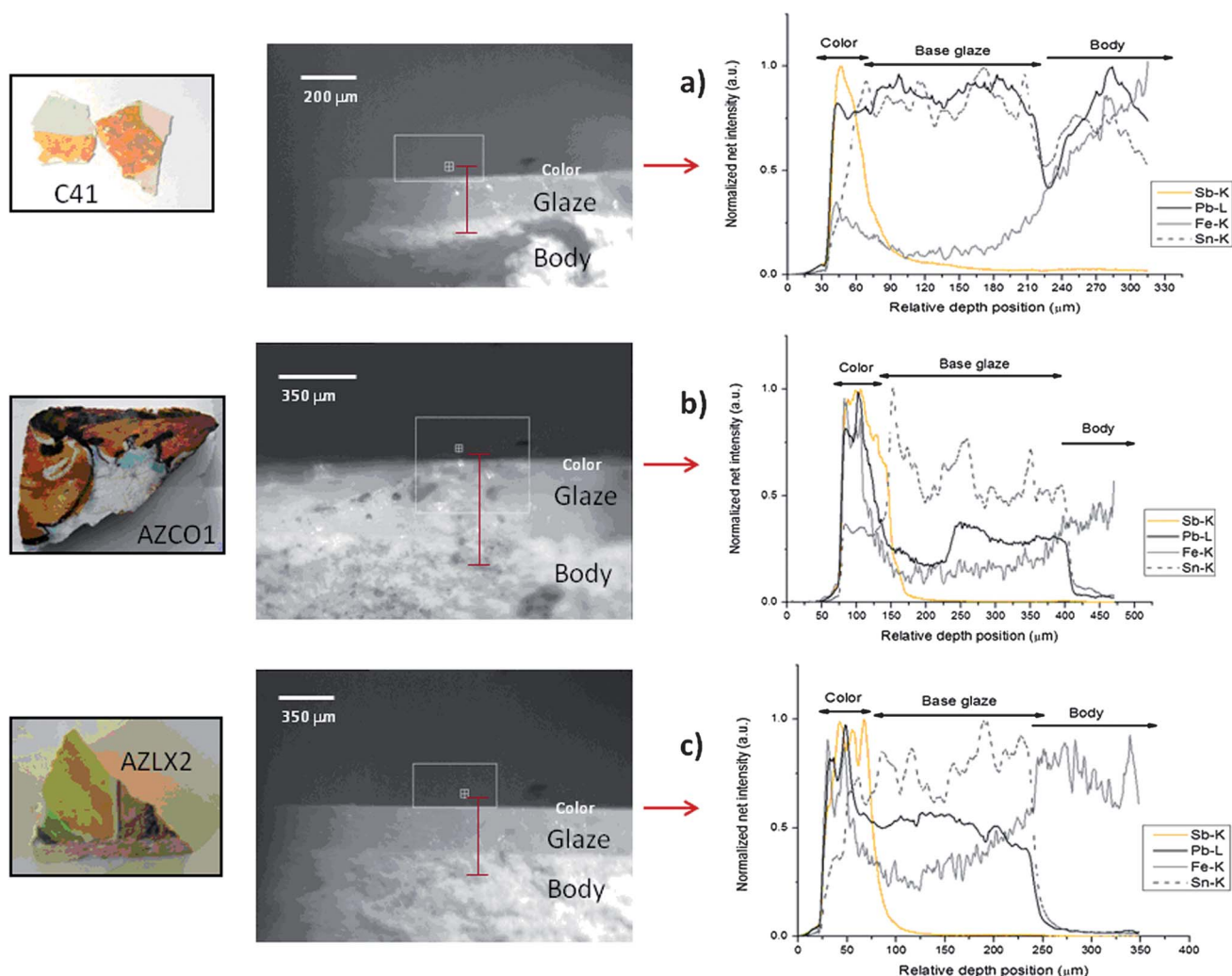
from Lisbon. At the interface glaze/body, the Pb and Fe signals are smoother in the sample from Lisbon (Fig. 8c) than in the sample from Coimbra (Fig. 8b).

### 3.2. Elemental mappings with a Color X-ray Camera (CXC)

Several images corresponding to elemental surface mappings are presented. These images were taken with the so-called Color X-ray Camera (CXC), and detailed explanation about the associated software can be found in ref. 7.

For these measurements, samples with a broad range of surface decorations were chosen in order to obtain a bigger elemental variety on these mappings. In Fig. 9 one can observe the pictures taken of 4 tile samples: AZCO3 (Fig. 9a), AZCO2 (Fig. 9b), AZLX9 (Fig. 9c) and AZLX2 (Fig. 9d). The red square marks the area of the image taken with the CXC. For each element a color was arbitrarily assigned. In both samples from Coimbra (Fig. 9a and b), the analyzed areas have a green base decoration together with purple motifs on top of it. This explains the abundant presence of Cu and Mn. The Cu signal is stronger in sample AZCO3 since it has a thicker layer of green than sample AZCO2.

For the sample from Fig. 9c (Lisbon), the examined area corresponds to green, blue and purple motifs over a white glaze base. One can see the characteristic Cu, Co and Mn signals from the respective colors. At last the sample from Fig. 9d (Lisbon) was examined in an area where three different parts are seen:

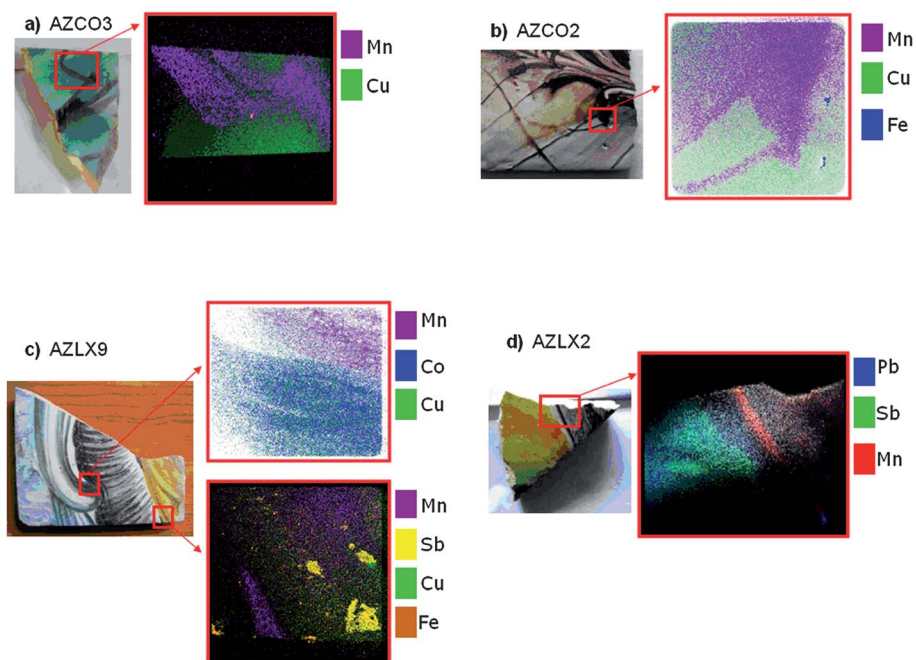


**Fig. 8** Cross-section scans were performed through the yellow/glaze/body of two samples from Coimbra – (a) a faience (C41) and (b) a tile (AZCO1) – and one sample from Lisbon, (c) a tile (AZLX2).

**Table 2** Summary of the properties of the Lisbon and Coimbra pieces for this set of samples. Differences in the pigment diffusion throughout the glaze between Lisbon and Coimbra tiles are observable

	Coimbra		Lisbon
	Faiences	Tiles	Tiles
Glaze	Thickness: max. 180 µm	Thickness: max. 400 µm	Thickness: max. 400 µm
Blue	Pigment (Co) completely dispersed into the glaze (Pb)	Pigment (Co) diffused down ~150 µm into the glaze (Pb)	Pigment (Co) diffused down ~125 µm into the glaze (Pb)
Purple	Pigment (Mn) completely dispersed into the glaze (Pb)	Pigment (Mn) well diffused into the glaze (Pb). Mn maximum at the surface ~50 µm broad	Pigment (Mn) well diffused into the glaze (Pb). Mn maximum at the surface <25 µm broad
Green	Pigment (Cu) completely dispersed into the glaze (Pb)	Pigment (Cu) well diffused into the glaze (Pb). Cu maximum at the surface ~50 µm broad	Higher pigment (Cu) intake into the glaze (Pb). Cu maximum at the surface ~25 µm broad
Yellow	Pigment (Sb) thickness: ~30 µm.	Pigment (Sb) thickness: ~100 µm. Strong drop in Pb signal together with Sb signal	Pigment (Sb) thickness: ~100 µm. Slight drop in Pb signal after the pigment layer (Sb)
General features	No color–glaze interface, except for yellow decorations	Broader maximum of the pigment signal. Slightly lower intake of the pigment through the glaze	Slightly higher intake of the pigment into the glaze. Smoother elemental exchange at the glaze–body interface ⇒ higher firing temperature





**Fig. 9** Surface elemental mappings were performed with a Color X-ray Camera (CXC) in two samples from Coimbra (a and b) and two samples from Lisbon (c and d).

yellow, glaze and purple. By the elemental mapping shown in this picture, one can see perfectly the characteristic Pb signal from the glaze lying underneath the Sb signal from yellow and the Mn signal from purple. An interesting feature is that the darker purple line in this area has less contribution from Pb than the brighter part of the purple decoration, where Mn is completely disseminated with the Pb, throughout the glaze.

#### 4. Conclusions

This study is part of an ongoing investigation, and the number of samples used here was chosen to be representative of each type of ceramic as well as the centre of production. The results reported are given as an example of application and the archaeometric conclusions hereby presented have a strong support from previous studies as mentioned throughout this manuscript.

The most important conclusion one can draw from this work is the usefulness of this method of investigation, and its potential in studying these types of CH objects is shown.

Cross-section elemental scans with a 1  $\mu\text{m}$  lateral resolution were performed and general features were extracted. In Table 2, a summary of the properties of the Lisbon and Coimbra samples is presented. The major difference is related to the glaze thicknesses of faiences and tiles. Faiences revealed a glaze thickness of up to 180  $\mu\text{m}$ , and tiles revealed a glaze thickness of up to 400  $\mu\text{m}$ .

In general, the maximum of each pigment's characteristic signal is broader in the tile samples from Coimbra than in the ones from Lisbon. However, a slightly higher intake of the pigment throughout the glaze in the tile samples from Lisbon is observable.

Another feature is that the tile samples from Lisbon seem to have a broader glaze/body interface than the ones from Coimbra.

This means that the chemical exchange between some elements from the glaze and some elements from the body took place in a more pronounced way in the samples from Lisbon. Taking these results into account, several points must be discussed. There is a high possibility that the glaze was applied raw, meaning that it had not undergone a previous firing process before being applied onto the bisque (fired ceramic body).<sup>23</sup> This conclusion derives from the fact that the glazes show defects like voids or cracks on naked eye inspection. This would have been much less probable if the glaze had been applied as a frit (pre-firing process) before application onto the bisque. The raw glaze is then mixed with water and applied onto the bisque to be fired. The lead compounds are water soluble and during the firing process, water is highly absorbed by the ceramic support and this process drags the lead compounds to the lower part of the glaze. This migration may also occur with other compounds, such as Fe. The fact that there is a smoother chemical exchange between Pb and Fe in the samples from Lisbon, as already mentioned, leads to the conclusion that Pb migrated further down the glaze and the samples from Lisbon were subjected to a higher firing temperature. This last conclusion is also supported by the fact that the pigment intake in the sample from Lisbon is higher than that in the samples from Coimbra.

Furthermore, the faiences reveal a typical thin glaze together with pigment application in a single firing stage. This conclusion comes from the fact that the signal from Pb and the element which typifies the color have similar profiles. However, the yellow decorations do not reveal this. The yellow pigment is much denser than the other ones (blue, green, purple) making its dissemination throughout the glaze difficult. Moreover, this could also be indicative of a single firing stage for the yellow pigment (mixed with glaze), which was then applied over the base glaze layer.

With regard to the elemental mappings provided by the CXC, it was interesting to visualize how the important elements, which characterize each color or glaze, are distributed. The characteristic elements that confer each color are clearly identified by these pictures. Some of the motifs are applied on top of other colors, as observed in Fig. 9a and b. The lead in sample AZLX2 (Fig. 9d) is clearly well distributed throughout the whole glaze layer and mixed with the pigments as well. This is an indication that the pigment was applied with glaze, even if a base glaze layer existed in the sample.

The information about tracing manufacturing techniques used to fabricate these pieces and the raw materials and mixtures used complements former investigations. In addition, it is of great importance for the Portuguese Cultural Heritage field to increase the knowledge about glazed ceramics.

## Acknowledgements

We acknowledge the Helmholtz-Zentrum Berlin – Electron storage ring BESSY II for the provision of synchrotron radiation at BAMline. The authors also wish to acknowledge Oliver Scharf and IAP (Institute for Applied Photonics e.V.) for providing the Color X-ray Camera (CXC) and helping with the data acquisition obtained from it.

## References

- 1 R. Padilla, O. Schalm, K. Janssens, R. Arzacaeta and P. Van Espen, Microanalytical characterization of surface decoration in Majolica pottery, *Anal. Chim. Acta*, 2005, **535**, 201–211.
- 2 R. Arletti, G. Vezzalini, S. Quartieri, D. Ferrari, M. Merlini and M. Cotte, Polychrome glass from Etruscan sites: first non-destructive characterization with synchrotron  $\mu$ -XRF,  $\mu$ -XANES and XRPD, *Appl. Phys. A: Mater. Sci. Process.*, 2008, **92**, 127–135.
- 3 L. De Viguerie, A. Duran, A. Bouquillon, V. A. Solé, J. Castaing and P. Walter, Quantitative X-ray fluorescence analysis of an Egyptian faience pendant and comparison with PIXE, *Anal. Bioanal. Chem.*, 2009, **395**, 2219–2225.
- 4 W. Tanthanuch, W. Pattanasiriwisawa, W. Somphon and S. Srilomsak, Synchrotron studies of Ban Chiang ancient pottery, *Suranaree J. Sci. Technol.*, 2011, **18**(1), 15–28.
- 5 F. Bardelli, G. Barone, V. Crupi, F. Longo, D. Majolino, P. Mazzoleni and V. Venuti, Combined non-destructive XRF and SR-XAS study of archaeological artefacts, *Anal. Bioanal. Chem.*, 2011, **399**, 3147–3153.
- 6 G. Bultrini, I. Fragalà, G. M. Ingo and G. Lanza, Characterisation and reproduction of yellow pigments used in central Italy for decorating ceramics during Renaissance, *Appl. Phys. A: Mater. Sci. Process.*, 2006, **83**, 557–565.
- 7 J. Pérez-Arantegui, A. Larrea, J. Molera, T. Pradell and M. Vendrell-Saz, Some aspects of the characterization of decorations on ceramic glazes, *Appl. Phys. A: Mater. Sci. Process.*, 2004, **79**, 235–239.
- 8 M. S. Tite, The production technology of Italian Maiolica: a reassessment, *J. Archaeol. Sci.*, 2009, **36**, 2065–2080.
- 9 A. Zucchiatti, A. Bouquillon, I. Katona and A. D'Alessandro, The 'DELLA ROBBIA BLUE': a case study for the use of cobalt pigments in ceramics during the Italian Renaissance, *Archaeometry*, 2006, **48**(1), 131–152.
- 10 M. Gulmini, L. Appolonia, P. Framarin and P. Mirti, Compositional and technological features of glazed pottery from Aosta Valley (Italy): a SEM–EDS investigation, *Anal. Bioanal. Chem.*, 2006, **386**, 1815–1822.
- 11 R. J. H. Clark and P. J. Gibbs, Non-destructive *in situ* study of ancient Egyptian faience by Raman microscopy, *J. Raman Spectrosc.*, 1997, **28**, 99–103.
- 12 D. de Waal, Micro-Raman and portable Raman spectroscopic investigation of blue pigments in selected Delft plates (17–20th century), *J. Raman Spectrosc.*, 2009, **40**, 2162–2170.
- 13 M. O. Figueiredo, T. P. Silva and J. P. Veiga, A XANES study of the structural role of lead in glazes from decorated tiles, manufactured between XVI and XVIII century, *Appl. Phys. A: Mater. Sci. Process.*, 2006, **83**, 209–211.
- 14 D. Barilaro, V. Crupi, D. Majolino, V. Venuti and G. Barone, Decorated pottery study: analysis of pigments by X-ray absorbance spectroscopy measurements, *J. Appl. Phys.*, 2007, **101**, 064909.
- 15 R. B. Mason and M. S. Tite, The beginnings of tin-opacification of pottery glazes, *Archaeometry*, 1997, **39**, 41–58.
- 16 A. Guilherme, J. Coroado, J. M. F. dos Santos, L. Lühl, T. Wolff, B. Kanngießner and M. L. Carvalho, X-ray fluorescence (conventional and 3D) and scanning electron microscopy for the investigation of Portuguese polychrome glazed ceramics: advances in the knowledge of the manufacturing techniques, *Spectrochim. Acta, Part B*, 2011, **66**(5), 297–307.
- 17 A. Guilherme, M. L. Carvalho, S. Pessanha, J. M. F. dos Santos and J. Coroado, Micro energy dispersive X-ray fluorescence analysis of polychrome lead-glazed Portuguese faiences, *Spectrochim. Acta, Part B*, 2010, **65**(4), 328–333.
- 18 A. Guilherme, J. Coroado and M. L. Carvalho, Chemical and mineralogical characterization on glazes of ceramics from Coimbra (Portugal) from XVI–XIX centuries, *Anal. Bioanal. Chem.*, 2009, **395**, 2051–2059.
- 19 H. Riesemeier, K. Ecker, W. Gorner, B. R. Muller, M. Radtke and M. Krumrey, Layout and first XRF applications of the BAMline at BESSY II, *X-Ray Spectrom.*, 2005, **34**(2), 160–163.
- 20 <http://x-ray-optics.de/>, accessed 5 December 2011.
- 21 O. Scharf, S. Ihle, I. Ordavo, V. Arkadiev, A. Bjeoumikhov, S. Bjeoumikhova, G. Buzanich, R. Gubzhokov, A. Günther, R. Hartmann, M. Kühbacher, M. Lang, N. Langhoff, A. Liebel, M. Radtke, U. Reinholz, H. Riesemeier, H. Soltau, L. Strüder, A. F. Thünemann and R. Wedell, Compact pnCCD-based X-ray camera with high spatial and energy resolution: a color X-ray camera, *Anal. Chem.*, 2011, **83**, 2532–2538.
- 22 V. A. Solé, E. Papillon, M. Cotte, Ph. Walter and J. Susini, A multiplatform code for the analysis of energy-dispersive X-ray fluorescence spectra, *Spectrochim. Acta, Part B*, 2007, **62**, 63–68.
- 23 J. Coroado and C. Gomes, Physical and Chemical Characterisation of Ceramic Wall Tiles, Dated from the XVII Century, from the "Convento de Cristo", in Tomar, Portugal, in *Understanding People Through Their Pottery. Proceedings of the 7th European Meeting of Ancient Ceramics*, IPA, Lisboa, 2005, pp. 33–39.



# X-ray fluorescence (conventional and 3D) and scanning electron microscopy for the investigation of Portuguese polychrome glazed ceramics: Advances in the knowledge of the manufacturing techniques

A. Guilherme<sup>a</sup>, J. Coroado<sup>b</sup>, J.M.F. dos Santos<sup>c</sup>, L. Lühl<sup>d</sup>, T. Wolff<sup>d</sup>, B. Kanngießner<sup>d</sup>, M.L. Carvalho<sup>a,\*</sup>

<sup>a</sup> Departamento de Física da Faculdade de Ciências, Centro de Física Atómica da Universidade de Lisboa, Av. Prof. Gama Pinto, 2, 1649-003 Lisboa, Portugal

<sup>b</sup> Instituto Politécnico Tomar, Dep. Arte Conservação & Restauro, P-2300313 Tomar, Portugal

<sup>c</sup> GIAN, Departamento de Física, Universidade de Coimbra, 3004-516 Coimbra, Portugal

<sup>d</sup> Institut für Optik und Atomare Physik, Technische Universität Berlin, Hardenbergstr. 36 D-10623 Berlin, Germany

## ARTICLE INFO

Available online 4 March 2011

### Keywords:

Portuguese ceramic  
Polychrome glaze  
Micro X-Ray fluorescence  
Confocal system  
Scanning Electron Microscopy

## ABSTRACT

This work shows the first analytical results obtained by X-Ray Fluorescence (XRF) (conventional and 3D) and Scanning Electron Microscopy with Energy Dispersive System (SEM-EDS) on original Portuguese ceramic pieces produced between the 16th and 18th centuries in Coimbra and Lisbon. Experts distinguished these productions based only on the color, texture and brightness, which originates mislabeling in some cases. Thanks to lateral and spatial resolution in the micrometer regime, the results obtained with  $\mu$ -XRF were essential in determining the glaze and pigment thicknesses by monitoring the profile of the most abundant element in each "layer". Furthermore, the dissemination of these elements throughout the glaze is different depending on the glaze composition, firing temperature and on the pigment itself. Hence, the crucial point of this investigation was to analyze and understand the interfaces color/glaze and glaze/ceramic support. Together with the XRF results, images captured by SEM and the corresponding semi-quantitative EDS data revealed different manufacturing processes used by the two production centers. Different capture modes were suitable to distinguish different crystals from the minerals that confer the color of the pigments used and to enhance the fact that some of them are very well spread through the glassy matrix, sustaining the theory of an evolved and careful procedure in the manufacturing process of the glaze.

© 2011 Elsevier B.V. All rights reserved.

## 1. Introduction

Glazed ceramics are very challenging objects of study. By naked eye inspection, there are several characteristics about a certain piece, which one can extract immediately: the brightness of a glaze and the color palette, among others. Although these characteristics give hints about how the piece was produced, they are not sufficient to characterize it.

To extend knowledge about the manufacturing procedures involved in the glazing and surface decoration is the main goal of this investigation. The items, which served as object of study, were originally produced between the 16th and 18th centuries in two main centers in Portugal: Coimbra and Lisbon.

A glazed ceramic object can be divided in three main parts: (1) the ceramic support, (2) the glaze and (3) the surface decoration (Fig. 1). The areas marked in red correspond to the interface color/glaze and glaze/ceramic support. Interface is defined here as an area where a mixture of two distinctive "layers" can be found. The surface

decoration can be more or less dispersed within the glassy matrix, depending on the kind of glaze (in terms of chemical composition) and/or the firing temperature used. Information about the historical background of the pieces as well as the chemical composition that characterizes each part, including the pigments composition, is available in previously published works [1,2].

According to the limited documentation about the possible manufacturing procedures involved in Portuguese glazed ceramics based on historical facts [3], several opinions have been developed about the raw materials, the glaze and color application as well as the firing stages and temperatures used at different centers of production, such as Coimbra and Lisbon.

It is known that Coimbra was a less wealthy center of production, when compared to Lisbon and, hence, the expensive raw materials were spared as much as possible. Therefore, one would find a broader range of elements used to confer the intended color. One example is given by the blue pigments, in which the source of cobalt (Smalt: a ground blue containing Co) is the main and expensive element. In the samples from Coimbra, additional elements can be found, such as Mn to spare the cobalt source. For that reason, in the samples from Coimbra the blue color has a kind of old-"pinkish" tone mixed to it. Further assumptions are related with the history of the country itself,

\* Corresponding author. Tel.: +351 21 7904776, +351 21 7500941; fax: +351 21 7954288.

E-mail address: [luisa@cii.fc.ul.pt](mailto:luisa@cii.fc.ul.pt) (M.L. Carvalho).

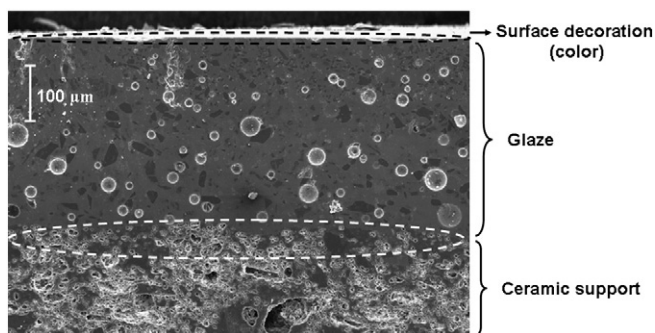


Fig. 1. Model of a polychrome glazed ceramic. The areas marked in red correspond to the interface color/glaze and glaze/ceramic support.

particularly that Lisbon had more influence from the Muslim occupation than Coimbra, so the recipes may have kept rather different from each other [4].

There are several possibilities to obtain the final piece. In all cases, a firing process for the ceramic support took place and then, it may have happened just one firing process for the base glaze together with the decorative motives or a separate firing process for the decorative motives, after the firing for the base glaze. [5]. So, the piece may have been submitted to either two or three firing processes.

Regarding this study, we are interested in the interfaces: surface decoration/glaze and glaze/ceramic support, which helps us to distinguish differences in the manufacturing methods, as well as the chosen raw materials for the glaze formation in both production centers. Hence, a detailed study of the elemental profiles throughout the interface areas was carried out, by using laboratory X-Ray Fluorescence Spectroscopy techniques (conventional XRF and 3D Micro-XRF). To complement such qualitative data, elemental content of the surface decoration as well as the glaze beneath/within were also obtained by means of Scanning Electron Microscopy with an Energy Dispersive Spectroscopy system (SEM-EDS).

## 2. Experimental methodology

A set of fragments from pieces originally produced in Coimbra (11 samples) and in Lisbon (9 samples) (Fig. 2) was collected for investigation. The art historians made the assignation to Coimbra and Lisbon on a stylistic basis. All of the fragments were cut with a diamond saw and polished in order to obtain flat cross sections for SEM and  $\mu$ -XRF analyses.

The experimental approach was the following:

- i) *Conventional XRF* measurements were carried out with a 45° tube-detector geometry setup enclosed in a chamber submitted to a 10 mbar vacuum, belonging to the Atomic Physics Centre of the University of Lisbon, and fully described in Refs. [1,2]. The X-ray tube is from Oxford Instruments (California, USA); the polycapillary optics are from XOS (New York, USA); and the detector is a Vortex-60EX from SII NanoTechnology USA Inc. (California, USA). The measurements were performed using a collimator, which allows an excitation area of about 1.2 mm<sup>2</sup>, when the sample is placed at a 1.5 mm distance from the Kapton window, through which the excitation and fluorescence beams pass. The operating conditions were 50 kV and 1 mA, in order to excite the K-lines of such elements as Sn and Sb. Each spectrum was acquired for 300 s. Spectra were collected using a multichannel (4096 channels) and recorded both in binary mode and in ASCII data mode in order to perform their evaluation using the PyMCA software code [6]. With this spectrometer, measurements were performed

perpendicular to the surface of each sample on each color and on the glaze. By using the collimator, a large area of analysis is obtained, which is more representative of the whole sample. Decoration and glaze areas are in all cases larger than 1.2 mm<sup>2</sup>.

The purpose of this investigation is to have intensity ratios for specific elements, which will provide us fingerprints of both production centers.

- ii) *3D Micro-XRF* measurements were carried out with a tabletop setup from the Institute for Optics and Atomic Physics at the Technical University of Berlin. This system is a common development with ifG (Institute for Scientific Instruments). The X-ray tube is from Rtw Röntgen-Technik (Neunhagen, Germany); the polycapillary optics are from IfG (Berlin, Germany); and the detector is from Bruker nano (Berlin, Germany). The leading feature of this system is the ability to perform depth-resolving analysis as is fully described in Ref. [7]. Due to the high amount of lead in the samples, strong absorption effects took place. This leads to an information depth of several tens of micrometers, only, which prevents further depth resolution. Nevertheless, we took advantage of another feature of the confocal geometry, which is probing site selection. The probing volume created in the confocal geometry allows selective analysis in a certain volume in the micrometer regime, which reduces the amount of detected scattered radiation considerably. Therefore, scans just on the surface of the polished cross section of each sample were performed, in steps of 5  $\mu$ m (each during 60 s) through a length that varied according to the thickness of the relevant part of the sample. The operating conditions were the maximum for this system: 50 kV and 600  $\mu$ A. The Full Width at Half Maximum (FWHM) of the probing volume obtained for Cu-K $\alpha$  (8.04 keV) was approximately 42  $\mu$ m.

In addition to the measurements in confocal geometry (3D), Micro-XRF measurements (2D – with lenses in the excitation path only) were carried out at the same cross sections. Comparing scans along the same cross section obtained by the two methods, the confocal geometry enables a better resolving of the elemental profiles along the cross sections, as is shown in Fig. 3. In this figure we see two scans performed along the cross section of the same sample (C29) capturing the pigment (purple), glaze and ceramic support, in 3D mode (a) and in 2D mode (b). In 3D mode, we can clearly see that there is an interface layer between the pigment and the base glaze, while with the 2D mode the transition is not so clear. This may lead to wrong conclusions about the pigment application on the glaze (see Results and discussion section).

With these results, we are able to monitor the profiles of certain elements through the interface color/glaze and glaze/ceramic support. It enables conclusions about the diffusion ability of elements, which give color, and about the fusibility of the glaze for these elements. These results also contribute to revelations on firing temperatures used in both manufacturing centers.

- iii) *Examinations by SEM* were carried out with a Hitachi S4100 system from Bruker (Tokyo, Japan), equipped with Quantax 400 EDS system of Bruker AXS (XFlash Silicon Drift Detector) (Berlin, Germany). A 15 kV acceleration voltage and a current intensity of 32  $\mu$ A were applied. The chemical information by EDS was taken from an area of 300  $\times$  400  $\mu$ m<sup>2</sup> selected regarding its homogeneity and lack of voids, with spectrum acquisition times at a minimum of 60 s. The semi-quantitative results were based on a peak-to-background ZAF evaluation method (P/B-ZAF), being ZAF a matrix correction, mainly based on analytical expressions for atomic number (Z), X-ray yield, self-absorption (A) and secondary fluorescence enhancement

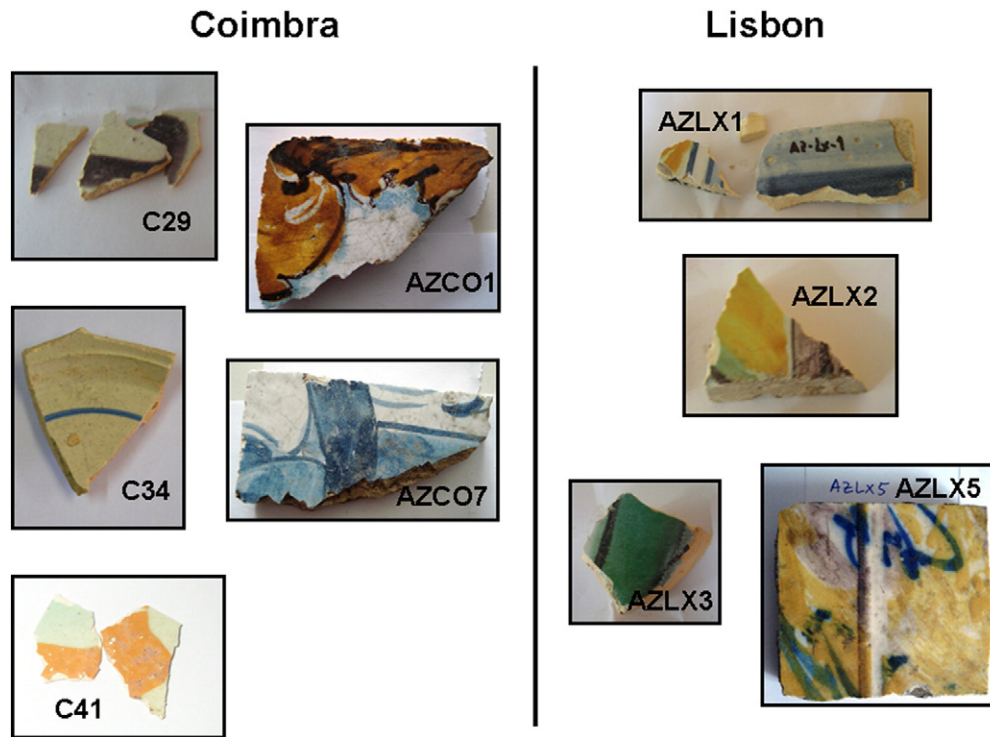


Fig. 2. Some analyzed samples: fragments from Coimbra and Lisbon.

(F), provided by the Esprit software from Bruker AXS microanalysis. With these measurements, we obtain the distribution and morphology of certain compounds, which

are crucial in the manufacturing process determination. In addition, the composition of color layer and glaze was obtained with the *EDS* coupling unit.

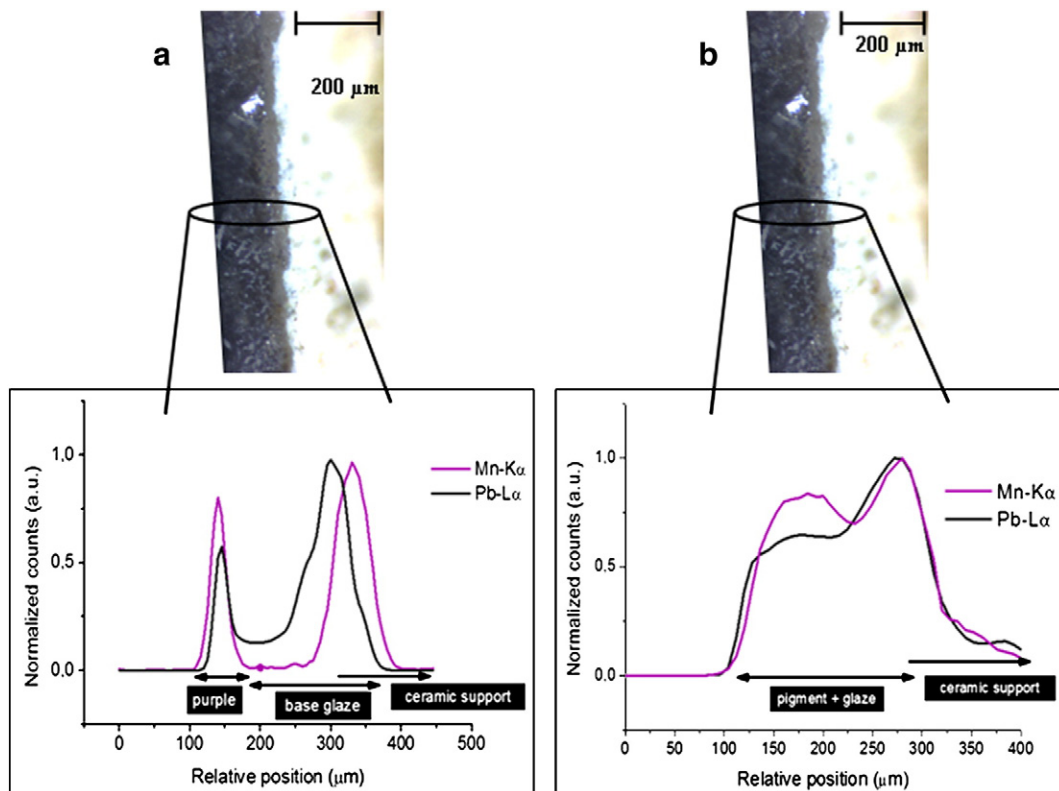


Fig. 3. Comparison between 3D (a) and 2D (b) cross-section scans of the same sample (C29). In 3D mode, we can an interface layer between the pigment and the base glaze (characterized by a drop on both line scans) while with the 2D mode this drop is not so clear.

### 3. Results and discussion

The results we present, are representative of the whole set of samples analyzed from both production centers. The measurements performed with all methods were carried out in all samples, and repeated in at least three spots.

#### 3.1. The (white) glaze

In a common way, the glazes from both production centers belong to a class of “tin opacified lead glazes”, in which the main components are  $\text{SiO}_2$ ,  $\text{PbO}$  and  $\text{SnO}_2$ . What differentiates the productions is the ratio between the amounts of these and other important oxides, such as  $\text{Na}_2\text{O}$ ,  $\text{K}_2\text{O}$  and  $\text{CaO}$ .

With SEM-EDS, the uniform distribution of cassiterite crystals ( $\text{SnO}_2$ ) throughout the glazes was evident. Tin and lead were usually burnt together and then added to the glaze. This way, tin oxide was first dissolved in a silica and lead vitreous matrix and during the firing process of the glaze, at a temperature of 650 °C, it recrystallized in the cassiterite structure ( $\text{SnO}_2$ ). Once in this form,  $\text{SnO}_2$  becomes insoluble in the glaze [8].

As an example, Fig. 4 displays an image taken perpendicular to the surface of the glaze (not colored) from the pieces (a) C41 from Coimbra and (b) AZLX1 from Lisbon. One can see how well distributed the tin oxide crystals are within the glassy matrix. Their length varies between 0.5 and 0.8  $\mu\text{m}$  for the former (a) and between 1 and 2  $\mu\text{m}$  for the latter (b). Furthermore, the EDS results (from SEM-EDS) in Table 1 reveal some differences between the two production centers worth to discuss. The glazes produced in Coimbra reveal relatively high amounts of  $\text{K}_2\text{O}$  (8.1–9.3 wt.%) and  $\text{CaO}$  (3.1–3.2 wt.%) when compared with the ones from Lisbon ( $\text{K}_2\text{O}$ : 4.3–5.8 wt.% and  $\text{CaO}$ : 0.8–1.1 wt.%). This in addition to the amounts of  $\text{Na}_2\text{O}$  (0.8–1 wt.%) and  $\text{PbO}$  (40.1–40.5 wt.%) in Coimbra compared to the ones in Lisbon ( $\text{Na}_2\text{O}$ : 3.5–4.2 wt.%, and  $\text{PbO}$ : 45.5–45.9 wt.%), leads us to the preliminary conclusion that the glazes of Lisbon have more fusibility

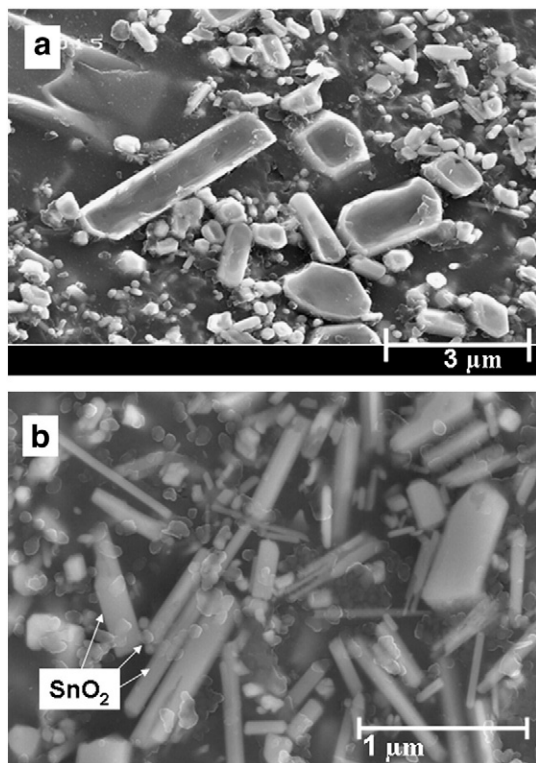


Fig. 4. SEM image perpendicular to the glaze surface of a sample from Coimbra (a: C41) and a sample from Lisbon (b: AZLX1).

than the ones from Coimbra. The higher amounts of  $\text{Na}_2\text{O}$  and  $\text{PbO}$  indicate that the melting point of the glaze is lower than the ones where higher amounts of  $\text{K}_2\text{O}$  and  $\text{CaO}$  are present. It is already known that Na and Pb compounds, acting as dominant fluxes in the glaze, lower the fusion temperature [9].

Other significant results are the ones obtained with the cross section lateral scans performed with the 3D Micro-XRF setup. Fig. 5a and b exhibits the profiles for one glaze from Coimbra (a: C41) and one from Lisbon (b: AZLX1), respectively, for the elements Pb, Sn and Ca. Scans performed in all the pieces from Coimbra showed that the glaze thicknesses vary between 150 and 350  $\mu\text{m}$ , whereas the ones from Lisbon vary between 300 and 400  $\mu\text{m}$ , by monitoring the energy line of the element, which mainly characterizes the glaze: Pb-L $\alpha$  (10.54 keV). These scans also support the results obtained by SEM-EDS: tin (Sn) is well distributed within the glassy matrix and the glazes from Coimbra reveal a higher concentration of Ca than the Lisbon ones, when compared to the other elements in the glaze of the same sample. Together with the images obtained by the microscope inside the confocal system, one can easily observe a very well defined interface glaze/ceramic support, being approximately 50  $\mu\text{m}$  for the Coimbra sample and smaller than 30  $\mu\text{m}$  for the Lisbon one.

#### 3.2. Colors and pigments

Concerning polychrome glazed ceramics, some facts must be taken into account. The colors employed on the pieces were usually obtained by metallic oxides, which could have been used in a “pure” state or in a mixture called *frit*, which is a pre-melting of the pigment together with fluxes, such as Pb, Na, and sometimes even Sn (to make it more opaque). After cooling down, this mixture (*frit*) was grinded until a powder was obtained and then applied over the “base glaze”. The brilliance or opacity and the migration ability of the elements, which grant the color, are some factors that help assign the way the pigment was applied onto/within the glaze [10].

##### 3.2.1. Blue

In general, blue is the most common color in glazed ceramics. The decorative motives as well as the tones used, make the difference. Measurements performed with the conventional XRF setup gave us the possibility analyzing bigger areas (due to the collimator) of the blue color from both production centers. These analyses were performed on the surface and, in order to identify the spectra from the blue color, spectra from the glaze next to these areas were subtracted. The typical elements detected were Fe, Ni, Co and As (Smalt) with the presence of Mn and Ba in certain cases mainly from Coimbra, as it was already discussed [2].

In Fig. 6 we can observe: a) comparison between spectra obtained on the blue color and the respective glaze of a sample from Coimbra (C34); b) comparison between spectra obtained on the blue color and on the respective glaze of a sample from Lisbon (AZLX1); c) comparison between the spectra obtained for the blue colors in Coimbra (C34) and Lisbon (AZLX1) and d) intensity ratios for the elements associated to the blue pigment (Smalt). From Fig. 6a and b, we can see the elements that are associated to the blue color: Mn–Fe–Co–Ni–As are free from interference coming from the glaze, except Fe, which is also present in the glaze. Fig. 6c shows that the samples from Coimbra have higher content of Mn and Ba and less of Co than the ones from Lisbon, which supports the assumption that Coimbra was a less wealthy center compared to Lisbon. However, as we can see from Fig. 6d not only the ratios Mn/Co are higher for Coimbra, but also the ratios Fe/Co, due to less pronounced values for Co in these samples.

In addition to these results, we present also cross section scans by 3D  $\mu$ -XRF together with pictures taken with the microscope. Fig. 7a and b shows an example of the different profiles obtained for a fragment from Coimbra (a: C34) and one from Lisbon (b: AZLX1). Due to the images provided by the microscope we clearly see two main

**Table 1**

Composition of the glazes from Coimbra and Lisbon (in% wt.). Analysis perpendicular to the surface obtained with SEM-EDS. The uncertainty varies between 0.1 and 2.8% (for the lowest and highest values, respectively). The uncertainties represent a Relative Error (in %) reported automatically by the software. The bold numbers give important information about the glaze properties. The glazes, which have higher amounts of Na<sub>2</sub>O and PbO are more fusible than the ones, which have higher amounts of K<sub>2</sub>O and CaO.

Local	Na <sub>2</sub> O	MgO	Al <sub>2</sub> O <sub>3</sub>	SiO <sub>2</sub>	K <sub>2</sub> O	CaO	Fe <sub>2</sub> O <sub>3</sub>	PbO	SnO <sub>2</sub>
Coimbra (N = 11)	<b>0.8–1</b>	0.2–0.3	2.8–3	31.3–31.9	<b>8.1–9.3</b>	<b>3.1–3.2</b>	3.6–3.7	<b>40.1–40.5</b>	10.4–10.8
Lisbon (N = 9)	<b>3.5–4.2</b>	0.6–0.8	3.1–3.7	28.9–29.4	<b>4.3–5.8</b>	<b>0.8–1.1</b>	2.1–2.5	<b>45.5–45.9</b>	9.8–10.3

(~150 μm) than the one from Lisbon (~400 μm); 2) by monitoring the Co K-line, the pigment distribution throughout the glaze is less in the Coimbra samples (~50 μm) than the ones from Lisbon (~100 μm). On one hand, either there is no interface between color and glaze in the sample from Coimbra or is less than the resolution allowed for the 3D Micro-XRF. This may indicate that glaze and pigment were applied together, as it is also proved by the Co–Kβ and Pb–Lα profiles (Fig. 7a). On the other hand, there is an interface color/glaze in the sample from Lisbon (Fig. 7b). However, the pigment seems to disseminate quite well through the glaze, which is also proved by the profiles obtained for Co–Kβ and Pb–Lα. In both cases the fact that Sn appears to be more abundant in the lower part of the glaze is noticeable (Fig. 7). In the case of the sample from Coimbra, it is evident that Sn is the dominant element on the lower part of the glaze (Fig. 7a). This is in agreement with the assumption that tin crystals are very dense and tend to deposit on the lower part of the glaze [8].

### 3.2.2. Purple

Analyses performed with conventional XRF showed similar chemical composition in all purple colors from both production centers (Fig. 8). The dominant element to give the purple color is Mn, and the presence of Ba in both spectra indicates that the mineral *Psilomelane* [(Ba,H<sub>2</sub>O)<sub>2</sub>Mn<sub>5</sub>O<sub>10</sub>] was used as raw material to obtain Mn [11].

Further analyses performed by SEM-EDS perpendicular to the purple surface revealed that the crystals in the purple layer could be

from Coimbra (Fig. 9a: C29) are more noticeable in comparison to the ones from Lisbon (Fig. 9b: AZLX2). The crystals formed on the sample from Lisbon appear to be more dispersed into the glaze matrix. The EDS results from these two samples were obtained by micro-spot analyses and are displayed in Table 2.

Furthermore, interesting results were also obtained with 3D μ-XRF. The profiles in Fig. 10 correspond to cross-section scans made on the same samples. In Fig. 10a, the Mn profile is similar to the one of Pb, where in the left side of the scan Mn corresponds to the purple color and in the right side it corresponds to the ceramic support. It is also evident that there is a drop in the Mn and Pb depth profiles between pigment and base glaze. This was a common result in all analyzed samples from Coimbra and it leads to the conclusion that the pigment was applied as a *frit*. The interface frit/“base glaze” clearly remained after the firing process and the two “layers” (frit and base glaze) were practically kept individualized from each other, indicating that the glaze has low fusibility (due to the presence of Ca also). When we compare these profiles with the ones from Lisbon (Fig. 10b), we see that the pigment is well dispersed into the glaze matrix. Furthermore, there is no accentuated drop in the Pb profile, revealing that the glaze is more fusible than the one in Coimbra, as it was already explained in Section 3.1: The (white) glaze. This allows a better dissemination of the frit in which the pigment was applied through the base glaze. Although we cannot compare the profiles of Ca obtained in both centers directly, when we evaluate the profiles Pb and Ca in each production center, the base glaze from Coimbra (Fig. 10a) has the

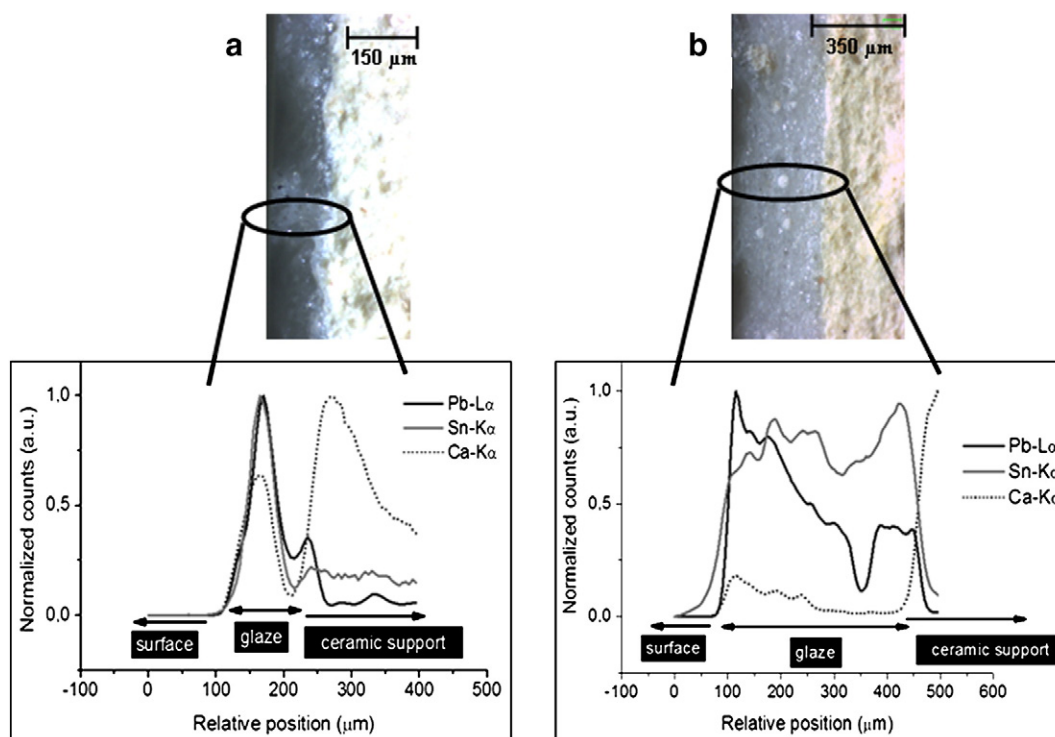


Fig. 5. 3D μ-XRF cross section scans performed on glaze + ceramic support on a sample from a) Coimbra (C41) and b) Lisbon (AZLX1).

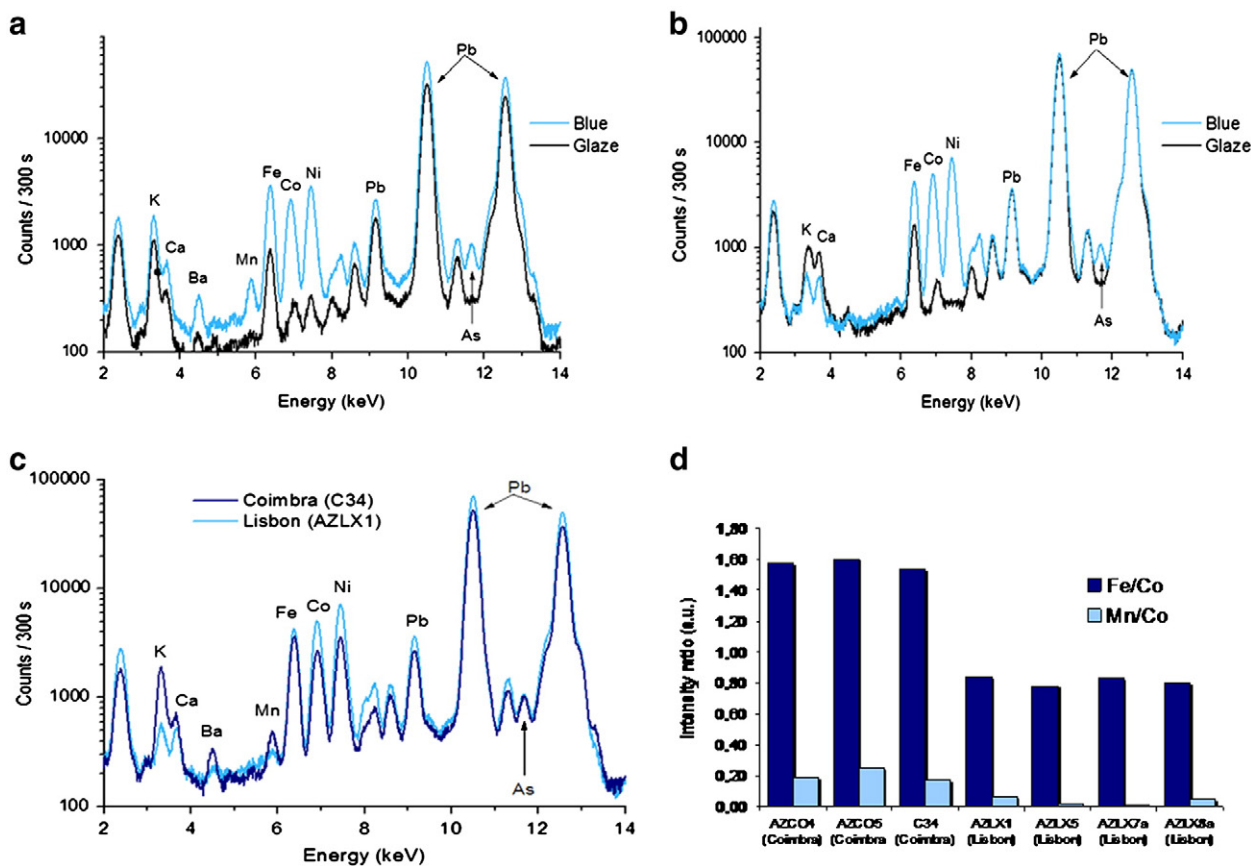


Fig. 6. a) Comparison between spectra on blue and glaze of a sample from Coimbra (C34); b) comparison between spectra on blue and glaze of a sample from Lisbon (AZLX1); c) comparison between spectra on the blue of the two samples; The samples from Coimbra have higher content of Mn and Ba and less of Co than the ones from Lisbon, which supports the assumption that Coimbra was a less wealthy center compared to Lisbon. d) intensity ratio of Fe and Mn with respect to Co, obtained on the blue in the set of samples from Coimbra and Lisbon.

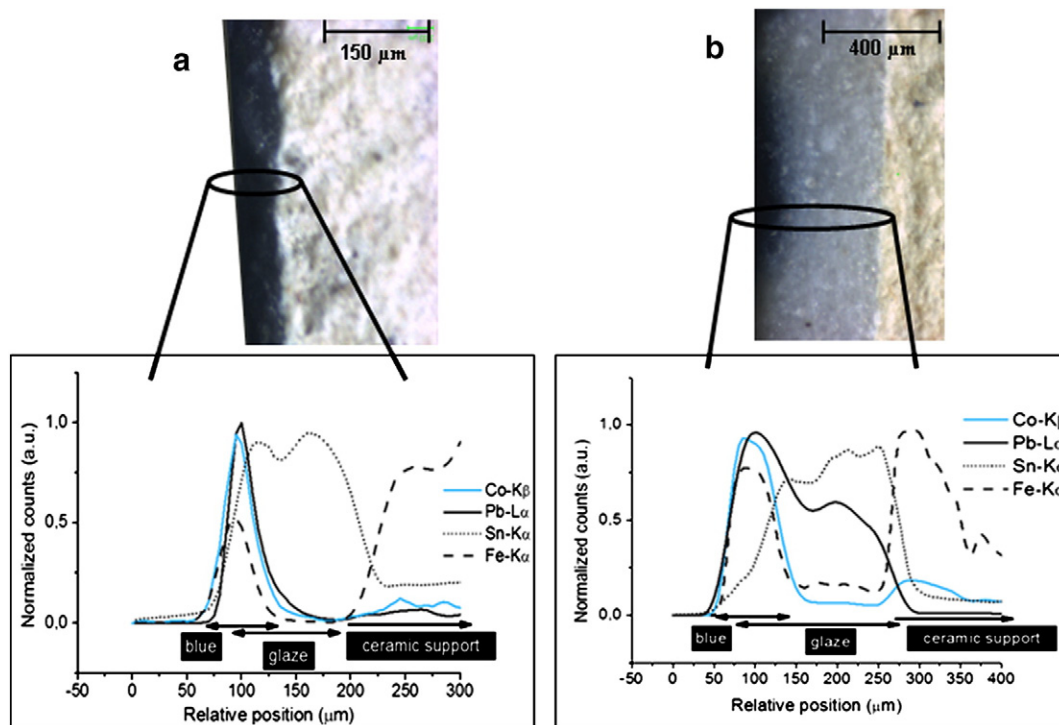


Fig. 7. 3D  $\mu$ -XRF cross section scans performed on blue + glaze + ceramic support of a sample from a) Coimbra (C34) and b) Lisbon (AZLX1).



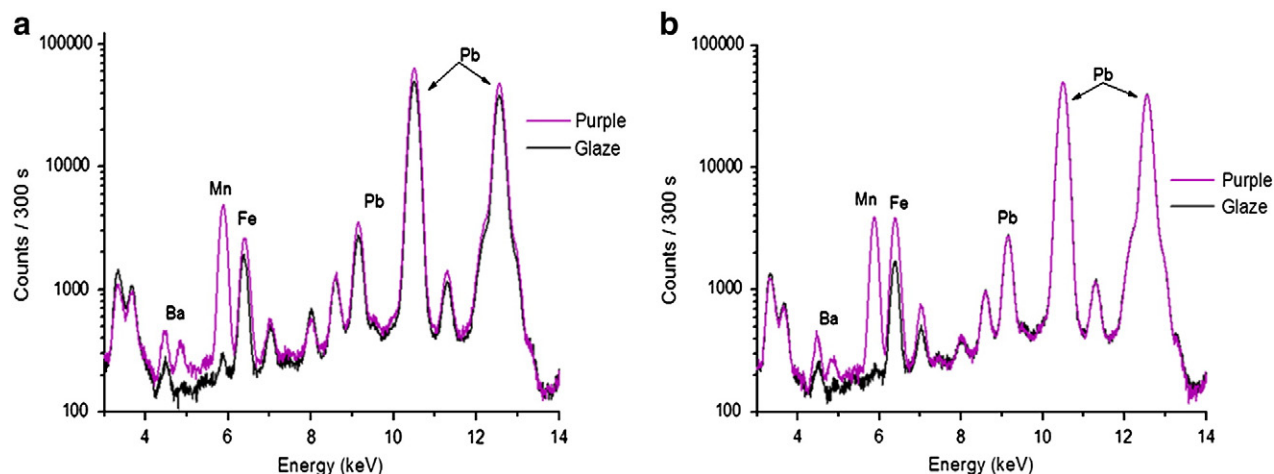


Fig. 8. Comparison of spectra obtained with conventional XRF for a) Coimbra (C29) and b) Lisbon (AZLX2) samples on the purple color.

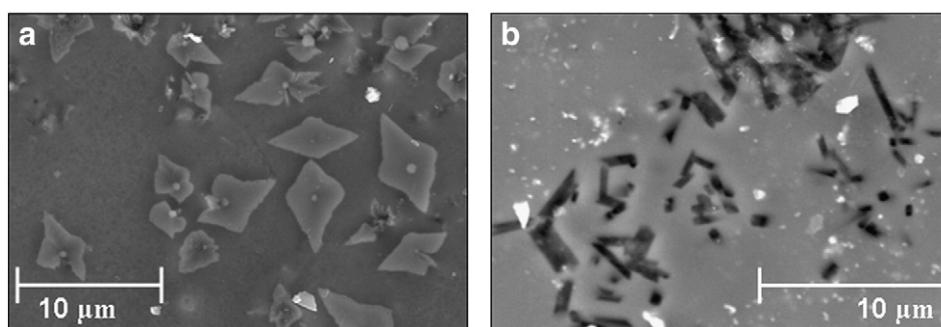


Fig. 9. SEM images perpendicular to the purple surface of a sample from Coimbra (a: C29) and a sample from Lisbon (b: AZLX2).

same intensity in Pb and Ca. Conversely, the base glaze from Lisbon (Fig. 10b) has much less Ca in comparison to the Pb signal. This is in agreement with the higher fusibility of the glazes from Lisbon.

### 3.2.3. Yellow/orange

From all the colors used in glazed ceramics, the yellow or orange comes out to be the most interesting one. By naked eye observation, we noticed that in Coimbra, this color tends to be orange and in Lisbon yellow.

The first results were obtained by conventional XRF, where different samples were analyzed from both centers and some differences are already noticed. Fig. 11 shows a spectrum of glaze and yellow from Coimbra (a: C41) and from Lisbon (b: AZLX1). From the spectra, we see that this pigment comes from the same compound, which is a lead–antimony ( $\text{Pb}_2\text{Sb}_2\text{O}_7$ ) composite called *Naples yellow* [12]. In Fig. 11c, we can see that the samples from Coimbra appear to have higher Fe and Mn count rate than the ones from Lisbon. This may be a justification for the orange tone exhibited by the samples from Coimbra. Furthermore, the ones from Lisbon revealed higher count rates in Sn and lower in Sb, which possibly indicates that  $\text{Sn}^{4+}$ , may have replaced the ion  $\text{Sb}^{3+}$  in the lead–antimony compound, provoking changes in the molecular structure [13].

Other relevant results are the ones we could obtain with SEM-EDS. Fig. 12a and b shows images taken perpendicular to the surface of the yellow color in one sample from Coimbra (a: C41) and one sample from Lisbon (b: AZLX2). Fig. 12c and d displays images taken perpendicular to the cross section of the samples in order to evaluate the interfaces in Coimbra (c) and in Lisbon (d).

The crystals identified in both images (a and b) have a triangular and hexagonal shape, which is typical for the Naples yellow pigment [12,14]. Additionally, the shape of the crystals is also a hint to estimate the firing temperature. According to Ref. [12], from 950 °C up some crystals start to form agglomerates, but in an irregular way (as it might be recognized in Fig. 12a, in Coimbra), and only from 1100 °C the nice hexagonal phase starts to appear (as it is shown on Fig. 12b, in Lisbon). In sample C41 (from Coimbra) (Fig. 11a) the crystals are somehow irregular and still very small (<1 μm) in comparison to the crystals in sample AZLX2 (Lisbon) (Fig. 12b), where they are very well shaped, having already a hexagonal shape.

Furthermore, the semi-quantitative results obtained from EDS (Table 3) on these samples lead to the assumption that different firing temperatures were used. The values of  $\text{Sb}_2\text{O}_5$  and  $\text{SiO}_2$  obtained for Coimbra and Lisbon show great discrepancy. This is because in Coimbra, the values represent the yellow chromophore phases within

Table 2

Comparison between the purple chromophore phases from Coimbra (C29) and from Lisbon (AZLX2). Analysis perpendicular to the surface obtained with SEM-EDS. The purple crystals (MnO) formed on the sample from Lisboa are more dispersed into the glaze matrix. This suggests the higher amount of MnO detected with the EDS. The uncertainties represent a Relative Error (in %) reported automatically by the software.

Sample	$\text{Na}_2\text{O}$	$\text{MgO}$	$\text{Al}_2\text{O}_3$	$\text{SiO}_2$	$\text{K}_2\text{O}$	$\text{CaO}$	$\text{MnO}$	$\text{Fe}_2\text{O}_3$	$\text{PbO}$
C29 Coimbra	$1.6 \pm 0.1$	$0.6 \pm 0.1$	$3.3 \pm 0.2$	$28.4 \pm 1.0$	$5.8 \pm 0.2$	$2.9 \pm 0.1$	<b><math>10.8 \pm 0.3</math></b>	$4.0 \pm 0.1$	$42.6 \pm 2.6$
AZLX2 Lisbon	$0.7 \pm 0.1$	$0.9 \pm 0.1$	$3.2 \pm 0.1$	$36.3 \pm 1.1$	$5.4 \pm 0.2$	$10.4 \pm 0.3$	<b><math>24.7 \pm 0.6</math></b>	$1.2 \pm 0.1$	$18.3 \pm 1.0$

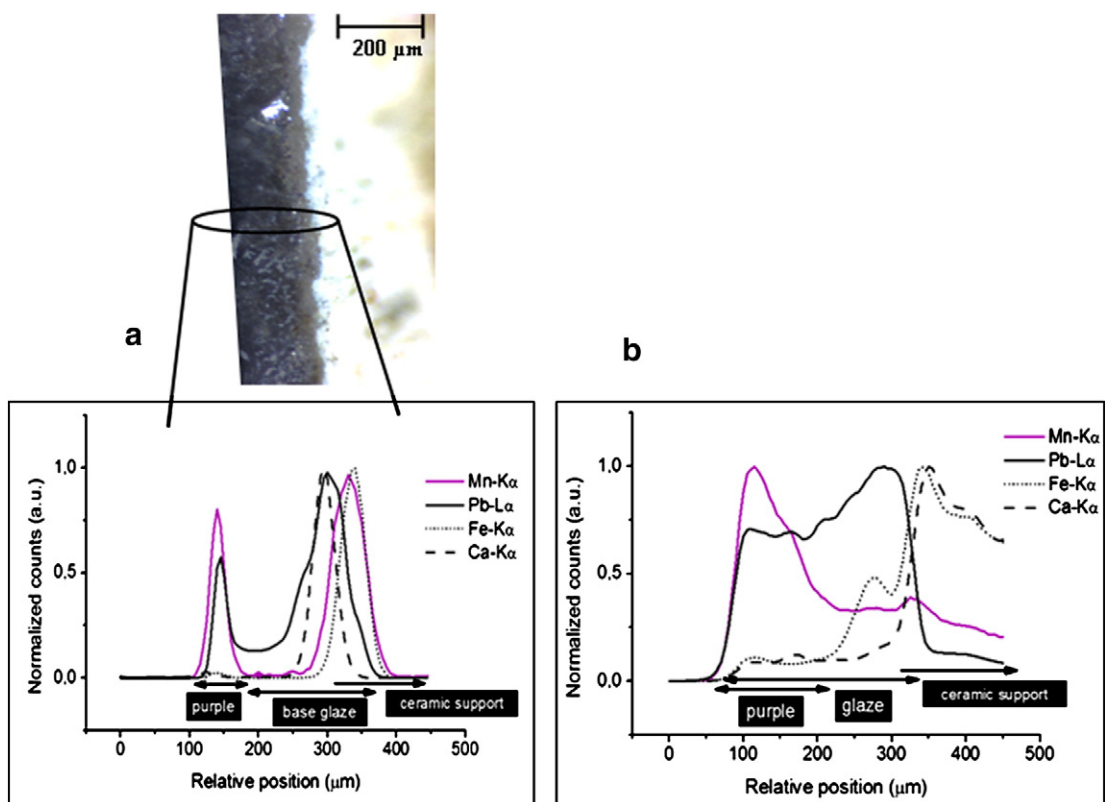


Fig. 10. 3D  $\mu$ -XRF cross section scans performed on purple + glaze + ceramic support on a sample from a) Coimbra (C29) and b) Lisbon (AZLX2).

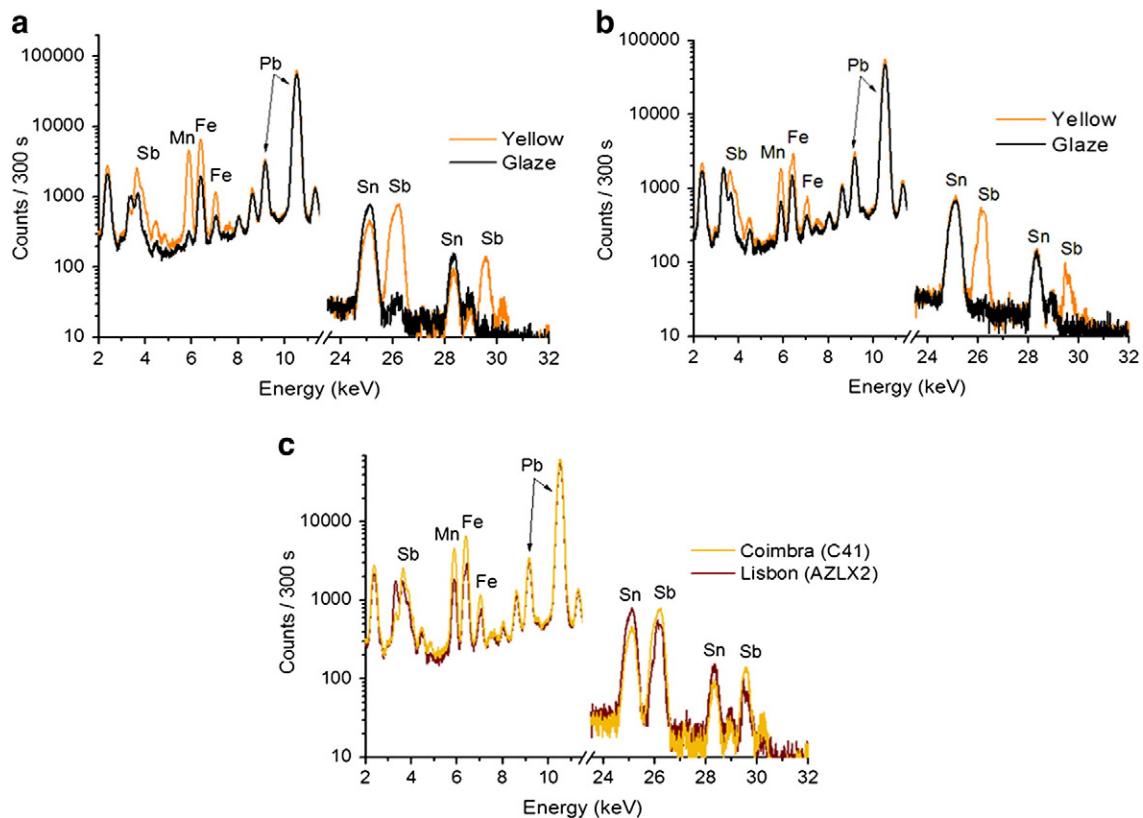
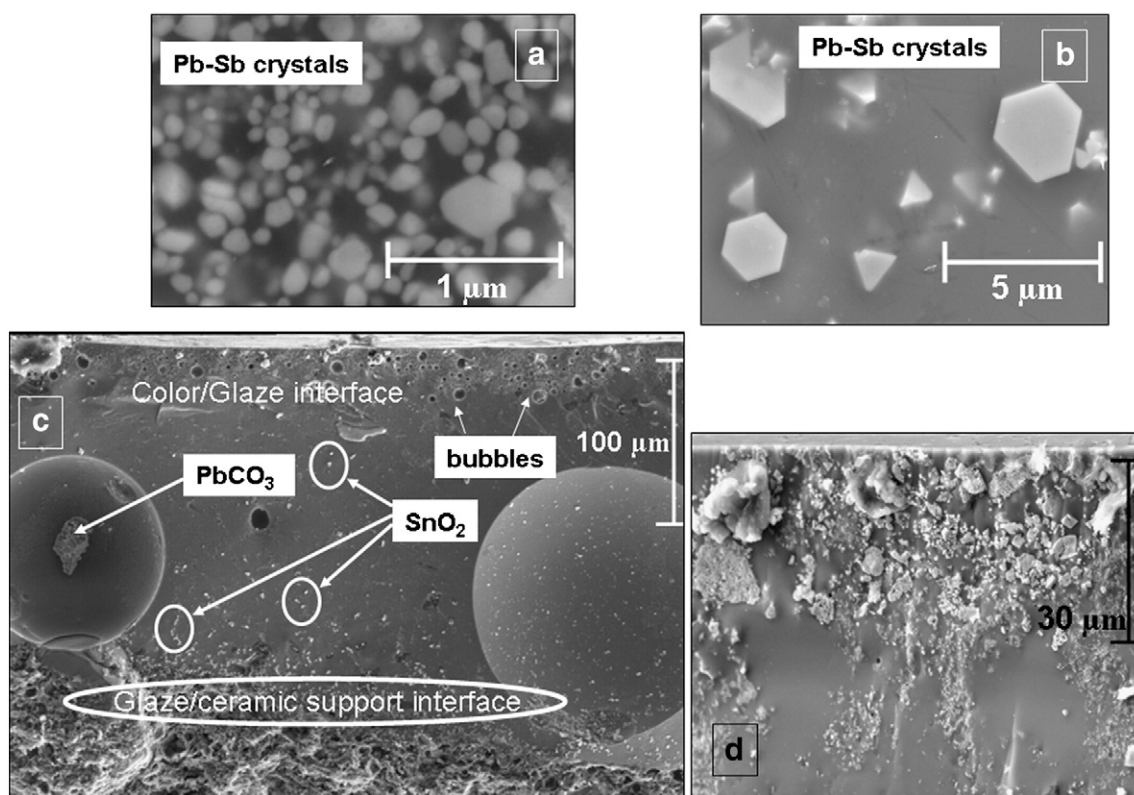


Fig. 11. a) Comparison between spectra on yellow and glaze of a sample from Coimbra (C41); b) comparison between spectra on yellow and glaze of a sample from Lisbon (AZLX2); c) comparison between spectra on the yellow in the two samples.



**Fig. 12.** SEM images perpendicular to the yellow surface of a sample from Coimbra (a: C41) and a sample from Lisbon (b: AZLX2). SEM images perpendicular to the cross section of sample C41 (c) and sample AZLX2 (d).

the glassy matrix (small crystals) and in Lisbon, the values represent the yellow chromophore phase (just onto the crystal: hexagonal). These semi-quantitative data are an indication that in fact some differences between the chromophore phases exist when we compare the two production centers.

Now, looking to Fig. 12c and d there are also some considerations. They both represent cross section images from sample C41 (c) and AZLX2 (d). The one from Coimbra (c) shows clearly an interface between color/glaze and glaze/ceramic support. These are characterized by a certain amount of bubbles, some of them contain *cerussite* (lead carbonate: PbCO<sub>3</sub>) due to weathering. The picture from the Lisbon piece (Fig. 12d) is a magnification of the possible interface color/glaze and in this case, it is not as evident as in the case of the sample from Coimbra. These are all indicative of different firing temperatures.

In complement to the results, we present also, the ones obtained with 3D  $\mu$ -XRF relative to the cross section scans. Fig. 13a represents a scan of the sample C41 (Coimbra) and Fig. 13b the sample AZLX2 (Lisbon). Once again, the profiles from the sample from Coimbra reveal a drop in the Pb-L $\alpha$  profile, which indicates non-homogeneity between base glaze and the frit in which the pigment was applied. The profiles of

However, the fact that the profile of Sb is more isolated from Pb suggests once again that the glaze in which the pigment is applied is more fusible than the one from Coimbra. In contrast, the Pb tends to go down the glaze due to its higher density. The Sn profiles indicate once again that the SnO<sub>2</sub> crystals tend to deposit on the lower part of the glaze.

#### 4. Conclusions

It is clear that Portuguese polychrome glazed ceramics have an intrinsic value by the way they were produced: the broad polychromic pallet, the obtained tones or even the careful manufacturing procedure in order to achieve such slight differences.

Comparing the data obtained for the two main important production centers, Lisbon and Coimbra, new results about the raw materials used as well as the possible manufacturing techniques have been achieved. Due to the lack of archaeometric information on Portuguese ceramic production, we used the knowledge from previous works performed on Spanish and Italian glazed ceramics [4,8,10,12–14], since we are dealing with similar types of samples. Hence, this work presents the first archaeometric results about Portuguese glazed ceramics produced in Coimbra and Lisbon as a comparative study.

**Table 3**

Comparison between the yellow chromophore phases from Coimbra (C41) and from Lisbon (AZLX2). Analysis perpendicular to the surface obtained with SEM-EDS. The EDS analysis on the sample from Lisbon were performed onto a single crystal which confers the yellow color. This justifies the higher amount of Sb<sub>2</sub>O<sub>5</sub> and a lower amount of SiO<sub>2</sub> when compared with the sample from Coimbra. The uncertainties represent a Relative Error (in %) reported automatically by the software.

Sample	Na <sub>2</sub> O	Al <sub>2</sub> O <sub>3</sub>	SiO <sub>2</sub>	K <sub>2</sub> O	Fe <sub>2</sub> O <sub>3</sub>	PbO	Sb <sub>2</sub> O <sub>5</sub>
C41 Coimbra	0.8 ± 0.1	1.9 ± 0.1	<b>20.8 ± 0.1</b>	5.1 ± 0.2	6.7 ± 0.4	47.9 ± 1.6	<b>16.7 ± 1.4</b>
AZLX2 Lisbon	2.5 ± 0.2	1.6 ± 0.1	<b>4.1 ± 0.2</b>	–	3.7 ± 0.2	47.5 ± 2.8	<b>40.1 ± 2.3</b>

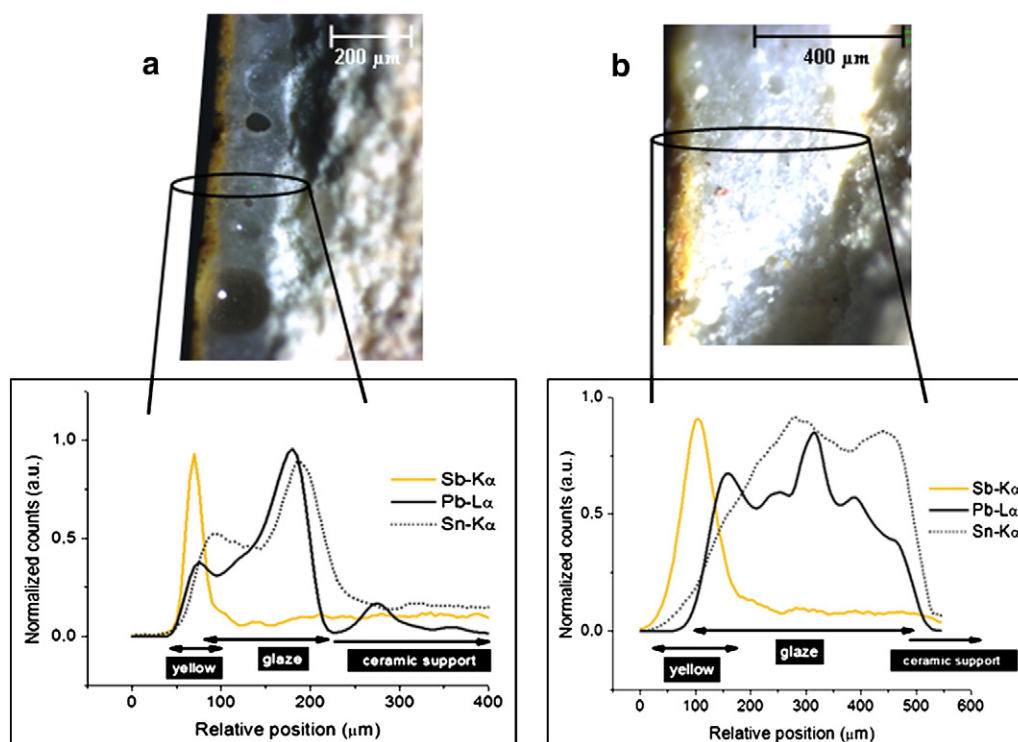


Fig. 13. 3D  $\mu$ -XRF cross section scans performed on yellow + glaze + ceramic support on a sample from a) Coimbra (C41) and b) Lisbon (AZLX2).

The compositional and microtextural data obtained for both groups of samples revealed differences in the properties of the glazes: the ones from Coimbra are less fusible than the ones from Lisbon. This was noticeable by all the results obtained with the different techniques. Glazes with a higher content of Na and Pb have a lower melting point than the ones with a higher content of K and Ca. This was also evident when the pigments were applied to the glaze in the form of *frit*. For this manufacture procedure, a more pronounced interface between pigment and glaze was found in the SEM images. However, when the *frit* and the base glaze onto which the pigment was applied had higher fusibility and/or if the firing temperature was higher than in other cases, the interfaces were not so distinguishable. This could be detected by the 3D Micro-XRF scans. In all images correspondent to the samples from Coimbra the elements are less disseminated throughout the glaze than the ones from Lisbon. This means that the element that gives the color (Co in the case of blue, Mn in the case of purple and Sb in the case of yellow) is more concentrated on the surface of the sample from Coimbra than the ones from Lisbon. This lack of ability in going further down into the glaze is more related with the glaze composition than with the pigment itself. However, blue and purple pigments have in principle more ability of diffusion than the yellow ones when applied to the same glaze. This is due to the molecule size and ability in homogenizing themselves into the glassy matrix.

Another conclusion can be drawn from the analysis of the yellow pigment. Not only the dissemination of the pigment throughout the glaze is less in the samples from Coimbra but also the irregularity of the crystals in the yellow seen in these samples is higher in comparison to the hexagonal shaped crystals from Lisbon. This indicates that the samples from Lisbon were submitted to a higher temperature than the ones in Coimbra.

Summarizing, in this study, some questions mainly related to the glaze properties have been clarified by comparing the manufacturing

centers of Coimbra and Lisbon as well as the pigment application and possible firing temperatures used.

As a next step of the project, it becomes necessary to evaluate the surface composition of all samples with  $\mu$ -XRD together with  $\mu$ -Raman in order to know the local composition of the pigments, and their evolution along the time.

### Acknowledgments

This work is within the frame of the Portuguese–German FCT/DAAD bilateral collaboration exchange program on “Investigation on glazed Portuguese ceramics through spectroscopy techniques (EDXRF, 3D Micro-XRF, XRD and SEM-EDS)”.

The authors would like to thank Dr. Alexandre Pais for having supplied the samples, property of the “Museu Nacional do Azulejo (MNAZ)” (National Tile Museum).

### References

- [1] A. Guilherme, J. Coroado, M.L. Carvalho, Chemical and mineralogical characterization on glazes of ceramics from Coimbra (Portugal) from the sixteenth to nineteenth centuries, *Anal. Bioanal. Chem.* 395 (2009) 2051–2059.
- [2] A. Guilherme, S. Pessanha, M.L. Carvalho, J.M.F. dos Santos, J. Coroado, Micro energy dispersive X-ray fluorescence analysis of polychrome lead-glazed Portuguese faiences, *Spectrochim. Acta Part B* 65 (2010) 328–333.
- [3] A. Pais, A. Pacheco, J. Coroado, *Cerâmica de Coimbra*, Ed. INAPA, Lisboa, (2007).
- [4] J. Molera, M. Vendrell-Saz, J. Pérez-Arantegui, Chemical characterization of tin glazes in Islamic ceramics from Eastern Spain, *J. Archaeol. Sci.* 28 (2001) 331–340.
- [5] Prudence M. Rice, *Pottery Analysis: a Sourcebook*, The University of Chicago Press, 1987.
- [6] V.A. Solé, E. Papillon, M. Cotte, Ph. Walter, J. Susini, A multiplatform code for the analysis of energy-dispersive X-ray fluorescence spectra, *Spectrochim. Acta Part B* 62 (2007) 63–68.
- [7] I. Mantouvalou, K. Lange, T. Wolff, D. Grötzsch, L. Lühl, M. Haschke, O. Hahn, B. Kanngießer, A compact 3D micro X-ray fluorescence spectrometer with X-ray tube excitation for archaeometric applications, *J. Anal. At. Spectrom.* 25 (2010) 554–561.

- [8] J. Molera, T. Pradell, N. Salvadó, M. Vendrell-Saz, Evidence of tin oxide recrystallization in opacified lead glazes, *J. Am. Ceram. Soc.* 82 (1999) 2871–2875.
- [9] A. Zucchiatti, A. Bouquillon, I. Katona, A. D'Alessandro, The 'Della Robbia Blue': a case study for the use of cobalt pigments in ceramics during the Italian renaissance, *Archaeometry* 48 (2006) 131–152.
- [10] M.S. Tite, The production technology of Italian maiolica: a reassessment, *J. Archaeolog. Sci.* 36 (2009) 2065–2080.
- [11] Data Web Mineral, Psilomelane Mineral Data. Retrieved Friday, 18th November, from, <http://webmineral.com/data/Psilomelane.shtml> 2010.
- [12] K. Sakellariou, C. Milian, A. Morresi, M. Ombelli, Spectroscopic investigation of yellow majolica glazes, *J. Raman Spectrosc.* 35 (2004) 61–67.
- [13] F. Rosi, V. Manuali, C. Miliani, B.G. Brunetti, A. Sgamellotti, T. Grygar, D. Hradil, Raman scattering features of lead pyroantimonate compounds. Part I: XRD and Raman characterization of Pb<sub>2</sub>Sb<sub>2</sub>O<sub>7</sub> doped with tin and zinc, *J. Raman Spectrosc.* 40 (2009) 107–111.
- [14] G. Bultrini, I. Fragalà, G.M. Ingo, G. Lanza, Characterisation and reproduction of yellow pigments used in central Italy for decorating ceramics during Renaissance, *Appl. Phys. A Mater. Sci. Process.* 83 (2006) 557–565.



## Analytical note

# Micro energy dispersive X-ray fluorescence analysis of polychrome lead-glazed Portuguese faiences <sup>☆</sup>

A. Guilherme <sup>a</sup>, S. Pessanha <sup>a</sup>, M.L. Carvalho <sup>a,\*</sup>, J.M.F. dos Santos <sup>b</sup>, J. Coroado <sup>c</sup>

<sup>a</sup> Departamento de Física da Faculdade de Ciências, Centro de Física Atómica da Universidade de Lisboa, Av. Prof. Gama Pinto, 2, 1649-003 Lisboa, Portugal

<sup>b</sup> GIAN, Physics Department, Coimbra University, 3004-516 Coimbra, Portugal

<sup>c</sup> Instituto Politécnico Tomar, Dep. Arte Conservação & Restauro, P-2300313 Tomar, Portugal

## ARTICLE INFO

## Article history:

Received 1 October 2009

Accepted 11 December 2009

Available online 24 December 2009

## Keywords:

Portuguese faience

Glaze

Micro X-ray fluorescence

Pigment

## ABSTRACT

Several glazed ceramic pieces, originally produced in Coimbra (Portugal), were submitted to elemental analysis, having as premise the pigment manufacture production recognition. Although having been produced in Coimbra, their location changed as time passed due to historical reasons. A recent exhibition in Coimbra brought together a great number of these pieces and *in situ* micro Energy Dispersive X-ray Fluorescence ( $\mu$ -EDXRF) analyses were performed in order to achieve some chemical and physical data on the manufacture of faiences in Coimbra.

A non-commercial  $\mu$ -EDXRF equipment for *in situ* analysis was employed in this work, carrying some important improvements when compared to the conventional ones, namely, analyzing spot sizes of about 100  $\mu$ m diameter. The combination of a capillary X-ray lens with a new generation of low power microfocus X-ray tube and a drift chamber detector enabled a portable unit for micro-XRF with a few tens of  $\mu$ m lateral resolution. The advantages in using a portable system emphasized with polycapillary optics enabled to distinguish proximal different pigmented areas, as well as the glaze itself.

These first scientific results on the pigment analysis of the collection of faiences seem to point to a unique production center with own techniques and raw materials. This conclusion arose with identification of the blue pigments having in its constitution Mn, Fe Co and As and the yellows as a result of the combination between Pb and Sb. A statistical treatment was used to reveal groups of similarities on the pigments elemental profile.

© 2009 Elsevier B.V. All rights reserved.

## 1. Introduction

The presence of coloration in an art object is one of the first characteristics to draw our attention and sometimes a starting point to make some cataloging about it. In fact, color has played an important role since ancient societies dated back to Egyptian times [1].

When the first Egyptians used color they believed it had magical abilities related with healing. They created the “Blue frit” by grinding down blue grass. The “Blue frit”, also known as “Egyptian blue”, is made from quartz, lime, a copper compound, and an alkali flux, all heated to a temperature between 850 and 1000 °C [2]. Frit is a ceramic composition that has been fused, quenched to form a glass, and granulated. Frits form an important part of the batches used in

ceramic glazes; the purpose of this pre-fusion is to render any soluble and/or toxic components insoluble by causing them to combine with silica and other added oxides and also to form a more uniform glaze surface on which the pigments can be applied more easily [3,4].

Color still creates an impact in our perception to define a certain object, regarding the cultural heritage of a country. For example, in Portuguese ceramic manufacture there was a marked preference for bluish glazes rather than yellowish in the decorative ceramic pieces. The ones which tend more to yellow-like color were seen as more commercial and not so fine as the blue-like ones [5].

In order to improve the knowledge of Portuguese glazed ceramics, this work aims to identify the colors used on this special type of pottery, which intend to identify “faiences of Coimbra”. Therefore, we quantify the kind of used pigments, as a key to classify the museum pieces. This investigation brings additional information regarding a former study already published by the authors [6], where the ceramic support and glaze of the same kind of pottery were characterized.

Historical and documental research based on examination of style, decorative motives and manufacture techniques provide a crucial set of information regarding typological and provenance matters. In

<sup>☆</sup> This paper was presented at the Colloquium Spectroscopicum Internationale XXXVI, held in Budapest, Hungary, August 30–September 3, 2009 and is published in the special issue of Spectrochimica Acta Part B, dedicated to that conference.

\* Corresponding author.

E-mail address: [luisa@cii.fc.ul.pt](mailto:luisa@cii.fc.ul.pt) (M.L. Carvalho).

addition to this classification method we will provide scientific results, in particular through the use of *in situ* micro Energy Dispersive X-ray Fluorescence ( $\mu$ -EDXRF).

Many special features like providing a good elemental coverage, high sensitivity for a wide range of elements and non-destructiveness, have labeled the XRF technique the most popular and the best starting point of a detailed scientific investigation [7–11]. These features together with a good quantification method and accomplished with a good statistical data treatment are in many cases enough to characterize the kind of objects at stake.

## 2. Materials

### 2.1. Provenance context

The type of pottery we study in this investigation is influenced by Northern Africa cultures especially from Maghreb. During the Renaissance, the tin glaze method applied to the ceramic body was manufactured in that region, which was rapidly spread to the southern European countries [3].

The ceramic pieces with this kind of glaze may have two designations: majolica or faience. The designation is associated to the place from where they were exported: from Majorca (Spain) or from Faenza (Italy), respectively. The faïences according to this technique were for the first time produced in Portugal in potteries from Lisbon on the second half of the XVI century [12].

At this time (end of the 16th century until beginning of the 17th) the Portuguese ceramic production consisted on common objects with “fast-made” decorative motives, which made this faïence production the cheapest one and the preferred one from the middle class to use in their daily life.

In the first half of the XVII century we witness a reduction of the people involved in the ceramic production, maybe due to outcome of many cases of Pest diseases.

In the second half of the XVII century, an increase of production in Coimbra was noticeable. At this time there was an offspring of new designations for this kind of activities (porcelain painters, oil painters and ceramic tileworks—Portuguese *azulejo*).

From the polychromic patterns used in the pieces produced in Coimbra, it is possible to distinguish, in a clearly divergent way, the production of this region from the pieces produced in other big production centers. To the production in Coimbra we can assign several features, such as the colors used as contours (Fig. 1). These varied from purple manganese to blue cobalt, enhancing a better definition of the limits between different decorative motives.

Under these conditions and based on historical and documental research, supported by examination of the style, the polychromic pieces having a mate vitreous surface, covered by dense and earthy decorative tones, seem to be characteristic from Coimbra. However, some doubts are still remaining concerning the pieces where the only chromatic tone is the blue. Furthermore, in these pieces two other characteristics can be allocated. The first one is that a mold from which all these pieces were manufactured might be existed, and the second one is that these pieces were performed prior in white, and following the glaze firing process some of them have been painted. Other characteristics rely on the decorative motives used in these pieces only in blue, such as laces.

### 2.2. Sample set

The analyzed pieces belong to a period between the XVI and XIX centuries and they are thought to be originally produced in Coimbra.

Nowadays these pieces belong to different museums in different locations in Portugal but a recent exhibition, aiming to show a large set of Coimbra ceramic manufacture, brought them together. The micro-EDXRF analyses were carried out *in situ* at the Museu Machado Castro in Coimbra. So, from the large number of pieces and



**Fig. 1.** Examples of glazed ceramics from Coimbra: (a) polychrome piece “Prato Vasconcelos”:  $6 \times \varnothing 27$  cm (b) the use of purples “Prato Mulher Pássaro”:  $4.8 \times \varnothing 27.4$  cm; (c) old plate: decorative motives used in these pieces only in blue, such as laces (marked in the picture), typical from Coimbra “Prato Flor”:  $5.3 \times \varnothing 33.6$  cm; (d)  $\mu$ -EDXRF *in situ* analysis of an old piece from Coimbra:  $14.5 \times 24 \times \varnothing 15$  cm.

**Table 1**  
Description of the 49 analyzed pieces.

Designation	Primary glaze	Color decoration
Prato 1739	White	B, P
Bica	Light yellow	G, P
Bispo azul e branco	White	B, P
Bispo azul e verde	White	B, G
Caco amarelo	White	Y
Caco verde e amarelo	White	G, Y
Depósito	Light blue	B, G, Y, P
Esfinge amarela	Light yellow	B
Esfinge branca	White	B
Estatueta	White	B, P
Estatueta rapariga	White	B, G, Y, O
Lavabo	Light blue	B, G, Y, P
Prato “macaco”	White	B, P
Prato “mulher-pássaro”	Light yellow	B, P
Placa de Sto. António	Light blue	B, G, Y, BR
Pote	Light yellow	B, G, P
Pote “Agva Bendita”	White	B
Pote com asas	White	B, Y, P
Pote azul	White	B
Prato “vascomselos”	White	B, Y, P
Prato “Apalpar”	White	B
Prato “brazão amarelo”	Light yellow	B, Y, P
Prato “brazão azul”	White	B
Prato “brazão leão”	Light yellow	B, P
Prato “çaçadores”	White	B, P
Prato “Anto Da Rocha”	White	B, P
Prato “cara”	White	B, P
Prato “coelho”	Light yellow	B, P
Prato “caravelas”	Light blue	B, BR
Prato “D. Quixote”	Light blue	B, G, Y, P
Prato “flor”	White	B
Prato “história”	White	B, P
Prato “Joaquim Pessoa”	White	B
Prato “laranja”	Light blue	B, G, O
Prato “leão”	White	B, P
Prato “lobo”	White	B, P
Prato “menina”	White	B, Y
Prato “menina pavão”	White	B
Prato “mocho”	White	B, P
Prato “MPerêra”	White	B
Prato “rainha”	White	B, G, P
Prato “rainha santa”	White	B, P
Prato “roza”	White	B
Prato “sétimo centenário”	White	B, G, BR
Prato “soldado”	White	B, G, Y, P
Prato “capacete”	Light yellow	B, BR
Estatueta “Sto. António”	White	B, P
Terrina	White	B, G, Y, P
Virgem	White	B, G

B—Blue; P—Purple G—Green; Y—Yellow; BR—Brown; O—Orange.

after a careful tracking from the historical point of view, 49 pieces have been chosen for analysis. Looking at Table 1 we see that blue is in 46 pieces, purple in 27 pieces, green in 15 pieces, yellow in 13 and brown and orange in just 6 pieces. These are the colors to be characterized.

### 3. Experimental

#### 3.1. $\mu$ -EDXRF method

For elemental determination, an Energy Dispersive X-ray Fluorescence (EDXRF) spectrometer, with micro beam capabilities was used.

The  $\mu$ -EDXRF system consists of a sided-Be window with a Mo anode OXFORD XTF5011 X-ray tube and a Silicon Drift Detector (SDD) Thermoelectrically Cooled (TEC) Vortex-60EX<sup>®</sup> (FWHM at 160 eV at Fe-K $\alpha$  line energy) with an active area of 50 mm<sup>2</sup> and a 25  $\mu$ m thickness Be window. The instrumentation is on a 45 degree detector to tube XRF geometric arrangement.

The characteristic radiation and Bremsstrahlung were emitted by means of polycapillary focusing optics [13], allowing a focal spot of 100  $\mu$ m for Fe–K $\alpha$ . The distance positioning was accomplished owed to two laser points and the analyzed spot could be visualized due to a camera. The X-ray beam as well as the detector snout is housed in a vacuum chamber, down to a 10 mbar pressure [14]. These measurements were performed *in situ* directly on the pieces (Fig. 1d).

Each spectrum was collected during 300 s by a digital pulse processor with PI-SpecA software application and the spectral qualification and further quantitative results obtained by using the PymCA software code [15].

#### 3.2. Statistical data handling

After quantifying the elements from the several analyzed pieces, we tried to find some correlations between the elements characteristics to each color used in the decoration of the pieces. In order to accomplish those correlations we resorted to two statistical applications, the Pearson test and the Scatter Matrix Plot.

The Pearson Correlation Coefficient is usually signified by  $r$  (rho), and can have the values from  $-1.0$  to  $1.0$ . A perfect negative (inverse) correlation corresponds to  $-1.0$ ;  $0.0$  means no correlation, and  $1.0$  corresponds to a perfect positive correlation.

Another interesting tool is the Scatter Matrix Plot. A scatter matrix is a pair-wise scatter plot of several variables presented in a matrix format. It can be used to determine whether the variables are

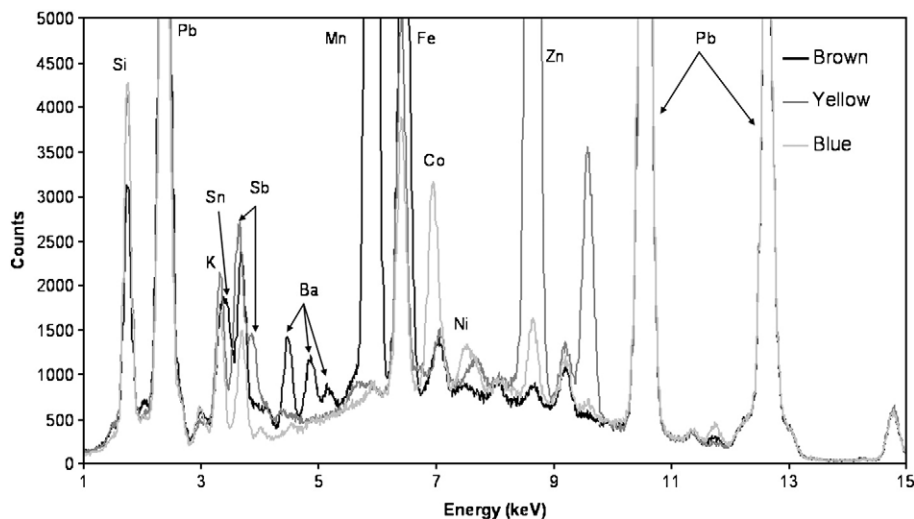


Fig. 2. Overlapping of spectra from three different colored areas (purple, yellow and blue) in a polychrome piece.



**Table 2**

Correlation matrix performed for the blue color. In bold are the significant correlations.

	Cl	K	Ca	Ti	Mn	Fe	Co	Ni	Cu	Zn	As	Pb		
Cl														
K		0.304												
Ca			0.129											
Ti				0.291										
Mn					0.013									
Fe						0.297								
Co							0.372							
Ni								0.400						
Cu									−0.037					
Zn										−0.014				
As											0.285			
Pb												0.104		
													0.032	
														−0.114
														−0.026
														−0.221
														0.041
														0.229
														0.248
														0.206
														0.171
														0.045

correlated and whether the correlation is positive or negative [16]. If one draws the line  $Y=x$  in the square of the relation between two elements, and the dots seem to tend to this line, their relation is positive; if they tend to  $Y=-x$ , their relation is negative.

#### 4. Results and discussion

In each piece all colors were analyzed in several points and some pattern arose from the evaluation of the spectra.

We started by noticing which elemental profile arises from the kind of pieces that definitely characterize the ceramics from Coimbra.

In the blue painted areas (Fig. 2) the elements Fe, Co Ni and As are present. Furthermore, the Pearson test (Table 2) revealed strong positive correlation between these elements which is indicative of its use to produce the blue pigment, like ground cobalt glass ( $\text{Co}(\text{SiO}_2)_n$ ) namely smalt, which is a blue glass matrix where tetrahedral holes are partly filled with  $\text{Co}^{2+}$  ions. The high correlation between Co and Ni (0.812) and Co and As (0.714) and also Fe and As (0.725) and Co and Fe (0.621) indicates that the raw material is related with cobaltite group mix minerals mainly Cobaltite a Cobalt Arsenic Sulfide ((Co, Fe) AsS) and Gersdorffite a Nickel Arsenic Sulfide NiAsS, or the related weathered mineral erythrite ( $\text{Co}_3(\text{AsO}_4)_2 \cdot 2.8\text{H}_2\text{O}$ ), more common as a blue pigment [17].

The purple (Fig. 2) was the second most used color. Through  $\mu$ -EDXRF spectra inspection we could testify that its characteristic element is Mn, which indicates that it was obtained by the use of ground manganite mineral originating Manganese Oxide Hydroxide  $\text{MnO}(\text{OH})$ . From the Scatter Matrix Plot (Fig. 3a) for the purple color we can see a positive relation with Fe since manganite is

commonly related with iron hydroxides (goethite) and iron carbonates (siderite) in surface sedimentary deposits.

The spectra corresponding to the green areas revealed Cu as the characteristic element for this pigment. An exception was revealed by the piece Prato “sétimo centenário”, containing high amounts of Ti and Zn and a very low content of Cu. This might be indicative that the piece is a recent one, maybe belonging to the XIX century. In fact, the motives and color densities are different than the rest of the set. In addition, the piece has some writings regarding the celebration at the year 1895. The performed tests did not reveal any correlations between the elements present in the green areas (Fig. 3b).

The measurements in the yellow colors revealed the presence of Sb together with very strong peaks of Pb. This suggests a crystalline phase of antimony and lead like the synthetic yellow pigment of Naples yellow ( $\text{Pb}_3(\text{SbO}_4)_2$ ) [18].

Nevertheless a positive correlation for these elements was not found (Table 3). This can be explained considering that the pieces are lead-based glazes, so the measurements of Pb are always affected by the Pb of the glaze.

Other colors such as orange and brown were also analyzed and the obtained spectra present mainly Mn and Fe in their composition. This suggests the use of ochres of these elements. These results are in agreement with the documented hypothesis that manganese oxides and iron oxides and hydroxides were responsible for the orange and brown colors [5].

The ceramic production in Coimbra is also distinguished by another characteristic which is the careful and detailed contours between the painted areas, usually in purple. In Fig. 4 we can observe that the contours are more dense colored areas and this is evidenced

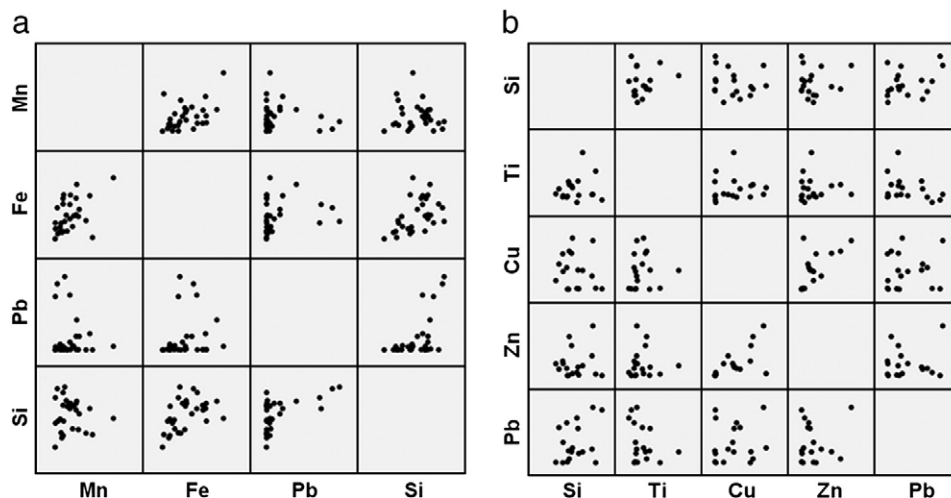


Fig. 3. Scatter matrix plots. (a) Purple color b) green color.

**Table 3**

Correlation matrix performed for the yellow color. In bold are the significant correlations.

	Cl	K	Ca	Ti	Mn	Fe	Ni	Cu	Zn	Sb	Pb
Cl		−0.375	−0.133	0.090	−0.449	0.611	−0.324	0.137	−0.135	−0.102	−0.010
K			−0.112	0.382	0.584	−0.066	0.317	0.112	−0.213	−0.340	0.554
Ca				0.350	0.416	0.460	0.274	0.469	−0.153	0.216	0.236
Ti					0.537	0.525	−0.010	0.339	−0.355	−0.006	0.397
Mn						−0.089	<b>0.655</b>	0.428	−0.334	0.021	0.578
Fe							−0.320	0.432	−0.185	−0.213	0.148
Ni								0.291	−0.360	0.208	0.449
Cu									<b>−0.783</b>	0.146	0.028
Zn										−0.109	−0.165
Sb											−0.484
Pb											

by the increase in manganese and the decrease of lead (characteristic from the glaze), due to a thicker layer of purple color.

## 5. Conclusions

From this work we can conclude that the glaze decoration performed after the primary glaze was obtained mainly by cobalt oxide pigments that confer the blue tones, the iron oxides and hydroxides responsible for the colors between orange and brown, the purple out of manganese oxides (typically used for contours), the green pigments essentially out of copper, and the yellows are a pigment based on antimony and lead. The remaining colors or tones result from the “chromatic density” and the combination of these pigments application.

This work is a successful application of a polycapillary lens in EDXRF portable equipment in order to study the colors, ornaments and contours in these exceptional pieces. Furthermore, this also emphasizes the use of a non-destructive *in situ* technique, which is a requisite to study valuable pieces that cannot be removed from the museums.

As a final remark we would like to end this work citing an old description of the ceramics from Coimbra belonging to Joaquim de Vasconcelos:

“The only one in Portugal representing the oriental tradition and preserving characteristics from the Arabic style. This paint, simulating birds, peacock tails, traced over a background formed by green areas, produces a unique effect at one sight, gives to this ceramics an archaic aspect, which is impossible to confuse it with any other region” [5].

## References

- [1] Little monkey murals. The history of colour. Retrieved Friday, 25 September 2009 from <http://www.littlemonkeymurals.com/ColoursHistory.htm>.
- [2] G.D. Hatton, A.J. Shortland, M.S. Tite, The production technology of Egyptian blue and green frits from second millennium BC Egypt and Mesopotamia, *Journal of Archaeological Science* 35 (2008) 1591.
- [3] Prudence M. Rice, *Pottery Analysis: A Sourcebook*, The University of Chicago Press, 1987.
- [4] A. Dodd, D. Murfin (Eds.), *Dictionary of Ceramics*, 3rd Edition, Institute of Materials, 1994.
- [5] A. Pais, A. Pacheco, J. Coroado *Cerâmica de Coimbra*. Ed. INAPA, Lisboa, 2007.
- [6] A. Guilherme, J. Coroado, M.L. Carvalho, Chemical and mineralogical characterization on glazes of ceramics from Coimbra (Portugal) from the sixteenth to nineteenth centuries, *Anal. Bioanal. Chem.* (2009), doi:10.1007/s00216-009-3132-y.
- [7] R. Padilla, P. Van Espen, P.P. Godo Torres, The suitability of XRF analysis for compositional classification of archaeological ceramic fabric: a comparison with a previous NAA study, *Anal. Chim. Acta.* 558 (2005) 283–289.
- [8] D.N. Papadopoulou, G.A. Zachariadis, A.N. Anthemidis, N.C. Tsirliganis, J.A. Stratis, Development and optimisation of a portable micro-XRF method for *in situ* multi-element analysis of ancient ceramics, *Talanta* 68 (2006) 1692–1699.
- [9] K. Tantrakarn, N. Kato, A. Hokura, I. Nakai, Y. Fujii, S. Glušćević, Archaeological analysis of Roman glass excavated from Zadar, Croatia, by a newly developed portable XRF spectrometer for glass, *X-Ray Spectrom.* 38 (2009) 121–127.
- [10] E. Ochandio-Cardo, S. Sagrado, G. Ramis-Ramos, Systematic procedure for the preparation of sets of calibration standards for X-ray fluorescence analysis of ceramic materials, *X-Ray Spectrom.* 27 (1998) 401–406.
- [11] A. Guilherme, A. Cavaco, S. Pessanha, M. Costa, M.L. Carvalho, Comparison of portable and stationary X-ray fluorescence spectrometers in the study of ancient metallic artefacts, *X-Ray Spectrom.* 37 (2008) 444–449.
- [12] A. Sandão, *Faianças Portuguesas: séculos XVIII e XIX*. Livraria Civilização Ed. Companhia Editora do Minho, Barcelos, 1985.
- [13] X-ray optical systems. Polycapillary focusing X-ray optics. Retrieved Friday, 25 September 2009 from [http://www.xos.com/index.php?page\\_id=12&m=1&sm=1](http://www.xos.com/index.php?page_id=12&m=1&sm=1).
- [14] G. Buzanich, P. Wobrauschek, C. Strelj, A. Markowicz, D. Wegrzynek, E. Chinea-Cano, S. Bamford, A portable micro-X-ray fluorescence spectrometer with

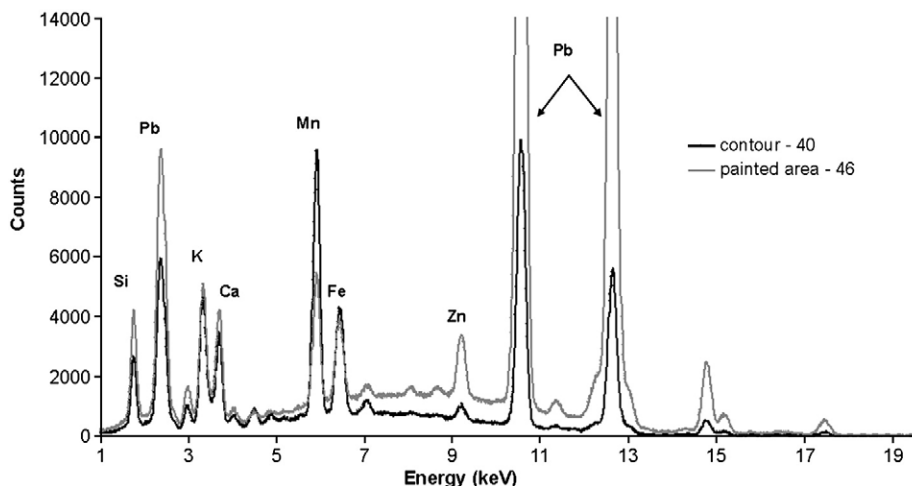


Fig. 4. Comparison of purple colors between a line contour and a painted area.

- polycapillary optics and vacuum chamber for archaeometric and other applications, *Spectrochim. Acta Part B* 62 (2007) 1252–1256.
- [15] V.A. Solé, E. Papillon, M. Cotte, Ph. Walter, J. Susini, A multiplatform code for the analysis of energy-dispersive X-ray fluorescence spectra, *Spectrochim. Acta Part B* 62 (2007) 63–68.
- [16] OriginLab. Retrieved Friday, 25 September 2009 from <http://www.originlab.com/index.aspx?s=8&lm=214&pid=1061>.
- [17] A. Zucchiatti, A. Ucchiatti, A. Bouquillon, I. Katona, A. D'alessandro, The 'Della Robbia blue: a case study for the use of cobalt pigments in ceramics during the Italian renaissance, *Archaeometry* 48, no. 1 (2006) 131–152.
- [18] J. Dik, F. Tichelaar, K. Goubitz, R. Peschar, Henk Schenk, 19th Century Naples yellow re-examined, *Zeitschrift fuer Kunsttechnologie und Konservierung*, 16, 2001, pp. 291–306.

# Chemical and mineralogical characterization on glazes of ceramics from Coimbra (Portugal) from the sixteenth to nineteenth centuries

A. Guilherme · J. Coroado · M. L. Carvalho

Received: 6 June 2009 / Revised: 27 August 2009 / Accepted: 2 September 2009 / Published online: 22 September 2009  
© Springer-Verlag 2009

**Abstract** Chemical, mineralogical and textural characterizations were performed on glazed pieces prepared in laboratory as well as on faïences fragments collected from the existing remains in “Santa Clara-a-Velha” monastery (Coimbra, Portugal). The chemical investigation was carried out using micro X-ray fluorescence ( $\mu$ -EDXRF) and wavelength dispersive X-ray fluorescence (WDXRF); the mineralogical results using X-ray diffraction (XRD) and the textural profile was obtained by scanning electron microscopy coupled with an energy dispersive spectroscopy system (SEM-EDS). Attention has been drawn to the glaze mineralogical changes during the firing temperature process, where three different types of glazes were submitted to three different firing temperatures (800 °C, 900 °C and 1,000 °C). Under these conditions, it is possible to relate the mineralogical content of the fragments to their firing temperature. Furthermore, we focused our purposes on identifying the technological aspects of the ceramic production in Coimbra, such as the raw materials, manufacture techniques and firing temperature adopted for the glaze. The latter aspect is highly dependent on the ceramic materials. In the framework of a more general project, this survey has as premise the recognition of a pattern, which is thought to be exclusively typical from the region of Coimbra. The perspective developed in the present work is

towards reliable archaeometric criteria, which can be used to characterise scientifically the ceramics from Coimbra.

**Keywords** Portuguese faïences · Glaze characterization · Spectrometry techniques · Authenticity · X-ray spectroscopy (XPS | XRF | EDX) · Diffraction methods (LEED | X-ray) · Archaeometry/fine arts

## Introduction

Many ceramic studies are easily found through the inspection of scientific international journals [1–6]. However, there is an apparent lack of scientific results concerning the ceramic Portuguese cultural Heritage.

Several faïence fragments, out of a large number, collected originally from the “Santa Clara-a-Velha” monastery remains, were examined through spectroscopic techniques to obtain their chemical and mineralogical profile. With this statement, we aim to perform consistent criteria that lead to scientific results and define a group of glazed ceramics (faïences), produced in Coimbra from the sixteenth to nineteenth centuries.

Between the sixteenth to nineteenth centuries, the production of ceramics in Portugal was based on three big production centres: Coimbra, Lisbon and Alcobaça. However, the different productions of these workshops cannot, nowadays, be easily separated.

The classification of these pieces is exclusively based on the inscriptions associated to the label of the workshop manufactures. It is essential to establish scientific tracers, like physical, chemical, mineralogical, textural and technological ones, which allow to distinguish these productions centres.

The importance of the ceramic production in Coimbra is very well documented [7–11]. However, in most of the

A. Guilherme · M. L. Carvalho (✉)  
Departamento de Física da Faculdade de Ciências,  
Centro de Física Atómica da Universidade de Lisboa,  
Av. Prof. Gama Pinto, 2,  
1649-003 Lisbon, Portugal  
e-mail: luisa@cii.fc.ul.pt

J. Coroado  
Dep. Arte Conservação & Restauro, Instituto Politécnico Tomar,  
2300313 Tomar, Portugal

cases, it is difficult to combine documental and material information, taking into account that most of the documents rely on unassigned pieces, which were produced in Coimbra.

A recent exhaustive documental work [12] describes clearly and in detail the manufacture from Coimbra, but such a complete study is still missing for other locations. The development of a scientific methodology can afterwards be applied to other manufacture centres, opening the path for the identification and characterization of the Portuguese ceramic production.

Taking these assumptions into account, this article presents chemical, mineralogical and textural data, concerning the glaze coatings used in the type of Coimbra faïences. For this purpose, two parallel approaches were considered: first, we studied the glaze coatings applied in the bisque (fired ceramic body) in simulated pieces prepared in laboratory. These model samples intend to reproduce the composition of the old ones (Fig. 1). We submitted these samples to three different temperatures, selected according to the range of temperatures that might be used in the original production of the sixteenth to nineteenth centuries. The glazes applied in the laboratory were obtained commercially in the form of frit, which means that the raw materials are pre-melted, then cooled down and grinded until obtain a uniform powder. With this process, the glaze acquires a bigger uniformity (concerning density and granularity) and the toxicity is reduced [13].

These pieces were analysed by several spectrometric techniques in order to obtain the data.

In parallel, we analysed by the same techniques, some original faïence fragments from Coimbra in order to identify characteristic tracers from this production centre (Fig. 2).

The existing recognised studies on these faïence fragments is supported basically by their chromatic and decorative characteristics, and were based on detailed descriptions of the ceramic production of Coimbra [12]. From this reference, important information can be extracted, namely, from the geologic point of view: (1) the ceramic support is generically characterised by a fine texture, light colour and sometimes red spots where non plastic elements are millimetric or eye visible, long pores oriented parallel to the surface are dispersed in the matrix. These aspects reveal the use of several raw materials and carelessness in the paste preparation.

(2) The glaze that is often associated to the ceramics from Coimbra is mostly characterised by a typical layer, which is used to masquerade the natural colour from the bisque (fired ceramic body), resulting in a matte aspect due to its textural composition.

The studied fragments were identified as belonging to the class of the *majolica* ceramics (sixteenth to nineteenth centuries).

Some of the most important aspects of *majolica* produced in Coimbra can be summarised: in 1514 is primarily established the price list of each kind of ceramic, but still no information about the used production technique. In this period, the glazed objects start to be frequent in Coimbra, due to the bad quality of the clay used for the ceramic body. In the seventeenth century, for the first time, appeared the reference to three different types of ceramic produced in Coimbra—the white one, the green, the yellow one and the red clay. The oxides could eventually be applied in a third firing process, which can explain the revealed chromatic density, and also the matte appearance and small white areas. In the eighteenth century, the ceramic from Coimbra reached the highest point. During this century, some of the masterpieces of the faïence from Coimbra were created and became famous all over the world through the Portuguese trade market with colonies from India, China, etc. In the nineteenth century, a new kind of faïence was produced in Coimbra called “*Ratinha*”. It is characterised by having a coarser paste aspect and a yellowish glaze, due to the bigger amount of tin included in the mixture.

The selected techniques for this study were:  $\mu$ -EDXRF, WDXRF, XRD and SEM-EDS. EDXRF and XRD are non-destructive and give elemental and chemical composition of the glaze. SEM-EDS allows mostly to identify the homogeneity of the material and WDXRF, besides being destructive, was used in this study as a complementary technique of  $\mu$ -EDXRF, for quantitative analysis.

All are well-established techniques and especially EDXRF, due to its portability, have been used successfully to study several characteristics in cultural heritage objects [14–16].

## Experimental

### Experimental setup

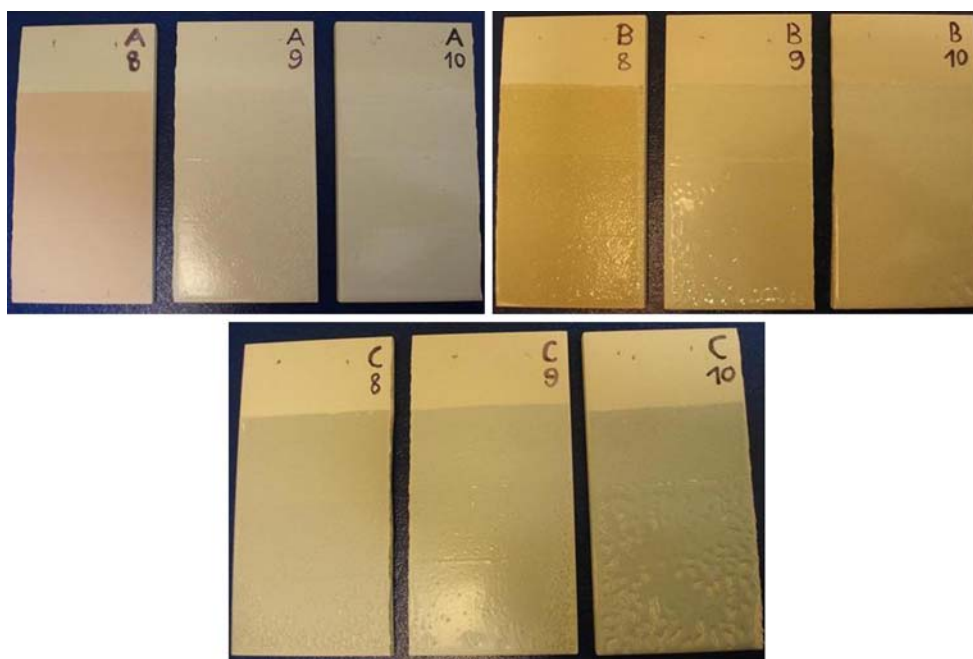
The experimental techniques at our disposal were:  $\mu$ -EDXRF, WDXRF, XRD and SEM-EDS. With these techniques we were able to extract the desired information: chemical, mineralogical and textural profiles.

The chemical profile of the prepared glazed pieces as well as the faïence fragments was undertaken by  $\mu$ -EDXRF and WDXRF.

The  $\mu$ -EDXRF system consists on a sided-Be window with a Mo anode OXFORD XTF5011 X-ray tube and a silicon drift detector thermoelectrically cooled Vortex 60EX (FWHM $\approx$ 160 eV at Fe-K $\alpha$  line energy) with an active area of 50 mm<sup>2</sup> and a 25  $\mu$ m thickness Be window. The instrumentation is on a 45° detector to tube X-ray fluorescence spectrometer (XRF) geometric arrangement.

The characteristic radiation and Bremsstrahlung can be emitted whether by means of a polycapillary lens or by a

**Fig. 1** Glazes A, B and C (8 submitted to 800 °C, 9 submitted to 900 °C, 10 submitted to 1,000 °C)



collimator, allowing a focal spot of 100  $\mu\text{m}$  for the former and 1.2 mm for the latter. The distance positioning was accomplished owing to two laser points and the analysed spot could be visualised by a camera.

The X-ray beam as well as the detector snout is housed in a vacuum chamber, down to a 10 mbar pressure [17]. These measurements were performed through a non-destructive method.

The WDXRF system consists on an XRF spectrometer Philips PW 1410/00, using a Cr-K $\alpha$  radiation. Lost on

ignition (LOI) values were obtained by heating samples at 1,000 °C for 3 h.

The mineralogical results were obtained through XRD. These analyses were performed with a Philips X'Pert PW 3040/60 goniometer, using Cu-K $\alpha$  radiation, 50 kV and 30 mA, automatic divergent notch graphite monochromator and a step size of 1°/2 $\theta$ /min in the 4–65° 2 $\theta$  range, with data acquisition by Philips X'Pert Data Collector v1.2. After samples have dried at 60 °C, were grinded and pulverised in an agate mortar. Identification of crystalline phases by XRD was carried out using the International Centre for Diffraction Data Powder Diffraction Files (ICDD PDF).

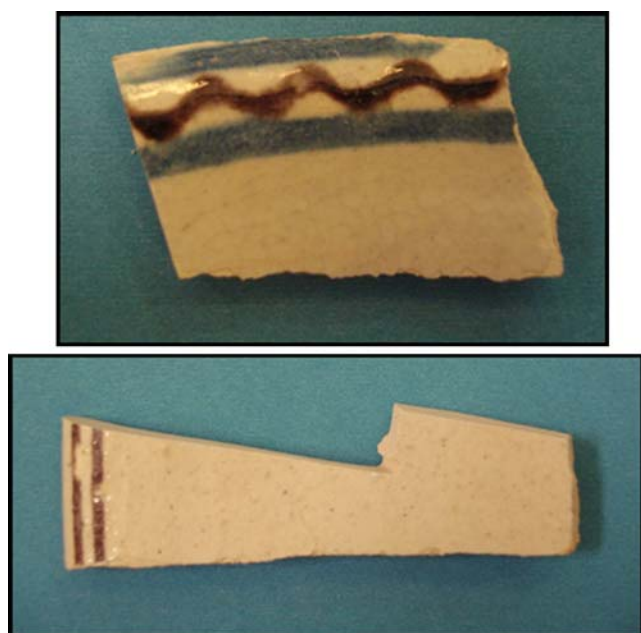
The surface microchemistry and texture profile of the analysed materials were obtained using SEM-EDS. The specification of this system is a Hitachi S4100, equipped with micro-analysis. The operating conditions were a 25 kV accelerating voltage and a 16 mm working distance.

For all the  $\mu$ -EDXRF measurements, the working conditions were: 40 kV, 1 mA, 10 mbar and 300 s acquisition time. The X-rays were emitted through the polycapillary lens mode, in order to obtain a detailed mapping area of each piece.

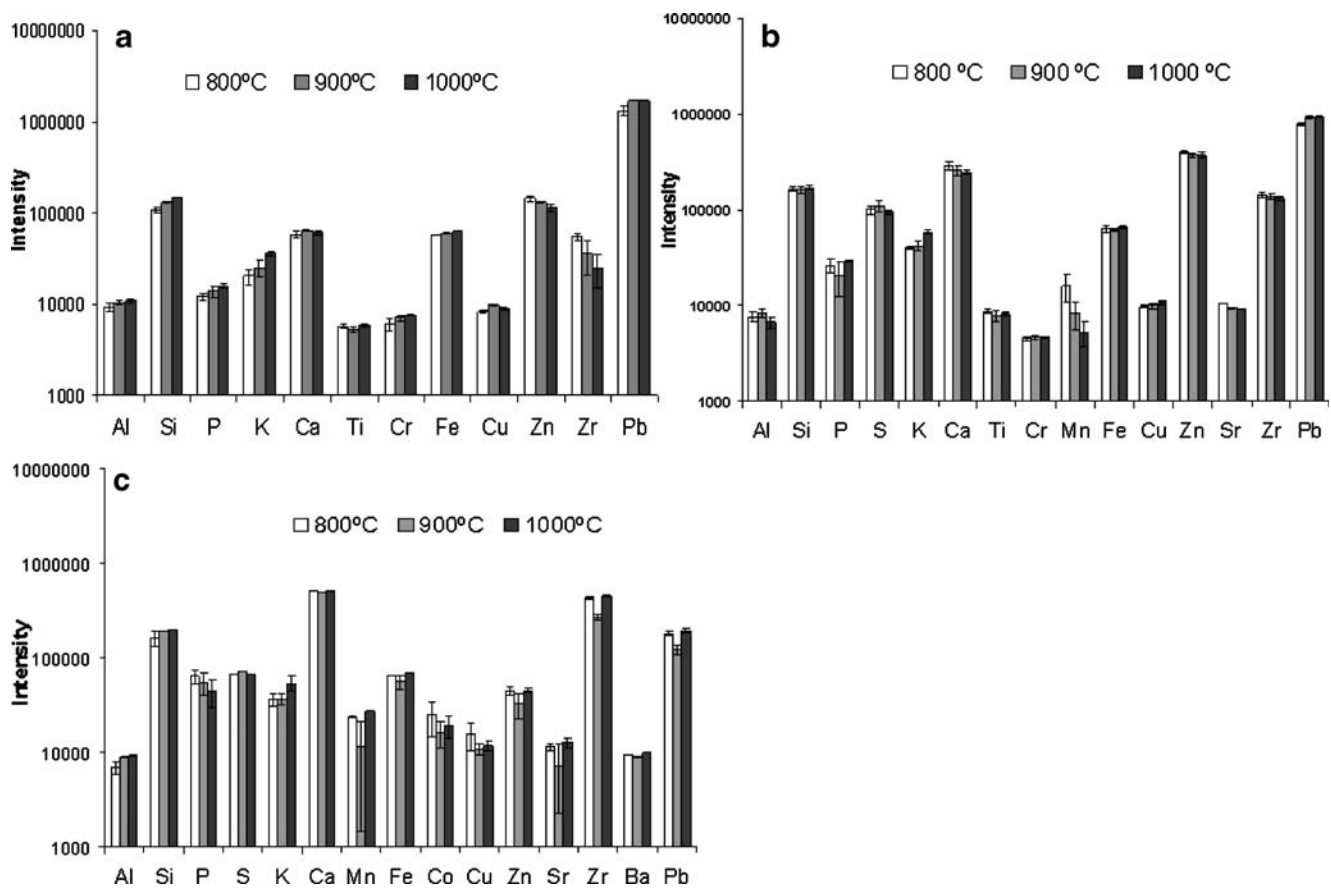
#### Sample collection and preparation

As previously referred, two parallel studies were undertaken in this work.

1. Pieces of three different types of glaze were prepared in laboratory (Fig. 1), labelled: A—“old-like” glass (seventeenth century), B—“old-like” glass (eighteenth century), C—rustic glass.



**Fig. 2** Faience fragments from the “Santa Clara-a-Velha” monastery (Coimbra, Portugal)



**Fig. 3** Elemental firing temperature dependence obtained by  $\mu$ -EDXRF for the glazes *A*, *B* and *C* submitted to 800 °C, 900 °C and 1,000 °C, respectively

Each type was previously mixed with water, applied on nine fired ceramic bodies (bisques) via submersion and then submitted to three different firing temperatures (800 °C, 900 °C and 1,000 °C, respectively). The purpose of this survey using the three different glazes with known chemical and mineralogical composition is to observe the phase differences and mineralogical changes after each thermal transformation. Following the identification of the mineralogical changes in the simulated samples, we can correlate the obtained results for the old glazes, allowing to estimate the production firing temperature. These temper-

atures were chosen considering the possibilities of working conditions for the original production.

These pieces were analysed by  $\mu$ -EDXRF and WDXRF in order to appraise the elemental characteristics of each glaze type, and the influence of firing temperature on morphological changes.

- Faience fragments, C-23, C-24 and C-26 (Fig. 2), collected from the “Santa Clara-a-Velha” Monastery remains were analysed by  $\mu$ -EDXRF, WDXRF, XRD and SEM-EDS.

**Table 1** Mineralogical firing temperature dependence obtained by XRD for the glaze *A*, submitted to 800 °C, 900 °C and 1,000 °C, respectively

Firing temp. (°C)	Compound						
	Kaolinite [Al <sub>2</sub> Si <sub>2</sub> O <sub>5</sub> (OH) <sub>4</sub> ]	Zircon (ZrSiO <sub>4</sub> )	Sodium aluminium-trisilicate (NaAlSi <sub>3</sub> O <sub>8</sub> )	Quartz (SiO <sub>2</sub> )	Cristobalite (polymorph of SiO <sub>2</sub> )	Skuterrudite (CoAs <sub>3</sub> )	Illite (K,H <sub>3</sub> O)(Al,Mg,Fe) <sub>2</sub> (Si,Al) <sub>4</sub> O <sub>10</sub> [(OH) <sub>2</sub> ,(H <sub>2</sub> O)]
Powder	✓	✓		✓			✓
800		✓	✓	✓			
900		✓	✓	✓		✓	
1000		✓	✓	✓	✓		

**Table 2** Mineralogical firing temperature dependence obtained by XRD for the glaze B, submitted to 800 °C, 900 °C and 1,000 °C, respectively

Firing temp. (°C)	Compound					
	Kaolinite [Al <sub>2</sub> Si <sub>2</sub> O <sub>5</sub> (OH) <sub>4</sub> ]	Zircon (ZrSiO <sub>4</sub> )	Cassiterite (SnO <sub>2</sub> )	Quartz-low (SiO <sub>2</sub> )	Cristobalite (polymorph of SiO <sub>2</sub> )	Anorthite (CaAl <sub>2</sub> Si <sub>2</sub> O <sub>8</sub> )
Powder	✓					
800		✓	✓	✓	✓	
900		✓		✓	✓	✓
1000		✓		✓		✓

The use of raw glazes on traditionally fired products is a well-established practise. However, the documental facts of the ceramic production in Coimbra [12] report a general carelessness in the production procedure, as it was mentioned previously, and those facts together with archaeological research leads us to believe that the universe of glazed ceramic production in Coimbra is based on both raw and fritted applications on the bisque. During the firing process of raw glazes, different processes can occur, such as: decomposition of raw materials, chemical reactions giving either crystalline or glassy products, and melting followed by nucleation and crystallisation of the melt [18].

**Results and discussion**

Glazed pieces prepared in laboratory

The μ-EDXRF analyses were performed on the three pieces and for the three different temperatures and for each sample, ten points were studied. The obtained results are displayed in Fig. 3 and correspond to an average of all measurements. As expected, no elemental changes were obtained for the three glazes having different firing temperatures (Fig. 3). The confirmation of this fact was necessary considering that the penetration of the glaze into the ceramic body could be temperature dependent.

Furthermore, from the semi-quantitative results, considering that the thickness and matrix composition of the

pieces are similar, we can conclude that the three types of glazes are different in terms of elemental composition. Both A and B are richer in Pb and poorer in Zr, while the rustic one presents a very high concentration in Zr. Type B, simulating the eighteenth century, is richer in Zn. These three elements are crucial to characterise the type of the glaze. Besides these three elements, Sn is also characteristic of old glazes, which is not present in the commercial ones.

All glazes (A, B and C) were obtained by commercial frits and the similarity with old glazes elemental content is decreasing from A to C (Tables 1, 2 and 3). The simulation of old-like glazes production is performed by introducing quartz and clay minerals to the frit, as it is exhibited in the XRD profile of glazes A and B. Moreover, in glazes A and B, kaolinite becomes amorphous at 550 °C and vanishes after the firing process is finished and at 1,000 °C the changes are basically due to mineral orientation, rather than thermal modifications (Tables 1 and 2).

Additional important aspects are the fact that glaze A exhibits more kaolinite and ilite and after the firing process is finished, it reveals a more matte appearance than glaze C (Fig. 1).

Glaze C is mainly composed by zircon (ZrSiO<sub>4</sub>), which assigns it as a modern one. In its profile is also shown a peak of cristobalite, characteristic from a high-temperature polymorph of quartz—this means that it has the same chemistry as quartz but a different structure (Table 3).

Some of the compounds are only formed after the glaze reaches the so called “working point”. This is the stage where all components have melted and this liquid matrix state of the glaze originates the formation of some

**Table 3** Mineralogical firing temperature dependence obtained by XRD for the glaze C, submitted to 800 °C, 900 °C and 1,000 °C, respectively

Firing temperature (°C)	Compound	
	Cristobalite (polymorph of SiO <sub>2</sub> )	Zircon (ZrSiO <sub>4</sub> )
Powder		✓
800		✓
900	✓	✓
1000	✓	✓



**Table 4** Mineralogical composition obtained by XRD for the fragments C-23, C-24 and C-26

Fragment	Compound				
	Quartz (SiO <sub>2</sub> )	Anorthite (CaAl <sub>2</sub> Si <sub>2</sub> O <sub>8</sub> )	Diopside (MgCaSi <sub>2</sub> O <sub>6</sub> )	Analcime (NaAlSi <sub>2</sub> O <sub>6</sub> ·H <sub>2</sub> O)	Augite (Ca,Mg,Fe)SiO <sub>3</sub>
C-23	✓	✓	✓	✓	
C-24	✓	✓	✓	✓	
C-26	✓	✓	✓	✓	✓

mineralogical components such as skutterudite (CoAs<sub>3</sub>), anorthite (CaAl<sub>2</sub>Si<sub>2</sub>O<sub>8</sub>) and sodium aluminium-trisilicate (NaAlSi<sub>3</sub>O<sub>8</sub>). Furthermore, cassiterite (SnO<sub>2</sub>) crystallises from 800 °C. Depending on the amount and on the original components from the raw frit, the “working point” can be reached at different temperatures for each kind of glaze [19].

At this point, an interesting fact should be mentioned. Skutterudite only appears due to the initial presence of cobalt oxide in the raw frit. This compound causes an interesting optic effect on the glaze and it was commonly used to confer some bluish coloration to glaze in order to reduce the typical commercial yellowish nature from the glazes. From an esthetical point of view, in general people tended to prefer the less yellowish glazes. One can even prove this fact by observation of the three different glazes applied on the ceramic pieces (Fig. 1), where glaze A is less yellow than the other two.

From the textural point of view, the SEM analyses confirm a certain homogeneity in the glaze composition, as one can see in Fig. 6. The obtained thickness for the glaze is approximately 200 µm.

Faience fragments (from the sixteenth to nineteenth centuries)

The general mineralogical composition of the ceramic supports associated to the decorative faiences (C-23, C-24 and C-26), obtained by XRD is formed by the crystalline phases of quartz (SiO<sub>2</sub>) and minerals of the melillite (calcium silicates) (Table 4).

The glazed surface was obtained, like for the model ones, during the second firing process by a method that allows the reaction between the various raw materials, in order to promote the glass formation, which gives rise to the glaze, as well as the used pigments. The firing

temperature in an oxidant atmosphere for these glazes must have been approximately 950 °C. This conclusion arises from the presence of diopside (MgCaSi<sub>2</sub>O<sub>6</sub>), due to its particular sensitivity for temperatures above 900 °C and analcime (CaAl<sub>2</sub>Si<sub>2</sub>O<sub>8</sub>) being weakly electrostatic when heated at higher temperatures [20].

Calcite and ilite are of great help to determine the firing temperature at which the pieces were submitted. Complete thermal decomposition of calcite can go up to 850 °C and the presence of augite [(Ca,Mg,Fe)SiO<sub>3</sub>] indicates precisely that the primary calcite was decomposed [21].

The chemical composition obtained by WDXRF revealed the content of the major elements, as well as the loss values at 1,000 °C, which are exhibited in Table 5. The water absorption of this material is (about 20 %), which from the technological point of view helps the glaze application.

The elemental profile from the glaze of each fragment obtained by µ-EDXRF is exhibited in Fig. 4 and shows great similarity between several analysed pieces, suggesting that the used raw material might be the same. Actually, existing documents corroborate this result stating that during this period (sixteenth to nineteenth centuries) the raw material was identical. The glaze is chemically characterised as a tin glaze, typical from the majolica type of ceramic, as it is confirmed by the presence of Sn in the spectra of Fig. 4.

The SEM-EDS measurements were performed via two operation modes: wide-area (where inclusions can be visualised) and spot-sized-area (where particular structure details are observed).

Through lateral observation of the fragments we could calculate the thickness of the glaze, which was approximately 400 µm.

Furthermore, SEM-EDS observations allowed us to access not only the glaze texture but also its semi-

**Table 5** Major elements composition obtained by WDXRF (%) and loss at 1,000 °C of the ceramic body from the C-23, C-24 and C-26 fragments (± 5% error analysis)

%	SiO <sub>2</sub>	Al <sub>2</sub> O <sub>3</sub>	Fe <sub>2</sub> O <sub>3</sub>	MnO	MgO	CaO	Na <sub>2</sub> O	K <sub>2</sub> O	TiO <sub>2</sub>	P <sub>2</sub> O <sub>5</sub>	Loss
C-23	51.10	18.72	3.72	0.04	4.77	16.35	1.24	2.23	0.79	0.14	0.90
C-24	52.82	17.35	3.75	0.04	4.57	15.52	1.71	1.21	0.81	0.11	2.10
C-26	50.59	18.43	3.78	0.04	4.79	16.21	1.60	2.02	0.79	0.15	1.60

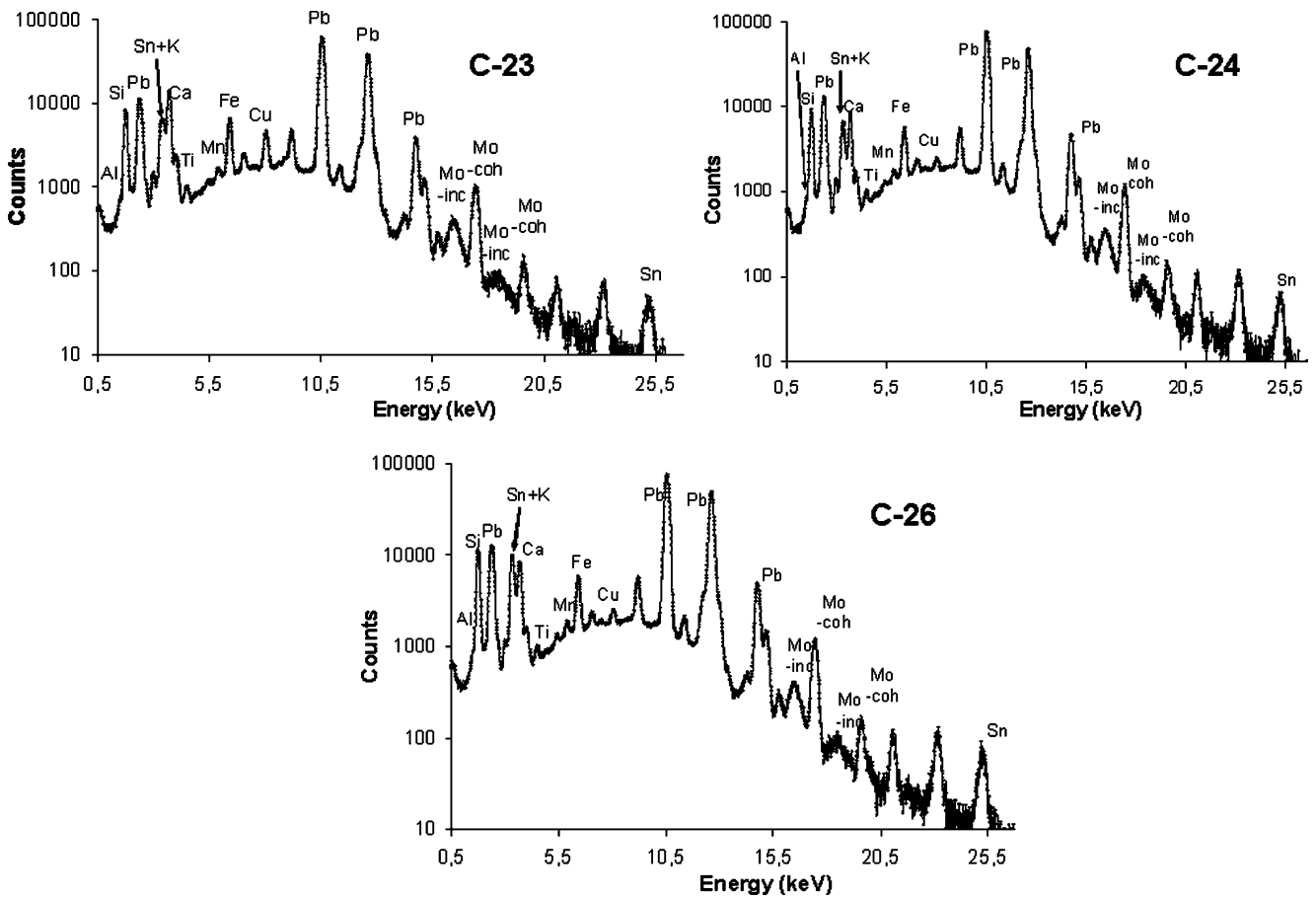
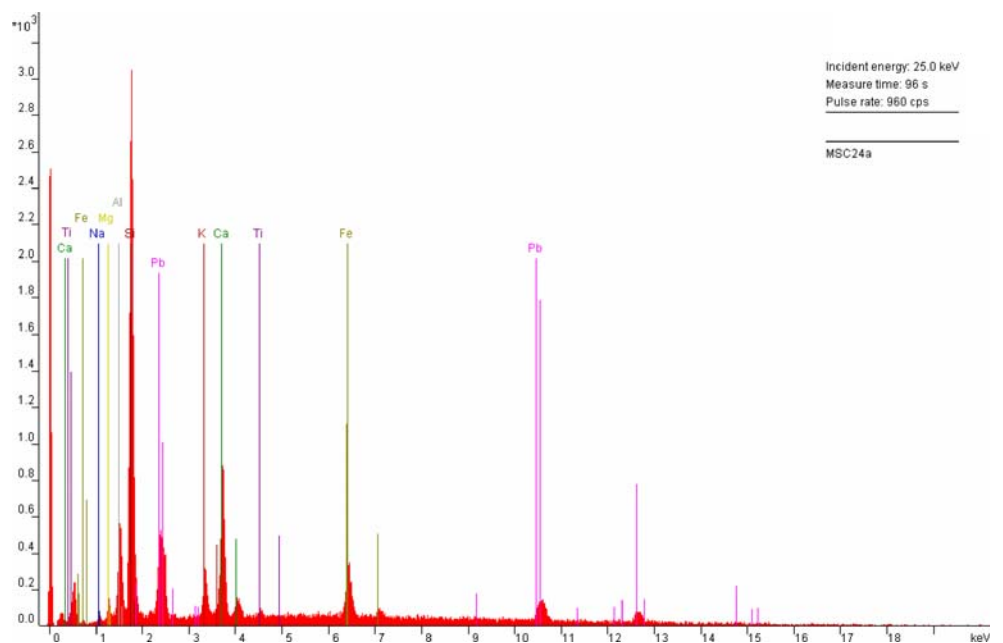
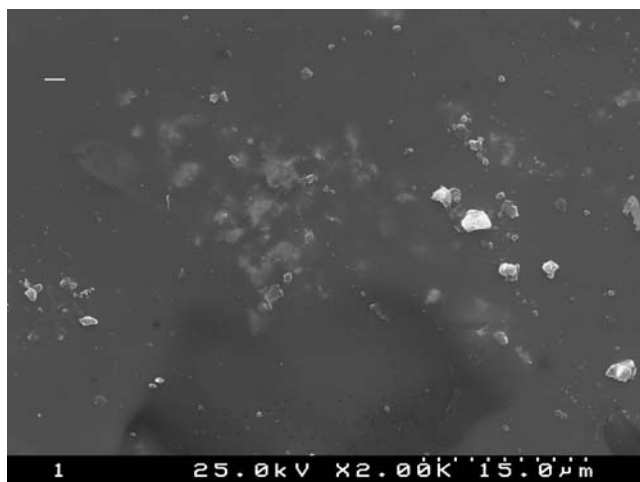


Fig. 4 Elemental profile obtained by  $\mu$ -EDXRF for the fragments C-23, C-24 and C-26

Fig. 5 EDS spectrum from the glaze of the C-24 fragment, where the number of counts is in arbitrary units

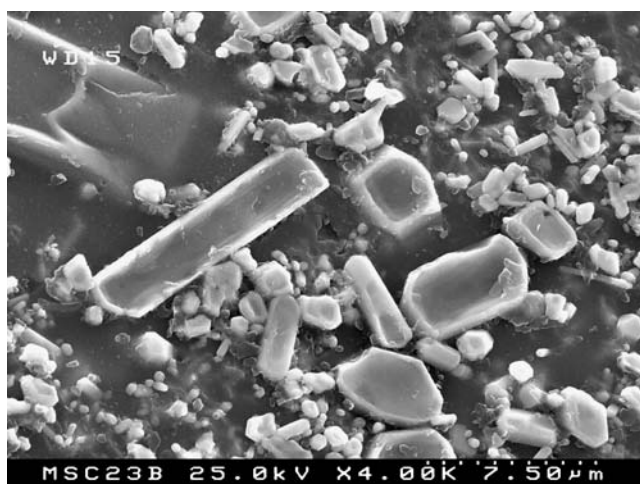




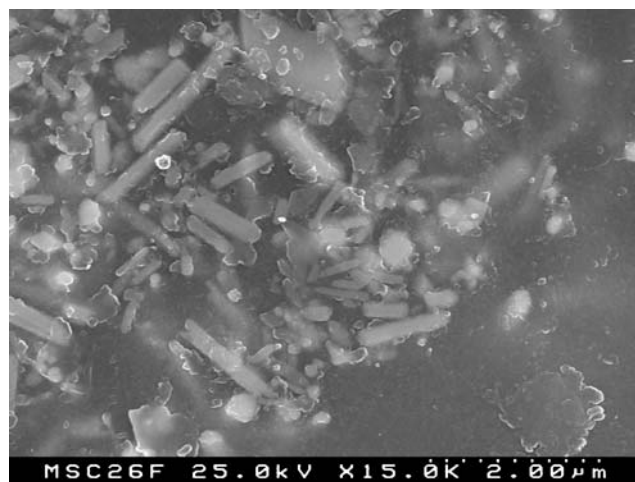
**Fig. 6** SEM image from the modern glaze A (frit) applied to the bisque. Magnification  $\times 2.0 \times 10^3$

quantitative elemental composition especially for the light elements: Na, Mg and Al not detected by EDXRF. From the obtained results, we conclude that the glaze main composition is micrometric-sized quartz grains, amorphous particles, rich in  $\text{SiO}_2$  and  $\text{Al}_2\text{O}_3$  which result from the de-hydroxylation of the clay minerals and closed pores (bubbles). All together, they confer an earthy and mate aspect to these glazes.

These features indicate that the glazes would be an aqueous suspension of its respective raw materials, namely clay minerals, which contribute to the glaze network formers ( $\text{SiO}_2$ ) and the network stabilisers ( $\text{Al}_2\text{O}_3$ ). The chemical composition of the glazes from Coimbra confirms the presence of these components and reveals that the fusing agents, the network modifiers were basically  $\text{PbO}$ ,  $\text{K}_2\text{O}$  and  $\text{Na}_2\text{O}$ , as we could confirm by the EDS spectra



**Fig. 7** SEM image from the glaze of the C-23 fragment showing cassiterite crystals ( $\text{SnO}_2$ ) included in the vitreous matrix. Magnification  $\times 4.0 \times 10^3$



**Fig. 8** SEM image from the glaze of the C-26 fragment, showing cassiterite crystals ( $\text{SnO}_2$ ) included in the vitreous matrix. Magnification  $\times 15.0 \times 10^3$

corresponding to the C-24 fragment (Fig. 5). Tin, in the cassiterite crystal structure ( $\text{SnO}_2$ ), which accumulates in the lower part of the glaze (close to the body), was used as an opaque agent, giving a white aspect, as we can see for the C-23 and C-26 pieces (Figs. 7 and 8).

## Conclusions

This work proposes a reliable scientific methodology to identify and characterise the Portuguese ceramics. The employment of EDXRF, with the advantage of its portability and non-destructiveness of the sample provided elemental identification. This allowed to characterise the raw materials used in the glaze preparation of the old fragments and hence to assign the type of ceramic: in this case, lead- and tin-based (*majolica*).

Another issue is the mineralogical identification, which gave rise to the second stage of our approach. Through XRD, we were able to identify the minerals existent in the analysed samples in the several stages we performed. This technique has also the advantage of being non-destructive even when bigger sized pieces had to be studied. To corroborate the analyses previously mentioned, we also performed SEM analyses to evaluate the textural content of the samples, which aid the mineralogical identification.

This work is a successful combination of several techniques:  $\mu$ -EDXRF, WDXRF, XRD and SEM-EDS, in order to achieve the chemical, mineralogical and the textural profiles of ceramics.

The two parallel studies carried out in this work allowed us to obtain important results showing the dependence of the firing temperature process on the mineralogical composition. These results are also extremely important

in conservation–restoration ceramic processes. In addition, this work emphasises the possibility to distinguishing the main features of Coimbra production centre, scarcely mentioned or even misdated due to non-existing information.

By a careful visual analysis of the SEM pictures for each kind of glaze, we could testify that one of the major characteristics relies on the in-homogeneity for old ceramics and homogeneity for the recent ones (Fig. 6, 7, and 8). This is related to the manufacturing process. Glazes from original pieces are obtained with “raw” materials which, after the firing process, create a more heterogenic pattern than the ones from the simulated pieces, where the glazes were obtained through a fritting process with pre-melted material. This also highlights the big importance of this study in identification of old and modern glazing processes.

## References

- Alaimo R, Bultini G, Fragalà I, Giarrusso R, Montana G (2004) *App Phys A* 79:263–272
- Padilla R, van Espen P, Godo Torres PP (2006) *Analytical Chemical Acta* 558:283
- Inanez JG, Speakman RJ, Garrigós JB, Glascock MD (2008) *J Archaeol Sci* 35:425–440
- Padeletti G, Fermo P, Gilardoni S, Galli A (2004) *App Phys A* 79:335–339
- Borgia I, Brunetti B, Mariani I, Sgamellotti A, Cariati F, Fermo P, Mellini M, Viti C, Padeletti G (2002) *Appl Surf Sci* 185:206–216
- Alaimo R, Bultrini G, Fragalà I, Giarrusso R, Iliopoulos I, Montana G (2004) *App Phys A* 79:221–227
- Teixeira de Carvalho JM (1921) *A Cerâmica Coimbrã no Século XVI*. Imprensa da Universidade, Coimbra
- Gonçalves AA (1912) In: *Estudo Químico e Tecnológico sobre a Cerâmica Portuguesa Moderna, Breve Noção para o Estudo da Cerâmica Coimbrã 2ª edição anotada*, Lisboa
- Gonçalves AN, Fonseca JC (1947) *Museu Machado de Castro: Secção de Cerâmica I Faiança Portuguesa: Catálogo—Guia*. Coimbra Editora, Coimbra
- Sandão A (1985) *Faianças Portuguesas: séculos XVIII e XIX*. Livraria Civilização, Barcelos
- Queiroz J (1907) *Cerâmica Portuguesa*. Typographia do Anuário Commercial, Lisboa
- Pais A, Pacheco A, Coroado J (2007) *Cerâmica de Coimbra*. Ed. INAPA, Lisboa
- Rice PM (1987) *Pottery analysis: a sourcebook*. The University of Chicago Press, Chicago
- Guilherme A, Cavaco A, Pessanha S, Costa M, Carvalho ML (2008) *X Ray Spectrom* 37:444–449
- Gil M, Carvalho ML, Seruya A, Ribeiro I, Alves P, Guilherme A, Cavaco A, Mirão J, Candeias A (2008) *X-Ray Spectrom* 37:328–337
- Pessanha S, Guilherme A, Manso M, Carvalho ML (2008) *Spectrosc Eur* 20:9–11
- Buzanich G, Wobrauschek P, Strelci C, Markowicz A, Wegrzynek D, Chinea-Cano E, Bamford S (2007) *Spectrochim Acta B* 62:1252–1256
- Fröberg L, Kronberg T, Hupa L, Hupa M (2007) *J Eur Ceram Soc* 67:1671–1675
- Rasteiro MG, Gassman T, Santos R, Antunes E (2007) *Ceram Int* 33:345–354
- Bagnasco MB, Casoli A, Chiari G, Compagnoni R, Davit P, Mirti P (2001) *J Cult Herit* 2:229–239
- Iordanidis A, Garcia-Guinea J, Karamitrou-Mentessidi G (2009) *Mater Charact* 60:292–302